厚生労働科学研究費補助金

難治性疾患等政策研究事業

染色体微細欠失重複症候群の包括的診療体制の構築

令和２年度　総括・分担研究報告書

研究代表者　倉橋　浩樹

令和３（２０２１）年　３月

目　　次

・講師）

厚生労働科学研究費補助金（難治性疾患等政策研究事業）
総括研究報告書

染色体微細欠失重複症候群の包括的診療体制の構築

研究代表者　倉橋　浩樹
藤田医科大学・総合医科学研究所・分子遺伝学・教授

研究要旨
本研究では、マイクロアレイ染色体検査により診断される、多発奇形・発達遅滞を主症状とする染色体微細欠失重複症候群の包括的診療体制の構築を目的として、代表的な疾患群に関して、全国調査による国内患者の把握や、診療情報の収集と分析、診断基準、診療ガイドラインの策定を実施する。エマヌエル症候群に関して、ウェブサイトを利用した患者登録を開始し、現在、16名の登録がある。また、COVID-19 の影響も後押しし、第２回オンライン家族会「エマヌエル症候群の日」を開催した。新規登録患者 6 名も含め、合計 18 家族が参加し、成人期と小児期の患者をつなぐことができた。医療情報の提供を行うとともに、個々の患者の臨床情報を得ることができた。また、その他の疾患に関しては、継続してマイクロアレイ染色体検査により診断を行った。マイクロアレイ染色体検査の保険収載に向けて、研究班の班員の経験を生かして、一般診療における診療ガイドラインを策定し、学会承認を得て、発出することができた。

研究分担者
大橋博文　埼玉県立小児医療センター・遺伝科・科長兼部長
黒澤健司　地方独立行政法人神奈川県立病院機構神奈川県立こども医療センター・遺伝科・部長
山本俊至　東京女子医科大学・遺伝子医療センター･教授
涌井敬子　信州大学医学部・遺伝医学教室・講師

A. 研究目的

染色体の欠失や重複のような微細構造異常によるコピー数の変化（copy number variation: CNV）は、量的効果により遺伝子機能に直接影響するため、先天性疾患や知的障害の原因となることが多い。CNV のある染色体領域に依存して含まれる遺伝子の種類が異なるので、症状にはバリエーションがある。ただ、CNV に含まれる数多くの遺伝子量が同時に変化するため、症状は複数の遺伝子の量的変化の効果の合算として現れ（隣接遺伝子症候群）、単一遺伝子病よりも重症となることが多い。従来は G 分染法による染色体検査によるスクリーニングや、特定の疾患に関しては FISH 法での診断が行われてきたが、近年、マイクロアレイ染色体検査が臨床応用され、検出感度が飛躍的に向上した。欧米では 2005 年頃から臨床応用され、多発奇形・発達遅滞の患者で G 分染法では３％であった異常検出率が、マイクロアレイ染色体検査の導入により、15-20％の患者で責任変異を同定できるとされ、すでに欧米では多発奇形・発達遅滞の原因の精査としては従来の染色体検査にかわる第 1 選択の診断ツールとされている。日本でも、マイクロアレイ染色体検査が診断に必須な疾患が指定難病や小児慢性特定疾患に認定されはじめ、その臨床的有用性は高いという認識は拡大しているものの、一方で、高コストという問題があり、まだ保険収載されていない。

研究代表者を含む本研究班員はこれまで、厚労省難治性疾患克服研究事業の支援も受け、マイクロアレイ染色体検査で診断されるような多発奇形・発達遅滞の患者の診療をおこなう中で、個々の疾患の診断基準や重症度基準、診療ガイドライン作成を行ってきた。一部の代表的な疾患に関してはすでに先行研究班で臨床的実態調査がなされており、小児期の疾患の自然歴に関しては十分な情報が集まった。一方で、患者さんの多くは小児期の医療管理の充実化により疾患の予後が改善し長期生存が可能となっており、成人期治療へのトランジッションが重要となってきたが、これら稀少疾患の成人期の臨床情報は皆無に等しい。直面している患者さんやご家族は移行期や成人期の疾患の臨床情報を必要としており、また、小児期の患者さんのご家族も安心材料としての長期的な情報を欲している。そこで、本研究では先行研究を継続する形で、3 年間を通じて、現在すでに作成している患者レジストリーを利用して、長期生存例の直近の情報を入手し、疫学的調査を行うことを第一の目的とする。1 年目には、代表的な 5 疾患（1p36 欠失症候群、4p 欠失症候群、5p 欠失症候群、スミスマゲニス症候群、エマヌエル症候群）に関して、成人期患者の情報収集を行う。2 年目は、収集した情報を分析して、当該疾患の症状の特徴を抽出し、その対処法や合併症の予防法をリスト化する。そして、3 年目には、代表的な 5 疾患に関して、成人期移行も踏まえた新たな診療ガイドラインの作成を行う。そして、その他の染色体微細欠失・重複症候群に関しては、頻度の低い疾患群なので、引き続き患者サンプルの収集とマイクロアレイ染色体検査を行い、ある程度の情報が集積したら、マイクロアレイ染色体検査の保険診療に向けてその準備の一環として、一般の医療従事者に向けたマイクロアレイ染色体検査の診療ガイダンスの策定を行うことを目的とする。

B. 研究方法

代表的な 5 疾患に関しては、先行研究ですでに作成している患者レジストリーを利用して、患者情報を、とくに長期生存例の直近の情報を入手し、疫学的調査を行う。研究代表者倉橋浩樹がエマヌエル症候群（指定難病２０４）、大橋博文（以下、敬称略）が 5p 欠失症候群（指定難病１０９）、黒澤健司がスミスマゲニス症候群（指定難病２０２）、山本俊至が 1p36 欠失症候群（指定難病１９７）、涌井敬子が 4p 欠失症候群（指定難病１９８）を担当する。また、その他の染色体微細欠失・重複症候群に関しては、患者数の少ない稀少疾患であるので、さらに多くの診断未確定患者の発掘のために、日本全国の主な診療施設の小児科もしくは遺伝診療科に連絡を取り、染色体微細構造異常が疑われるような多発奇形・発達遅滞の患者の情報を得て、研究代表者を含む各研究分担者が個々の施設でマイクロアレイ染色体検査、必要に応じて FISH 解析にて診断を確定させ、詳細な臨床情報との関連を検討する。また、マイクロアレイ染色体検査の保険診療に向けてその準備の一環として、一般の医療従事者に向けたマイクロアレイ染色体検査の診療ガイダンスの策定を行う。この策定には、日本小児遺伝学会（黒澤健司理事長、本研究班の研究分担者）、日本先天異常学会、日本人類遺伝学会・臨床細胞遺伝学認定士制度委員会（大橋博文委員長、本研究班の研究分担者）、そして、厚生労働科学研究費補助金難治性疾患政策研究事業「先天異常症候群領域の指定難病等の QOL の向上を目指す包括的研究」研究班との連携のもとに行う。

（倫理面への配慮）

本研究は、ヒトゲノム・遺伝子解析研究に関する倫理指針、人を対象とする医学系研究に関する倫理指針を遵守して行った。解析試料の取得は書面でのインフォームドコンセントの上でおこない、研究対象者に対するプライ

バシーの保護など、人権擁護上の問題については十分に配慮したうえで行った。各関連施設から送付される試料は、試料提供機関において連結可能匿名化が行われ、研究代表者や研究分担者の所属機関には匿名化された試料と、予めチェックリストとして作成した臨床データのみが送付されることとした。試料は研究代表者や研究分担者の所属機関にて保管し、研究期間終了後に同意書に基づき破棄を行う予定である。データは研究代表者や研究分担者の所属機関内の鍵のかかるキャビネットに研究期間内、保管する。もしくは、同意が得られた場合にはスキャンして電子カルテに取り込む。報告又は発表に際しては、被験者のプライバシー保護に十分配慮する。偶発的所見を含めた、発生しうる諸問題には、各施設の遺伝カウンセリング部門が対応する。マイクロアレイ染色体検査や、アンケートによる疾患情報収集に関する研究は、すでに研究代表者や研究分担者の所属機関の倫理審査委員会の承認を得ている(「染色体コピー数異常症に関する研究」藤田医科大学・ヒトゲノム・遺伝子解析研究倫理審査委員会、HG13-003。「日本における t(11;22)染色体転座保因者およびエマヌエル症候群患者の疫学調査」藤田医科大学・医学研究倫理審査委員会、HM15-157。)。

C. 研究結果

（１）エマヌエル症候群について

エマヌエル症候群については、7 年前に完了した先行研究の終了後、徐々に把握している患者は加齢し成人期に達する患者が増えている。また、追加で把握している患者の数も増加している。本研究においては、患者登録を促進するために、患者の居住地がわかるような「友だちマップ」というレジストリー・システムを作成し、研究代表者が運営するエマヌエル症候群の患者と家族の支援サイトの上で運用している（資料１）。登録者数は昨年度より３名増え、現時点で 16 名が登録している（宮城 5、神奈川 3、大阪２，群馬、東京、岡山、山口、高知、熊本が各１名)、患者の家族がお互いの居住地と年齢とでできるようになる。必要な情報、とくに年長児や成人期の情報を、居住地の近隣の家族から得ることが可能になることが期待される。

先行研究や､把握している成人患者に対するアンケート調査において成人期の情報を集めるために、成人例に焦点を当てた質問表作成に取り組んでいる。まずは、若年患者の家族が成人例の何を知りたいのかを事前に調査することとした。

藤田医科大学病院・臨床遺伝科（遺伝カウンセリング室）には、全国から新規に診断されたエマヌエル症候群の患者が来談される（今期は COVID-19 特例でオンライン遺伝カウンセリングにて対応)。その面談の中で、成人期の患者の家族に何を聞きたいのか、質問リストを作成してもらっている。一昨年度は福岡（2018 年 4 月 21 日）と仙台（2018 年 5 月 12 日）で数組みの患者家族が集まる小規模な患者会を開催し、そこで成人期患者の情報や、小児期患者の家族が何を知りたがっているのかの情報を収集した。それらを質問表作成の材料とした。

この地域ごとの患者会はそれなりに家族同士をつなぐ役割を果たしたが、情報収集には患者数を増やす必要がある。しかし、移動が困難な患者さん同士が地域を越えてコミュニケーションを取るのは困難を伴う。そこで、２年目の昨年度は、オンライン会議システム Zoom を用いてオンライン家族会を開催した t(11;22)転座にちなんで、2019 年 11 月 22 日に第１回のオンライン家族会を開催した。首都圏、関西、四国、九州の患者さんとそのご家族が参加し、移動が困難である患者さん同士をつなぐことができた。また、このオンライン家族会で、本事業に関してもご家族にアナウンスし、情報収集が可能となった。、

そこで、毎年 11 月 22 日を「エマヌエル症候群の日」とし、その日にオンライン家族会を開催することとし、本年度は 2020 年 11 月 22 日に第２回の「エマヌエル症候群の日」を開催した（資料２）。新規登録患者６名も含め、合計 18 家族が参加した。北は東北、南は九州まで、全国規模でご家族に参加して頂けた。まず、北米の患者会の前代表者の Stephanie St.Pierre 夫人に、動画によるメッセージを頂き、拝聴した。北米の患者会の現代表者の Murney Rinholm さんも現地から現地時刻で深夜帯にオンラインで参加された。前半は、理学療法士と言語聴覚士の先生がたに、嚥下、歩行などに関する講座をして頂いた。そのあと後半は、患者同士のグループ・ワークを行い、終了後にアンケートを配布した。アンケート調査により得られたデータを分析したところ、継続的な開催の要望が強かった。患者会でのご家族の意見を総括して、成人期の患者の自然歴情報の収集のための調査票を作成した（資料３）。

さらには、オンライン開催であった第６５回日本人類遺伝学会の患者会のコーナーにはじめて出展し、エマヌエル症候群に患者会が存在することをアピールすることができた。

（２）その他の疾患について

マイクロアレイ染色体検査は染色体微細欠失重複症候群のような疾患の診断に必須であり、保険診療化を目指すため、これまでの多くの診断経験を踏まえて、日本小児遺伝学会の有志、日本人類遺伝学会・臨床細胞遺伝学認定士制度委員会のメンバーなどが中心となり、マイクロアレイ染色体検査の診療ガイダンスの策定を行った（資料４）。日本小児遺伝学会、日本先天異常学会、日本人類遺伝学会、そして、厚生労働科学研究費補助金難治性疾患政策研究事業「先天異常症候群領域の指定難病等の QOL の向上を目指す包括的研究」研究班、「染色体微細欠失重複症候群の包括的診療体制の構築」研究班の名のもとに発出した。

D. 考察

染色体微細欠失重複症候群のような稀少難病は小児期に診断されるため、診断時に症例報告がなされ、小児期の臨床情報は容易に入手可能であるが、予後の改善により長期生存例が増え、シームレスな移行期・成人期治療へのトランジッションが重要となってきている。本研究では、代表的疾患の成人期情報を収集し、診療ガイドラインに反映させる形で公開することを目指している。

代表的疾患の解析から進めているが、患者会のようなフェイストゥーフェイスの機会が、患者の家族は先輩方から直接に情報を聞くことができるし、じかに成人期の患者と接触することでイメージが湧きやすい。また、そこに参加した医療従事者も効率的に情報収集ができる。エマヌエル症候群の場合、長時間の移動が難しい患者が多いため、大都市で行われるような大規模な患者会では参加しにくいという問題がある。そこで、小規模ながらも各地方の主要都市で患者会を開催することができれば、短時間の移動で目的地に着くことができ、いろんな年齢層の患者の家族が患者の家族が集まる場ができ、そこで種々の情報を得ることができる。さらにはその小規模の患者会同士を繋ぐなど、種々の目的で、昨年度第１回のオンライン家族会を試みた。参加者はほとんどが個人参加であったが、自宅でパーソナルコンピューターやスマートフォンを利用して参加し、特にトラブル無く、また大変満足して頂いた。またわたしたちも研究の概要のアナウンスと情報収集を行うことができた。

本年度は、奇しくも COVID-19 の影響で、物理的な移動が困難となり、ますますオンライン情報伝達ツールが発達し、一般のかたが簡単に使えるようになりつつあることが、私たちの活動を大きく後押しした。第２回のオ

ンライン家族会合計 18 家族が参加した。家族会でのご家族からの意見を総括して、成人期の患者の自然歴情報の収集のための調査票を作成することができたので、今後に生かしていけると考えている。

来年度以降、COVID-19 が収束に向かえば、オンライン家族会はハイブリッド方式に進むことが期待される。すなわち、地域の拠点においては、患者さん同士が一同に集まって頂き、フェイストゥーフェイスで交流を深める。また、その拠点同士をオンラインで繋ぎ、情報交換することができればと考えている。

最後に、本研究のもう一つのゴールである、染色体微細欠失重複症候群の遺伝学的診断として必須のマイクロアレイ染色体検査の一般診療への普及がある。マイクロアレイ染色体検査のような網羅的解析法の保険診療化は種々の問題点があるが、機器承認などようやくその可能性が見えてきたため、診療において実施するマイクロアレイ染色体検査ガイダンス」として一般診療でのガイドラインを策定した。これらが今後のマイクロアレイ染色体検査の保険適応への後押しになれば良いと考えている。

E. 結論

本研究では、多発奇形・発達遅滞を主症状とする染色体微細欠失重複症候群の成人期移行を見据えた診療ガイドラインの確立を目的として、国内の多施設共同研究により、代表的な 5 疾患に関して、とくにエマヌエル症候群について全国調査による国内成人患者の実態調査を行った。その結果、（1）レジストリー・システムにより成人期患者の所在を把握した。（2）家族会の開催により、成人期移行の患者への質問表を作成できた。今後、地域ごとの小規模患者会とそれらを繋ぐオンラインシステムが充実すれば、医療サイドの対応に先行して、患者の家族が自ら対応して行ける体制が整うことが期待され、平行して進めてゆく。

F. 健康危険情報

特になし。

G. 研究発表

1．論文発表

(1) Bonora E, Chakrabarty S, Kellaris G, Tsutsumi M, Bianco F, Bergamini C, Ullah F, Isidori F, Liparulo I, Diquigiovanni C, Masin L, Rizzardi N, Cratere MG, Boschetti E, Papa V, Maresca A, Cenacchi G, Casadio R, Martelli P, Matera I, Ceccherini I, Fato R, Raiola G, Arrigo S, Signa S, Sementa AR, Severino M, Striano P, Fiorillo C, Goto T, Uchino S, Oyazato Y, Nakamura H, Mishra SK, Yeh YS, Kato T, Nozu K, Tanboon J, Morioka I, Nishino I, Toda T, Goto YI, Ohtake A, Kosaki K, Yamaguchi Y, Nonaka I, Iijima K, Mimaki M, Kurahashi H, Raams A, MacInnes A, Alders M, Engelen M, Linthorst G, de Koning T, den Dunnen W, Dijkstra G, van Spaendonck K, van Gent DC, Aronica EM, Picco P, Carelli V, Seri M, Katsanis N, Duijkers FAM, Taniguchi-Ikeda M, De Giorgio R. Biallelic variants in *LIG3* cause a novel mitochondrial neurogastrointestinal encephalomyopathy. **Brain**. 2021 Apr 15. [Epub ahead of print]

(2) Hitachi K, Nakatani M, Kiyofuji Y, Inagaki H, Kurahashi H, Tsuchida K. An analysis of differentially expressed coding and long non-coding RNAs in multiple models of skeletal muscle atrophy. **Int J Mol Sci.** 22(5):2558, 2021.

(3) Kumai T, Sadato A, Kurahashi H, Kato T, Adachi K, Hirose Y. Coexistence of *RASA1* and *COL4A2* variants caused pial arteriovenous fistula (AVF) in a patient with capillary malformation-arteriovenous malformation. **Clin Neurol Neurosurg**. 204:106612, 2021.

(4) Yokoi K, Nakajima Y, Yasui T, Yoshino M, Yoshikawa T, Kurahashi H, Ito T. Novel *ARG1* variants identified in a patient with arginase 1

deficiency. **Hum Genome Var**. 8(1):8, 2021.
(5) Kanai S, Okanishi T, Kawai M, Yoshino G, Tsubouchi Y, Nishimura Y, Sakuma H, Kurahashi H, Maegaki Y. Late-onset cerebral arteriopathy in a patient with incontinentia pigmenti. **Brain Dev**. S0387-7604(20):30350-8, 2021.
(6) Tsutsumi M, Miura H, Inagaki H, Shinkai Y, Kato A, Kato T, Hamada-Tsutsumi S, Tanaka M, Kudo K, Yoshikawa T, Kurahashi H. An aggressive systemic mastocytosis preceded by ovarian dysgerminoma. **BMC Cancer**. 20(1):1162, 2020.
(7) Ohwaki A, Nishizawa H, Kato A, Kato T, Miyazaki J, Yoshizawa H, Noda Y, Sakabe Y, Ichikawa R, Sekiya T, Fujii T, Kurahashi H. Placental genetic variants in the upstream region of the *FLT1* gene in pre-eclampsia. **J Reprod Infertil**. 21(4):240-246, 2020.
(8) Kawai M, Kato T, Tsutsumi M, Shinkai Y, Inagaki H, Kurahashi H. Molecular analysis of low-level mosaicism of the IKBKG mutation using the X chromosome inactivation pattern in incontinentia pigmenti. **Mol Genet Genomic Med**. e1531, 2020.
(9) Miura H, Kawamura Y, Ohye T, Hattori F, Kozawa K, Ihira M, Yatsuya H, Nishizawa H, Kurahashi H, Yoshikawa T. Inherited chromosomally integrated human herpesvirus 6 is a risk factor for spontaneous abortion. **J Infect Dis**. 2020, jiaa606. [Epub ahead of print]
(10) Tsukamoto K, Shinzawa N, Kawai A, Suzuki M, Kidoya H, Takakura N, Yamaguchi H, Kameyama T, Inagaki H, Kurahashi H, Horiguchi Y, Doi Y. The Bartonella autotransporter BafA activates the host VEGF pathway to drive angiogenesis. **Nat Commun**. 2020, 11(1):3571.
(11) Yokoi K, Nakajima Y, Matsuoka H, Shinkai Y, Ishihara T, Maeda Y, Kato T, Katsuno H, Masumori K, Kawada K, Yoshikawa T, Ito T, Kurahashi H. Impact of DPYD, DPYS, and UPB1 gene variations on severe drug-related toxicity in patients with cancer. **Cancer Sci**. 111(9):3359-3366, 2020.
(12) Yasuda T, Sanada M, Nishijima D, Kanamori T, Iijima Y, Hattori H, Saito A, Miyoshi H, Ishikawa Y, Asou N, Usuki K, Hirabayashi S, Kato M, Ri M, Handa H, Ishida T, Shibayama H, Abe M, Iriyama C, Karube K, Nishikori M, Ohshima K, Kataoka K, Yoshida K, Shiraishi Y, Goto H, Adachi S, Kobayashi R, Kiyoi H, Miyazaki Y, Ogawa S, Kurahashi H, Yokoyama H, Manabe A, Iida S, Tomita A, Horibe K. Clinical utility of target capture-based panel sequencing in hematological malignancies: A multicenter feasibility study. **Cancer Sci**. 111(9):3367-3378, 2020.
(13) Kato T, Inagaki H, Miyai S, Suzuki F, Naru Y, Shinkai Y, Kato A, Kanyama K, Mizuno S, Muramatsu Y, Yamamoto T, Shinya M, Tazaki Y, Hiwatashi S, Ikeda T, Ozaki M, Kurahashi H. The involvement of U-type dicentric chromosomes in the formation of terminal deletions with or without adjacent inverted duplications. **Hum Genet**. 139(11):1417-1427, 2020.
(14) Ikeda M, Taniguchi-Ikeda M, Kato T, Shinkai Y, Hagiwara H, Sasaki N, Masaki T, Matsumura K, Sonoo M, Kurahashi H, Saito F. Unexpected mutations by CRISPR/Cas9 CTG repeat excision in myotonic dystrophy and use of CRISPR interference as an alternative approach. **Mol Ther Methods Clin Dev**. 18:131-144, 2020.
(15) Kawamura R, Kato T, Miyai S, Suzuki F, Naru Y, Kato Tanaka M K, Nagasaka M, Tsutsumi M, Inagaki H, Ioroi T, Yoshida M, Nao T, Conlin LK, Iijima K, Kurahashi H, Taniguchi-Ikeda M. A case of a parthenogenetic 46,XX/46,XY chimera presenting ambiguous genitalia. **J Hum Genet**. 65(8):705-709, 2020.
(16) Kato T, Kawai M, Miyai S, Suzuki F, Tsutsumi M, Mizuno S, Ikeda T, Kurahashi H.

Analysis of the origin of double mosaic aneuploidy in two cases. **Cytogenet Genome Res**. 160(3):118-123, 2020.

(17) Kato M, Yagami A, Tsukamoto T, Shinkai Y, Kato T, Kurahashi H. Novel mutation in the KITLG gene in familial progressive hyperpigmentation with or without hypopigmentation. **J Dermatol**. 47(6):669-672, 2020.

(18) Miura H, Ohye T, Kozawa K, Hattori F, Kawamura Y, Ihira M, Kurahashi H, Yoshikawa T. Coinfection with human herpesvirus (HHV)-6B in immunocompetent, healthy individuals with chromosomally integrated HHV-6A. **J Pediatric Infect Dis Soc**. 10(2):175-178, 2021.

(19) 倉橋浩樹、着床前診断　技術の進歩と見えてきた課題、遺伝子医学 35 号 11(1): 18-19, 2021.

(20) 倉橋浩樹、PGT-HLA、遺伝子医学 35 号 11(1): 55-61, 2021.

(21) 加藤武馬、杉本岳、倉橋浩樹、PGT の現状と課題、BIO Clinica 36(2), 108-112, 2021.

(22) 七里由衣、加藤武馬、倉橋浩樹、着床前遺伝学的検査の技術的進歩と限界、産科と婦人科 88(1), 45-51, 2021.

(23) 倉橋浩樹、HHV-6 のヒトゲノムへの挿入―ciHHV-6―, IASR, 41(12), 220-221,　2020.

(24) 倉橋浩樹、遺伝子診断の臨床応用　現在と未来　各論（４）出生前診断、日本医師会雑誌;149(11):1970-1974, 2020.

(25) 吉澤ひかり、西澤春紀、倉橋浩樹、PGT-M で診断できる疾患、できない疾患、Hormone Frontier in Gynecology 27(4), 53-57, 2020.

(26) 加藤良美、加藤武馬、宮井俊輔、倉橋浩樹、遺伝子増幅に関する選択肢と課題、産婦人科の実際 69(8), 817-821, 2020.

(27) 森山育実、倉橋浩樹、着床前診断の遺伝カウンセリング、52(8), 1116-1121, 2020.

２．学会発表

(1) Yokoi K, Nakajima Y, Matsuoka H, Shinkai Y, Ishihara T, Maeda Y, Kato T, Katsuno H, Masumori K, Kawada K, Yoshikawa T, Ito T, Kurahashi H. Impact of DPYD, DPYS and UPB1 gene variations on severe drug-related toxicity in cancer patients. 70th annual meeting of American Society of Human Genetics. Virtual, October 27-30, 2020.

(2) Kato T, Miyai S, Suzuki F, Naru Y, Inagaki H, Shinya M, Ikeda T, Kurahashi H. Fetoplacental chromosomal structural abnormalities are originated from repeated breakage-fusion-bridge cycles. 70th annual meeting of American Society of Human Genetics. Virtual, October 27-30, 2020.

(3) Nagasaka M, Taniguchi-Ikeda M, Harada R, Yamamoto T, Kurahashi H, Kuroda R, Iijima K, Toda T. Assessment of upper limb muscles in patients with Fukuyama muscular dystrophy: noninvasive assessment using ultrasound and shear wave elastography. 70th annual meeting of American Society of Human Genetics. Virtual, October 27-30, 2020.

(4) Watanabe S, Yoshikai K, Tomida M, Suzuki S, Matsuda Y, Miyai S, Kato T, Kurahashi H, Nakano E, Sawada S. Irregular cleavage in early embryogenesis does not reduce the euploidy after reaching the blastocyst. ESHRE Virtual 36th Annual Meeting, July 5-8, 2020.

(5) 倉橋浩樹．着床前胚染色体異数性検査、第 72 回 日本産科婦人科学会学術講演会、web、Apr 24, 2020.

(6) 倉橋浩樹．PGT-A の現状と課題、第 139 回 関東連合産科婦人科学会学術集会、web、Jun 4, 2020.

(7) 倉橋浩樹．着床前診断の遺伝カウンセリング、第 16 回 広島臨床遺伝研究会、web, Aug 8, 2020.

(8) 倉橋浩樹．網羅的遺伝子診断における遺伝カウンセリング、第 60 回日本リンパ網内系

学会総会、web, Aug 20, 2020.
(9) 倉橋浩樹．出生前診断の問題を回避できるか : 着床前診断、第 123 回 日本小児科学会学術集会、web, Aug 22, 2020.
(10) 倉橋浩樹. PGT-A 解析技術の進歩と問題点、第 139 回 生殖バイオロジー東京シンポジウム 2020, web, Sep 4, 2020.
(11) 倉橋浩樹．PGT-M 解析技術の進歩と課題、第 38 回 日本受精着床学会総会・学術講演会、web, Oct 1, 2020.
(12) 倉橋浩樹．遺伝子検査と健康管理、株式会社 OVUS オンライン・セミナー、web、web, Oct 30, 2020
(13) 倉橋浩樹. PGT-A/SR における モザイク胚の扱い、第 2 回 日本不育症学会学術集会、web, Nov 14-15, 2020.
(14) 倉橋浩樹. 染色体と私 ―２つのＧトリソミー―、日本人類遺伝学会第 65 回大会、web, Nov 18-21, 2020.
(15) 倉橋浩樹、PGT-A と遺伝カウンセリング、第 6 回 日本産科婦人科遺伝診療学会学術講演会、web, Dec 9-15, 2020.
(16) 倉橋浩樹、2 段階エキスパートパネルによる希少未診断疾患に対する診断プログラムの開発に関する研究．IRUD 令和 2 年度班会議、web、Dec 18, 2020.
(17) 倉橋浩樹. モザイク胚移植における 遺伝カウンセリング、南九州 PGT 研究会、web, Dec 19, 2020.
(18) 倉橋浩樹．モザイク胚移植における 遺伝カウンセリング、第 5 回 せとうち ART 研究会、web, Mar 13, 2021.
(19) 加藤武馬, 倉橋浩樹. 染色体異常のゲノム解析, High-throughput genome analysis of chromosomal rearrangements.日本人類遺伝学会第 65 回大会, web、Nov18-21, 2020.
(20) 稲垣秀人、加藤武馬、豊田敦、蒔田芳男、倉橋浩樹、ロングリードシーケンシング技術を用いた 22q11 のギャップ領域の解析.日本人類遺伝学会第 65 回大会, web、Nov18-21, 2020.
(21) 堤真紀子、加藤良美、稲垣秀人、倉橋浩樹．A cell culture model to analyze the mechanism of age-related increase of oocyte aneuploidy. 日本人類遺伝学会第 65 回大会, web、Nov18-21, 2020.
(22) 河村理恵、大江瑞恵、長坂美和子、森山育実、池田真理子、佐藤労、倉橋浩樹．With コロナにおける新しい教育様式を考える−藤田医科大学大学院遺伝カウンセリング分野実践報告−．日本人類遺伝学会第 65 回大会, web、Nov18-21, 2020.
(23) 七里由衣、稲垣秀人、河村理恵、宮井俊輔、倉橋浩樹、DMD の欠失変異はなぜ生じるか？日本人類遺伝学会第 65 回大会, web、Nov18-21, 2020.
(24) 西山幸江、朝日啓司、清水勇輔、北村智志、青木淳子、西山幸男、倉橋浩樹、PGT-A の処分胚の検討、日本人類遺伝学会第 65 回大会, web、Nov18-21, 2020.
(25) 黒木裕子、桑鶴ゆかり、德留茉里、福元由美子、渡邉みあ、燃脇晴恵、溝部大和、橋元恵里奈、岩川富貴子、田平達則、田平満里奈、竹内美穂、竹内一浩、加藤武馬、倉橋浩樹、当院における着床前遺伝子検査（PGT）の臨床成績、日本人類遺伝学会第 65 回大会, web、Nov18-21, 2020.
(26) 石原尚子、帽田仁子、稲垣秀人、倉橋浩樹、てんかん性脳症および先天性ネフローゼ症候群を呈した SLC35A1-CDG の 1 例、日本人類遺伝学会第 65 回大会, web、Nov18-21, 2020.
(27) 鈴木綾子、倉橋浩樹、佐藤労、大江瑞恵、青年期から成人期におけるダウン症候群のある人の親の性意識に影響を与える要因、日本人類遺伝学会第 65 回大会, web、Nov18-21, 2020.
(28) 原鐵晃、頼英美、佐藤景子、三浦貴弘、渡邉陽子、西村加奈子、吉田亜矢子、植田彩、姫野真由子、加藤武馬、宮井俊輔、倉橋浩樹、当科で経験した挙児希望のある常染色体相互

転座および X-常染色体相互転座夫婦に着床前診断(PGT-SR/A)を行い、その情報のみでは移植胚を決定することが難しい場合の検討、日本人類遺伝学会第65回大会, web、Nov18-21, 2020.
(29) 永岡晋一、利光正岳、小堀周作、小川真紀、倉橋浩樹、室月淳、P3H1（LEPRE1）遺伝子に変異を認めた骨形成不全症の同胞再発と考えられる家族例に対し出生前遺伝学的検査を行い生児を得た一例、日本人類遺伝学会第 65 回大会, web、Nov18-21, 2020.
(30) 尾崎守, 池田敏郎, 遠藤俊明, 佐々木愛子, 倉橋浩樹, 浦大樹, 硎澄仁, 岩田由美子, 高瀬悦子, 新井田要、相互転座保因者に関するアプリケーション公開とこれまでに寄せられた改良点について、日本人類遺伝学会第 65 回大会, web、Nov18-21, 2020.
(31) 池田敏郎、宮井俊輔、加藤武馬、倉橋浩樹、Weaver 症候群の合併が生後に判明したトリプル X 症候群の出生前診断例、日本人類遺伝学会第 65 回大会, web、Nov18-21, 2020.
(32) 古俣知里、倉橋浩樹、河村理恵、大江瑞恵、佐藤労、地域基幹病院の遺伝診療部門における認定遺伝カウンセラーの役割についての検討、日本人類遺伝学会第65回大会, web、Nov18-21, 2020.
(33) 七里由衣、大江瑞恵、佐藤労、倉橋浩樹、筋ジストロフィーの子どもをもつ夫婦が親役割を果たすための円環的認識論の活用 第 44 回遺伝カウンセリング学会、web、Jul 3-5, 2020.
(34) 加藤良美、倉橋浩樹、佐藤労、大江瑞恵、ダウン症候群の成人期までの支援の現状と支援モデル、第 44 回遺伝カウンセリング学会、web、Jul 3-5, 2020.
(35) 長柄美保子、佐藤労、倉橋浩樹、大江瑞恵、思春期にあるマルファン症候群患者の疾患への認識と自己開示、第 44 回遺伝カウンセリング学会、web、Jul 3-5, 2020.
(36) 木下孝一、中山要、岩下寿子、加藤武馬、宮井俊輔、河合美紀、鳥嶋雅子、山田崇弘、倉橋浩樹、DMD 保因者診断における SNV による誤判定の一例、第 44 回遺伝カウンセリング学会、web、Jul 3-5, 2020.
(37) 佐藤優香、倉橋浩樹、大江瑞恵、佐藤労、「重篤な疾患を持つ新生児の家族と医療スタッフの話し合いのガイドライン」の使用と１８トリソミー児における治療の現状、第 44 回遺伝カウンセリング学会、web、Jul 3-5, 2020.
(38) 尾崎守, 池田敏郎, 遠藤俊明, 倉橋浩樹, 浦大樹, 硎澄仁, 岩田由美子, 高瀬悦子, 新井田要、相互転座保因者パキテン図等の作成アプリケーションの公開について、第 44 回遺伝カウンセリング学会、web、Jul 3-5, 2020.
(39) 古俣知里、倉橋浩樹、河村理恵、大江瑞恵、佐藤労、ゲノム関連医療の発展に伴う遺伝診療部門の必要性と新規開設の課題に関する検討、第 44 回遺伝カウンセリング学会、web、Jul 3-5, 2020.
(40) 堤真紀子、倉橋浩樹. Mechanism of age-related aneuploidy of oocytes: Toward the development of methods for its prevention. 第 43 回日本分子生物学会年会、web、Dec 2-4, 2020.
(41) 堤真紀子、稲垣秀人、加藤 武馬、河村理恵、倉橋 浩樹、培養細胞モデル系を用いた卵母細胞コヒーシンの加齢による減少機構の解析、第 52 回藤田学園医学会、豊明、Oct 1-2, 2020.
(42) 斉藤史明、池田美樹、池田真理子、加藤武馬、新海保子、田中園子、萩原宏毅、佐々木直道、真先敏弘、松村喜一郎、倉橋浩樹、園生雅弘、CRISPR/Cas9 による筋強直性ジストロフィーの CTG リピート除去に伴う遺伝子変異と CRISPR interference 法の有用性に関する検討、第 6 回筋学会学術集会、web、Dec 18-20, 2020.
(43) 七里由衣、加藤良美、稲垣秀人、石原尚子、宮田昌史、帽田仁子、小島有紗、三宅未紗、倉橋浩樹、GATA 4 病的バリアントによ

って生じたと考えられる 先天性心疾患を伴う 46,XY 性分化疾患の一例、第 43 回日本小児遺伝学会学術集会、web、Jan 8-9, 2021.
(44) 横井克幸、中島葉子、近藤朋実、松川昇平、加藤武馬、池住洋平、倉橋浩樹、伊藤哲哉、C5DC 陽性の経過観察中、高インスリン性低血糖を認め診断に至った HAD 欠損症の姉妹例、第 43 回日本小児遺伝学会学術集会、web、Jan 8-9, 2021.
(45) 佐藤優香、倉橋浩樹、大江瑞恵、佐藤労、過去２年間における 18 トリソミーの経験と転機、第 43 回日本小児遺伝学会学術集会、web、Jan 8-9, 2021.
(46) 渡辺真一、吉貝香里、冨田麻莉、鈴木篤智、野呂麻理子、松田有希野、宮井俊輔、加藤武馬、中野英子、倉橋浩樹、澤田富夫、タイムラプスモニタリングで胚発生能と正倍数性はどこまで評価できるか. 第 38 回日本受精着床学会総会学術講演会、web、Oct 1-2, 2020.

H. 知的財産権の出願・登録状況
特になし

（資料１）

友だちマップ

ハートをクリックしてください。メッセージが開きます。

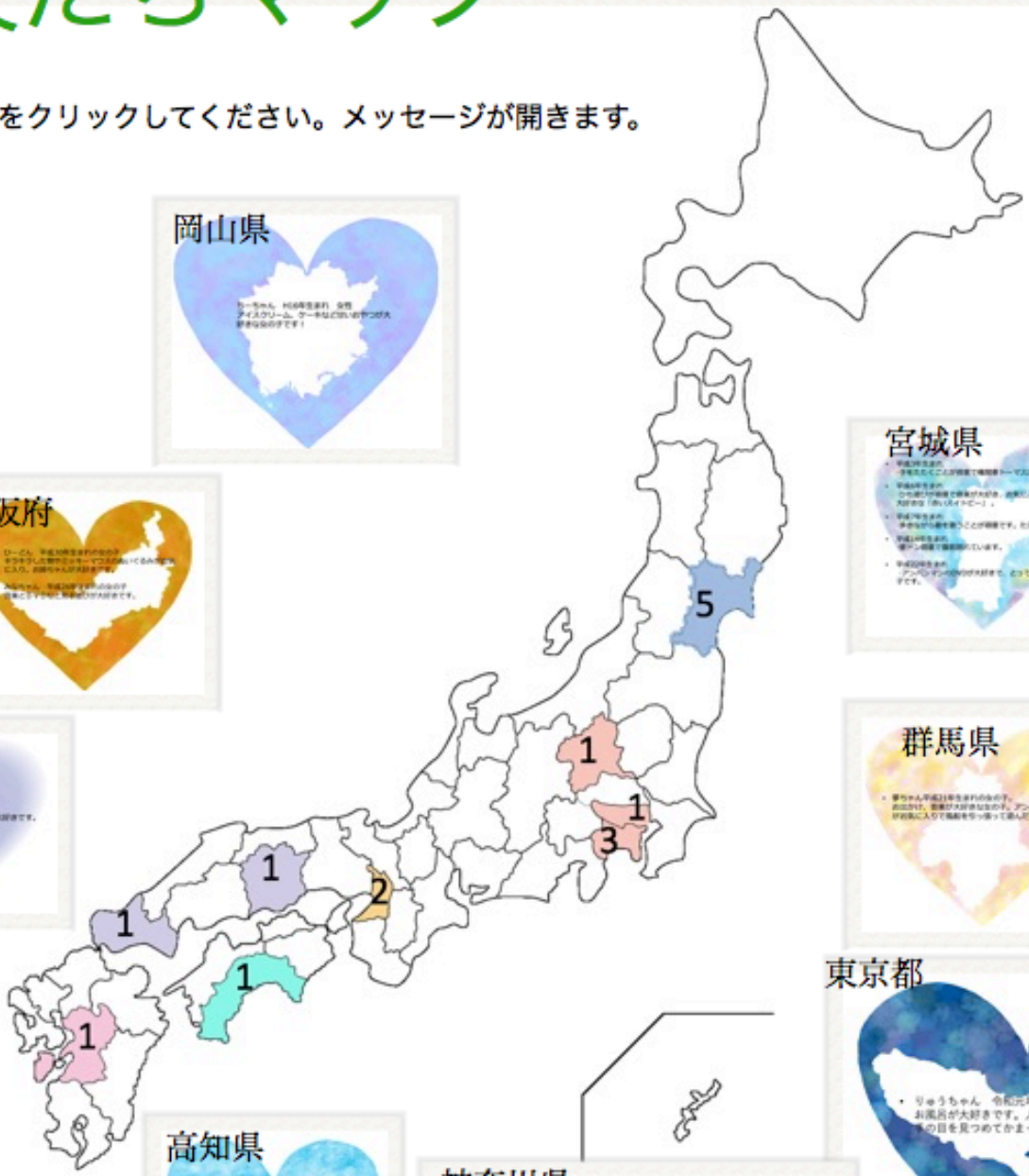

岡山県

宮城県

大阪府

山口県

群馬県

東京都

高知県

神奈川県

- トアくん　平成28年生まれの男の子
タンバリン、絵本、ぬいぐるみが好きです。
- アオイちゃん。平成19年生まれの女の子です。
友達や人と関わる事が大好きで、手を叩いたり、声出し、表情でコミュニケーションをとります。ローリングやほふく前進、座位姿勢を組み合わせて動く事も大好きです！
- むっちゃん。2011年生まれの男の子
人とのスキンシップが大好きで、抱っこしてもらうとニヤニヤが止まりません。日々腹筋の筋トレをし、細マッチョ目指してます。

熊本県

（資料２）

エマヌエル症候群の日

『オンライン家族会』

11月22日（日）15時から17時まで

参加者、募集中

今年も11月22日をt(11;22)に因んでエマヌエル症候群の日として、患者、ご家族の皆様がお住いの全国各地をノートパソコンで結んだオンライン家族会を開催いたします。
インターネットを通じて、楽しいひと時を過ごしましょう。

<プログラム>
- ご挨拶（プロジェクト代表・倉橋より）
- 参加ご家族の自己紹介
- 事前質問のお返事
- ご家族同士の交流

申込方法：事前の申し込みが必要です。
メールでご連絡ください。genome@fujita-hu.ac.jp
詳細は 『t(11;22)とエマヌエル症候群』のウェブページをご覧ください。
http://www.fujita-hu.ac.jp/~genome/11&22

http://www.fujita-hu.ac.jp/~genome/11

藤田医科大学
担当者：倉橋浩樹、大江瑞恵
事務担当：河村理恵
厚生労働科学研究費難治性疾患等政策研究事業「染色体微細欠失重複症候群の包括的診療体制の構築研究班」

本日の予定

15時スタート

- 倉橋先生からの挨拶とお話
- 歩行リハビリについて
  松田文浩先生（理学療法士）
- 嚥下について
  栗飯原けい子先生（言語聴覚士)
- 事前質問

16時頃　休憩

- 人類遺伝学会への家族会の紹介
- 参加ご家族の自己紹介
- ご家族間の交流-1

17時頃　休憩

- ご家族間の交流-2
- その他
  来年度のオンライン家族会
  記念撮影

18時頃　解散

エマヌエル症候群オンライン家族会アンケート

n=12

通信状況

Zoomの通信状態（音声、画像）はいかがでしたか。

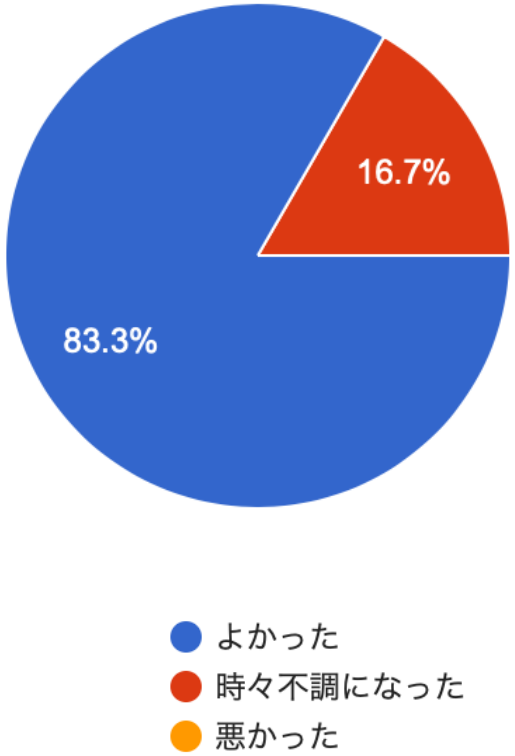

オンライン家族会で必要になったインターネットのデータ通信容量は、負担になりましたか。

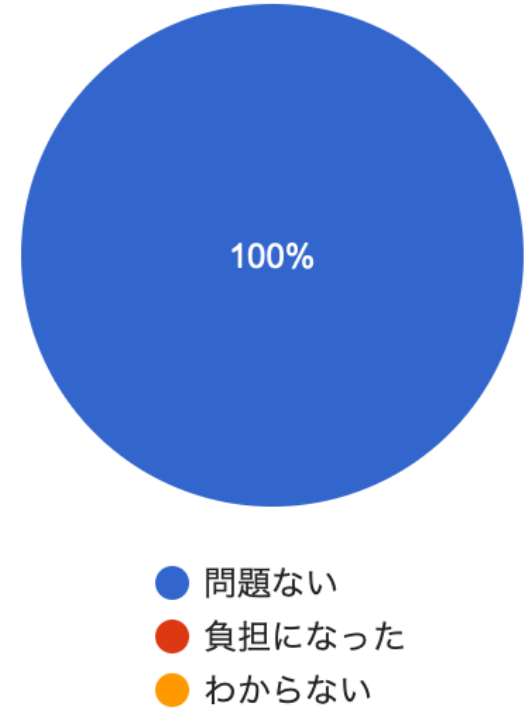

日程について

オンライン家族会の開催日時（11月22日）は、いかがでしたか。

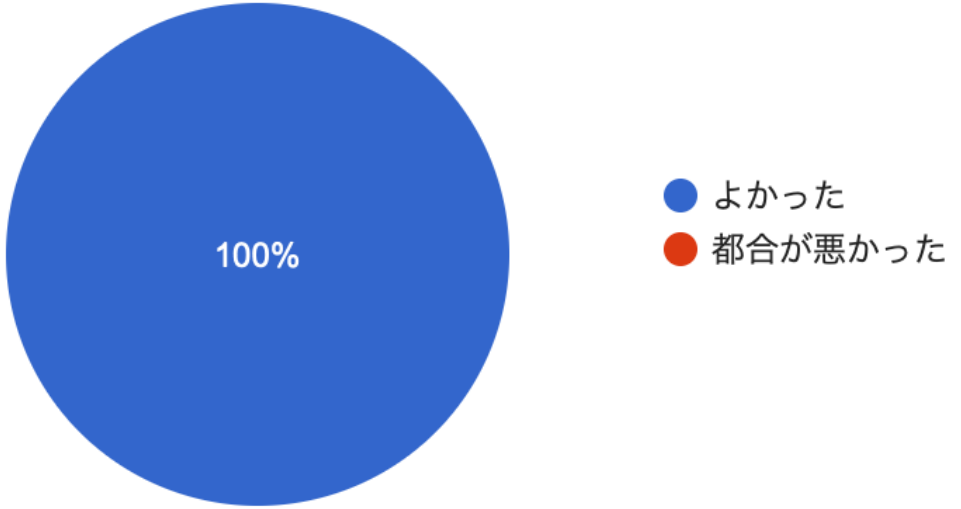

オンライン家族会の開催日のご希望はありますか（複数選択可）

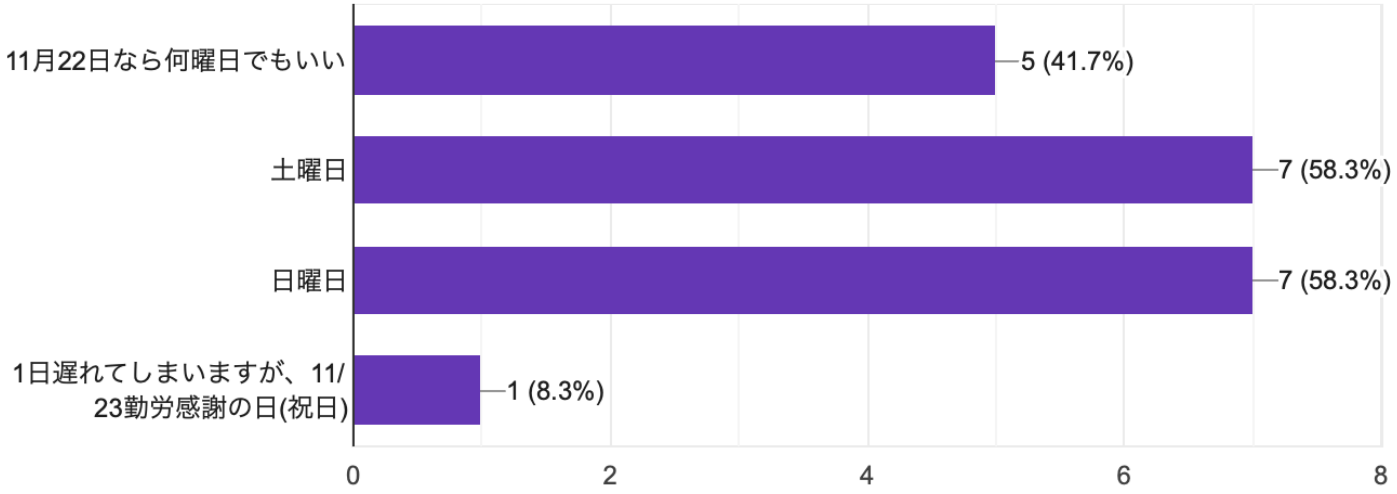

開催時間について

オンライン家族会の開催時間の長さはいかがでしたか。

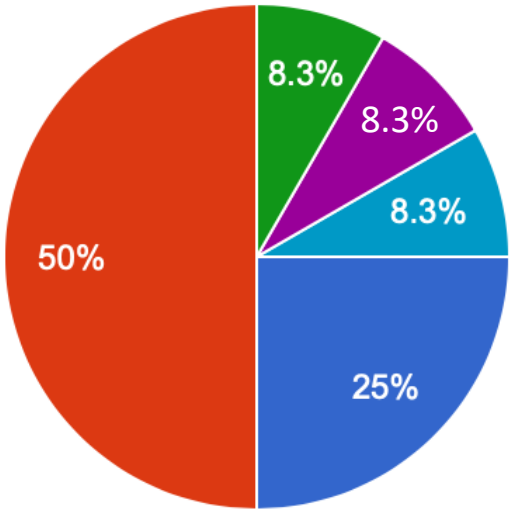

- ちょうど良い
- 長すぎる
- 短すぎる
- 少し長く感じました
- ほんの少し長いかな？と感じました。子供達が小さいので、2時間くらいだと良いのかもしれません。ただ、内容はとても素晴らしく、削れそうな所もないので、3時間は仕方ないのかなとも感じています。
- 勉強会があったので少し長く感じました。

システムの改善点

オンライン家族会のシステム（連絡、通信手段など）で困ったこと、改善した方がいいことがありましたら、教えてください。

ZOOMに不慣れで、テストの時に使い方を教えてもらったけれど、やはり当日少し混乱しました。『ここをクリックで参加者みんなが表示される』とか『話す時だけミュートを解除する』などの簡単な説明を、直前メールに付け足してもらえるとありがたいです。

正確な開始と終了時間は明示頂きたい。

プログラムについて

よかったプログラムはどれですか（複数回答可）

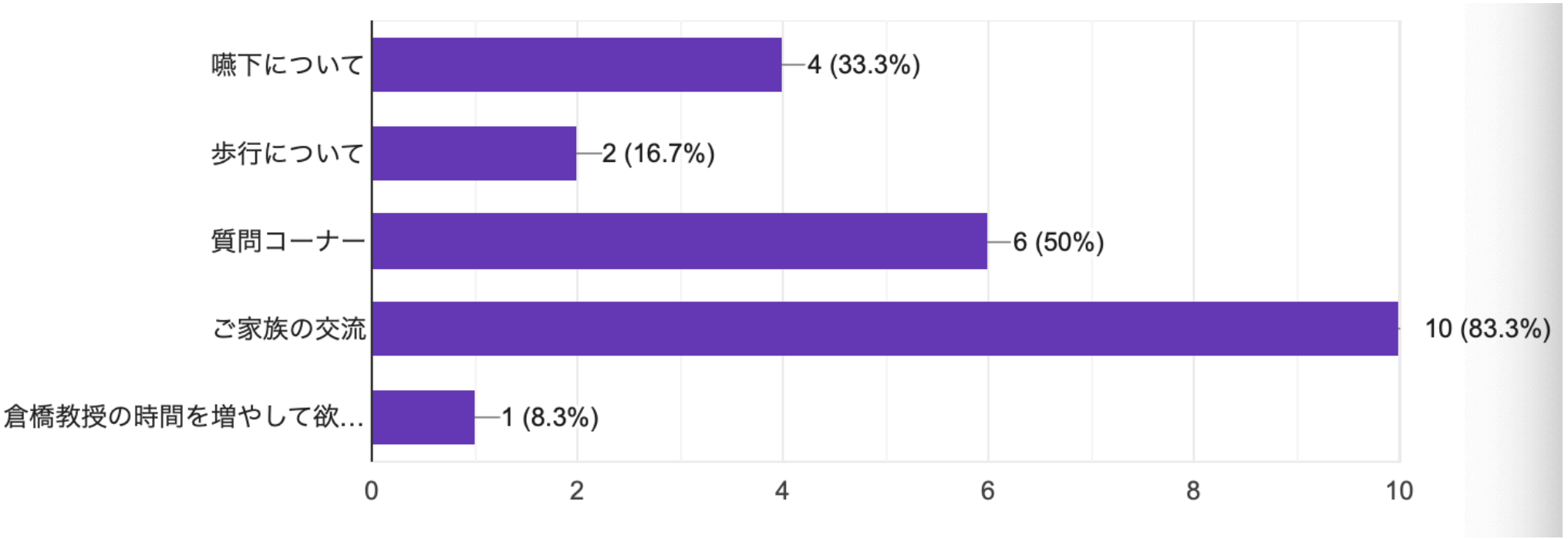

プログラムについて

嚥下と歩行についての講演時間はいかがでしたか。

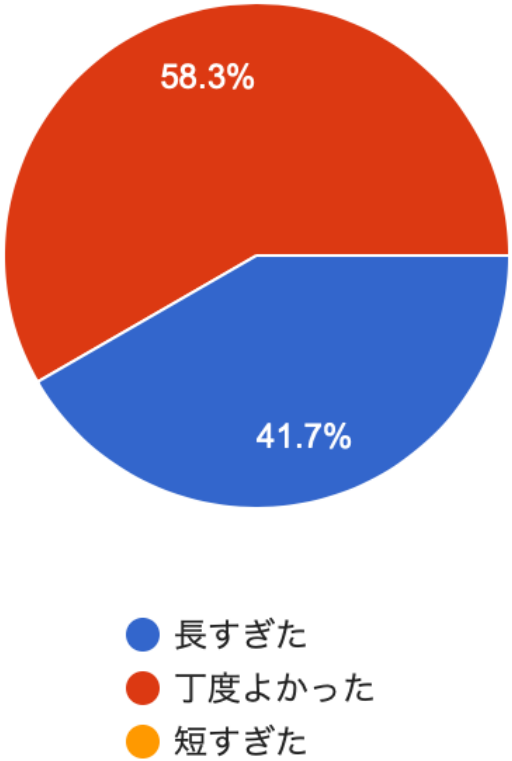

ご家族の交流の時間はいかがでしたか。

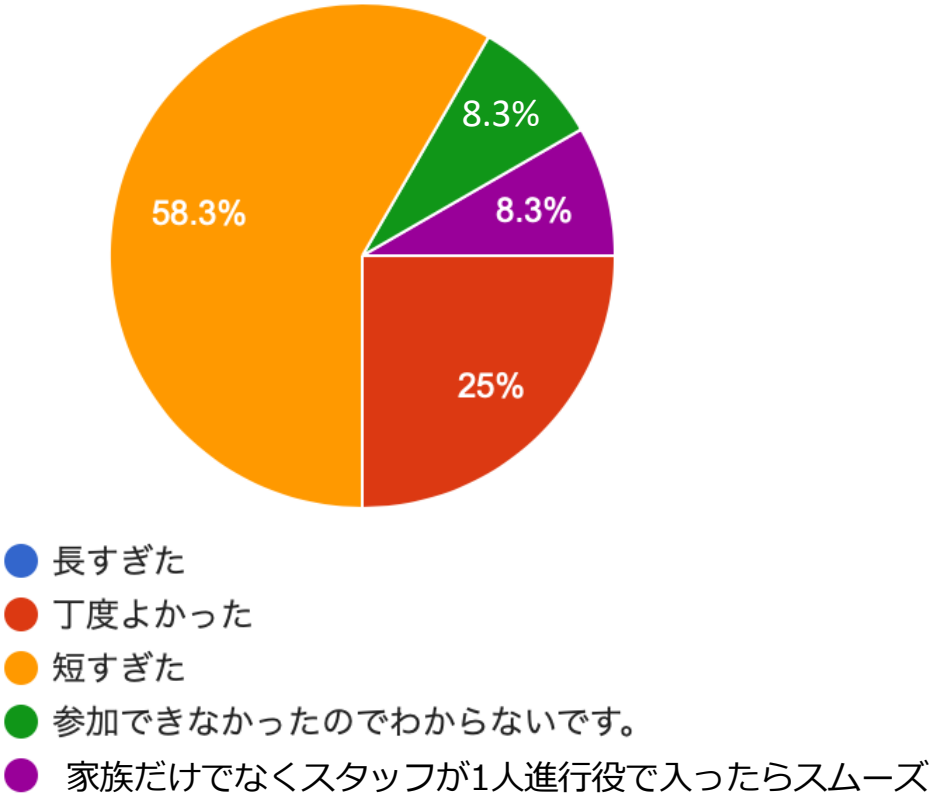

今回のオンライン家族会に参加している中で、お気づきになったことがあったら教えてください。

最初に家族紹介をして、現在の状態などをもっと詳しく（決まった項目に沿って）話してもらってから始まったら良かったなぁと思いました。

話は尽きないので、時間は必要だが、エマヌエルの子だけでなく兄弟児もいると今回は長かったと思う。

開始時間を15時からではなく、13時とか13時半から3時間ですと、夕食の時間に重ならず、参加しやすいと感じました。

自己紹介がもっと詳しければよかったかなと思いました。質問もしやすくなるかなって思いました。病歴や今困っていることなど。

交流の場で進行役がいてくれるとスムーズだと思います。
自己紹介の際にスピーカービューにしていたところ、ミュートにしていない方がいて、自己紹介家族が映らないことが何度かありました。必要な時にホスト側でミュートにしてあげるとよいかと思いました。

前半の講演と後半の交流を別にして、二部構成にするのはどうでしょうか。講演内容によっては興味のない方もおられるかもしれません。講演内容を事前にお伝え頂き、参加するかどうかを決めておいて好きなタイミングから参加する、でもいいと思います。

家族の交流の中で2つに分けたときに進行役がいるともっとスムーズに話せたのではないかと思います。

進行係りは必ず欲しい。

グループ分けをして様々な方とお話させていただき話しやすかったです。

家族交流の際に進行役の方がいるとスムーズに進んで良いと思います。

オンライン家族会で行うと良いプログラムは何ですか。リクエストをお願いします。

可能なら誰かをピックアップして、こういうことができるよというような動画を流してほしいと思いました。例えば、歩きながら歌を歌われている方の動画など。話でこういうことができると聞くよりは動画で見せて頂けると更に励みになるので。ただ個人情報なので、難しい面もあるかと思いますが、、、

PT、STの話は興味深かったが、家族会なので自己紹介や家族交流にもっと時間を使って、もっと話を深くしたかった

リハビリの先生が参加してくれたので、色々相談したかったです。みんながどんなリハビリをしているなかも知りたかったです。

家族間での質問や交流にもっと時間があっても良かったと思います。

リハビリ内容の詳細が知りたい。合併症も知りたい。

11月22日とは別に平日の昼間にこどもがいない状態でもゆっくり話をしてみたいです。

既にあるプログラムですが、家族交流の時間を長くとっていただけると良いかと思います。

今回のオンライン家族会のご感想をお聞かせください。私たちのホームページに掲載させて頂きたいと思います。宜しくお願いいたします。

その1

普段なかなか会えないので全国にいる仲間に会えたようで嬉しかったです

オンライン家族会ではお世話になりました。ありがとうございました。
オンライン会議をするのは初めてで不安があったのですが、テストの日を設けて頂いて、当日はスムーズにつなげることができました。ありがとうございました。
久しぶりにお会いするご家やラインでつながっていても会ったことがなかったご家族、今回初めてお会いするご家族、皆さんに会えたことがとても嬉しかったです！
病気についてもまだまだ分からないことが多く、先生方や皆さんの話しをこれからも聞かせて頂きたいので、ぜひこれからも継続して家族会を開いてください。よろしくお願いします。

今年も素敵な機会を作ってくださり、ありがとうございました。
こどもたちが疲れないうち(時間帯)に自己紹介をもうちょっとゆっくりやって、ほかのエマヌエルの方がどんな子なのか見たかった。
その方が家族交流の時間がもっと盛り上がったと思う。
ピエールさんからメッセージ良かった

前回よりも参加家族も多く、プログラムも盛りだくさんで、とても勉強になりました。
嚥下については、カメラでの映像がとても勉強になり、これからの子供への食事や水分摂取の仕方などな工夫に繋げられる内容でとても素晴らしかったです、
また、カナダの家族会のメッセージには感動しました。
離れた地域に居るご家族と交流する事ができ、オンライン家族会はとても素晴らしいものだと感じています。
来年度も楽しみにしています。
有難うございました。

たくさんのご家族に会えてうれしかったです。講演もとても勉強になりましたし、他のご家族からの色んなお話も聞けて良かったです。貴重な時間をありがとうございました。来年もぜひ参加したいです。

今回名前、年齢があったので質問もしやすく分かりやすかったです。
一年ぶりですが、去年より成長が見れてよかったです。
もっとお話ししたかったですが、いつか会える日があればいいのになって思いました。貴重な時間になりました。
ありがとうございました！

0歳から29歳まで、全国の仲間たちがつながるとても良い機会だと思いました。不安や悩みを相談しあえる出会いになったのではないでしょうか。

多くの家族の意見や情報を得られ、有意義な時間でした。また次回参加したいと思います。

初めてオンライン家族会に参加しましたが、楽しかったです。
家族の交流の時間がもっと長かったら良かったと思います

初めて参加しました。意見交換時の情報共有がとても参考になりました。

今回は前回に比べて年齢の高い方のお話を聞くことができて、とても有意義な時間てした。ありがとうございました!

全国のご家族の方と交流を持つことができ、また様々なお話しを聞くことができてとても有意義な時間を、過ごさせていただきました。ほかのお子さまより年齢が上ということもあり、何かこれまでの経験でお力になれることがあればという思いもあって参加させていただきました。微力ながら今後ともお子さまのご成長にお役に立つ機会があれば幸いです。

（資料３）

エマヌエル症候群の患者様に関するアンケート調査

1. 患者さんの年齢、性別、身長、体重
　　＿＿＿＿＿＿才　　男性　・　女性
　身長＿＿＿＿＿cm　体重＿＿＿＿＿kg

2. 診断された経緯（何歳の時に、どのような状況や、症状で診断されましたか）

3. 疾患が疑われてから、どのくらいの期間で診断されましたか。
　　年　　ケ月

4. エマヌエル症候群と診断される前に、言われていた診断名があれば、教えてください。

5. 診断のために行った検査について教えてください。
　a.染色体検査　　b.行っていない　　c.わからない

6. 検査を行う前にどのような説明を受けましたか
　a.染色体のこと　　b.遺伝子のこと　c.エマヌエル症候群の症状のこと
　d.染色体転座のこと　　e.遺伝のこと　　f.次のお子さんのこと
　g.その他（　　）

7. 検査を行う前にどのような情報が欲しかったですか。

8. 検査を行った後にどのような説明を受けましたか
   a.染色体のこと　　b.遺伝子のこと　　c.エマヌエル症候群の症状のこと
   d.染色体転座のこと　e.遺伝のこと　　f.次のお子さんのこと
   g.その他（　　）

9. 診断された時に、どのような情報が欲しかったですか。

10. 生後すぐにみられた症状を記載してください。該当する項目に○をつけてください。
    また治療の有無と、治療した年齢について教えてください。

	診断名	治療
a. 心疾患	（　　）	（　有　無　、　歳）
b. 口唇口蓋裂	（　　）	（　有　無　、　歳）
c. 腎疾患	（　　）	（　有　無　、　歳）
d. 外表の特徴	（　　）	（　有　無　、　歳）
e. 鎖肛	（　　）	（　有　無　、　歳）
f. 繰り返す感染症	（　　）	（　有　無　、　歳）
g. 耳の疾患	（　　）	（　有　無　、　歳）
h. けいれん	（　　）	（　有　無　、　歳）
i. 呼吸の問題	（　　）	（　有　無　、　歳）
その他		
j.	（　　）	（　有　無　、　歳）
k.	（　　）	（　有　無　、　歳）
l.	（　　）	（　有　無　、　歳）
m.	（　　）	（　有　無　、　歳）
n.	（　　）	（　有　無　、　歳）

11. 出生時にはなく、その後にみられた症状について該当する項目に○をつけ、発症した年齢を教えてください。また治療の有無と、治療した年齢を教えてください。

	診断名		治療		
a. 中耳炎	（	、 歳）	（ 有	無 、	歳）
b. けいれん	（	、 歳）	（ 有	無 、	歳）
c. 難聴	（	、 歳）	（ 有	無 、	歳）
d. 視力の問題	（	、 歳）	（ 有	無 、	歳）
e. 嚥下の問題	（	、 歳）	（ 有	無 、	歳）
その他					
f.	（	、 歳）	（ 有	無 、	歳）
g.	（	、 歳）	（ 有	無 、	歳）
h.	（	、 歳）	（ 有	無 、	歳）
i.	（	、 歳）	（ 有	無 、	歳）
j.	（	、 歳）	（ 有	無 、	歳）

12. 治療に関して困ったことや不安だった事がありましたら、教えてください。

13. 病院や訓練施設で行ったリハビリテーションや訓練について教えてください。

a. 歩行
年齢： ～ 歳
内容：

b. 食事
年齢： ～ 歳
内容：

c. トイレ
年齢：　　～　　歳
内容：

d. 言語・コミュニケーション
年齢：　　～　　歳
内容：

e. 音楽
年齢：　　～　　歳
内容：

f. その他
年齢：　　～　　歳
内容：

＜発達について＞

1. 寝返りからお座り、立つ、歩行のそれぞれの有無に○をつけ、その年齢と困ったことや工夫をされたことがあったら具体的に教えてください。
   （例：歩行：10 歳くらいに援助者が支えながら、ゆっくりと部屋の移動程度。1 歳から 3 歳まで、こんな工夫をした。）

定頸： 有　　無　　歳

寝返り：　有　　無　　歳

お座り：　有　　無　　歳

立つ：　有　　無　　歳

歩行：　有　　無　　歳

トイレの自立と状況：　有　　無　　歳

常時とっている姿勢：　有　　無

その他の運動について：

2. コミュニケーションはどのようにとっていますか。困ったことや工夫したことがあったら具体的に教えてください。
（例：指を使ったサインを行っている。～に困ったので、こんな工夫した。）

3. 食事は、生後から現在まで、どの様に取られていますか。困ったことや工夫されたことがあったら具体的に教えてください。
（例：10 歳までミキサー食、11 歳から柔らかいもの、20 歳から普通食。こんな工夫をした。）

年齢　　食事形態や工夫されたことなど

（　　歳）（　　）

（　　歳）（　　）

（　　歳）（　　）

（　　歳）（　　）

（　　歳）（　　）

4. よく行う動作があれば教えてください。

5. 好きなことや得意なことを教えてください。

6. 苦手なことを教えてください。

＜15 歳以上の方に伺います。＞

1. 15 歳の時点でみられた症状を教えてください。また、かかっている診療科と行っている治療について教えてください。

診断名	診療科	治療内容
( )	( )	( )
( )	( )	( )
( )	( )	( )
( )	( )	( )
( )	( )	( )
( )	( )	( )
( )	( )	( )
( )	( )	( )
( )	( )	( )
( )	( )	( )
( )	( )	( )

2. 成人期の一般診療科（小児科以外）への移行について教えてください。

1）小児科への通院は現在もされていますか。通院していない場合は、小児科から移行した時期を教えてください。

している　　していない（移行した時期：　　歳）

2）一般診療科（小児科以外）への移行はスムーズにできましたか。
　　はい　　いいえ

3）一般診療科（小児科以外）に移行する際に困ったことはありますか

4）移行の時には、どのように病院を決めましたか？
　（例：小児科の医師からの紹介、自分で探して判断した）

3. 現在、医療支援について困っていることがあれば、教えてください。

4. 成人期への医療体制に望むことがあれば教えてください。

<就学・就労について>

1. 就学先について教えてください。
（例：通常学級・通級指導教室・特別支援学級・特別支援学校など）

小学校：
中学校：
高校：

2. 学校を卒業後、就労していますか。
はい　いいえ

はいの方→就労先：一般就労・就労継続支援事業 A 型・就労移行支援事業 B 型
その他（　　）
1 日の勤務時間：

3. 学校などを選択するにあたり、迷ったこと、困ったことがあったら教えてください。

<医療費助成,福祉・児童手当について>

1. 交付を受けている手帳の種類に○を付けてください。
   a. 身体障害者手帳　（等級：　　）
   b. 療育手帳　　（等級：　　）
   c. 精神障害者保健福祉手帳
   d. その他（　　）

2. 受けている手当に○を付けてください。
   小児期
   a. 特別児童扶養手当（1 級・2 級）
   b. 障害児福祉手当
   c. その他（　　）

   成人期
   a. 特別障害者手当
   b. 経過的福祉手当
   c. 障害基礎年金
   d. その他（　　）

3. 利用している制度に○を付けてください。
   a. 小児慢性特定疾病医療費助成制度
   b. 心身障害者医療費助成制度
   c. その他（　　）

<補装具について>

1．使用したことのある補装具に○を付けてください。

a. 座位保持装置
b. 歩行補助杖
c. 眼鏡
d. 補聴器
e. 車イス
f. 電動車イス
g. 座位保持イス
h. 起立保持具
i. 歩行器
j. 頭部保持具
k. 排便補助具
l. 意思伝達装置
m. 障害児向けバギー
n. その他（　　）

２．補装具費支給制度等の助成を受けた補装具があれば教えてください。

＜社会支援について＞

1. 利用していた、又は現在利用している社会支援に○を付けてください。

小児期

通所支援

a. 児童発達支援センター・児童発達支援事業所
b. 医療型児童発達支援センター
c. 放課後等デイサービス
d. 居宅訪問型児童発達支援（看護師など専門スタッフの自宅訪問）
e. 保育所等訪問支援（保育所などに専門スタッフが訪問）
d. その他（　　）

入所支援

a. 福祉型障害児入所施設（長期・短期）
b. 医療型障害児入所施設（長期・短期）
c. その他（　　）

成人期

居宅系

a. 居宅介護（ホームヘルプ）
b. 短期入所（ショートステイ）
c. 行動援護
d. その他（　　）

居住系

a. 施設入所・グループホーム
b. その他（　　）

2. 今後利用するつもりである、又は利用してみたい社会資源がありましたら教えてください。

3. 生活する上で、困っていること、知りたいこと、あったら良いと思う社会資源やシステムなどがありましたら教えてください。

＜保護者様について＞

1. 保護者様の勤務形態ついて教えてください。
（例：正社員・派遣社員・パート・アルバイト・自営業・無職など）

続柄		勤務形態
（ 父	：	）
（ 母	：	）
（	：	）
（	：	）

ご協力ありがとうございました。

（資料４）

診療において実施するマイクロアレイ染色体検査のガイダンス

日本小児遺伝学会
日本先天異常学会
日本人類遺伝学会
厚生労働省難治性疾患政策研究事業
「先天異常症候群領域の指定難病等の QOL の向上を目指す包括的研究」研究班
「染色体微細欠失重複症候群の包括的診療体制の構築」研究班

はじめに

このガイダンスは、出生後の生殖細胞系列遺伝学的検査として実施するマイクロアレイ染色体検査が適切に用いられることを目的としている［注 1］。

マイクロアレイ染色体検査は、ゲノムのコピー数変化（Copy number variant: CNV）を評価する検査であり、生殖細胞系列の網羅的遺伝学的検査の一つでもあることから、その実施にあたっては関連学会等からのガイドライン［注 2］や種々の提言［注 3］を遵守することが求められる。既に海外ではマイクロアレイ染色体検査は臨床検査として定着し、ガイドラインや提言が公表されている［注 4］。このガイダンスでは、マイクロアレイ染色体検査の基本原理や特性に留意した対応をまとめた。

１．マイクロアレイ染色体検査の基本原理［注 5］

マイクロアレイ染色体検査は、基本原理から２つのプラットフォームに分類される。一つはオリゴヌクレオチドプローブなどによる比較ゲノムハイブリダイゼーション（comparative genomic hybridization : CGH）アレイで、もうひとつは、1 塩基多型（Single nucleotide polymorphism : SNP）アレイである。前者は基盤に固定されたオリゴヌクレオチドプローブに対し、患者検体と対照検体のゲノム DNA を競合的にハイブリダイゼーションさせることにより CNV を評価する［注 6］。後者は、SNP プローブに対する患者検体ゲノム DNA のハイブリダイゼーションによる単色シグナル強度を専用アルゴリズムで評価し CNV を算出する。いずれのプラットフォームでも CNV を評価することを基本としているが、SNP アレイではヘテロ接合性の喪失（absence of heterozygosity: AOH）の連続性により、片親性ダイソミー（uniparental disomy: UPD）、家系同一性（identity-by-descent: IBD）なども同定や推定が可能である。両プラットフォームとも、検出原理に合わせた解析アルゴリズムで評価する。検出感度は、設計されたプローブの座位・間隔・密度や、解析アルゴリズムの検出閾値にも依存する。

２．検査の適応

マイクロアレイ染色体検査の適応には、出生後の原因不明の知的障害、先天性多発形態異常が含まれる。臨床的に特定の染色体異常症が強く疑われる場合（ダウン症候群や 18 トリソミー症候群など）は、染色体 G 分染法の実施が勧奨される。

３．検査の実施

マイクロアレイ染色体検査の実施に際しては、検査方法の原理や限界、適応、留意点を理解

し、得られたデータを正しく解釈し、追加すべき検査を含めて患者家族に適切に説明することが求められる。臨床遺伝専門医と連携するなど総合的な遺伝医療の体制が敷かれている施設で行うことが望ましい［注 7］。

４．検査の限界［注 8］

１）均衡型染色体再構成（相互転座、逆位など）は検出できない。
２）低頻度モザイクの検出が困難である。
３）ゲノムコピー数異常をもたらした染色体再構成は確認できない。CNV が検出された際に、その理由が単純な欠失／重複か不均衡型転座等による欠失／重複かの区別ができない。
４）倍数性異常を検出することが困難である。
５）プローブが配置されていない領域（セントロメア、ヘテロクロマチン、テロメア領域等）の CNV は検出できない。
６）プローブの密度と設定閾値以下の微細な範囲の CNV は検出できない。また、臨床症状に影響を与える CNV 以外の遺伝子の点変異や発現状態、メチル化状態なども検出することはできない。
７）目的とする CNV が検出できないことは、臨床診断を否定することにならない。

５．検査前の説明事項

遺伝学的検査実施時に考慮される説明事項［注 9］に加え、一定の頻度で、現在の症状と関連性がないものの、臨床的意義ある病的 CNV（二次的所見）が検出されうることや、二次的所見が発端者のみならず血縁者にも影響を与える可能性があることを伝える［注 10］。臨床的意義不明な CNV の解釈では血縁者の遺伝学的検査が発端者の診断に有用となることも伝える。

６．マイクロアレイ染色体検査後に検討される追加の遺伝学的検査

検出された CNV が親の染色体再構成（均衡型相互転座や逆位等）や低頻度モザイクの保因状態に起因したものであるかを評価するために、本人および両親の染色体 G 分染法、当該領域を検出するプローブを用いた FISH（fluorescence in situ hybridization）法、マイクロアレイ染色体検査、リアルタイム PCR 法等の遺伝学的検査が有用な場合がある。

７．マイクロアレイ染色体検査の結果解釈と報告に必要な事項

１）アレイプラットフォームごとに、基本原理や解析アルゴリズム（検出閾値設定など）に由来する限界を理解する。
２）ゲノムデータベース［注 11］やゲノムブラウザー［注 12］の使用方法を熟知する。表現型のない集団における CNV の範囲や頻度、欠失領域内に含まれる Loss-of-function intolerant genes（ハプロ不全により疾患発症が予測される遺伝子）の有無とヒト疾患関連遺伝子の情報を考慮する。
３）検出されたテキスト情報をゲノムブラウザーで可視化し、CNV および隣接領域に含まれる遺伝子の量的効果と対象患者の臨床症状との相関を検討する。
４）マイクロアレイ染色体検査の結果解釈の留意点（家系内の浸透率、表現度、追加検査の適応、臨床的意義のない良性の CNV［注 13］等）を理解する［注 14］。
５）表現型の確実な評価が得られない状況下では、検査結果の解釈が困難である。

６）診療科担当医が臨床遺伝の専門家でない場合は、臨床遺伝の専門家を含むカンファレンス等で検査結果と臨床症状との合致を確認し、総合的に解釈する［注 15］。

８．結果開示における留意点［注 15］

１）検査後の結果の解釈は、診療科担当医と臨床遺伝専門医との連携のもとで行われることが望ましい。
２）患者および家族・血縁者に対する結果の意義について丁寧な説明を行う。
３）遺伝カウンセリングを通じて、疾患情報を整理し、患者、家族および血縁者に対する心理社会的支援を継続する。
４）患者家族および血縁者に対する追加の遺伝学的検査（染色体 G 分染法、FISH 法、マイクロアレイ染色体検査、リアルタイム PCR 法等）が必要と判断された場合、臨床遺伝専門医との診断連携を考慮する。
５）二次的所見の開示は、臨床的有用性や医療管理の実現性を考慮し、慎重に検討する。

おわりに

次世代シーケンサーによる生殖細胞系列網羅的遺伝学的解析においては、得られたデータをもとに全ゲノム領域の CNV 検出が技術的に可能で、その精度が高まっている［注 16］。そのため、マイクロアレイ染色体検査は、新しく開発されたゲノム解析技術により検出された CNV の確認として用いられることもあり、生殖細胞系列網羅的遺伝学的検査とみなすことができる。したがって、本ガイダンスは、今後、全ゲノムを対象とした網羅的遺伝学的検査のガイドラインや提言に沿って活用されることが望ましい。

厚生労働科学研究費補助金（難治性疾患等政策研究事業）

分担研究報告書

染色体微細欠失重複症候群の包括的ケアの検討

研究分担者　大橋博文・埼玉県立小児医療センター遺伝科科長

研究要旨

マイクロアレイ染色体検査で診断される微細欠失重複症候群の包括的診療体制構築を目指す本研究班の活動において、成人期への移行に関わる研究は特に重要なテーマである。その分担研究として、昨年度には遺伝性疾患に関する本人への情報開示（告知）の実態調査を行い、378人中157人（回収率41.5%）から回答を得た。本人へ疾患情報は67件（43%）で伝えられていた。本年度はさらにその内容について、情報開示のきっかけや理由、開示の内容、気を付けたこと、情報開示で役に立った情報、開示後に疾患について話す頻度とその理由、伝えたことに関する気持ち、親としての想い、に分けて検討を進めた。それをもとに実診療において本人への疾患説明を家族とともに考える少なくとも契機の一つとなることを期待して小冊子“親から子どもへ疾患の情報を伝えること～176人の親のメッセージ～”の作成を行い、本邦において微細欠失重複症候群の遺伝診療に深く関わる学術集団である日本遺伝カウンセリング学会ならびに日本小児遺伝学会会員に配布した。また以前より継続している先天異常症候群の集団外来はコロナウィルス感染蔓延下にあって例年のような開催が困難だったが、年度半ばからのスタートながらZoomによって５疾患（カブキ症候群、22q11.2欠失症候群、プラダー・ウィリー症候群、ウィリアムズ症候群、5pモノソミー症候群）の集団外来を開催し、合計で６２家族（県外３１家族）が参加した。

研究協力者

大場　大樹　（埼玉県立小児医療センター遺伝科）

井坂　美帆　（埼玉県立小児医療センター遺伝科）

金子実基子　（慈恵医科大学遺伝子診療部）

A．研究目的

染色体微細欠失重複症候群を含む先天異常症候群にでの包括的ケアを考えた時、大きなテーマは成人期への移行であり、本研究班が取り組む課題となっている。その課題の中で、重要な点の１つに本人への疾患情報の提供（告知）があり、それは成人期に自律的な健康管理を維持するためには必須と考えられる。しかしながらこの重大な課題についての検討は未だ十分ではない状況から、昨年度の分担研究として遺伝性疾患に関する本人への情報開示（告知）の実態調査を行った。その結果 378 人中 157 人（回収

率 41.5%）から回答が得られ、本人へ疾患情報は 67 件（43%）で伝えられていた。本年度はさらにその内容についての検討を進めることを目的とした。また以前より継続している先天異常症候群集団外来も計画することとした。

B．研究方法

１．遺伝性疾患に関する本人への情報開示（告知）の実態調査のまとめ。

情報開示のきっかけや理由、開示の内容、気を付けたこと、情報開示で役に立った情報、開示後に疾患について話す頻度とその理由、伝えたことに関する気持ち、親としての想い、についてまとめた。

２．先天異常症候群集団外来の推進

2020 年 9 月～同年 12 月までの間に、5 疾患（カブキ症候群、22q11.2 欠失症候群、プラダー・ウィリー症候群、ウィリアムズ症候群、5p モノソミー症候群）の集団外来を開催した。

C．研究結果

１．遺伝性疾患に関する本人への情報開示（告知）の実態調査のまとめ（複数回答可とした）。

１）情報開示のきっかけや理由

病院に行く理由を理解してもらいたかった（43%）、理解できる年齢に達したと思った（30%）、病院に行く理由をきかれた(25%)、就学・就職・結婚などのイベントがあった(16%)、身体的な症状についてきかれた(13%)、周りの友だちに何か言われた (10%)、身体的な症状を気にしていそうだった (7%)の順であった。そのほか、「自分のことを知ってほしい」、「自分で対処できるように」、「納得して治療を受けてもらいたい」、「自分の健康管理への理解」、「自然と知った」などの記載もあった。

２）開示の内容

症状（73%）、疾患名（70%）、通院理由（57%）、健康管理（49%）、原因（16%）、遺伝（7%）の順だった。そのほか、「誰のせいでもないこと」、「苦手なこともあるけど得意なこともあること」、「知的障害について」、「なぜ通院のたびに採血が必要なのか」、「身体的な特徴」、「できないことの原因は病気であること」の記載もあった。

３）気を付けたこと

わかりやすく伝えるよう心がけた（67%）、シンプルに伝えるよう心がけた（49%）、安心できるように心がけた（48%）、正直に伝えるよう心がけた（36%）、疾患＝異常と扱わないように気を付けた（27%）、大きな問題ではないと伝えるよう心がけた（25%）、直接的に、正しい用語を使って伝えるよう心がけた（3%）の順だった。そのほか、「一人ではないないこと」、「家族みんな　で乗り越えよう」、「手術を乗り越え頑張ってきたこと、たくさんの人に助けられてきたこと」、「個性・特性の１つと前向きにとらえられるように」、「家族も協力するよということ」、「いろいろな病気があること、その中でみんな生きていること」の記載もあった。

４）情報開示で役に立った情報

患者・主治医（42%）、家族の会（32%）、Web 情報（16%）の順だった。そのほか、「主治医からもらった説明文書」、「親の職業上の情報入手」、「本、「治療・術後の情報」、「受診時の情報」、「家族の支え」
などがあった。

5）開示後に疾患について話す頻度とその理由

何度か話している（45% ;「勉強会や通院・入院があるとき」、「本人が聞いてくる、本人が困ったりつらいとき」、「話題になったとき」）、いつでも話している（43% ;「本人が困ったときにいつでも」、「勉強会やテレビなど何かの機会の折に触れて」、「聞いてきたときにいつでも」、「手術の後などに写真や楽しかったことを話す」、「疾患のことを気にしていそうなときにいつでも」、「今後の自分自身のため」、「困ったときの対処法など伝えるため」）、一度も話していない（12% ;「まだ伝えたばかり」、「まだ理解していない様子」、「本人が話題にしない」、「聞いてこない」）の順だった。

6）伝えたことに関する気持ち

気持ちの程度を、伝えてよかった-よくなかった、後悔していない- 後悔している、いつでも話題にできる- 話題にするのは辛い を、100 から 0 で表現すると、伝えてよかった 88、後悔していない 95、いつでも話題にできる 79 であった。

６）親としての想い

伝える目的、時期はさまざまであり、相反する想いが混在していた。 伝えた親は、早期から自然に徐々に伝えたほうがいいという傾向にあり、伝えていない親は、子どもが理解できるようになったら伝えたいという傾向がみられた。伝えることへの難しさ、悩ましさがあげられており、伝えることは親の気持ちの負担になる可能性はあるが全ての親が当てはまるわけではなかった。そして、伝えるにあたっては、わかりやすく、正確に、前向きに捉えられるよう伝え、本人・きょうだいの不安や心配を払拭し、それぞれの人生が満足できる生き方であって欲しいという親の願いが込められていた。 伝えた後の心のケア、寄り添う気持ち、いつでも支えになることは、親として本人・きょうだいに対して同じ想い

親なき後のことも含め、本人・きょうだいともに助け合っていきて欲しいという願いがある一方で、きょうだいに負担をかけたくない、きょうだい自身の人生をいきて欲しいという想いがあった。

２．先天異常症候群集団外来の推進

本年度、集団外来はやむなく Zoom での開催となった。参加家族総数は合計で６２家族（県外３１家族）だった。Zoom 集団外来でも従来通り、情報提供、参加者全員の自己紹介、座談会形式の交流会の構成とした。パソコン・スマートフォンからの Zoom 参加手順を図解した資料を事前に郵送していたが、実際に参加してみてどうであったかを質問したところ、“問題なく参加できた”が 63.6%、“参加までの手順に少し戸惑った”が 36.4%、“参加までの手順が分かり難くて困った”が 0%であった。

表1 先天異常症候群集団外来の開催状況

疾患名	テーマ	Zoom集団外来参加者（家族）	その内県外からの参加者
22q11.2欠失症候群	本人への疾患情報の提供について	9	1
5pモノソミー症候群	5p モノソミー症候群の概要	6	1
Prader-Willi症候群	本人への疾患情報の提供について	9	6
Williams症候群	本人への疾患情報の提供について	16	5
Kabuki症候群	本人への疾患情報の提供について	22	18

自由記述では、Zoom 集団外来のメリットとして、“小さいきょうだいがいる、コロナウイルス感染が心配、自宅が遠い（沖縄県）、等の理由で自宅から参加できて良かった”、“コロナ禍の生活で普段よりも孤独を感じる事が多かったので、交流できる場所があって安心できた”等の意見が挙げられた。一方、“初対面で画面越しだと間の取り方や雰囲気を掴むのが難しい”、“対面だとちょっとした時に横の人と話せるが、Zoom だとできないのが残念”、“直接お会いして色々な方と話すのが一番良い”、“親だけでなく子供達同士の触れ合いの時間も欲しい”等の声もあった。コロナ禍においてオンラインであっても同じ疾患をもつ患者家族同士が繋がりをもつことは、“悩んでいるのは自分だけじゃないと分かり心の支えになっている”というアンケート記載からも、意味があったと考えた。しかし、“Zoom 開催なら参加しない”とした家族も複数あり、アンケートでも“現状では仕方ないがやはり皆と直接会いたい”との意見も当然ながらあった。

D．考察

.染色体微細欠失重複症候群を含めた先天異常疾患の成人期移行（トランジション）は重大なテーマである。疾患情報を本人が十分に理解しておくことはトランジションそして本人の自立的な成人期の生活の前提となると思われる。今回行った本人への疾患情報開示の実態調査はその課題を検討する上で重要な資料となると思われる。なお、この調査結果をもとに冊子“親から子どもへ疾患の情報を伝えること～176人の親のメッセージ～”の作成を行い、実診療において本人への疾患説明を家族とともに考える少なくとも契機の一つとなることを期待して、本邦において微細欠失重複症候群の遺伝診療に深く関わる学術集団である日本遺伝カウンセリング学会ならびに日本小児遺伝学会会員に配布した。

先天異常症候群集団外来は疾患情報を提供と家族間交流を通して本人・家族支援を目指す試みであるが、本年度は初めてZoomを用いた開催した。この経験はコロナウイルス感染収束後の新たな遺伝診療に生かしたい。また、こういった集団外来に本人も参加する過程そのものが本人への疾患情報開示の場となり得

ることも想定して今後の外来に取り組んで行きたい。

Ｆ．研究発表

（発表誌名巻号・頁・発行年等も記入）

1. 論文発表

1) Machida M, Katoh H, Machida M, Miyake A, Taira K, Ohashi H: The Association of Scoliosis and NSD1 Gene Deletion in Sotos Syndrome Patients. Spine (Phila Pa 1976). 2020 Dec 15;Publish Ahead of Print.

2) 井坂美帆、大場大樹、小林美和、大橋博文：埼玉県小児医療センターに置けるコロナ禍下の遺伝診療対応の報告。日本遺伝カウンセリング学会雑誌 41 巻, p269-271, 2020

2. 学会発表

１) 金子実基子、井上絢香、大場大樹、小林美和 、大橋博文：遺伝性疾患をもつ子ども本人への情報開示の調査。第 65 回日本人類遺伝学会、2020 年 11 月、Web 開催。

２）井坂美帆、大場大樹、小林美和、 阿久津シルビア夏子、宮本達雄、松浦伸也、大橋博文 : 先天異常症候群集団外来 : モザイク型ダウン症候群外来の報告。第 65 回日本人類遺伝学会、2020 年 11 月、Web 開催。

Ｇ．知的財産権の出願・登録状況（予定を含む。）

1. 特許取得

該当なし

2. 実用新案登録

該当なし

3. その他

特になし

別紙３

厚生労働科学研究費補助金（難治性疾患等政策研究事業）
分担研究報告書

次世代シーケンスとマイクロアレイ染色体の組み合わせによる染色体微細構造解析

黒澤　健司
神奈川県立こども医療センター遺伝科　部長

研究要旨
エクソーム解析は、全遺伝子に対して網羅的ではあるものの、CNV（Copy number variant）評価としては限界がある。XHMM（eXome Hidden Markov Model）は、一定のアルゴリズムで CNV 評価を行うが、パラメーター設定によっては、ある程度の物理的範囲が必要である。エクソン単位での評価は、今後の臨床応用で極めて需要である。今回このデータ処理により 2 例の症例でエクソン単位での CNV が発症原因であることを明らかにした。診断未確定症例では、マイクロアレイ解析が次世代シーケンス後の CNV 確認として有用となる可能性がある。

A．研究目的

全ゲノムシーケンスの臨床応用が視野に入りつつある現在、得られたシーケンスデータによる構造解析および CNV 解析は極めて重要となる。次世代シーケンスの臨床応用の適応範囲は極めて広く、従来染色体微細構造異常としてマイクロアレイで検出してきた疾患特異的コピー数変化（Copy number variant）も、次世代シーケンスデータの、データ変換解析により、エクソン単位、あるいは遺伝子単位で、検出することが可能となりつつある。現在まで、我々の研究グループでは、視覚的に理解しやすく、データの解釈が一般臨床医でも可能となるエクソン単位の CNV 評価を取り入れてきた。

今回、さらに症例を追加して次世代シーケンスデータによる CNV 評価とマイクロアレイ染色体検査の併用による臨床診断のプロセスを検討した。

B．研究方法

対象は、知的障害および先天性の多発形態異常を身体特徴とする症例で、臨床症状の組み合わせおよび通常の診療で行われる生化学的検査及び染色体検査からは、特定の診断確定に至らない症例であった。次世代シーケンサーによる疾患原因遺伝子変異スクリーニングは、卓上型次世代シーケンサーMiSeq（イルミナ社）ないしは HiSeq3000（イルミナ社）を用い、ゲノム上のターゲット領域のキャプチャーは、MiSeq プラットフォームでは TruSight One Sequencing Panel（イルミナ社）、HiSeq3000 では SureSelect（アジレント・テクノロジーズ社）を使用した。解析パイプラインは、GATK、BWA、snpEff を主軸として、病原性予測として CADD、PolyPhen-2、SIFT、PROVEAN を用い、参照データベースとして gnomAD、jMorp、HGVD、ClinVar、HGMD などを用いた。このバリアント評価は、施設内倫理承認のもと、親権者からの同意書を取得したのちに進めた。マイクロアレイ解析は、Agilent 社製マイクロアレイシステムを用い、アレイは SurePrint G3 Human CGHMicroarray kit 8x60K を用いた。解析手順は、Agilent 社による標準プロトコールに準じて進めた。得られたデータの解析は Agilent Genomic Workbench ソフトウェアを用いた。データは DLR spread 値< 0.30 を採用した。比較対照 DNA は、Promega 社製 Female および Male genomic DNA を用いた。

(倫理面への配慮)
まとめるにあたって、個人情報の取り扱い留意し、連結可能匿名化のもとで解析を進めた。

C．研究結果

症例 1 は、聴力低下を主訴に来院の男児で、頭部 MRI などから超神経腫瘍が疑われた。原因検索としてメンデル遺伝病パネル解析を施行、NF2 遺伝子エクソン 9-14 の約 13 から 20Kb の欠失が疑われた。定量 PCR 法によりコントロールと比較し、欠失を確認した。

症例２は、軽度の発達遅滞とカフェオーレ斑を主訴に来院した 4 歳男児。身体所見から神経線維腫症 1 型を疑い、メンデル遺伝病パネル解析を施行。NF1 遺伝子を含む欠失を確認。マイクロアレイ染色体検査で、NF1 を含む 17q11.2 の 1.2Mb の欠失を確認した。

D．考察

エクソーム解析で得られたデータから１エクソ

ン単位の微細欠失を検出することが可能であることを、実際の臨床症例で確認できた。既存の同様機能を有すプログラムとして XHMM があるが、1 エクソン単位は事実上困難である。我々の方法では、エクソン単位の評価が可能で、極めて臨床的意義が高い。しかし、限界もあり、候補遺伝子が事前に明確にされている必要がある。また、エクソン内に埋もれる微細欠失は検出できない。全ゲノムシーケンスデータを視野に入れた場合、データ量は各段に増加し、アルゴリズムに従う計算方法の工夫が必要となる。

E. 結語

次世代シーケンスデータを変換することにより CNV 評価を行った。症例によってはエクソン単位で評価が可能であった。特に、ハプロ不全で発症する疾患では、一塩基の変化(SNV)と CNV 同時に評価できることを確認した。今後、マイクロアレイ解析は、alternative m,ethods としての有用性が期待されるかもしれない。

F．研究発表

1. 論文発表

Ohashi I, Kuroda Y, Enomoto Y, Murakami H, Masuno M, Kurosawa K. 6p21.33 Deletion encompassing CSNK2B is associated with relative macrocephaly, facial dysmorphism, and mild intellectual disability. Clin Dysmorphol. 2021 Mar 19. doi: 10.1097/MCD.0000000000000372.

Yokoi T, Enomoto Y, Tsurusaki Y, Harada N, Saito T, Nagai JI, Naruto T, Kurosawa K. An efficient genetic test flow for multiple congenital anomalies and intellectual disability. Pediatr Int. 2020 May;62(5):556-561.

2. 学会発表

西村直人(遺伝科), 熊木達郎, 村上博昭, 黒澤健司 4p16.3 微細欠失の遺伝子型と表現型の相関性に関する検討　第 123 回日本小児科学会 2020.8.21-23.　オンライン

榎本友美、鶴崎美徳、小林 眞司、井上 真規、藤田和俊、相田 典子、熊木 達郎、村上博昭、黒澤健司　POLR1B の recurrent 変異, c.3007C>T (p.Arg1003Cys)はトリーチャーコリンズ症候群 4 において外耳道閉鎖と小耳症に関与する　第 65 回日本人類遺伝学会 2020.11.19-21　名古屋

G．知的財産権の出願・登録状況（予定を含む。）

1. 特許取得

なし

2. 実用新案登録

なし

3. その他

なし

厚生労働科学研究費補助金(難治性疾患政策研究事業)
分担研究報告書

日本人において疾患概念が未確立の染色体サブテロメア欠失

研究分担者　山本　俊至　東京女子医科大学遺伝子医療センターゲノム診療科・教授

研究要旨
研究目的:
本研究班においては、染色体微細欠失重複症候群の包括的診断体制を構築することが目的である。今年度は、症例が少ないため日本人においては疾患概念が未だに確立しているとは言い難い、9q モノソミーについて報告する。
研究方法:
未診断疾患患者に対してマイクロアレイによるゲノムコピー数解析を行い、診断のサポートを行った中で、9q モノソミーを示す例が2例明らかになった。
結果と考察:
2症例の欠失はサブテロメアから 600-kb 以上あり、EHMT1 遺伝子を含んでいた。EHMT1 は Kleefstra 症候群の原因遺伝子として報告され、9q モノソミー症候群の症状とほぼ一致するため、EHMT1 は 9q モノソミーの責任遺伝子でもある。
結論:
Kleefstra 症候群、9q モノソミーともには日本人における報告が少なく、臨床的な疾患概念が未確立である。疾患概念の確立させ、診療ガイドラインを作成するためには、症例をさらに集積していくことが必要である。

A. 研究目的

本研究班においては、染色体微細欠失重複症候群の包括的診断体制を構築することが目的である。今年度は、症例が少ないため日本人においては疾患概念が未だに確立しているとは言い難い、9q モノソミーについて報告する。

B. 方法

未診断疾患患者に対してマイクロアレイによるゲノムコピー数解析を行った。なお、本研究は学内倫理委員会の承認を得て行い、患者サンプルの収集においては、書面による家族の同意を得て行った。

今年度診断のサポートを行った中で、9q モノソミーを示す例が2例明らかになった。

C. 研究結果

症例は下記のとおりである。

症例1:3歳男児。3歳で歩行不能、有意語なs。自閉スペクトラム症の症状を示す。体格は大き目も、頭囲は平均以下。

症例2:1歳8か月女児。VSD 自然閉鎖。5か月で無熱性けいれんあり。1歳半で独座付加、有意語なく、頭囲は 44.5cm と小さ目であった。

臨床所見:眼間開離、鼻根部扁平、アーチ状の眉などの共通した顔貌所見あり。

解析結果:両症例とも EHMT1 を含む 9q サブテロメア微細欠失を認め、Kleefstra 症候群と診断した。

D. 考察

9q サブテロメア欠失症候群の患者に共通する特徴は、重度の精神遅滞、低緊張、短頭頭蓋、てんかん発作、両眼隔離症、鼻根

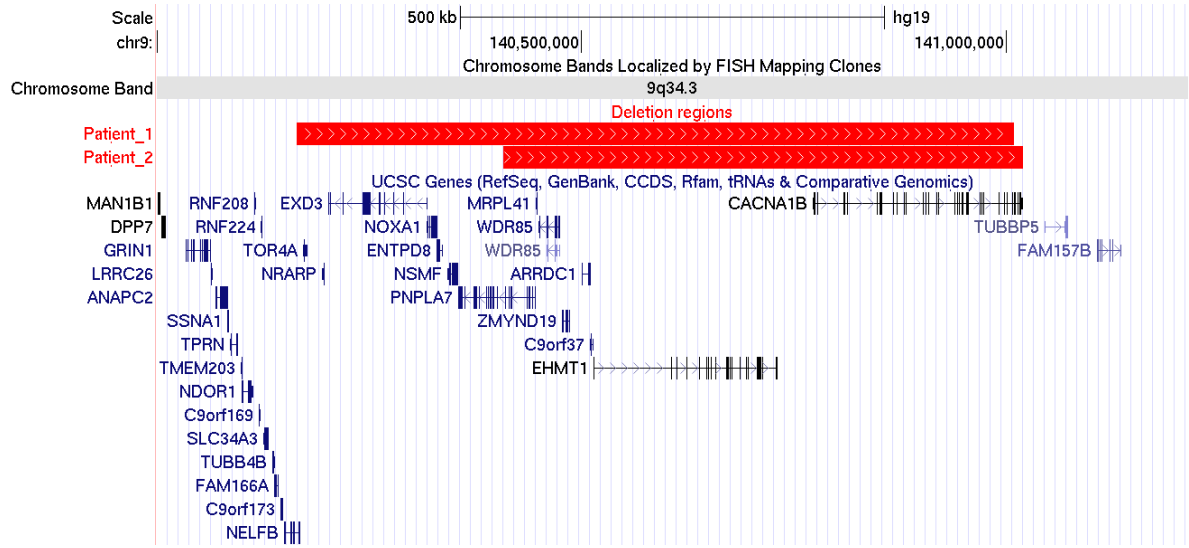

部平坦、テント状の上口唇、および先天性心疾患などであり、2009 年、Kleefstra らは、9q サブテロメア欠失症候群類似の症例において、EHMT1 変異を明らかにし、EHMT1 が 9q サブテロメア欠失症候群の責任遺伝子であることを突き止め、以来 Kleefstra 症候群という呼称が一般化している。しかしながら、本邦における報告例は少なく、長期的な予後や合併症の頻度などの自然歴は定かではない。

E. 結論

Kleefstra 症候群、9q モノソミーともには日本人における報告が少なく、臨床的な疾患概念が未確立である。疾患概念の確立させ、診療ガイドラインを作成するためには、症例をさらに集積していくことが必要である。

F. 研究発表

1. 論文発表

1. Yamamoto-Shimojima K, Osawa K, Saito M, Yamamoto T: iPSCs established from a female patient with Xq22 deletion confirm that BEX2 escapes from X-chromosome inactivation. Congenit Anom 61; 63-67, 2021.
2. 柳下友映, 下島圭子, 西 恵理子, チョン ピンフィー, 山田 博之, 岡本 伸彦, 永田智, 山本俊至: 日本人 Potocki-Lupski 症候群 7 症例の臨床症状. 脳と発達 in press
3. Imaizumi T, Yamamoto-Shimojima K, Yanagishita T, Ondo Y, Nishi E, Okamoto N, Yamamoto T: Complex chromosomal rearrangements of human chromosome 21 in a patient manifesting clinical features partially overlapped with that of Down syndrome. Hum Genet 139; 1555-1563, 2020.
4. Yanagishita T, Imaizumi T, Yamamoto-Shimojima K, Yano T, Okamoto N, Nagata S, Yamamoto T: Breakpoint junction analysis for complex genomic rearrangements with the caldera volcano-like pattern. Hum Mutat 41; 2119-2127, 2020.
5. Akiyama T, Hyodo Y, Hasegawa K, Oboshi T, Imai K, Ishihara N, Dowa Y, Koike T, Yamamoto T, Shibasaki J, Shimbo H, Fukuyama T, Takano R,

Shiraku H, Takeshita S, Okanishi T, Baba S, Kubota M, Hamano S, Kobayashi K: Pyridoxal may be a better indicator of vitamin B6 dependent epilepsy than pyridoxal 5-phosphate. Pediatr Neurol 113; 33-41, 2020.

6. Cappuccio C, Sayou C, Tanno PL, Tisserant E, Bruel AL, Kennani SE, Sá J, Low KJ, Dias C, Havlovicová M, Hančárová M, Eichler EE, Devillard F, Moutton S, MD, Van-Gils J, Dubourg C, Odent S, Piton A, Yamamoto T, Okamoto N, Firth H, Metcalfe K, Moh A, Kimberly A. Chapman, Aref-Eshghi E, Kerkhof J, Torella A, Nigro V, Perrin L, Piard J, Le Guyader G, Jouan T, Thauvin-Robinet C, Duffourd Y, George-Abraham JK, Buchanan CA, Williams D, Kini U, Wilson K, Telethon Undiagnosed Diseases Program, The DDD study, Sousa SB, Hennekam RCM, Sadikovic B, Thevenon J, Govin J, Vitobello A, Brunetti-Pierri N: De novo SMARCA2 variants clustered outside the helicase domain cause a new recognizable syndrome with intellectual disability and blepharophimosis distinct from Nicolaides-Baraitser syndrome. Genetics in Med 22; 1838-1850, 2020.
7. Ogura H, Ohga S, Aoki T, Utsugisawa T, Takahashi H, Iwai A, Watanabe K, Okuno Y, Yoshida K, Ogawa S, Miyano S, Kojima S, Yamamoto T, Yamamoto-Shimojima K, Kanno H: Novel COL4A1 mutations identified in infants with congenital hemolytic anemia in association with brain malformations. Hum Genome Var 7; 42, 2020.
8. Imaizumi T, Yamamoto-Shimojima K, Yanagishita T, Ondo Y, Yamamoto T: Analyses of breakpoint-junctions of complex genomic rearrangements comprising multiple consecutive microdeletions by nanopore sequencing. J Hum Genet 65; 735-741, 2020.
9. Kamio T, Kamio H, Aoki T, Ondo Y, Uchiyama T, Yamamoto-Shimojima K, Watanabe M, Okamoto T, Kanno H, Yamamoto T: Molecular Profiles of Breast Cancer in a Single Institution. Anticancer Res 40; 4567-4570, 2020.
10. Kato T, Inagaki H, Miyai S, Suzuki F, Naru Y, Shinkai Y, Kato A, Kanyama K, Mizuno S, Muramatsu Y, Yamamoto T, Shinya M, Tazaki Y, Hiwatashi S, Ikeda T, Ozaki M, Kurahashi H: The involvement of U-type dicentric chromosomes in the formation of terminal deletions with or without adjacent inverted duplications. Hum Genet 139; 1417-1427, 2020.
11. Hirose S, Tanaka Y, Shibata M, Kimura Y, Ishikawa M, Higurashi N, Yamamoto T, Ichise E, Chiyonobu T, Ishii A: Application of Induced Pluripotent Stem Cells in Epilepsy. Molecular and Cellular Neuroscience 108; 103535, 2020.
12. Wakabayashi K, Osaka H, Kojima K, Imaizumi T, Yamamoto T, Yamagata T: MCT8 deficiency in a patient with a novel frameshift variant in the SLC16A2 gene. Hum Genome Var 8: 10, 2021.

13. Yamamoto-Shimojima K, Akagawa H, Yanagi K, Kaname T, Okamoto N, Yamamoto T: Deep intronic deletion in intron 3 of PLP1 associated with severe phenotype of Pelizaeus-Merzbacher disease. Hum Genome Var in press
14. Yamamoto-Shimojima K, Kimoto Y, WatanabeY, Yamamoto T: Two different MLC1 variants compounded with a common variant S93L in Japanese patients of megalencephalic leukoencephalopathy with subcortical cysts. Tokyo Women's Medical University Journal 4; 94-97, 2020.
15. Yanagishita T, Eto K, Yamamoto-Shimojima K, Imaizumi T, Nagata S, Yamamoto T: A novel PAFAH1B1 splicing variant identified in a patient with classical lissencephaly. Tokyo Women's Medical University Journal in press
16. Fujita T, Ihara Y, Hayashi H, Ishii A, Ideguchi H, Inoue T, Imaizumi T, Yamamoto T, Hirose S: Coffin‐Siris syndrome with bilateral macular dysplasia caused by a novel exonic deletion in ARID1B. Congenital Anomalies in press
17. Yamamoto-Shimojima K, Ono H, Imaizumi T, Yamamoto T: Novel LAMA2 variants identified in a patient with white matter abnormality. Hum Genome Var 7; 16, 2020.

2. 著書

1. 山本俊至: 遺伝子検査. お医者さんオンライン h00391. プレシジョン, 東京, 2020.
2. 山本俊至: 脊髄性筋萎縮症. 周産期遺伝カウンセリングマニュアル 146-148. 中外医学社, 東京, 2020.5.

3. 学会発表

1. 山本俊至:【シンポジム:わが国における NIPT の在り方を考える】「小児科医の立場から」. 第12回日本小児科学会倫理委員会公開フォーラム-出生前診断を考える-, 東京(WEB), 2021/03
2. 山本圭子, 澤石由記夫, 山本俊至: Inverted-duplication-deletion の領域にさらに不均衡転座が付加された過去に報告のない染色体構造異常の1例. 第43回日本小児遺伝学会学術集会, 松本(WEB), 2021/01
3. 山本俊至, 山本圭子, 岡本伸彦: SMARCA2 の hot spot 変異は従来の SWI/SNF 複合体症候群とは異なる表現型を示す. 第43回日本小児遺伝学会学術集会, 松本(WEB), 2021/01
4. 西恵理子, 上原朋子, 要匡, 山本俊至, 小崎健次郎, 岡本伸彦: EBF3 遺伝子のハプロ不全を有する患者の臨床症状. 第43回日本小児遺伝学会学術集会, 松本(WEB), 2021/01
5. 山本俊至:【生殖シンポジウム1:PGT】日本における遺伝学的検査の現状と PGT の問題点. 第6回日本産科婦人科遺伝診療学会学術集会, 金沢(WEB), 2020/12

6. 山本俊至:【シンポジウム1 わが国のPGT-A はどこへ？】解析技術; Pros and cons. 第65回 日本生殖医学会学術講演会・総会, 東京(WEB), 2020/12
7. 山本圭子, 小野浩明, 今泉太一, 山本俊至: 白質異常を端緒に特定された新規 LAMA2 バリアント. 日本人類遺伝学会第 65 回大会, 名古屋(Web), 2020/11
8. 山本圭子, 赤川浩之, 荒木 敦, 柳 久美子, 要 匡, 岡本伸彦, 山本俊至: エクソン近傍のイントロン欠失によって生じるPLP1スプライシング異常. 日本人類遺伝学会第 65 回大会, 名古屋(Web), 2020/11
9. 山本俊至:【シンポジウム 4;日本における PGT～臨床研究から倫理まで～】PGT-A における本邦の課題. 日本人類遺伝学会第 65 回大会, 名古屋(Web), 2020/11
10. 山本俊至, 柳下友映, 今泉太一, 山本圭子, 岡本伸彦: ナノポアシーケンスによって明らかになるゲノム構造異常. 日本人類遺伝学会第 65 回大会, 名古屋(Web), 2020/11
11. 相馬未来, チョン・ピンフィー, 今泉太一, 柳下友映, 山本圭子, 山本俊至: 臨床症状より Coffin-Siris 症候群が疑われた患者において認められた新規 EP300 変異. 日本人類遺伝学会第 65 回大会, 名古屋(Web), 2020/11
12. 村松みゆき, 山本俊至: WAGR 症候群を持つ児への早期療育、特別支援教育の取組みに関する研究;システマティックレビュー. 日本人類遺伝学会第 65 回大会, 名古屋(Web), 2020/11
13. 今泉太一, 柳下友映, 山本圭子, 西恵理子, 岡本伸彦, 山本俊至: ロングリードシーケンサーを用いた染色体構造異常の解析. 第 62 回日本小児神経学会学術集会, 幕張(Web), 2020/08
14. 柳下友映, 山本圭子, 今泉太一, 恩藤由美子, 岡本伸彦, 矢野珠巨, 永田智, 山本俊至: 重複の両端のコピー数がさらに増えている新規染色体構造異常のメカニズム. 第 62 回日本小児神経学会学術集会, 幕張(Web), 2020/08
15. 山本圭子, 今泉太一, 赤川浩之, 菅野仁, 山本俊至: 選択的 IgG2 低下を示し中耳炎を反復した ZBTB20 の de novo 変異による Primrose 症候群の 1 例. 第 62 回日本小児神経学会学術集会, 幕張(WEB), 2020/08
16. 山本俊至: 小児神経科医が知っておくべき出生前診断の現状. 第 62 回日本小児神経学会学術集会, 幕張(WEB), 2020/08
17. 山本俊至: 脳と発達・B&D 編集委員会主催合同セミナー:和文・英文両機関誌に求められる使命と役割分担「脳と発達の役割」. 第 62 回日本小児神経学会学術集会, 幕張(WEB), 2020/08
18. 山本俊至: 遺伝学的検査普及のため NPO 法人を設立して:その経緯と課題. 第 62 回日本小児神経学会学術集会, 幕張(WEB), 2020/08
19. 山本俊至, 山本圭子: 疾患特異的

iPS 細胞を用いた CDKL5 てんかん脳症の病態解明. 第 62 回日本小児神経学会学術集会, 幕張(WEB), 2020/08

20. 大松泰生, 高橋幸利, 植田佑樹, 永井康平, 井田久仁子, 臼井大介, 山口解冬, 大谷英之, 池田浩子, 重松秀夫, 今井克美, 加藤光広, 山本俊至: STXBP1 遺伝子異常 10 症例のてんかんの特徴. 第 62 回日本小児神経学会学術集会, 幕張(WEB), 2020/08
21. 山崎あや, 宮田理英, 恩藤由美子, 山本圭子, 山本俊至: 14q サブテロメア欠失の表現型に関する一報告. 第 44 回日本遺伝カウンセリング学会学術集会, 宜野湾市(Web), 2020/07
22. 山本圭子, 長谷川結子, 岡本伸彦, 菅野 仁, 山本俊至: Acrocentric な染色体の短腕への転座を示した 2 例. 第 44 回日本遺伝カウンセリング学会学術集会, 宜野湾市(Web), 2020/07
23. 山本俊至, 山本圭子, 恩藤由美子, 谷本綾子, 藤井裕士: G 分染法では2つの染色体間での均衡転座と診断された 3 染色体間での不均衡転座. 第 44 回日本遺伝カウンセリング学会学術集会, 宜野湾市(Web), 2020/07
24. 村松みゆき, 柳下友映, 下島圭子, 三浦健一郎, 山本俊至: WAGR 症候群患者の実態調査と家族会サポート. 第 44 回日本遺伝カウンセリング学会学術集会, 宜野湾市(Web), 2020/07
25. 柳下友映, 佐藤孝俊, 石垣景子, 永田智, 山本俊至: 新規 BICD2 バリアントにより歩容異常・下肢優位の筋力低下を示した母子例. 第 44 回日本遺伝カウンセリング学会学術集会, 宜野湾市(Web), 2020/07.

H. 知的所有権の取得状況

1. 特許取得
   なし
2. 実用新案登録
   なし
3. その他

厚生労働科学研究費補助金(難治性疾患政策研究事業)
分担(総合)研究報告書

進行性白質脳症の研究成果情報収集と診断支援

研究分担者　山本　俊至　東京女子医科大学遺伝子医療センターゲノム診療科・教授

研究要旨

研究目的:
本研究班においては、染色体微細欠失重複症候群の包括的診断体制を構築することが目的である。17p11.2 微細欠失は Smith-Magenis 症候群の責任領域として知られており、非アリル間相同染色体組換によって生じる。非アリル間相同染色体組換は欠失だけではなく、同じ領域の重複を生じることがあるが、長らくその存在は認識されてこなかった。マイクロアレイによる網羅的なゲノムコピー数解析によって、このような未知の染色体微細異常が次々と明らかになり、Smith-Magenis 責任領域の 17p11.2 の重複は、Smith-Magenis 症候群とはまったく別の Potocki-Lupski 症候群を示すことが明らかになった。しかしながら、本邦における報告はなく、疾患概念や自然歴も明らかでないため、日本人 Potocki-Lupski 症候群患者の実態を明らかにするため、症例をまとめた。

研究方法:
未診断の精神運動発達遅滞患者を対象に網羅的なゲノムコピー数解析を行い、17p11.2 重複を示す患者の情報を収集した。

結果と考察:
日本人 Potocki-Lupski 症候群患者7例の情報を収集することができた。全例精神運動発達遅滞・非特異的な顔貌所見を示した。筋緊張低下、および自閉スペクトラム症状を疑わせる常同行為などの症状はそれぞれ 4 例において認められ、てんかんは 2 例で認められた。全 7 例で認められた表現型は、海外から過去に報告された所見と矛盾はなかった。

結論:
Smith-Magenis 症候群は先天性心疾患や特徴的顔貌などから比較的鑑別が容易であるが、今回 Potocki-Lupski 症候群と確認できた7例の臨床症状は精神運動発達遅滞や顔貌所見、筋緊張低下、行動の特徴など、いずれも非特異的であるため、臨床症状だけで Potocki-Lupski 症候群を鑑別することは難しいと考えられた。Potocki-Lupski 症候群の臨床的特徴をより理解するために、患者情報をさらに詳しく調査する必要があると考える。

A. 研究目的

17 番染色体短腕 11.2 領域(17p11.2)の約 3-Mb の微細欠失によって Smith-Magenis 症候群を生じる。この 17p11.2 領域の欠失両端には反復配列領域が存在しており、非アリル間相同染色体組換によって欠失が生じやすいことで知られている。非アリル間相同染色体組換では重複をきたすこともあるが、Smith-Magenis 症候群の責任領域 17p11.2 が重複した場合、Smith-Magenis 症候群とはまったく別の Potocki-Lupski 症候群の原因となる。Potocki-Lupski 症候群は生後の筋緊張低下、体重増加不良、精神運動発達遅滞、自閉スペクトラム症を主な症状とし、2007 年 Potocki らによって提唱された。頻度は 25,000 人に一人と言われ、常染色体優性遺伝形式を示す。Smith-Magenis 症候群と同様に, ほとんどの重複は両端の切断点が共通しており約 3-Mb である。Potocki-Lupski 症候群本邦における報告はなく、疾患概念や自然歴も

明らかでないため、日本人 Potocki-Lupski 症候群患者の実態を明らかにするため、症例をまとめた。

B. 研究方法

未診断の精神運動発達遅滞患者を対象に網羅的なゲノムコピー数解析を行い、17p11.2 重複を示す患者の情報を収集した。

C. 研究結果

日本人 Potocki-Lupski 症候群患者7例の情報を収集することができた。全例精神運動発達遅滞・非特異的な顔貌所見を示した。筋緊張低下、および自閉スペクトラム症状を疑わせる常同行為などの症状はそれぞれ 4 例において認められ、てんかんは 2 例で認められた。 全 7 例で認められた表現型は、海外から過去に報告された所見と矛盾はなかった（詳細は文献1を参照）。

D. 考察

MLC 疑い患者においては、日本人では S93L 変異が common 変異であるため、この変異の有無を同定することが診断に直結する。S93L をヘテロで示した患者においては、予想どおりもう一方の変異が認められたため、まずこの変異の有無を調べることが効率的であるということが確認できた。それ以外の進行性白質脳症は、効率的な方法としてエクソーム解析が推奨される。

E. 結論

Smith-Magenis 症候群は先天性心疾患や特徴的顔貌などから比較的鑑別が容易であるが、今回 Potocki-Lupski 症候群と確認できた7例の臨床症状は精神運動発達遅滞や顔貌所見、筋緊張低下、行動の特徴など、いずれも非特異的であるため、臨床症状だけで Potocki-Lupski 症候群を鑑別することは難しいと考えられた。Potocki-Lupski 症候群の臨床的特徴をより理解するために、患者情報をさらに詳しく調査する必要があると考える。

F. 研究発表

1. 論文発表

1. 柳下友映, 下島圭子, 西 恵理子, チョン ピンフィー, 山田 博之, 岡本 伸彦, 永田智, 山本俊至: 日本人 Potocki-Lupski 症候群 7 症例の臨床症状. 脳と発達 (in press)
2. Yamamoto-Shimojima K, Akagawa H, Yanagi K, Kaname T, Okamoto N, Yamamoto T: Deep intronic deletion in intron 3 of PLP1 associated with severe phenotype of Pelizaeus-Merzbacher disease. Hum Genome Var (in press)
3. Wakabayashi K, Osaka H, Kojima K, Imaizumi T, Yamamoto T, Yamagata T: MCT8 deficiency in a patient with a novel frameshift variant in the SLC16A2 gene. Hum Genome Var 8; 10, 2021.
4. Yamamoto-Shimojima K, Osawa K, Saito M, Yamamoto T: iPSCs established from a female patient with Xq22 deletion confirm that BEX2 escapes from X-chromosome inactivation. Congenit Anom 61; 63-67, 2021.
5. Imaizumi T, Yamamoto-Shimojima K, Yanagishita T, Ondo Y, Nishi E, Okamoto N, Yamamoto T: Complex chromosomal rearrangements of human

chromosome 21 in a patient manifesting clinical features partially overlapped with that of Down syndrome. Hum Genet139; 1555-1563, 2020.

6. Yanagishita T, Imaizumi T, Yamamoto-Shimojima K, Yano T, Okamoto N, Nagata S, Yamamoto T: Breakpoint junction analysis for complex genomic rearrangements with the caldera volcano-like pattern. Hum Mutat 41; 2119-2127, 2020.
7. Akiyama T, Hyodo Y, Hasegawa K, Oboshi T, Imai K, Ishihara N, Dowa Y, Koike T, Yamamoto T, Shibasaki J, Shimbo H, Fukuyama T, Takano R, Shiraku H, Takeshita S, Okanishi T, Baba S, Kubota M, Hamano S, Kobayashi K: Pyridoxal may be a better indicator of vitamin B6 dependent epilepsy than pyridoxal 5-phosphate. Pediatr Neurol 113; 33-41, 2020.
8. Cappuccio C, Sayou C, Tanno PL, Tisserant E, Bruel AL, Kennani SE, Sá J, Low KJ, Dias C, Havlovicová M, Hančárová M, Eichler EE, Devillard F, Moutton S, MD, Van-Gils J, Dubourg C, Odent S, Piton A, Yamamoto T, Okamoto N, Firth H, Metcalfe K, Moh A, Kimberly A. Chapman, Aref-Eshghi E, Kerkhof J, Torella A, Nigro V, Perrin L, Piard J, Le Guyader G, Jouan T, Thauvin-Robinet C, Duffourd Y, George-Abraham JK, Buchanan CA, Williams D, Kini U, Wilson K, Telethon Undiagnosed Diseases Program, The DDD study, Sousa SB, Hennekam RCM, Sadikovic B, Thevenon J, Govin J, Vitobello A, Brunetti-Pierri N: De novo SMARCA2 variants clustered outside the helicase domain cause a new recognizable syndrome with intellectual disability and blepharophimosis distinct from Nicolaides-Baraitser syndrome. Genet Med 22; 1838-1850, 2020.
9. Hirose S, Tanaka Y, Shibata M, Kimura Y, Ishikawa M, Higurashi N, Yamamoto T, Ichise E, Chiyonobu T, Ishii A: Application of Induced Pluripotent Stem Cells in Epilepsy. Mol Cell Neurosci 108; 103535, 2020.
10. Ogura H, Ohga S, Aoki T, Utsugisawa T, Takahashi H, Iwai A, Watanabe K, Okuno Y, Yoshida K, Ogawa S, Miyano S, Kojima S, Yamamoto T, Yamamoto-Shimojima K, Kanno H: Novel COL4A1 mutations identified in infants with congenital hemolytic anemia in association with brain malformations. Hum Genome Var 7; 42, 2020.
11. Imaizumi T, Yamamoto-Shimojima K, Yanagishita T, Ondo Y, Yamamoto T: Analyses of breakpoint-junctions of complex genomic rearrangements comprising multiple consecutive microdeletions by nanopore sequencing. J Hum Genet 65; 735-741, 2020.
12. Kamio T, Kamio H, Aoki T, Ondo Y, Uchiyama T, Yamamoto-Shimojima K, Watanabe M, Okamoto T, Kanno H, Yamamoto T: Molecular Profiles of Breast Cancer in a Single Institution. Anticancer Res 40; 4567-4570, 2020.

13. Kato T, Inagaki H, Miyai S, Suzuki F, Naru Y, Shinkai Y, Kato A, Kanyama K, Mizuno S, Muramatsu Y, Yamamoto T, Shinya M, Tazaki Y, Hiwatashi S, Ikeda T, Ozaki M, Kurahashi H: The involvement of U-type dicentric chromosomes in the formation of terminal deletions with or without adjacent inverted duplications. Hum Genet 139; 1417-1427, 2020.
14. Kanda S, Ohmuraya M, Akagawa H, Horita S, Yoshida Y, Kaneko N, Sugawara N, Ishiduka K, Miura K, Harita Y, Yamamoto T, Oka A, Araki K, Furukawa T, Hattori M: Deletion in the Cobalamin Synthetase W Domain-Containing Protein 1 Gene Is associated with Congenital Anomalies of the Kidney and Urinary Tract. J Am Soc Nephrol 31; 139-147, 2020.
15. Yamamoto-Shimojima K, Kimoto Y, WatanabeY, Yamamoto T: Two different MLC1 variants compounded with a common variant S93L in Japanese patients of megalencephalic leukoencephalopathy with subcortical cysts. TWMUJ 4; 94-97, 2020.
16. Fujita T, Ihara Y, Hayashi H, Ishii A, Ideguchi H, Inoue T, Imaizumi T, Yamamoto T, Hirose S: Coffin‐Siris syndrome with bilateral macular dysplasia caused by a novel exonic deletion in ARID1B. Congenit Anom 60; 189-193, 2020.
17. Yamamoto-Shimojima K, Ono H, Imaizumi T, Yamamoto T: Novel LAMA2 variants identified in a patient with white matter abnormality. Hum Genome Var 7; 16, 2020.
18. Abe Y, Yamamoto T, Izumita Y, Tsukano S: Gitelman syndrome caused by a novel hemi-allelic missense mutation of SLC12A3 unveiled by 16q12.2q21 microdeletion. Hum Genome Var 7; 17, 2020.
19. Imaizumi T, Yamamoto-Shimojima K, Yamamoto H, Yamamoto T: Establishment of a simple and rapid method to detect MECP2 duplications using digital polymerase chain reaction. Congenit Anom 60; 10-14, 2020.
20. Nozawa A, Ozeki M, Kawasaki R, Nakama M, Iwata H, Yamamoto T, Fukao T: Identification of homozygous somatic DICER1 mutation in pleuropulmonary blastoma. J Pediatr Hematol Oncol 42; 307-309, 2020.
21. Sato T, Sugiura-Ogasawara M, Ozawa F, Yamamoto T, Kato T, Kurahashi H, Kuroda T, Aoyama N, Kato K, Kobayashi R, Fukuda A, Utsunomiya T, Kuwahara A, Saito H, Takeshita T, Irahara M, Japan Society of Obstetrics and Gynecology: Preimplantation genetic testing for aneuploidy: a comparison of live birth rates in patients with recurrent pregnancy loss due to embryonic aneuploidy or recurrent implantation failure. Hum Repro 34; 2340-2348, 2019.
22. Yamamoto T, Imaizumi T, Yamamoto-Shimojima K, Lu Y, Yanagishita T,

Shimada S, Chong P-F, Ryutaro Kira R, Ueda R, Ishiyama A, Takeshita E, Momosaki K, Ozasa S, Akiyama T, Kobayashi K, Oomatsu H, Kitahara H, Yamaguchi T, Imai K, Kurahashi H, Okumura A, Oguni H, Seto T, Okamoto N: Genomic backgrounds of Japanese patients with undiagnosed neurodevelopmental disorders. Brain Dev 41; 776-782, 2019.

23. Okumura A, Shimojima K, Kurahashi H, Numoto S, Shimada S, Ishii A, Ohmori I, Takahashi S. Awaya T, Kubota T, Sakaki T, Ishihara N, Hattori A, Torisu H, Tohyama J, Inoue T, Haibara A, Nishida T, Yamamoto T: PRRT2 mutations in Japanese patients with benign infantile epilepsy and paroxysmal kinesigenic dyskinesia. Seizure 71; 1-5, 2019.
24. Yamamoto-Shimojima K, Kouwaki M, Kawashima Y, Itomi K, Momosaki K, Ozasa S, Okamoto N, Yokochi K, Yamamoto T: Natural histories of patients with Wolf-Hirschhorn syndrome derived from variable chromosomal abnormalities. Congenit Anom 59; 169-173, 2019.
25. Imaizumi T, Yamamoto-Shimojima K, Yamamoro T: Advantages of ddPCR in detection of PLP1 duplications. Intractable & Rare Diseases Research 8; 198-202, 2019.
26. Yamamoto-Shimojima K, Imaizumi T, Aoki Y, Inoue K, Kaname T, Okuno Y, Muramatsu H, Kato K, Yamamoto T: Elucidation of the pathogenic mechanism and potential treatment strategy for a female patient with spastic paraplegia derived from a single nucleotide deletion in PLP1. J Hum Genet 64; 665-671, 2019.
27. Yamamoto-Shimojima K, Imaizumi T, Akagawa H, Kanno H, Yamamoto T: Primrose syndrome associated with unclassified immunodeficiency and a novel ZBTB20 mutation. Am J Med Genet A 182; 521-526, 2019.
28. Hoshina T, Seto T, Shimono T, Sakamoto H, Okuyama T, Hamazaki T, Yamamoto T: Narrowing down the region responsible for 1q23.3q24.1 microdeletion by identifying the smallest deletion. Hum Genome Var 6; 47, 2019.
29. Tomita Y, Chong P-F, Yamamoto T, Akaminea S, Imaizumi T, Kira R: Sequential radiologic findings in osteopathia striata with cranial sclerosis. Diagn Interv Imaging 100; 529-531, 2019.
30. Yanagishita T, Yamamoto-Shimojima K, Nagata S, Yamamoto T: Compound heterozygous ALDH7A1 mutation causes the hemi-allelic expression in a patient with pyridoxine-dependent epilepsy. TWMUJ 3; 73-77, 2019.
31. Miyamoto s, Nakashima M, Ohashi T, Hiraide T, Kurosawa K, Yamamoto T, Takanashi J, Osaka H, Inoue K, Miyazaki T, Wada Y, Okamoto N, Saitsu H: A case of de novo splice site variant in SLC35A2 showing developmental delays, spastic paraplegia, and delayed

myelination. Mol Genet Genomic Med 7; e814, 2019.

32. Yanagishita T, Yamamoto-Shimojima K, Nakano S, Sasaki T, Shigematsu H, Imai K, Yamamoto T: Phenotypic features of 1q41q42 microdeletion including WDR26 and FBXO28 are clinically recognizable: The first case from Japan. Brain Dev 41; 452-455, 2019.
33. Yamamoto-Shimojima K, Okamoto N, Matsumura W, Okazaki T, Yamamoto T: Three Japanese patients with 3p13 microdeletions involving FOXP1. Brain Dev 41; 257-262, 2019.
34. Yanagishita T, Eto K, Yamamoto-Shimojima K, Imaizumi T, Nagata S, Yamamoto T: A novel PAFAH1B1 splicing variant identified in a patient with classical lissencephaly. TWMUJ 3; 73-77, 2019.
35. Tsukada I, Shimada S, Shono T, Nishizaki N, Oda H, Suzuki K, Niizuma T, Obinata K, Yamamoto T, Shimizu T: PRRT2 mutation in a sporadic case of paroxysmal kinesigenic dyskinesia. Juntendo Medical Journal 65; 95-98, 2019.
36. Imaizumi T, Mogami Y, Okamoto N, Yamamoto-Shimojima K, Yamamoto T: A de novo 1p35.2 microdeletion including PUM1 identified in a patient with sporadic West syndrome. Congenit Anom 59; 193-194, 2019.
37. Imaizumi T, Kumakura A, Yamamoto-Shimojima K, Ondo Y, Yamamoto T: Identification of a rare homozygous SZT2 variant due to uniparental disomy in a patient with a neurodevelopmental disorder. Intractable Rare Dis Res 7; 245-250, 2018.
38. Akizawa Y, Yamamoto T, Tamura K, Kanno T, Takahashi N, Ohki T, Omori T, Tokushige K, Yamamoto M, Saito K: A novel MLH1 mutation in a Japanese family with Lynch syndrome associated with small bowel cancer. Hum Genome Var 5; 13, 2018.
39. Shimada S, Hirasawa K, Takeshita A, Nakatsukasa H, Yamamoto-Shimojima K, Imaizumi T, Nagata S, Yamamoto T: Novel compound heterozygous EPG5 mutations consisted with a missense mutation and a microduplication in the exon 1 region identified in a Japanese patient with Vici syndrome. Am J Med Genet A 176; 2803-2807, 2018.
40. Shimada S, Oguni H, Otani Y, Nishikawa A, Ito S, Eto K, Nakazawa T, Yamamoto-Shimojima K, Takanashi J, Nagata S, Yamamoto T: An episode of acute encephalopathy with biphasic seizures and late reduced diffusion followed by hemiplegia and intractable epilepsy observed in a patient with a novel frameshift mutation in HNRNPU. Brain Dev 40; 813-818, 2018.
41. Babaya N, Noso S, Hiromine Y, Ito H, Taketomo Y, Yamamoto T, Kawabata Y, Ikegami H: Early-Onset Diabetes Mellitus in a Patient With a Chromosome 13q34qter Microdeletion Including IRS2. J Endocr Soc 2; 1207-1213, 2018.

42. Yamamoto T, Lu Y, Nakamura R, Shimojima K, Kira R: Novel A178P mutation in SLC16A2 in a patient with Allan-Herndon-Dudley syndrome. Congenit Anom 58; 143-144, 2018.
43. Yamamoto T, Yamamoto-Shimojima K, Ueda Y, Imai K, Takahashi Y, Imagawa E, Miyake N, Matsumoto N: Independent occurrence of de novo HSPD1 and HIP1 variants in brothers with different neurological disorders - leukodystrophy and autism. Hum Genome Var 5; 18, 2018.
44. Akaboshi K, Yamamoto T: Interstitial deletion within 7q31.1q31.3 in a woman with mild intellectual disability and schizophrenia. Neuropsychiatr Dis Treat 14; 1773-1778, 2018.
45. Akizawa Y, Yamamoto T, Tamura K, Kanno T, Takahashi N, Ohki T, Omori T, Tokushige K, Yamamoto M, Saito K: A novel MLH1 mutation in a Japanese family with Lynch syndrome associated with small bowel cancer. Hum Genome Var 5; 13, 2018.

2. 著書

1. 山本俊至: 網羅的ゲノム解析による着床前診断. 遺伝子医学 11; 26-33, 2021.
2. 山本俊至: 網羅的遺伝子診断としての次世代シーケンス結果の評価と診断. 脳と発達 52; 361-367, 2020.
3. 山本俊至: 網羅的遺伝子診断. 小児科臨床 73; 587-592, 2020.
4. 山本俊至: Williams 症候群の遺伝学. 小児科診療 82; 895-900, 2019.
5. 山本俊至, 山本圭子: マイクロアレイ染色体検査の実際. 遺伝子医学 9; 122-127, 2019.
6. 山本俊至: XV その他 11p13 欠失症候群(WAGR 症候群). 別冊日本臨牀領域別症候群シリーズ No.4 (2019年3月31日発行) 別刷 内分泌症候群(第 3 版) IV ―その他の内分泌疾患を含めて― 625-629. 日本臨床社, 東京, 2019.3
7. 山本俊至: 遺伝性腫瘍症候群とその対応. 小児科診療 Up-to-Date 33; 9-12, 2018.

3. 学会発表

1. 山本俊至:【シンポジム:わが国における NIPT の在り方を考える】「小児科医の立場から」. 第12回日本小児科学会倫理委員会公開フォーラム-出生前診断を考える-, 東京(WEB), 2021/03
2. 山本圭子, 澤石由記夫, 山本俊至: Inverted-duplication-deletion の領域にさらに不均衡転座が付加された過去に報告のない染色体構造異常の1例. 第43回日本小児遺伝学会学術集会, 松本(WEB), 2021/01
3. 山本俊至, 山本圭子, 岡本伸彦: SMARCA2 の hot spot 変異は従来の SWI/SNF 複合体症候群とは異なる表現型を示す. 第43回日本小児遺伝学会学術集会, 松本(WEB), 2021/01
4. 西恵理子, 上原朋子, 要匡, 山本俊至, 小崎健次郎, 岡本伸彦: EBF3 遺伝子のハプロ不全を有する患者の臨床症状. 第43回日本小児遺伝学会学術集会,

松本(WEB), 2021/01

5. 山本俊至:【生殖シンポジウム1:PGT】日本における遺伝学的検査の現状とPGT の問題点. 第6回日本産科婦人科遺伝診療学会学術集会, 金沢(WEB), 2020/12
6. 山本俊至:【シンポジウム1 わが国のPGT-A はどこへ？】解析技術; Pros and cons. 第65回 日本生殖医学会学術講演会・総会, 東京(WEB), 2020/12
7. 山本圭子, 小野浩明, 今泉太一, 山本俊至: 白質異常を端緒に特定された新規 LAMA2 バリアント. 日本人類遺伝学会第 65 回大会, 名古屋(Web), 2020/11
8. 山本圭子, 赤川浩之, 荒木 敦, 柳 久美子, 要 匡, 岡本伸彦, 山本俊至: エクソン近傍のイントロン欠失によって生じる PLP1 スプライシング異常. 日本人類遺伝学会第 65 回大会, 名古屋(Web), 2020/11
9. 山本俊至:【シンポジウム 4;日本における PGT～臨床研究から倫理まで～】PGT-A における本邦の課題. 日本人類遺伝学会第 65 回大会, 名古屋(Web), 2020/11
10. 山本俊至, 柳下友映, 今泉太一, 山本圭子, 岡本伸彦:ナノポアシーケンスによって明らかになるゲノム構造異常. 日本人類遺伝学会第 65 回大会, 名古屋(Web), 2020/11
11. 相馬未来, チョン・ピンフィー, 今泉太一, 柳下友映, 山本圭子, 山本俊至: 臨床症状より Coffin-Siris 症候群が疑われた患者において認められた新規 EP300 変異. 日本人類遺伝学会第 65 回大会, 名古屋(Web), 2020/11
12. 村松みゆき, 山本俊至:WAGR 症候群を持つ児への早期療育、特別支援教育の取組みに関する研究;システマティックレビュー. 日本人類遺伝学会第 65 回大会, 名古屋(Web), 2020/11
13. 今泉太一, 柳下友映, 山本圭子, 西恵理子, 岡本伸彦, 山本俊至: ロングリードシーケンサーを用いた染色体構造異常の解析. 第 62 回日本小児神経学会学術集会, 幕張(Web), 2020/08
14. 柳下友映, 山本圭子, 今泉太一, 恩藤由美子, 岡本伸彦, 矢野珠巨, 永田智, 山本俊至:重複の両端のコピー数がさらに増えている新規染色体構造異常のメカニズム. 第 62 回日本小児神経学会学術集会, 幕張(Web), 2020/08
15. 山本圭子, 今泉太一, 赤川浩之, 菅野仁, 山本俊至: 選択的 IgG2 低下を示し中耳炎を反復した ZBTB20 の de novo 変異による Primrose 症候群の 1 例. 第 62 回日本小児神経学会学術集会, 幕張(WEB), 2020/08
16. 山本俊至: 脳と発達・B&D 編集委員会主催合同セミナー:和文・英文両機関誌に求められる使命と役割分担「脳と発達の役割」. 第 62 回日本小児神経学会学術集会, 幕張(WEB), 2020/08
17. 山本俊至: 小児神経科医が知っておくべき出生前診断の現状. 第 62 回日本小児神経学会学術集会, 幕張(WEB), 2020/08
18. 山本俊至: 遺伝学的検査普及のため NPO 法人を設立して:その経緯と課題. 第 62 回日本小児神経学会学術集会, 幕張(WEB), 2020/08

19. 山本俊至, 山本圭子:疾患特異的 iPS 細胞を用いた CDKL5 てんかん脳症の病態解明. 第 62 回日本小児神経学会学術集会, 幕張(WEB), 2020/08
20. 21. 大松泰生, 高橋幸利, 植田佑樹, 永井康平, 井田久仁子, 臼井大介, 山口解冬, 大谷英之, 池田浩子, 重松秀夫, 今井克美, 加藤光広, 山本俊至: STXBP1 遺伝子異常 10 症例のてんかんの特徴. 第 62 回日本小児神経学会学術集会, 幕張(WEB), 2020/08
21. 山崎あや, 宮田理英, 恩藤由美子, 山本圭子, 山本俊至: 14q サブテロメア欠失の表現型に関する一報告. 第 44 回日本遺伝カウンセリング学会学術集会, 宜野湾市(Web), 2020/07
22. 山本圭子, 長谷川結子, 岡本伸彦, 菅野 仁, 山本俊至: Acrocentric な染色体の短腕への転座を示した 2 例. 第 44 回日本遺伝カウンセリング学会学術集会, 宜野湾市(Web), 2020/07
23. 山本俊至, 山本圭子, 恩藤由美子, 谷本綾子, 藤井裕士: G 分染法では2つの染色体間での均衡転座と診断された 3 染色体間での不均衡転座. 第 44 回日本遺伝カウンセリング学会学術集会, 宜野湾市(Web), 2020/07
24. 村松みゆき, 柳下友映, 下島圭子, 三浦健一郎, 山本俊至: WAGR 症候群患者の実態調査と家族会サポート. 第 44 回日本遺伝カウンセリング学会学術集会, 宜野湾市(Web), 2020/07
25. 柳下友映, 佐藤孝俊, 石垣景子, 永田智, 山本俊至: 新規 BICD2 バリアントにより歩容異常・下肢優位の筋力低下を示した母子例. 第44回日本遺伝カウンセリング学会学術集会, 宜野湾市(Web), 2020/07
26. Yamamoto T, Imaizumi T, Yamamoto-Shimojima K, Yanagishita T, Seto T, Okamoto N: Genomic backgrounds of Japanese patients with undiagnosed neurodevelopmental disorders. The 59th Annual Meeting of the Japanese Teratology Society/ The 13th World Congress of the International Cleftlip and Palate Foundation -CLEFT 2019-, Nagoya, 2019/07
27. Akamine S, Chong P F, Yamamoshita F, Maeda K, Yamamoto T, Kira R: A case of chromosome 8p inverted duplication deletion syndrome with infantile spasms and severe developmental delay. International Symposium on Neonatal Seizures: Deepening Insights into Developmental Brain Injury: The 20th Annual Meeting of Infantile Seizre Society, Nagoya, 2019/05
28. Sunag A, Fujita K, Hikita N, Sakuma S, Hamazaki T, Yamamoto T, Seto T: Successful treatment with perampanel to control myclonic seizure in an infant with neuronal ceroid lipofuscinosis type 14. International Symposium on Neonatal Seizures: Deepening Insights into Developmental Brain Injury: The 20th Annual Meeting of Infantile Seizre Society, Nagoya, 2019/05
29. 山本俊至: 小児神経科医が知っておくべき臨床遺伝学的検査. 第 20 回 常総セミナー, つくば市, 2020/02
30. 山本俊至: 新型出生前診断(NIPT)に

おける懸念. 第 2 回日本ダウン症会議, 東京, 2019/11

31. 柳下友映, 衛藤薫, 山本圭子, 今泉太一, 永田智, 山本俊至: LIS1 の de nobo スプライシング変異による滑脳症の 1 例. 日本人類遺伝学会第 64 回大会, 長崎, 2019/11
32. 井上陽子, 今泉太一, 柳下友映, 山本圭子, 岡本伸彦, 山本俊至: 重度発達遅滞を示した SATB2 を含む 2q33.1 領域の染色体重複例. 日本人類遺伝学会第 64 回大会, 長崎, 2019/11
33. 岩﨑直子, 大澤真里, 長谷美智代, 松尾真理, 山本俊至, 馬場園哲也, 齋藤加代子: Consensus guidline に基づいた糖尿病個別化医療のアウトカム. 日本人類遺伝学会第 64 回大会, 長崎, 2019/11
34. 今泉太一, 山本圭子, 柳下友映, 恩藤由美子, 山本俊至: ロングリードシーケンサーを用いた複雑な染色体構造異常の切断点解析. 日本人類遺伝学会第 64 回大会, 長崎, 2019/11
35. 山本圭子, 鈴村宏, 岡本伸彦, 山本俊至: NKX2-5 が位置する 5q35.1 領域の中間部欠失を示した3例. 日本人類遺伝学会第 64 回大会, 長崎, 2019/11
36. 山本俊至, 今泉太一, 山本圭子, 柳下友映, 瀬戸俊之, 岡本伸彦: 神経発達障害に対するクリニカルシーケンスの診断効率. 日本人類遺伝学会第 64 回大会, 長崎, 2019/11
37. 青木貴子, 小倉浩美, 槍澤大樹, 山本俊至, 中原衣里菜, 矢ケ崎博, 森岡一朗, 菅野仁: 先天性溶血性貧血関連遺伝子パネルを用いた新生児溶血性疾患の病因解析. 日本人類遺伝学会第 64 回大会, 長崎, 2019/11
38. 村松みゆき, 今泉太一, 柳下友映, 山本圭子, 岡本伸彦, 山本俊至: MED13 遺伝子を含む 17q23 微細欠失を示した男児例. 日本人類遺伝学会第 64 回大会, 長崎, 2019/11
39. 柳下友映, 山本圭子, 今泉太一, 恩藤由美子, 岡本伸彦, 山本俊至: 超ロングシーケンスによる染色体構造異常の新たなメカニズムの解析. 日本人類遺伝学会第 64 回大会, 長崎, 2019/11
40. 宮本祥子, 中島光子, 大橋伯, 平出拓也, 宮崎岳大, 黒澤健司, 山本俊至, 髙梨潤一, 小坂仁, 井上健, 和田芳直, 岡本伸彦, 才津浩智: De novo スプライスサイト変異が同定された SLC35A2-CDG の 1 例. 日本人類遺伝学会第 64 回大会, 長崎, 2019/11
41. 堀田純子, 馬場遥香, 濱崎考史, 山本俊至, 瀬戸俊之: 2q23.3q24.2 欠失の 1 女児例. 日本人類遺伝学会第 64 回大会, 長崎, 2019/11
42. 村松みゆき, チョンピンフィー, 吉良龍太郎, 山本圭子, 岡本伸彦, 山本俊至: 13 番染色体構造異常 6 例の遺伝子型・表現型相関. 臨床遺伝 2019 in Sapporo/第 26 回日本遺伝子診療学会大会・第 43 回日本遺伝カウンセリング学会学術集会合同学術集会, 札幌, 2019/08
43. 柳下友映, 山本圭子, 小池敬義, 那須裕郷, 高橋幸利, 秋山倫之, 永田智, 山本俊至: ALDH7A1 の複合ヘテロ変異が同定できたビタミン依存性てんかんの1例. 臨床遺伝 2019 in Sapporo/

第 26 回日本遺伝子診療学会大会・第 43 回日本遺伝カウンセリング学会学術集会合同学術集会, 札幌, 2019/08

44. 井上陽子, 本岡里英子, 今泉太一, 恩藤由美子, 山本圭子, 山本俊至: 皮質下嚢胞をもつ大脳型白質脳症亜系遺伝子MLC2のヘテロ変異が同定された1例. 臨床遺伝 2019 in Sapporo/第 26 回日本遺伝子診療学会大会・第 43 回日本遺伝カウンセリング学会学術集会合同学術集会, 札幌, 2019/08
45. 今泉太一, チョンピンフィー, 吉良龍太郎, 山本圭子, 山本俊至:NGS 解析で診断された MECP2 重複症候群の1家系. 臨床遺伝 2019 in Sapporo/第 26 回日本遺伝子診療学会大会・第 43 回日本遺伝カウンセリング学会学術集会合同学術集会, 札幌, 2019/08
46. 山本圭子, 今泉太一, 赤川浩之, 山本俊至:全エクソーム解析で診断された Primrose 症候群の本邦第1例. 臨床遺伝 2019 in Sapporo/第 26 回日本遺伝子診療学会大会・第 43 回日本遺伝カウンセリング学会学術集会合同学術集会, 札幌, 2019/08
47. 山本俊至, 山本圭子, 恩藤由美子, 青山直樹, 黒田知子, 加藤恵一: 着床前染色体異数性診断(PGT-A)に用いる染色体数的異常の診断方法の検討. 臨床遺伝 2019 in Sapporo/第 26 回日本遺伝子診療学会大会・第 43 回日本遺伝カウンセリング学会学術集会合同学術集会, 札幌, 2019/08
48. 矢川陽介, 成宮孝祐, 工藤健司, 前田新介, 豊島幸憲, 有賀淳, 山本俊至, 大杉治司, 山本雅一: ニボルマブが奏功している食道悪性黒色腫術後肝転移の 1 例. 第 73 回日本食道学会学術集会, 福岡, 2019/06
49. 荒井 篤, 熊倉 啓, 吉田真衣, 石嶺里枝, 佐々木宏太, 山本俊至, 岡本伸彦, 秦 大資: てんかんと自閉症スペクトラム症を伴った SZT2 変異例と CHD2 変異例の報告. 第 61 回日本小児神経学会学術集会, 名古屋, 2019/06
50. 比屋根真彦, 松岡剛司, 山本俊至, 井上 健: 1 ヵ月時難治てんかんで発症し、肝脾腫、呼吸不全が急激に進行した大脳白質消失病の男児例. 第 61 回日本小児神経学会学術集会, 名古屋, 2019/06
51. 若林 慶, 小坂 仁, 小林華林, 今泉太一, 山本俊至, 山形崇倫: 乳児期から大脳半球の萎縮とジストニアを認めた MCT8 欠損症の 1 例. 第 61 回小児神経学会学術集会, 名古屋, 2019/05
52. 山本圭子, 青木雄介, 井上 健, 山本俊至:女性 Pelizaeus-Merzbacher 病患者の発症メカニズムと治療戦略の検討. 第 61 回日本小児神経学会学術集会, 名古屋, 2019/05
53. 柳下友映, 山本圭子, 恩藤由美子, 岡本信彦, 永田 智, 山本俊至: 精神運動発達遅滞・特徴的顔貌・心奇形を認める 19q13.32 欠失の新規症例. 第 61 回日本小児神経学会学術集会, 名古屋, 2019/05
54. 今泉太一, 山本圭子, 椎原 隆, 岡本伸彦, 山本俊至: 10 番染色体長腕サブテロメア欠失の 6 例.第 61 回日本小児神経学会学術集会, 名古屋, 2019/05

55. 山本俊至：「脳と発達」で論文 accept を勝ち取るには？. 第 61 回日本小児神経学会学術集会, 名古屋, 2019/05
56. 森岡景子, 高橋幸利, 臼井大介, 東本和紀, 大星大観, 伊藤智城, 木村暢佑, 植田祐樹, 山口解冬, 大谷英之, 今井克美, 重松秀夫, 井上有史, 加藤光広, 山本俊至：CDKL5 遺伝子異常による難治てんかん 10 例の検討:発達の特徴. 第 61 回日本小児神経学会学術集会, 名古屋, 2019/05
57. 橋詰拓摩, 衛藤薫, 鈴木美穂, 佐藤友哉, 柳下友映, 南雲薫子, 西川愛子, 中務秀嗣, 伊藤進, 平澤恭子, 山本俊至, 永田 智：LIS1 遺伝子のスプライシング変異を認めた古典型滑脳症一例. 第4 回 副都心小児科カンファレンス, 東京, 2019/06
58. 山本俊至:【シンポジウム3 着床前遺伝子スクリーニング:今後の展望】網羅的染色体診断技術の可能性. 第 15 回日本 A-PART 学術講演会, 東京, 2019/03
59. 服部元史, 石塚喜世伸, 薮内智朗, 金子直人, 三浦健一郎, 橋本多恵子, 山本俊至, 張田豊, 佐藤秀則：臨床・病理・遺伝学的解析に基づく腎移植後 FSGS 再発リスク. 第 52 回日本臨床腎移植学会, 大阪市, 2019/02
60. 山本圭子, 柳下友映, 村松みゆき, 今泉太一, 山本俊至：1p36 欠失症候群家族会の活動と本邦における実態. 第 41 回日本小児遺伝学会学術集会, 名古屋, 2019/01
61. 今泉太一, 山本圭子, 山本俊至：デジタル PCR を用いたアレイ CGH 解析結果の検証. 第 41 回日本小児遺伝学会学術集会, 名古屋, 2019/01
62. 柳下友映, 山本圭子, 今泉太一, 恩藤由美子, 西恵理子, 岡本伸彦, 永田智, 山本俊至：15q サブテロメア欠失 2 症例からの考察. 第 41 回日本小児遺伝学会学術集会, 名古屋, 2019/01
63. 遠山潤, 小松原孝夫, 小林悠, 眞柄慎一, 放上萌美, 中山有美, 松井亨, 加藤光広, 下島圭子, 山本俊至：石灰化をともなう多小脳回をきたした Pallister-Killian 症候群. 第 41 回日本小児遺伝学会学術集会, 名古屋, 2019/01
64. 山本俊至：パイロット試験を経験して（医療者の立場から）. 日本産婦人科学会倫理委員会公開シンポジウム【着床前診断-PGT-A 特別臨床研究の概要と今後の展望】, 東京, 2018/12
65. 矢川陽介, 有賀淳, 山本俊至, 成宮孝祐, 工藤健司, 前田新介, 豊島幸憲, 大杉治司, 山本雅一：ホルマリン固定パラフィン包理手術標本におけるマイクロサテライト不安定性の測定. 第 31 回日本バイオセラピィ学会学術集会総会, 東京, 2018/12
66. 服部元史, 秋岡祐子, 石塚喜世伸, 薮内智朗, 金子直人, 三浦健一郎, 白井陽子, 谷口洋平, 長澤武, 伴英樹, 髙木陽子, 橋本多恵子, 飯田貴也, 山本俊至, 張田豊, 佐藤秀則：腎移植を受けた小児 FSGS 患者の病因分類および再発リスク評価:臨床＋病理＋遺伝学的アプローチ. 第 40 回日本小児腎不全学会学術集会, 宮崎市, 2018/11

67. 山本俊至:【特別講演】小児神経科医が知っておくべきゲノム医療. 第 69 回日本小児神経学会関東地方会, 東京, 2018/1
68. 青木貴子、小倉浩美、槍澤大樹、山根孝久、山本俊至、菅野仁:遺伝子パネルシークエンスにより脱水型遺伝性有口赤血球症(DHSt)と診断し得た一例. 日本人類遺伝学会第63回大会, 横浜, 2018/10
69. 今泉太一、恩藤由美子、山本圭子、山本俊至:デジタル PCR を用いた MECP2 遺伝子重複検出法の確立. 日本人類遺伝学会第 63 回大会, 横浜, 2018/10
70. 秋澤叔香, 佐藤祐子, 浦野真理, 菅野俊幸, 山内あけみ, 熊切順, 山本俊至, 小川正樹, 齋藤加代子:当院における遺伝性乳がん・卵巣がんカウンセリング症例についての後方視的検討と課題. 日本人類遺伝学会第63回大会, 横浜, 2018/10
71. 藤原千代、竹内絵理子、楢原幸二、山本俊至: 自閉症スペクトラム障害と低身長を認めた19番環状染色体の一例. 日本人類遺伝学会第63回大会, 横浜, 2018/10
72. 柳下友映, 今泉太一, 山本圭子, 鞍嶋有紀, 岡本伸彦, 山本俊至: 多彩な症状を示す 1q21.1 微細欠失の 4 例. 日本人類遺伝学会第63回大会, 横浜, 2018/10
73. 山本圭子, 山本俊至: INV-DUP-DEL のほとんどは U-type-exchange による. 日本人類遺伝学会第63回大会, 横浜, 2018/10
74. 山本俊至: シンポジウム7【着床前診断の現状と問題点】着床前染色体異数性診断の現状と課題. 日本人類遺伝学会第 63 回大会, 横浜, 2018/10
75. 赤星恵子、大野由美子、松井秀司、松田光展、和田恵子、牧野道子、椎貴俊秀、山本俊至: Interstitial deletion of 7q31 in a patient with Schizopherenia. 日本人類遺伝学会第63回大会, 横浜, 2018/10
76. 村松みゆき, 今泉太一, 柳下友映, 山本圭子, 岡本伸彦, 山本俊至: OTX2 を含む 14q22.3q23.1 微細欠失を示した両側無眼球症の 1 例. 日本人類遺伝学会第 63 回大会, 横浜, 2018/10
77. 白井謙太朗、渡辺章充、浦野真理、佐藤裕子、松尾真理, 山本俊至: ナンセンス変異による Duchenne 型筋ジストロフィーの遺伝カウンセリングの一例. 日本人類遺伝学会第 63 回大会, 横浜, 2018/10
78. 柳下友映, 今泉太一, 岡本伸彦, 山本圭子, 山本俊至: USP7 を含む 16p13.2 領域の欠失を示す知的障害の1例. 第 58 回日本先天異常学会学術集会, 東京, 2018/07
79. 柳下友映, 山本-下島圭子, 西川恵里子, 岡本伸彦, 山本俊至: FMR1 を含む X 染色体微細欠失により過成長と精神運動発達遅滞を来した女児例. 第 42 回日本遺伝カウンセリング学会学術集会, 仙台, 2018/06
80. 岩渕恵美, 田中竜太, 塚越隆司, 鈴木竜太郎, 佐藤琢郎, 福島富士子, 泉維昌, 中山純子, 森山伸子, 山本俊至: 成長障害、発達遅滞、てんかんおよび

高サイトカイン型急性脳症を来し、網羅的な遺伝子解析で 1q44 欠失が見い出された一例. 第 60 回日本小児神経学会学術集会, 千葉, 2018/06

81. 山本-下島圭子, 松村渉、岡崎哲也, 前垣義弘, 岡本伸彦, 山本俊至: FOXP1 を含む 3p13 領域の微細欠失を示した 4 症例における遺伝子型表現型相関解析. 第 60 回日本小児神経学会学術集会, 千葉, 2018/06
82. 山本俊至, 山本-下島圭子, 幸脇正典, 鞍嶋有紀, 糸見和也, 百崎謙, 小篠史郎, 岡本伸彦, 横地健治: 4p モノソミー症候群10例における遺伝子型・表現型相関解析. 第60回日本小児神経学会学術集会, 千葉, 2018/06
83. 柳下友映, 今泉太一, 山本-下島圭子, 北原光, 今井克美, 山本俊至: 高度脳波異常を示した MED13L 変異によるてんかん性脳症の 1 例. 第 60 回日本小児神経学会学術集会, 千葉, 2018/05
84. 今泉太一, 岡本伸彦, 山本-下島圭子, 恩藤由美子, 山本俊至: BAI2 を含む 1p35 領域の欠失を示す West 症候群の 1例. 第 60 回日本小児神経学会学術集会, 千葉, 2018/05
85. 保科孝男, 瀬戸俊之, 藤田賢司, 匹田典克, 佐久間悟, 山本俊至, 新宅治夫: 早期に診断しえた STXBP1 遺伝子変異による新生児期発症てんかんの 1 例. 第 60 回日本小児神経学会学術集会, 千葉, 2018/05

H. 知的所有権の取得状況

1. 特許取得

なし

2. 実用新案登録

なし

3. その他

厚生労働科学研究費補助金（難治性疾患政策研究事業）
分担研究報告書

染色体微細欠失重複症候群の包括的診療体制の構築

研究分担者　涌井 敬子　信州大学医学部遺伝医学教室 講師

研究要旨：マイクロアレイ染色体検査でみつかる染色体微細欠失重複症候群を含む稀少疾患のひとつであるWolf-Hirschhorn症候群について，成人期の臨床症状等に関する情報収集を行った．合併症によって長く生きられない患者も少なくないが，成人として生活している症例もいる．患者のＱＯＬ向上のためにも，介護者のためにも，新たな医学的知見を得る研究に繋がる可能性からも，稀少遺伝性疾患患者の登録制度をつくり，各症例のゲノム情報とともに臨床症状を継続的に情報収集し蓄積してゆくための体制構築が急務である．

A．研究目的

マイクロアレイ染色体検査でみつかる染色体微細欠失重複症候群の医療水準の向上や患者のQOL向上をめざし，特に成人期治療へのトランジッションを充実させるために成人期の臨床情報を収集する．

B．研究方法

１．マイクロアレイ染色体検査

信州大学医学部遺伝医学教室にてマイクロアレイ染色体検査を実施した症例の中に，Wolf-Hirschhorn症候群（WHS）と確定診断された成人の一症例を認めたので提示する．

対象は，他施設から信州大学医学部附属病院遺伝子医療研究センターに紹介された，口唇口蓋裂，てんかん，胎児期からの発育遅延，重度精神運動発達遅滞，知的障害，顔貌上の特徴などを伴う43歳女性．緑内障にて30歳過ぎに失明した．小児期に染色体検査が実施されたが（おそらくＧ分染法とおもわれるが詳細不明），異常は検出されなかったとのことであった．

受診目的は，両親が結婚を控えた同胞の子供への遺伝を心配したことの遺伝カウンセリングで，まず対象の確定診断が検討された．臨床遺伝専門医による診察で，臨床的にWHSが疑われ，遺伝学的確定診断のためマイクロアレイ染色体検査（60K, CGHアレイ，パーキンエルマー）が実施された．

２．文献検索

WHS症例の成人期の臨床情報に関する文献を検索した．

2018年度の本研究報告においても，WHS症例の成人期の臨床情報の文献情報について報告しており，今回はその後報告されたWHS関連の新たな文献を検索，内容を確認した．

（倫理面への配慮）

本研究の実施に際しては，倫理指針等を遵守し，関係する多発奇形・発達遅滞を有する患者やその家族が不利益を被ることの無いよう，個人情報の保護に留意する．

C．研究結果

１．マイクロアレイ染色体検査

43歳の重症心身障害者である対象に，確定診断目的にマイクロアレイ染色体検査が施行され，4番染色体短腕（4p）端部に約13Mbのコピー数減少を検出した（下図）．

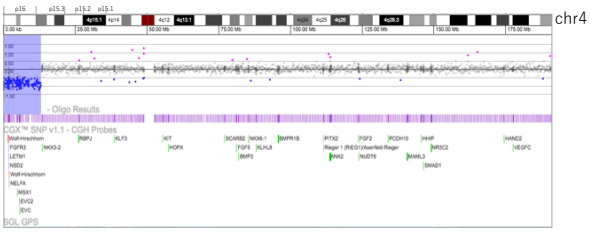

口唇口蓋裂を伴うWHSを示唆する顔貌上の特徴，子宮内発育遅延，てんかん，重度精神運動発達遅滞，知的障害などの既往から，臨床遺伝専門医が対象は典型的なWHSとして矛盾ないことを確認，確定診断された．

WHSのうち不均衡型転座による染色体再構成を約10-15%に認める（Nevado j, et al. 2019）ということから，対象の異常4番染色体が他の染色体腕端部の重複を伴う不均衡型構造異常である可能性についても検討した．今回用いたプラットフォームのマイクロアレイ染色体検査結果からは，直接的にそのことを示唆する他の染色体腕末端部のコピー数増加は認めなかったため，対象は単純な4p端部欠失である可能性が高いと考えられた．

しかしながら，不均衡型転座の転座相手が染色体末端部のテロメアリピート配列領域や端部着糸型染色体の短腕などマイクロアレイのプローブが配置できない繰り返し配列領域である場合には，親の均衡型構造異常に由来する不均衡型構造異常染色体であっても，対象の解析結果は関与する染色体のうち一方の染色体のコピー数異常しか検出されないという場合もありうる．今回の対象の異常4番染色体が不均衡型転座による再構成であり，それがいずれかの親の均衡型転座に由来し，さらにその同じ均衡型転座を同胞も有している可能性を完全に否定するには，両親および同胞の染色体分裂像について400-バンドレベル以上のG分染法，あるいは対象の4p欠失領域に座位するプローブと4番のコントロールプローブを用いた分裂像FISH解析を実施し，関連する均衡型転座がないことを確認することが必要である．

対象は乳児期から現在まで，原因不明の重症心身障害児として療育施設に入所し継続的に対応されてきたことで，医療の成人移行ついては大きな問題はなかったようである．診療にあたった臨床遺伝専門医から「成人WHS患者は地域病院で診療を受けていると推測されるが全貌がわかっていない．できれば成人も対応する大学病院の遺伝子医療部門などで1〜3年に一度でもフォローをしてゆくことが望ましいと考える．」とのコメントを得た．

謝辞：成人WHS患者の診療を担当し情報を提供くださった，信州大学医学部附属病院遺伝子医療研究センターの臨床遺伝専門医・古庄知己教授と認定遺伝カウンセラー・石川真澄様に感謝申し上げます．

2．成人WHS症例の臨床情報の文献検索

WHS症例研究の第一人者である，Battaglia（イタリア）とCarey（米国）らにより，成人WHSの自然歴に関する以下の論文２報が，オンライン版で先行公表された．

1）Natural history study of adults with Wolf-Hirschhorn syndrome 1: Case series of personally observed 35 individuals. Battaglia A, Lortz A, Carey JC. Am J Med Genet A. 2021 Mar 24. doi: 10.1002/ajmg.a.62176. Online ahead of print.

2）Natural history study of adults with Wolf-Hirschhorn syndrome 2: Patient-reported outcomes study. Carey JC, Lortz A, Mendel A, Battaglia A. Am J Med Genet A. 2021 May 5. doi: 10.1002/ajmg.a.62220. Online ahead of print.

1）の研究対象は計35名（19〜55歳，女性26名/男性9名）で，25名はBattagliaが5〜20年間に渡りフォローしてきたWHS症例で，10名はCareyらが米国の4p-サポートグループから抽出したWHS症例であった．

2）の研究対象は，2018年度の本研究班報告においてその活動を紹介した米国のSanford Research が取り組んでいる，7000以上の希少疾患を登録対象とした患者・家族（未診断患者も含む，保因者も含む）と研究者をつなぐための自然歴調査を担う，Coordination of Rare Diseases at Sanford (CoRDS) Registry database に登録されているWHS症例のうち，22〜64歳（平均30歳）の30名で，米国在住 : 26名/それ以外 : 4名，女性21名/男性7名/性別不明2名）であった．そのうち，親あるいは介護者からの患者報告アウトカム調査により，現在の日常生活の情報を得られたのは12名であった．

調査対象のWHS成人の日常生活における自立状態は，要全面介護（食事，排泄，入浴，衣類着脱，歩行など）: 70%［1）23/35名，2）10/12名，計33/47名］，食事など一部自立 : 28%［1）11/35名，2）2/12名，計13/47名］自立 : 2%［1）1/35名，計1/47名］であった．

心疾患，泌尿器系疾患，消化器系疾患，難聴などを有している症例もあるが，健康状態については72%［1）23/35名，2）11/12名，計34/47名］が健康と感じられているとのことであった．以前より指摘されている肝腫瘍は13%［1）6/35名，計6/47名］，歯の異常が68%［1）22/35名，2）10/12名，計32/47名］と頻度が高く，他には，側彎［1）17/35名，2）2/12名］，骨量減少［1）12/35名，2）1/12名］，白内障［1）5/35名，2）0/12名］，緑内障［1）4/35名，2）1/12名］，睡眠障害［1）3/35名，2）0/12名］，糖尿病［1）2/35名，2）1/12名］などの罹患が確認された．

Battaglia ら（2021）によると，てんかんについては，35名中34名が2〜14歳の間におさまっており，しかし10名（16〜34歳）は抗てんかん薬の投与は継続されていた．すべての対象症例は主に身ぶり手ぶりで（3名はそれ以外の手段でも）周りの家族や友人とコミュニケーションをとり，幸福そうで，友好的で，慈しみ深く，社交的であると評されていた．約25%は，診察時，初めてのことなど理解できない状況を怖いと感じているような不安傾向を表した．発達障害の程度は，個人差はあるが，概ね中等度から重度で広範な認知障害を有しており，適応性の発達は概ね24ヵ月相当であった．さらに，35名すべての対象症例が，理学療法，作業療法，言語療法，摂食療法など，何らかの個別のリハビリテーションプログラムに参加していた．また，3名は自国のワークショップに参加した経験があり，2名はグループホームで生活しており，1名はフードバンクにおいて棚に缶を並べたり食料品を箱詰めしたりするボランティア活動をしながら自立生活を送っていた．

Battagliaら（2021）は，WHS症例の臨床的定期チェックとして，血算，生化学検査，腎機能検査，肝腫瘍確認のための腹部超音波検査，眼科検診，てんかんが継続していれば神経科の診察，DXA法による骨密度検査，歯科検診，整形外科における側彎のチェックおよび治療などを提案した．

D．考察

43歳でWHSと確定診断された女性症例を経験した．小児期に染色体異常症が疑われ染色体検査を実施されたものの異常を検出されず，またDysmorphologyの専門家であれば臨床的に強く疑える顔貌の特徴などを有していながら，確定診断される機会を逸し，重症心身障害者として療育施設にてフォローされていた．

WHSはその原因となる4番染色体短腕端部欠失が約2Mb程度から>30Mbと大きな差がある隣接遺伝子症候群である．本対象は初回の染色体検査で異常が検出されなかったとの情報だったため，マイクロアレイ染色体検査で4pに欠失が確認されるとしても微細であろうと考えていたが，欠失サイズは約13Mbと決して小さくなかった．約13Mbの4p端部欠失は，先天異常の染色体検査に求められる400-バンドレベルのG分染では，4番染色体短腕の末端のバンドである4p16バンドの多くの部分が欠失してみえる大きさの欠失である．300〜400-バンドレベルの4p16バンドは淡染バンドであるためその欠失の検出はやや難しいが，このサイズの欠失であればG分染法にて検出されていなければならなかった．しかし約40年前は，G分染法を実施できた施設はごく限られており，また当時検査の標準化の概念はなく，形態学的検査である核型分析の解析精度は施設により大きな差があったことが推察される．検査センターで染色体検査が実施されるようになり，FISH法用が項目に加わった時期に，本対象も再検が検討されてもよかったと考える．

染色体微細欠失重複症候群の確定診断は，特定の染色体微細欠失重複症候群を臨床的に疑い，適した遺伝学的検査を依頼する臨床側のスキルと，高い解析精度で検査を実施する検査側の技術が必要なため，確定診断されずに自宅や療育施設等で過ごしている症例がまだ多く存在する可能性が示唆される．

対象は，30歳過ぎに緑内障により失明していた．緑内障の合併はWHS症例には多くないと考えられていたようであるが，稀ではあるが比較的大きなサイズの欠失例の中に先天性あるいは小児期発症の緑内障の報告もあり（Curtin J, et al. 2010, Dickmann A, et al. 2009, Finzi S, et al. 2001），またBattagliaら（2021）とCareyら（2021）によると，成人WHSの11%（5/47名）に緑内障の合併を認めている．一方40歳以上の一般成人約20人にひとりが罹患しているといわれており，自覚症状がない場合も多く気がついた時には悪化している場合も少なくないといった病気の特徴，さらに緑内障の責任遺伝子が特定されていないことを考慮すると，4p端部欠失と緑内障との因果関係は否定できないと考えた．

Battagliaら（2021）により提案されたチェック項目を，WHS症例の臨床的定期チェックとして，血算，生化学検査，腎機能検査，肝腫瘍確認のための腹部超音波検査，眼科検診，てんかんが継続していれば神経科の診察，DXA法による骨密度検査，歯科検診，整形外科における側彎のチェックおよび治療などを提案した．

Limeresら（2020）は，WHS患者の口腔内症状について詳細に検討し，4pの欠失サイズと部分無歯の有無が関係している可能性，その責任遺伝子が*MSX1*遺伝子を含む2.3-5.5Mb領域にある可能性を示唆した（Oral Manifestations of Wolf-Hirschhorn Syndrome: Genotype-Phenotype Correlation Analysis. J. Clin.

Med. 2020, 9, 3556）. Battagliaら（2021）とCareyら（2021）も成人WHS患者の68%（32/47名）が歯の異常を有していることを示したが，2021年の自然歴調査報告では各症例の欠失サイズを明らかにしておらず，責任遺伝子については言及していない. しかし, WHSのような欠失領域に大きな差がある隣接遺伝子症候群においては，欠失領域と症状の比較からある症状の責任遺伝子を特定する研究に結びつく可能性があることについて考察しており，今後検討してゆく予定を示唆していた.

マイクロアレイ染色体検査でみつかる染色体微細欠失重複症候群はそれぞれ非常に頻度が低く，自然歴を明らかにすることは容易でない．染色体微細欠失重複症候群症例のほとんどは，新生児期～小児期に小児科で診断され，小児病院の遺伝科や先天異常患者を多く診察している小児科でフォローされている症例もいるが，成人まで至る患者は比較的合併症が軽い場合が多く，在宅で介護されたり療育施設に入所した症例は，決まった医療機関でのフォローも途切れてしまう場合も少なくないと推測される．そのため，各患者の出生時から成人までの臨床症状は継続して記録されず，臨床症状の推移，転帰，死亡した場合の年齢・原因等の詳細もまとめて記録されていないのが，現在の我が国の現状である.

染色体微細欠失重複症候群を疑う症例について，諸外国で普及しているようにマイクロアレイ染色体検査を第一選択として保険で実施できるような医療体制を構築し，ひとりでも多くの症例を確定診断につなげることがまず必要である．新規症例のみならず，すでに臨床的にあるいはG分染法あるいはFISH法でWHSと診断された症例についてもマイクロアレイ染色体検査により欠失領域を確定することも重要である．そして，診断された各症例を英国のように国レベルでゲノム情報とともに登録し，長期に継続的に臨床情報を蓄積してゆく体制を構築することが望まれる．あるいは米国のCoRDSに参画するための体制を構築することを検討してもよいかもしれない．蓄積された情報から，将来，新たな医学研究に結びつく成果が得られる可能性も期待できる.

E．結論

染色体微細欠失重複症候群のひとつであるWHSについて，成人期の臨床症状等に関する情報収集を行った.

患者のＱＯＬ向上のためにも，介護者のためにも，新たな医学的知見を得る研究に繋がる可能性からも，染色体微細欠失重複症候群を含む稀少疾患患者の各ゲノム情報を登録制とし，それぞれの自然歴を長期に継続的に情報収集し蓄積してゆくことが非常に重要で，そのための登録体制構築が急務である.

G．研究発表

１． 論文発表

涌井敬子．遺伝子関連検査を知る．細胞遺伝学的検査結果を理解するために：染色体核型記載の基本. 遺伝子医学. 10 巻 1 号 pp.104-110, 2020

Hara-Isono K, Matsubara K, Hamada R, Shimada S, Yamaguchi T, Wakui K, Miyazaki O, Muroya K, Kurosawa K, Fukami M, Ogata T, Kosho T, Kagami M. A patient with Silver-Russell syndrome, multilocus imprinting disturbance, and Schimuke Immunoosseous Dysplasia unmasked by uniparental isodisomy of chromosome 2. J Hum Genet. accepted (2021.5.11)

２． 学会発表

Copy number losses of 11p14.3-p13 and 11p13-p12 detected by CGH array revealed to be heterozygous deletion of 11p14.3-p12 on one chromosome 11 and heterozygous duplication within 11p13 on the other chromosome 11 by metaphase FISH analysis（ポスター発表）. Wakui K, Kosho T, Fukushima Y. 欧州人類遺伝学会, 20206.6-9，ベルリン（Web 開催）

マイクロアレイ染色体検査結果解釈の留意点．SNP アレイ解析で 15 番染色体の一部に AOH を検出した Prader-Willi 症候群の解析結果から（ポスター発表）. 涌井敬子, 高野亨子, 久保田紀子, 小林純, 武田良淳, 山口智美, 古庄知己, 福嶋義光．第 44 回日本遺伝カウンセリング学会学術集会, 2020.7.3-5, 那覇 (web 開催)

発達の遅れ又は知的障害を伴う先天異常症候群を有する患者のきょうだいに関する研究（ポスター発表）. 佐久彰子, 小島朋美, 石川真澄, 黄瀬恵美子, 高野亨子, 湊川真理, 中村勝哉, 涌井敬子, 山口智美, 古庄知己. 第 44 回

日本遺伝カウンセリング学会学術集会，2020.7.3-5，那覇（web 開催)

SYNGAP1 関連知的障害の 5 例（ポスター発表）．高野亨子, 福山哲広, 本林光雄, 山崎佐和子, 山口智美, 涌井敬子, 柳久美子, 要匡, 古庄知己, 第 62 回日本小児神経学会学術集会, 2020.8.17-20，幕張（web 開催)

モザイクを示唆するゲノムコピー数増加のデータをきっかけに確認した染色体異数性異常／構造異常のモザイク症例の検証と考察（口頭発表）. 涌井敬子, 髙野亨子, 水野誠司, 江口真理子, 松田和之, 重藤翔平, 根岸達哉, 山口智美, 古庄知己, 福嶋義光. 日本人類遺伝学会第 65 回大会, 2020.11.18-12.2, 名古屋（web 開催）

“Ion AmpliSeq data の CNV 検出法”を用いた CNV 解析が遺伝学的診断に有用であった 2 例（ポスター発表）．高野亨子、西尾信哉、山口智美、涌井敬子、福山哲広、久保田紀子、武田良淳、古庄知己．日本人類遺伝学会第 65 回大会，2020.11.18-12.2，名古屋（web 開催）

TRIO 遺伝子関連知的障害の親子例（ポスター発表）．阪下達哉，高野亨子，柴直子，小島朋美，山口智美，涌井敬子，古庄知己．日本人類遺伝学会第 65 回大会，2020.11.18-12.2，名古屋（web 開催）

7p 端部欠失と 7q 端部重複をみとめた環状 7 番染色体の 1 例（ポスター発表）. 阪下達哉，涌井敬子，水野史，湊川真理，花房宏昭，高野亨子，古庄知己．第 43 回日本小児遺伝学会学術集会，2021.1.8-9，松本（web 開催）

H. 知的財産権の出願・登録状況

1. 特許取得

なし

2. 実用新案登録

なし

3.その他

なし

別紙４

研究成果の刊行に関する一覧表

書籍

著者氏名	論文タイトル名	書籍全体の編集者名	書　籍　名	出版社名	出版地	出版年	ページ
Hiroki Kurahashi	Microarray and Next Generation Sequencing	Hideaki Matsuzaki	Fetal Morph Functional Diagnosis	Springer	Singapore	2020	335-344

雑誌

発表者氏名	論文タイトル名	発表誌名	巻号	ページ	出版年
Bonora E, Chakrabarty S, Kellaris G, Tsutsumi M, Bianco F, Bergamini C, Ullah F, Isidori F, Liparulo I, Diquigiovanni C, Masin L, Rizzardi N, Cratere MG, Boschetti E, Papa V, Maresca A, Cenacchi G, Casadio R, Martelli P, Matera I, Ceccherini I, Fato R, Raiola G, Arrigo S, Signa S, Sementa AR, Severino M, Striano P, Fiorillo C, Goto T, Uchino S, Oyazato Y, Nakamura H, Mishra SK, Yeh YS, Kato T, Nozu K, Tanboon J, Morioka I, Nishino I, Toda T, Goto YI, Ohtake A, Kosaki K, Yamaguchi Y, Nonaka I, Iijima K, Mimaki M, Kurahashi H, Raams A, MacInnes A, Alders M, Engelen M, Linthorst G, de Koning T, den Dunnen W, Dijkstra G, van Spaendonck K, van Gent DC, Aronica E M, Picco P, Carelli V, Seri M, Katsanis N, Duijkers FA M, Taniguchi-Ikeda M, De Giorgio R.	Biallelic variants in *LIG3* cause a novel mitochondrial neurogastrointestinal encephalomyopathy.	**Brain**	In press.	In press.	2021
Hitachi K, Nakatani M, Kiyofuji Y, Inagaki H, Kurahashi H, Tsuchida K.	An analysis of differentially expressed coding and long non-coding RNAs in multiple models of skeletal muscle atrophy.	**Int J Mol Sci**	22(5)	2558	2021

Kumai T, Sadato A, Kurahashi H, Kato T, Adachi K, Hirose Y.	Coexistence of *RASA1* and *COL4A2* variants caused pial arteriovenous fistula (AVF) in a patient with capillary malformation-arteriovenous malformation.	**Clin Neurol Neurosurg**	204	106612	2021
Yokoi K, Nakajima Y, Yasui T, Yoshino M, Yoshikawa T, Kurahashi H, Ito T.	Novel *ARG1* variants identified in a patient with arginase 1 deficiency.	**Hum Genome Var**	8(1)	8	2021
Kanai S, Okanishi T, Kawai M, Yoshino G, Tsubouchi Y, Nishimura Y, Sakuma H, Kurahashi H, Maegaki Y.	Late-onset cerebral arteriopathy in a patient with incontinentia pigmenti.	**Brain Dev**	S0387-7604(20)	30350-8	2021
Tsutsumi M, Miura H, Inagaki H, Shinkai Y, Kato A, Kato T, Hamada-Tsutsumi S, Tanaka M, Kudo K, Yoshikawa T, Kurahashi H.	An aggressive systemic mastocytosis preceded by ovarian dysgerminoma.	**BMC Cancer**	20(1)	1162	2020
Ohwaki A, Nishizawa H, Kato A, Kato T, Miyazaki J, Yoshizawa H, Noda Y, Sakabe Y, Ichikawa R, Sekiya T, Fujii T, Kurahashi H.	Placental genetic variants in the upstream region of the *FLT1* gene in pre-eclampsia.	**J Reprod Infertil**	21(4)	240-246	2020
Kawai M, Kato T, Tsutsumi M, Shinkai Y, Inagaki H, Kurahashi H.	Molecular analysis of low-level mosaicism of the IKBKG mutation using the X chromosome inactivation pattern in incontinentia pigmenti.	**Mol Genet Genomic Med**.	-	e1531	2020
Miura H, Kawamura Y, Ohye T, Hattori F, Kozawa K, Ihira M, Yatsuya H, Nishizawa H, Kurahashi H, Yoshikawa T.	Inherited chromosomally integrated human herpesvirus 6 is a risk factor for spontaneous abortion.	**J Infect Dis**	-	jiaa606	2020
Tsukamoto K, Shinzawa N, Kawai A, Suzuki M, Kidoya H, Takakura N, Yamaguchi H, Kameyama T, Inagaki H, Kurahashi H, Horiguchi Y, Doi Y.	The Bartonella autotransporter BafA activates the host VEGF pathway to drive angiogenesis.	**Nat Commun**	11(1)	3571	2020
Yokoi K, Nakajima Y, Matsuoka H, Shinkai Y, Ishihara T, Maeda Y, Kato T, Katsuno H, Masumori K, Kawada K, Yoshikawa T, Ito T, Kurahashi H.	Impact of DPYD, DPYS, and UPB1 gene variations on severe drug-related toxicity in patients with cancer.	**Cancer Sci**	144(1)	111(9)	2020

Yasuda T, Sanada M, Nishijima D, Kanamori T, Iijima Y, Hattori H, Saito A, Miyoshi H, Ishikawa Y, Asou N, Usuki K, Hirabayashi S, Kato M, Ri M, Handa H, Ishida T, Shibayama H, Abe M, Iriyama C, Karube K, Nishikori M, Ohshima K, Kataoka K, Yoshida K, Shiraishi Y, Goto H, Adachi S, Kobayashi R, Kiyoi H, Miyazaki Y, Ogawa S, Kurahashi H, Yokoyama H, Manabe A, Iida S, Tomita A, Horibe K.	Clinical utility of target capture-based panel sequencing in hematological malignancies: A multicenter feasibility study.	**Cancer Sci**	111(9)	3367-3378	2020
Kato T, Inagaki H, Miyai S, Suzuki F, Naru Y, Shinkai Y, Kato A, Kanyama K, Mizuno S, Muramatsu Y, Yamamoto T, Shinya M, Tazaki Y, Hiwatashi S, Ikeda T, Ozaki M, Kurahashi H.	The involvement of U-type dicentric chromosomes in the formation of terminal deletions with or without adjacent inverted duplications.	**Hum Genet**	139(11)	1417-1427	2020
Ikeda M, Taniguchi-Ikeda M, Kato T, Shinkai Y, Hagiwara H, Sasaki N, Masaki T, Matsumura K, Sonoo M, Kurahashi H, Saito F.	Unexpected mutations by CRISPR/Cas9 CTG repeat excision in myotonic dystrophy and use of CRISPR interference as an alternative approach.	**Mol Ther Methods Clin Dev**	18	131-144	2020
Kawamura R, Kato T, Miyai S, Suzuki F, Naru Y, Kato Tanaka M K, Nagasaka M, Tsutsumi M, Inagaki H, Ioroi T, Yoshida M, Nao T, Conlin L K, Iijima K, Kurahashi H, Taniguchi-Ikeda M.	A case of a partheno genetic 46,XX/46,XY chimera presenting ambiguous genitalia.	**J Hum Genet**	65(8)	705-709	2020
Kato T, Kawai M, Miyai S, Suzuki F, Tsutsumi M, Mizuno S, Ikeda T, Kurahashi H.	Analysis of the origin of double mosaic aneuploidy in two cases.	**Cytogenet Genome Res**	160(3)	118-123	2020
Kato M, Yagami A, Tsukamoto T, Shinkai Y, Kato T, Kurahashi H.	Novel mutation in the KITLG gene in familial progressive hyperpigmentation with or without hypopigmentation.	**J Dermatol**	47(6)	669-672	2020
Miura H, Ohye T, Kozawa K, Hattori F, Kawamura Y, Ihira M, Kurahashi H, Yoshikawa T.	Coinfection with human herpesvirus (HHV)-6B in immunocompetent, healthy individuals with chromosomally integrated HHV-6A.	**J Pediatric Infect Dis Soc**	10(2)	175-178	2020

doi:10.1093/brain/awab056 BRAIN 2021: Page 1 of 17 | 1

BRAIN
A JOURNAL OF NEUROLOGY

Biallelic variants in *LIG3* cause a novel mitochondrial neurogastrointestinal encephalomyopathy

Elena Bonora,[1,†] Sanjiban Chakrabarty,[2,†] Georgios Kellaris,[3,†] Makiko Tsutsumi,[4,†] Francesca Bianco,[1,‡] Christian Bergamini,[5,‡] Farid Ullah,[3] Federica Isidori,[1] Irene Liparulo,[5] Chiara Diquigiovanni,[1] Luca Masin,[5] Nicola Rizzardi,[5] Mariapia Giuditta Cratere,[1,6] Elisa Boschetti,[1] Valentina Papa,[7] Alessandra Maresca,[8] Giovanna Cenacchi,[7] Rita Casadio,[9] Pierluigi Martelli,[9] Ivana Matera,[10] Isabella Ceccherini,[10] Romana Fato,[5] Giuseppe Raiola,[11] Serena Arrigo,[10] Sara Signa,[10] Angela Rita Sementa,[10] Mariasavina Severino,[10] Pasquale Striano,[10] Chiara Fiorillo,[10] Tsuyoshi Goto,[12] Shumpei Uchino,[13,14] Yoshinobu Oyazato,[15] Hisayoshi Nakamura,[16] Sushil K. Mishra,[17] Yu-Sheng Yeh,[12] Takema Kato,[4] Kandai Nozu,[18] Jantima Tanboon,[16] Ichiro Morioka,[19] Ichizo Nishino,[16] Tatsushi Toda,[20] Yu-ichi Goto,[21] Akira Ohtake,[22] Kenjiro Kosaki,[23] Yoshiki Yamaguchi,[24] Ikuya Nonaka,[16] Kazumoto Iijima,[18] Masakazu Mimaki,[13] Hiroki Kurahashi,[4] Anja Raams,[2] Alyson MacInnes,[25] Mariel Alders,[26] Marc Engelen,[27] Gabor Linthorst,[25] Tom de Koning,[28] Wilfred den Dunnen,[29] Gerard Dijkstra,[30] Karin van Spaendonck,[26] Dik C. van Gent,[2] Eleonora M. Aronica,[31] Paolo Picco,[10] Valerio Carelli,[7,8,§] Marco Seri,[1,§] Nicholas Katsanis,[3,§] Floor A. M. Duijkers,[26,§] Mariko Taniguchi-Ikeda[4,18,32,§] and Roberto De Giorgio[33,§]

[†,‡,§]These authors contributed equally to this work.

Abnormal gut motility is a feature of several mitochondrial encephalomyopathies, and mutations in genes such as *TYMP* and *POLG*, have been linked to these rare diseases. The human genome encodes three DNA ligases, of which only one, ligase III (*LIG3*), has a mitochondrial splice variant and is crucial for mitochondrial health.

We investigated the effect of reduced LIG3 activity and resulting mitochondrial dysfunction in seven patients from three independent families, who showed the common occurrence of gut dysmotility and neurological manifestations reminiscent of mitochondrial neurogastrointestinal encephalomyopathy. DNA from these patients was subjected to whole exome sequencing. In all patients, compound heterozygous variants in a new disease gene, *LIG3*, were identified. All variants were predicted to have a damaging effect on the protein. The *LIG3* gene encodes the only mitochondrial DNA (mtDNA) ligase and therefore plays a pivotal role in mtDNA repair and replication. *In vitro* assays in patient-derived cells showed a decrease in LIG3 protein levels and ligase activity. We demonstrated that the *LIG3* gene defects affect mtDNA maintenance, leading to mtDNA depletion without the accumulation of multiple deletions as observed in other mitochondrial disorders. This mitochondrial dysfunction is likely to cause the phenotypes observed in these patients. The most prominent and consistent clinical signs were severe gut dysmotility and neurological abnormalities, including leukoencephalopathy, epilepsy, migraine, stroke-like episodes, and neurogenic bladder. A decrease in the number of myenteric neurons, and increased fibrosis and elastin levels were the most prominent changes in the gut. Cytochrome *c* oxidase (COX) deficient fibres in skeletal muscle were also observed. Disruption of *lig3* in zebrafish reproduced the brain alterations and impaired gut transit *in vivo*.

Received April 25, 2020. Revised November 13, 2020. Accepted December 9, 2020.

In conclusion, we identified variants in the *LIG3* gene that result in a mitochondrial disease characterized by predominant gut dysmotility, encephalopathy, and neuromuscular abnormalities.

1 Department of Medical and Surgical Sciences, St. Orsola-Malpighi Hospital, University of Bologna, Bologna, 40138, Italy
2 Department of Molecular Genetics, Erasmus MC, Rotterdam, 3000 CA, The Netherlands
3 Center for Human Disease Modeling, Duke University, Durham, NC 27710, USA
4 Division of Molecular Genetics, Institute for Comprehensive Medical Science, Fujita Health University, Aichi, 470-1192, Japan
5 Department of Pharmacy and Biotechnology, University of Bologna, Bologna, 40126, Italy
6 Division of Genetics and Cell Biology, San Raffaele Scientific Institute, Milan, 20132, Italy
7 Department of Biomedical and Neuromotor Sciences, University of Bologna, Bologna, 40123, Italy
8 IRCCS Istituto delle Scienze Neurologiche di Bologna, Programma di Neurogenetica, Bologna, 40139, Italy
9 Biocomputing Group, Department of Biological, Geological, Environmental Sciences, University of Bologna, Bologna, 40126, Italy
10 IRCCS Istituto Giannina Gaslini, Genova, 16128, Italy
11 Department of Paediatrics, Pugliese-Ciaccio Hospital, Catanzaro, 88100, Italy
12 Laboratory of Molecular Function of Food, Division of Food Science and Biotechnology, Graduate School of Agriculture, Kyoto University, Uji, 611-0011, Japan
13 Department of Pediatrics, Teikyo University School of Medicine, Tokyo, 173-8605, Japan
14 Department of Pediatrics, Graduate School of Medicine, The University of Tokyo, Tokyo, 113-0033, Japan
15 Department of Pediatrics, Kakogawa Central City Hospital, Kakogawa, Hyogo, 675-8611, Japan
16 Department of Neuromuscular Research, National Institute of Neuroscience, National Center of Neurology and Psychiatry, Tokyo, 187-8502, Japan
17 Glycoscience Group, National University of Ireland, Galway, H91 CF50, Ireland
18 Department of Pediatrics, Kobe University Graduate School of Medicine, Hyogo, 650-0017, Japan
19 Department of Pediatrics and Child Health, Nihon University School of Medicine, Tokyo, 173-8610, Japan
20 Department of Neurology, Graduate School of Medicine, The University of Tokyo, Tokyo, 113-0033, Japan
21 Department of Mental Retardation and Birth Defect Research, National Institute of Neuroscience, National Center of Neurology and Psychiatry, Tokyo, 187-8502, Japan
22 Department of Pediatrics & Clinical Genomics, Faculty of Medicine, Saitama Medical University, Saitama, 350-0495, Japan
23 Center for Medical Genetics, Keio University School of Medicine, Tokyo, 160-8582, Japan
24 Laboratory of Pharmaceutical Physical Chemistry, Tohoku Medical and Pharmaceutical University, Miyagi, 981-8558, Japan
25 Department of Metabolic Diseases, Amsterdam UMC, University of Amsterdam, Amsterdam, 1100 DD, The Netherlands
26 Department of Clinical Genetics, Amsterdam UMC, University of Amsterdam, Amsterdam, 1100 DD, The Netherlands
27 Department of Neurology, Amsterdam UMC, University of Amsterdam, Amsterdam, 1100 DD, The Netherlands
28 Department of Metabolic Diseases, UMCG, Groningen, 9700 RB, The Netherlands
29 Department of Pathology, UMCG, Groningen, 9700 RB, The Netherlands
30 Department of Gastroenterology, UMCG, Groningen, 9700 RB, The Netherlands
31 Department of Pathology, Amsterdam UMC, University of Amsterdam, Amsterdam, 1100 DD, The Netherlands
32 Department of Clinical Genetics, Fujita Health University Hospital, Aichi, 470-1192, Japan
33 Department of Morphology, Surgery and Experimental Medicine, St. Anna Hospital, University of Ferrara, Ferrara, 44124, Italy

Correspondence to: Professor Roberto De Giorgio
Department of Morphology, Surgery and Experimental Medicine, University of Ferrara, 44124 Ferrara, Italy
E-mail: roberto.degiorgio@unife.it

Correspondence may also be addressed to: Dr Floor A. Duikers
Department of Clinical Genetics. Amsterdam University Medical Centers, University of Amsterdam, 1105 AZ, Amsterdam, The Netherlands
E-mail: f.a.duijkers@amsterdamumc.nl

Associate professor Mariko Taniguchi-Ikeda
Department of Clinical Genetics, Fujita Health University Hospital, 1-98, Dengakugakubo, Kutsukake-cho Toyoake, Aichi 470-1192, Japan
E-mail: mtani@fujita-hu.ac.jp or taniguchi_mariko@me.com

Keywords: mtDNA repair; mtDNA replication; *LIG3*; MNGIE; CIPO

Abbreviations: CIPO = chronic intestinal pseudo-obstruction; dpf = days-post-fertilization; MNGIE = mitochondrial neurogastrointestinal encephalomyopathy; MO = morpholino; USC = urothelial sediment cell; WES = whole exome sequencing

Introduction

The human genome encodes three DNA ligases (I, III and IV). All DNA ligases are expressed in the nucleus, but only ligase III (*LIG3*) has a mitochondrial splice variant. Nuclear LIG3 interacts with X-ray repair cross-complementing protein 1 (XRCC1) for DNA maintenance by base excision repair, but other nuclear ligases can compensate for defects in the *LIG3* gene, which encodes the LIG3 protein.[1-5] However, LIG3 is crucial in mitochondria, as it is the only ligase responsible for mitochondrial DNA (mtDNA) replication and maintenance, working along with mtDNA polymerase gamma (POLG) and other mtDNA replisome factors.[6] The lethality of a *LIG3* null mutation can be alleviated by targeting another DNA ligase to mitochondria, whereas overexpression of the LIG3 protein appears to increase the resistance to oxidative damage in mitochondria.[7] Therefore, reduced LIG3 activity is expected to affect mitochondrial health and would lead to diseases resulting from mitochondrial dysfunction.

A key clinical feature of several mitochondrial diseases is severely abnormal gut motility, such as in patients with chronic intestinal pseudo-obstruction (CIPO). This is an impairment of gut propulsion, mimicking a mechanical obstruction without detectable anatomical causes.[8-10] Mitochondrial encephalomyopathies may also be characterized by prevalent leukoencephalopathy caused by mitochondrial dysfunction.[6] Mitochondrial neurogastrointestinal encephalopathy (MNGIE), the 'tip of the ice-berg' of such rare diseases, is caused by mutations in the *TYMP* gene, which encodes thymidine phosphorylase.[11] Similar phenotypes are also caused by mutations in *POLG*, or mutations in the mtDNA itself, as observed in patients with mitochondrial encephalomyopathy with lactic acidosis and stroke-like episodes (MELAS).[12]

We here report a novel mitochondrial gastrointestinal encephalomyopathy caused by biallelic variants in *LIG3*,[1,3,13,14] leading to a syndrome predominantly characterized by severe gut dysmotility (i.e. CIPO) and encephalomyopathy.

Patients and methods

In the present study, analyses of the patients were performed in three different institutes, which led to some differences in the methods used per family, as detailed below.

Ethical approval

Data from patients and controls were handled in accordance with the local ethics committees (St. Orsola Hospital Ethics Committee; Institutional Review Board of Kobe University School of Medicine and Medical Ethical Board of Amsterdam University) and analyses were performed after obtaining written informed consent from the patients or patients' parents, according to the declaration of Helsinki.

Next-generation sequencing analysis

Families were recruited from different institutions as follows: Italy, Family 1, Patients 1-1, 1-2, and 1-3; The Netherlands, Family 2, Patients 2-1 and 2-2; and Japan, Family 3, Patients 3-1 and 3-2. Details of patients are provided in the Supplementary material.

Sample collection and immunohistochemistry

Muscle, gut, skin and urothelial sediment cells (USCs) were collected and histologically analysed as described in the Supplementary material. Procedures for western blot analyses are also provided in the Supplementary material.

Immunofluorescence: Family 1

Immunofluorescence analysis was performed as described in the Supplementary material. The following primary antibodies were used: rabbit anti-LIG3 (26583-1-AP; 1:50, ProteinTech). Secondary antibodies used were the following: Alexa Fluor® 488 goat anti-rabbit IgG, Alexa Fluor® 555 goat anti-rabbit (all from Abcam; 1:800).

Analysis of mtDNA content by real-time quantitative PCR

Family 1

Total DNA was extracted from fibroblasts using the Qiagen Mini kit and from muscle biopsies by standard phenol-chloroform extraction. Real-time quantitative PCR was used to assess mtDNA content according to previously validated methods.[15]

Family 2

The mtDNA/nuclear DNA (nDNA) ratio was measured in duplicate on freshly obtained muscle tissue in a diagnostic setting (Radboud UMC Laboratory, The Netherlands) and compared to age-matched controls (above the age of 21 years) from reports in the literature.[16]

Family 3

Total DNA was extracted from fibroblasts or myoblasts using DNeasy Blood and Tissue Kit (Qiagen). The Human mtDNA Monitoring Primer Set (Takara) was used for amplification of mtDNA and nDNA. Real-time PCR was performed using SYBR Premix Ex Taq II (Takara) and 7300 Real-Time PCR System (Thermo Fisher) according to previously published protocols.[17,18]

DNA ligase assay: Patient 2-1

Mitochondrial protein extracts were prepared from primary fibroblasts as previously described.[19] Ligation of linearized pUC18 plasmid using mitochondrial extracts was performed as previously reported.[19] Briefly, PstI-linearized pUC18 was incubated at 16°C for 16 h with mitochondrial extracts

from control and mutant samples. Plasmid DNA was subsequently deproteinized, purified and separated on 1.2% analytical agarose gels. Reactions were supplemented by the addition of ATP; T4 DNA ligase (New England Biolabs) was used as a positive control. Each ligation assay was performed twice.

Quantitative PCR-based analysis of mtDNA repair activity

Wild-type and *LIG3*-mutant fibroblasts (10^6) from Patient 2-1 were seeded in 6-cm dishes 16–18 h prior to the experiments. Cells were washed once with Ham's F-10 medium without supplements, and the conditioned medium was used subsequently. Cells were exposed to 200 μM H_2O_2 for 15 min and harvested immediately or cultured with conditioned medium for 6 h. High-molecular weight genomic DNA was extracted from untreated or H_2O_2-treated wild-type and *LIG3*-mutant cell lines using Wizard® SV Genomic DNA Purification System (Promega). The quantitative PCR reaction was performed with the LongAmp® Taq PCR kit (New England Biolabs) as follows: 15 ng total DNA was added to a reaction mix of 50 μl with 100 ng/μl bovine serum albumin, 200 μM dNTPs each, 1–3 mM $MgO(Ac)_2$, and 20 pmol each of the two primers. PCR was performed with primer pairs to amplify an 8.9-kb fragment of mtDNA (long), and in a separate reaction to amplify a 221-bp fragment of mtDNA (short), to calculate mtDNA damage and copy number in untreated and H_2O_2-treated samples, respectively.[17] The primer sequences used were as previously described.[17] PCR products for both long and short mitochondria amplicons were quantified using the PicoGreen™ dsDNA quantification assay (Thermo Fisher). Fluorescent values obtained from the short PCR products of each sample were used to normalize the results from the long PCR products. These values were used to estimate the average number of lesions per 10 kb mitochondrial genome using a Poisson distribution.[17] Relative amplification was calculated by comparing treated samples with untreated samples for both wild-type and mutant cells and the unpaired *t*-test was performed for statistical analysis.

Ethidium bromide treatment: Patient 3-2

Fibroblasts were cultured in the presence of 50 ng/ml ethidium bromide (EtBr), 1 mM pyruvate, and 50 μg/ml uridine for 9 days followed by culturing without EtBr for 7 days. Subcultures were performed every 2 to 3 days to keep the confluency of the cells between 30% and 80%.

Mitochondrial oxygen consumption

Patient 1-1

To measure mitochondrial oxygen consumption 1.5×10^6 cells for each cell type (wild-type and Patient 1-1-derived fibroblasts) were harvested, washed in PBS, resuspended in complete medium and assayed for oxygen consumption at 37°C using a thermostatically regulated oxygraph chamber (Instech Mod.203). Basal respiration was measured in Dulbecco's modified Eagle medium and compared with data obtained after the injection of oligomycin (1 μM) and carbonyl cyanide 4-(trifluoromethoxy) phenylhydrazone (FCCP) (1–6 μM). Antimycin A (5 μM) was added at the end of the experiments to completely block the mitochondrial respiration.[20] Respiratory rates were expressed in nmol O_2/min/mg of total protein, which was determined by the Lowry assay.

Patient 3-2

In USCs, basal and maximal oxygen consumption rates (OCR) were analysed using Seahorse Bioscience XF-24 extracellular flux bioanalyzer (Agilent) and Seahorse XF Cell Mito Stress Test. USCs were seeded onto XF 24-well microplates in growth medium at 1.5×10^5/well ($n = 5$). The next day, growth medium was replaced with assay medium supplemented with glucose, pyruvate and L-glutamine, and the pH was adjusted to 7.4. Cells were equilibrated prior to Mito Stress testing in the analysis medium for 30 min at 37°C in a CO_2-free incubator. ATP-linked respiration was determined by oligomycin (1 μM) and maximal respiration was induced using FCCP (1 μM). Nonmitochondrial respiration was determined after injection of rotenone and antimycin A (1 μM each). Data were analysed using XF Cell Mito Stress Test Report Generator. After assay completion, cells were rinsed with PBS and frozen. After thawing, double stranded DNA of each well was measured using DNA Quantity kit (Cosmo BIO) using a microplate reader.

ATP determination: Patient 1-1

Nucleotides were extracted and detected using a Kinetex C18 column (250 × 4.6 mm, 100 Å, 5 μm; Phenomenex) with a two pump Agilent 1100 series system (Agilent).[21] Absorbance (260 nm) was monitored with a photodiode array detector (Agilent 1100 series system). Nucleotide peaks were identified by comparison and coelution with known standards and quantification by peak area measurement compared with standard curves.

Zebrafish husbandry

Embryos were obtained by natural mating of wild-type adults (TU/AB strain, Aquatica BioTech). Adults were maintained on a 14-h/10-h day/night cycle. Larvae were nurtured in embryo media (0.3 g/l NaCl, 75 mg/l $CaSO_4$, 37.5 mg/l $NaHCO_3$ and 0.003% methylene blue) at 28°C until phenotypic analysis at 3 days post fertilization (dpf), 5 dpf and 8 dpf, respectively. All zebrafish studies were approved by the Duke University Institutional Animal Care and Use Committee.

Gene suppression and complementation in zebrafish embryos

A splice-blocking morpholino (MO) was designed to target the *Danio rerio lig3* exon 11 splice donor (e11i11) and was

synthesized by Gene Tools LLC. To identify the optimal dose for *in vivo* complementation, a dose curve was generated by injecting 2, 4 and 6 ng (1 nl MO per embryo; one- to four-cell stage) into TU/AB embryos. Total RNA was extracted from 1 dpf embryos (15–20 per condition) using TRIzol® (Thermo Fisher) and was reverse transcribed using the SuperScript® III Reverse Transcriptase kit (Thermo Fisher). We used cDNA as the template for RT-PCR with primers flanking the *lig3* MO target site. PCR products were purified with QIAquick gel extraction kit (Qiagen) and cloned in TOPO-TA cloning vector (Thermo Fisher). Plasmids were purified and Sanger sequenced according to standard protocols. For rescue experiments, wild-type human *LIG3* open reading frame (Ultimate ORF collection; Clone ID: IOH40893) was subcloned into the pCS2+ vector by LR Clonase II®-mediated recombination (Thermo Fisher). To produce constructs containing the sequences of patient-associated variants, site-directed mutagenesis was performed.[22] Constructs were linearized with *NotI*, and the resulting template was transcribed with the mMessage mMachine® SP6 transcription kit (Thermo Fisher). Unless otherwise noted, 6 ng *lig3* MO was used either alone or in combination with 200 pg *LIG3* mRNA for *in vivo* complementation studies.

CRISPR/Cas9 genome editing of zebrafish embryos

Guide (g) RNAs targeting the *lig3*-coding region were designed with CHOPCHOP. A GeneArt precision gRNA synthesis kit (Thermo Fisher) was used to *in vitro* transcribe gRNAs, followed by injection of 1 nl of injection cocktail containing 100 pg/nl gRNA and 200 pg/nl Cas9 protein (PNA Bio) directly into the cell of TU/AB embryos (one-cell stage). Heteroduplex assays were used to determine targeting efficiency in founder (F0) mutants.[23,24] Genomic DNA was extracted from 2 dpf embryos. The region flanking the gRNA target site was amplified by PCR; PCR products were denatured (95°C for 2 min), reannealed (–2°C/s to 85°C and –0.1°C to 25°C), separated on a 15% TBE 1.0-mm polyacrylamide gel, stained with EtBr and imaged using the Chemi-Doc system (Bio-Rad). To estimate the percentage of mosaicism of *lig3* F0 mutants ($n = 5$), PCR products were gel-purified with QIAquick Gel extraction kit (Qiagen), cloned into the TOPO-TA vector (Thermo Fisher) and plasmids were isolated from individual colonies ($n = 10$–12 colonies/embryo) and Sanger sequenced according to standard procedures.

Phenotypic analysis of zebrafish larvae

Whole-mount immunostaining with anti-acetylated tubulin (T7451, Sigma-Aldrich) and anti-HuC/D (A-21271, Thermo Fisher) antibodies was performed to analyse the brain and enteric neurons along the gastrointestinal tract, respectively. Smooth muscle morphology of the gastrointestinal tract was assessed using the anti-phospho-myosin light chain 2 antibody (Ser19; 9970, CST). To quantify neurons in the cerebellar area, whole-mount acetylated tubulin immunostaining was performed.[22,25] Dorsal images were acquired manually with an AxioZoomV.16 microscope (Zeiss) and Axiocam 503 monochromatic camera (Zeiss). Cerebellar structures of interest were measured using ImageJ software. Total cerebellar area was measured blindly by two experts on acetylated tubulin-stained larvae by outlining the structures with a fluorescent signal. Quantitative evaluation of enteric neurons was performed via HuC/D staining in injected embryos at 5 dpf. For phospho-myosin staining, injected embryos were analysed at 8 dpf. Fluorescent cell counts were performed with ImageJ software. To assess peristalsis of the zebrafish gut, embryos at 8 dpf were anesthetized using 1× tricaine embryo media. Gastrointestinal motility was recorded with 2-min time lapse videos.

Statistical analysis

Chi-squared (χ^2), ANOVA and two-tailed parametric *t*-tests were performed as reported in the corresponding 'Results' sections and figure legends, using GraphPad Prism software v.7.00 (GraphPad). *P*-values < 0.05 were considered to indicate a statistically significant difference between two groups. For statistical analysis of cerebellum measurements in zebrafish, a non-parametric one-way ANOVA followed by the Tukey multiple comparison test was performed. For the gut peristalsis assay, the χ^2 test was used to perform pairwise statistical comparisons across experimental conditions.

The analysis of mtDNA deletions by droplet digital PCR, RNA extraction and transcript analysis, ultrastructural analysis, mitochondrial network analysis, reactive oxygen species quantification, and measurement of transmembrane potential are described in the Supplementary material.

Data availability

The authors confirm that the data supporting the findings of this study are available within the article and its Supplementary material.

Results

Clinical features of the patients

In seven affected individuals from three separate families compound heterozygous variants in the *LIG3* gene were identified by whole exome sequencing (WES) (Fig. 1A–C). These patients showed a largely overlapping phenotype and an overview of their clinical features is presented in Table 1. The clinical histories of each patient can be found in the Supplementary material. The clinical features of these patients for many aspects resembled the mitochondrial

disease MNGIE. Severe dysmotility of the gut was present in all patients and most patients fulfilled the diagnostic criteria for CIPO.[8-10,26] Brain MRI of all patients showed leukoencephalopathy and/or progressive cortical atrophy, whereas cerebellar atrophy was observed only in patients from Family 3 (Fig. 1D–F). In addition to the MNGIE-like features, all patients had other neurological features including epilepsy, stroke-like episodes, migraine and developmental delay, reminiscent of MELAS. Further clinical manifestations included neurogenic bladder and macular degeneration, which were present in most patients. Hearing loss was only observed in one patient (Table 1). Increased lactate/pyruvate ratio in the CSF was found in the patients of Family 3. Although the clinical phenotype was quite consistent across the three families, the age of onset and disease severity differed considerably ranging from paediatric severe disease with premature death to adult cases. In particular, the two patients of Family 3 manifested as infants with severe gut dysmotility, severe developmental delay and epilepsy, interpreted as West syndrome.[27] One of the two children in this family died at the age of 2 years. Conversely, the disease onset occurred much later in the three patients from Family 1 (between the ages of 9 and 10 years), with a rapid disease progression. The presentation in Family 2 was even later, with some features detectable at paediatric age, but the most severe manifestations only occurring at adult age with a slower disease progression compared with the other two families.

Evidence of mitochondrial dysfunction in patient tissue

Skeletal muscle biopsies of patients from all three families (Patients 1-1, 2-2 and 3-2) showed alterations that are observed in patients with mitochondrial myopathies, e.g. succinate dehydrogenase (SDH) hyper-reactivity, reduced cytochrome *c* oxidase (COX)-staining (Supplementary Fig. 1A–C) and altered myofibre structure (Patient 3-2) on electron microscopy (Supplementary Fig. 1D). Nevertheless, these muscle alterations were variable/subtle, as compared with the severe clinical phenotype observed in the gut and CNS of the patients.

Identification of *LIG3* mutations

The recurrent phenotype of CIPO and neuromuscular involvement in all sibs, along with unaffected parents, suggested a recessive disorder, with a possible mitochondrial aetiology. In all three families we identified compound heterozygous variants in *LIG3*, shared by the corresponding affected sibs and inherited from the corresponding heterozygous healthy parents (Fig. 2A and Supplementary Fig. 2A–C). The variants in Family 1 (p.K537N and p.G964R missense variants) were not present in public databases (Database of Single Nucleotide Polymorphisms, dbSNP; Genome Aggregation Consortium, gnomAD; ClinVar; 1000Genomes) or in an inhouse database (650 Italian exomes). In Family 2 the missense variant p.C999Y was novel and the premature stop codon p.R267Ter was present in dbSNP with a very low minor allele frequency (MAF) (Supplementary Table 1). In Family 3 we identified the missense variant p.P609L and the premature stop codon p.R811Ter. Both variants were present in dbSNP and gnomAD with a very low MAF (Supplementary Table 1). No deleterious variants in other genes compatible with a recessive or *de novo* inheritance were detected. All variants mapped to the conserved LIG3 domains[28,29] and *in silico* analyses predicted their pathogenicity (Fig. 2A, Supplementary Fig. 2D and Supplementary Tables 1 and 2).[30,31] No causative point mutations or deletions in mtDNA were identified in Patients 1-1, 2-2 and 3-2.

LIG3 mRNA and protein analysis

Detailed analyses on the consequences of the *LIG3* mutations were conducted using primary skin fibroblasts derived from Patients 1-1, 2-1 and 3-2. The missense p.K537N variant identified in Family 1, mapping to the most 3′ nucleotide of exon 9, was predicted to alter splice-site recognition (Human Splicing Finder v3.0, HSF; Supplementary Fig. 3A). RT-PCR with the primers in exon 8 and exon 10 showed only one band of the expected size for exon 9 inclusion in control cDNA, but the cDNA from patient cells also gave rise to a shorter transcript lacking exon 9 (Fig. 2B). Exon 9 skipping results in a protein lacking 52 amino acids (495–537 in-frame deletion) in the conserved adenylation-nucleotidyltransferase (NTase) domain of the ATP- and POLG-binding regions (Fig. 2C).[13,14,28] Exon skipping in this mutant protein results in the loss of ~5 kDa of the LIG3 protein. However, we detected a severe reduction in the total amount of LIG3 protein without the appearance of a shorter LIG3 species on western blot analysis of control and patient fibroblast lysates (Fig. 2D) (a severe reduction in expression is also shown in Supplementary Fig. 3B–D). Concordantly, transient transfection of the cDNA encoding for human *LIG3* carrying the exon 9 deletion in HEK293 cells did not show any band smaller than that of the wild-type LIG3 protein (Supplementary Fig. 3E), suggesting that the protein is early degraded. Although in Patient 1-1 fibroblasts the exon 9 variant gave rise to exon skipping, we also evaluated its potential effect as missense change p.K537N in transient transfection of HEK293: the protein product was present (Supplementary Fig. 3F), but the co-immunoprecipitation assay using an antibody against LIG3, followed by western blotting for POLG, showed a very low affinity for POLG compared to wild-type LIG3 (Supplementary Fig. 3G). Based on western blot results in fibroblasts, we assumed that, in the Patient 1-1 fibroblasts, only the other human LIG3 allele (p.G964R) was expressed at the protein level and that this amino acid change caused reduced stability. In line with these observations, transient transfection of the cDNA encoding for human LIG3 with the missense change p.G964R in HEK293 revealed that LIG3 expression was comparable to that of the empty vector, at difference with

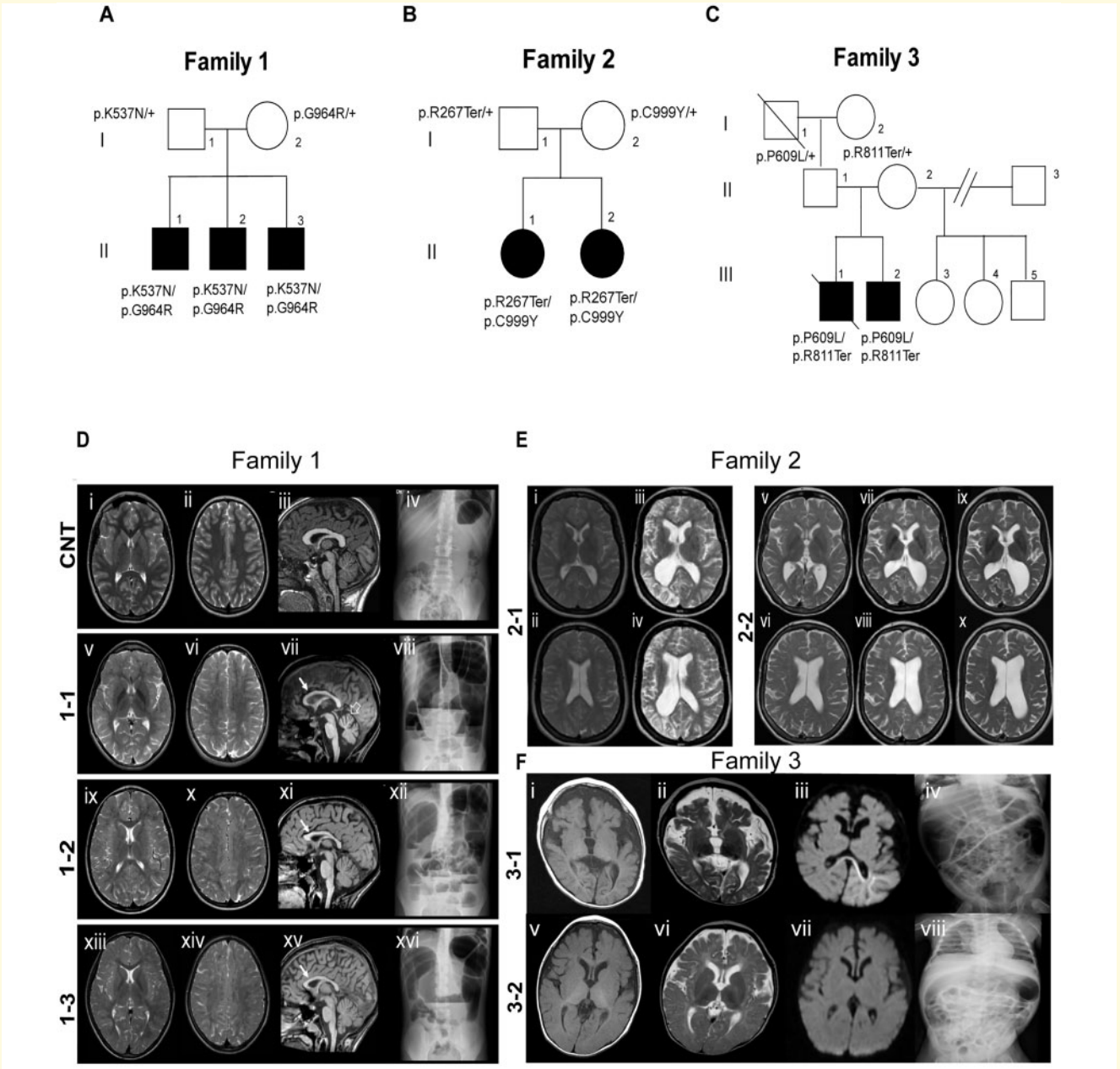

Figure 1 Identification of *LIG3* mutations. (**A**–**C**) Pedigrees of the three families with *LIG3* mutations. Filled and open symbols denote affected and healthy individuals, respectively; diagonal bars indicate deceased members. (**A**) Family 1: inheritance of paternal p.K537N and maternal p.G964R variants in the three affected brothers. (**B**) Family 2: inheritance of paternal p.R267Ter and maternal p.C999Y variants in the two affected sisters. (**C**) Family 3: inheritance of paternal p.P609L and maternal p.R811Ter variants in the two affected brothers. (**D**) Brain MRI and abdominal X-ray images of the patients in Family 1. (**ii**) Axial T_2-weighted, and (**iii**) sagittal T_1-weighted images of a control subject (CNT) demonstrating normal supratentorial white matter, corpus callosum and cerebellar vermis. Corresponding images for Patients 1-1 (**v**–**vii**), 1-2 (**ix**–**xi**) and 1-3 (**xiii**–**xv**) demonstrate leukoencephalopathy (involving periventricular and subcortical white matter, corpus callosum and internal capsules) characterized by diffuse but irregular T_2 hyperintensities with a peculiar 'leopard-skin' pattern due to the sparing of small white matter islets. Arrows (**vii**, **xi** and **xv**) indicate mild callosal hypoplasia. Patient 1-1 shows additional signs of cerebellar atrophy (**vii**, open arrow). (**viii**–**xvi**) Abdominal X-ray images displaying bowel dilatation with air-fluid levels compared with the control subject. (**E**) Brain MRI of the patients of Family 2. Axial T_2-weighted images of Patients 2-1 (*left*) and 2-2 (*right*) at different time points (**i**, t = 0 years and **iii**, t = +3 years; **v** and **vi**, t = 0; **vii** and **viii**, t = +2 years, **ix** and **x**, t = +4 years). In Patient 2-1 there is diffuse hyperintensity of the entire cerebral white matter. After several stroke-like episodes, progressive atrophy with asymmetrical '*ex vacuo*' dilatation of the ventricular system was noted. Patient 2-2 displays a similar pattern and evolution over time. (**F**) Brain MRI and abdominal X-ray images of patients in Family 3. In Patient 3-1 axial (**i**) T_1-weighted, (**ii**) T_2-weighted and (**iii**) diffusion-weighted images demonstrate brain atrophy and restricted diffusion in the left temporo-occipital, corticosubcortical regions extending to the corpus callosum. In Patient 3-2, brain MRI demonstrates generalized brain atrophy (**v**–**vii**). Abdominal X-ray images show marked bowel distension (**iv** and **viii**).

Table 1 Clinical features of the affected sibs with LIG3 compound heterozygous variants

	Patient 1-1	Patient 1-2	Patient 1-3	Patient 2-1	Patient 2-2	Patient 3-1	Patient 3-2
Current age, years	17	13	11	40	39	2 (deceased)	4
Age of onset, years	9	10	10	18	18	1	2
GI symptoms and surgery	Subacute and/or recurrent episodes of intestinal obstruction without an occluding lesion, malnutrition (parenteral nutrition), diarrhoea, ileostomy (at 16 years)	Subacute and/or recurrent episodes of intestinal obstruction without an occluding lesion, malnutrition (parenteral nutrition), abdominal distension and constipation, ileostomy (at 11 years)	Subacute and/or recurrent episodes of intestinal obstruction without an occluding lesion, diarrhoea/constipation, ileostomy (at 10 years)	Chronic intestinal pseudo-obstruction (18 years), TPN (from 33 years), enlarged liver, cholecystolithiasis	Chronic intestinal pseudo-obstruction (at 18 years), TPN (at 37 years).	Severe abdominal distension, hepatomegaly, NG tube (at 1 month)	Severe abdominal distension, hepatomegaly, NG tube (at 1 month), IVH (at 2 years)
Brain imaging	Diffuse leukoencephalopathy, cerebellar atrophy	Diffuse leukoencephalopathy, thin corpus callosum	Diffuse leukoencephalopathy	After a stroke-like event at 33 years, increasing degree of atrophy and gliosis over time, most prominent in parietal-occipital right hemisphere	Progressive diffuse leukoencephalopathy after stroke-like episodes	Leukoencephalopathy, cerebellar atrophy	Leukoencephalopathy, cerebellar atrophy
Neurological signs	Pyramidal signs, mild ataxia, dysmetria	Pyramidal signs	Pyramidal signs	Unilateral neglect and cognitive deterioration/decline after stroke-like episode at 33 years	Nystagmus and diminished feeling in the legs and cognitive deterioration at 36 years	Involuntary movements, jerks	Involuntary movements, jerks
Headache	Yes, complicated with motor deficits	Yes, complicated with motor deficits	Yes, complicated with motor deficits	Yes, migraine with aura, starting from teenage years	Yes, migraine with aura, starting from paediatric years	N/A	N/A
Psychiatric features	Repetitive pattern of behaviours and interests	Repetitive pattern of behaviours	None	None	None	N/A	N/A
Urogenital abnormalities	Neurogenic bladder, right mild pyelectasia	Neurogenic bladder	None	Possible voiding dysfunction, frequent retention bladder	Unilateral duplicated collecting system, frequent retention bladder	N/A	Neurogenic bladder
Additional features	Recurrent arthralgias, stomatitis, macular degeneration	Macular degeneration	None	Macular degeneration	Macular degeneration, frequent infections (recent years)	Apnoea, recurrent infections, pneumonia	Cataracts, hearing loss, dysphagia

GI = gastrointestinal; IVH = intravenous hydration; N/A = not assessed; NG = nasogastric; TPN = total parenteral nutrition.

the HEK293 cells transfected with wild-type LIG3 (Supplementary Fig. 3F). Molecular modelling showed that p.G964 interacts with p.R558 of murine XRCC1 (a residue conserved between human and murine proteins). The LIG3 variant p.G964R was predicted to hamper the interaction between LIG3 and XRCC1 because of the close proximity (0.44 nm) of two positively charged amino acids in the interacting site (p.R558 in XRCC1 and mutated p.R964; Supplementary Fig. 3H). This impairment prevented LIG3 translocation into the nucleus (Supplementary Fig. 3I).[1-3]

The compound heterozygous mutations in Family 2 (p.R267Ter and p.C999Y) were also analysed. RT-PCR on Patient 2-1 fibroblasts and controls showed that the c.799C>T allele (p.R267Ter variant) was not expressed, and only the c.2996G>A allele (p.C999Y variant) was present in the final transcript of the patient's fibroblasts (Fig. 2E), suggesting that mRNA carrying the c.799C>T variant (premature stop codon p.R267Ter) was degraded by nonsense-mediated decay. Transient transfection of HEK293 cells with the plasmid encoding the LIG3 p.C999Y variant did not show an increase in expression, compared to cells transfected with the empty vector, as seen for the vector with wild-type LIG3 (Supplementary Fig. 3F). Molecular modelling showed that the variant p.C999Y is predicted to severely destabilize LIG3 structure ($\Delta\Delta G$ = –2.02 kcal/mol; Supplementary Fig. 3H).[28-31] Western blot analysis in patient's fibroblasts indeed resulted in a marked decrease in LIG3 protein levels (Fig. 2D and Supplementary Fig. 3C).

The p.R811Ter variant in Family 3 was not expressed and only the c.1826C>T allele (p.P609L variant) was present in the final transcript (Fig. 2F), suggesting that mRNA carrying the c.2431C>T variant (premature stop codon p.R811Ter) was degraded by nonsense-mediated decay, as shown for the premature stop-codon found in patients of Family 2. The p.P609L variant, mapping to the end of an alpha-helix in the ATP-binding domain, was predicted to destabilize the protein ($\Delta\Delta G$ = –0.74 kcal/mol; Fig. 2C).[30,31]

Compared to controls, fibroblasts from Patient 3-2 showed very low amounts of LIG3 protein (Fig. 2D and Supplementary Fig. 3D), in agreement with the transient transfection of the construct carrying the p.P609L variant in HEK293 cells (Supplementary Fig. 3F). We also investigated whether protein instability could be rescued by the proteasome inhibitor MG132 which, however, evoked only a marginal increase of LIG3 levels in mutant cells (Supplementary Fig. 3D).

LIG3 mutations result in impaired ligase activity and mtDNA depletion

As LIG3 is the only mtDNA ligase, we investigated whether the ligase activity of mitochondrial extracts from patient cells was affected. The mitochondrial extracts from control and Patient 2-1 fibroblasts were incubated with linearized plasmid DNA (Fig. 3A). Indeed, mutant extracts were unable to religate the linearized plasmid DNA, whereas mitochondrial extracts from control cells showed clear ligation activity. Subsequently, the mtDNA ligation and repair capacity was analysed in control and patient fibroblasts, according to Furda et al.[17] Control and mutant cells were exposed to oxidative stress (H_2O_2 for 15 min) and then allowed to repair the DNA damage for 6 h (Fig. 3B). Normal fibroblasts showed a reduced amount of PCR amplification product directly after the H_2O_2 exposure and a significant recovery after 6 h ($P < 0.05$; Fig. 3B). However, mutant cells showed little or no recovery of intact mtDNA, consistent with a severe defect in mtDNA repair (Fig. 3B).

We also investigated whether mtDNA replication was affected. The replication capacity of mtDNA after EtBr treatment was impaired in fibroblasts from Patient 3-2. Control and patient cells lost their mtDNA content at a similar rate and after 9 days of EtBr treatment all cells contained only low levels of mtDNA (controls between 0.5% and 1.2%; patient 0.9% of the starting level). However, the controls showed a clear increase in mtDNA content 6 days after withdrawal of EtBr, whereas this recovery was not observed in the patient samples. This experiment demonstrates that the patient cells have a clearly decreased capacity of mtDNA replication, in addition to the previously shown impairment in mtDNA repair (Fig. 3C).

We subsequently investigated whether the *LIG3* defects also resulted in reduced mtDNA content. Quantitative assessment of mtDNA copy number in a skeletal muscle biopsy sample from Patient 1-1 demonstrated significant mtDNA depletion compared with controls ($P < 0.01$; Fig. 3D). In Patient 2-2, mtDNA content of the skeletal muscle biopsy was 66% of that in age-matched healthy controls (Supplementary Fig. 4A).[16] A significant decrease in mtDNA copy number was also observed in myoblasts derived from Patient 3-2 compared to controls ($P < 0.05$; Fig. 3E).

Patient 1-1-derived fibroblasts showed significant mtDNA depletion compared to controls ($P < 0.01$; Fig. 3F). Conversely, in skin-derived fibroblasts of Patient 3-2 mtDNA copy number was similar to control cells (Supplementary Fig. 4B).

A quantitative assessment of mtDNA deletions was performed as reported in the Supplementary material, but deletions were not detected in both fibroblasts and skeletal muscle of Patient 1-1 (Supplementary Fig. 4C and D).

Mitochondrial dysfunction caused by *LIG3* mutations

We next investigated how partial mtDNA depletion affected mitochondrial shape and function. Mitochondria were visualized with MitoTracker Green and analysed using confocal fluorescence microscopy. Overall, the mitochondria of mutant fibroblasts (Patient 1-1) displayed a fragmented network compared with control cells (Fig. 4A and Supplementary Fig. 5A–E). Compared to controls,

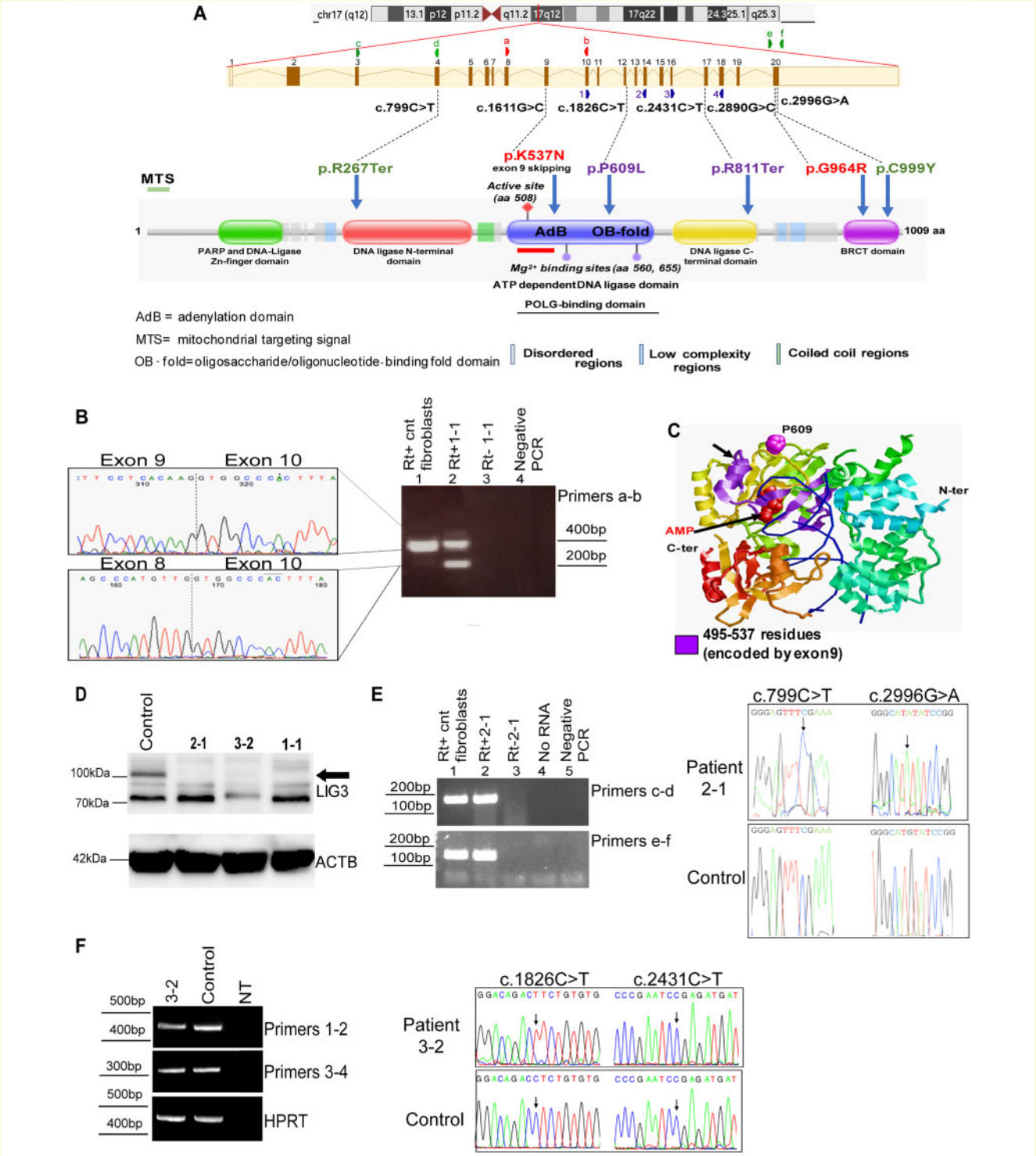

Figure 2 Identification of the molecular defects of *LIG3*. (**A**) Mutations mapped on the Pfam database (https://pfam.xfam.org/) domains of LIG3 [mitochondrial transport signal (MTS), ATP-binding domain, POLG and XRCC1-binding sites]. Variants in Family 1 are indicated in red, variants in Family 2 are indicated in green, and variants in Family 3 are indicated in violet. Arrowheads indicate the primer pairs used for subsequent RT-PCR analysis. aa = amino acids. (**B**) Splicing alteration induced by the p.K537N variant. Control fibroblasts (lane 1, cnt) show a band of the expected size for the transcript containing exon 9. Fibroblasts from Patient 1-1 (lane 2) show two bands: the higher band corresponds to the transcript with exon 9, and the lower band corresponds to a transcript without exon 9, as shown by the corresponding electropherograms. A cropped image of the gel electrophoresis is reported, without the marker lane (relevant sizes indicated; bp = base pairs). Lane 3: no RT = RT-PCR carried out without reverse transcriptase on Patient 1-1 mRNA; lane 4: negative control of RT-PCR (no template). (**C**) Structure of the ligase domain of human LIG3 (residues 257-833) in complex with DNA and AMP. The region encoded by exon 9 is in violet. The position p.P609 is represented in pink. (**D**) LIG3 western blot analysis in total cell lysates derived from human control and patient fibroblasts, showing a severely

(continued)

ultrastructural analysis in fibroblasts of Patient 1-1 showed qualitative and quantitative mitochondrial defects such as abnormal cristae and swollen mitochondria and a greater average mitochondrial area (0.011854 versus 0.00644 μm^2, respectively) (Supplementary Fig. 5F).

Analysis of the respiration rate confirmed the mitochondrial dysfunction in patient cells. We observed a significantly decreased uncoupled oxygen consumption (Fig. 4B) and lower ATP content (Fig. 4C) in Patient 1-1 fibroblasts. In addition, USCs which have high mitochondrial content,[32] were established from Patient 3-2 and tested for oxygen consumption rate. The results showed a decrease in oxygen consumption rate in USCs of Patient 3-2 compared with control USCs (Supplementary Fig. 5G). Although no differences in mitochondrial membrane potential were detected in intact control and Patient 1-1 fibroblasts (Supplementary Fig. 5H), in digitonin-permeabilized cells *LIG3*-mutant fibroblasts were less responsive to different respiratory substrates (glutamate malate, ADP, and succinate), inhibitors (oligomycin A and rotenone) and uncoupler (FCCP) compared to controls ($P = 0.0012$; Fig. 4D). MitoSOX^{TM} Red staining (a selective probe for mitochondrial superoxide) detected a significantly increased production of mitochondrial reactive oxygen species in mutant cells compared to control cells ($P = 0.0393$; Fig. 4E), confirming the mitochondrial dysfunction.[33]

As the addition of glutamine (6 mM) has been shown to increase the survival of cells carrying mitochondrial defects, but not control cells,[34] the glutamine concentration was increased in the culture medium from the standard 2 mM to 6 mM. In control fibroblasts a higher glutamine concentration resulted in a decreased growth rate (Supplementary Table 3), in agreement with previous findings,[34-36] indicating that in the absence of mitochondrial defects, excess glutamine may exert a detrimental effect. Conversely, fibroblasts from Patient 1-1 grew more efficiently when exposed to 6 mM than 2 mM glutamine (Fig. 4F and Supplementary Table 3; $P = 0.0248$ at 96 h culture).

In vivo modelling of *LIG3* mutations

As a final line of evidence that the *LIG3* mutations can indeed cause the phenotype observed in the patients, we investigated the intestinal and neuronal phenotypes in a zebrafish model. We evaluated the consequences of *LIG3* mutations on the cerebellar structure[25,37] and the developing digestive system.[38] Reciprocal BLAST with the human LIG3 protein sequence against the zebrafish genome (Zfin v.10) identified a single *lig3* orthologue on chromosome 5, encoding a single transcript for which the encoded protein (NP_001025345) had 69.7% identity to human LIG3 (NP_039269).

We engineered F0 mutants using CRISPR/Cas9 genome editing (Supplementary Fig. 6A and B). F0 clutches with a *lig3* gene disruption (at 3 dpf) showed a significant decrease in the overall cerebellar area compared with both uninjected embryos and embryos injected with gRNA alone (Fig. 5A and B). The observed cerebellar phenotype was consistent with published data from *Lig3*$^{-/-}$ mice.[2]

We also applied a splice-blocking MO antisense oligonucleotide targeting the splice donor site of *lig3* exon 11 (e11i11; Supplementary Fig. 6A). The MO resulted in the skipping of exon 11 and the induction of a frameshift soon thereafter (Supplementary Fig. 6C). Injection of this MO resulted in a dose-dependent decrease in cerebellar area phenocopying the F0 CRISPR mutants ($P < 0.0001$; Supplementary Fig. 7A and B). The cerebellar phenotype was rescued by co-injecting human wild-type *LIG3* mRNA (Supplementary Fig. 7B), but not by mRNA harbouring patient-derived mutant variants (p.K537N and p.G964R) ($P < 0.0001$; Fig. 5C).

We also tested whether *lig3* suppression (MO) or ablation (CRISPR) perturbed the morphology of the gut and the function of the gastrointestinal tract. Quantification of HuC/D-positive neurons showed no significant differences between MO-treated or F0 mutant zebrafish compared with controls (Supplementary Fig. 7C and D). Anti-phosphomyosin staining in the zebrafish gut (8 dpf) did not show any myopathic changes (Supplementary Fig. 7E). We assayed gastrointestinal function at 8 dpf (at which age the gastrointestinal system is developed) by analysing the pattern of peristalsis using high-speed video microscopy. Qualitative scoring by investigators blind to the injection cocktail showed a significant number of morphants and knockout zebrafish with abnormal gut peristalsis [Fig. 5D,

Figure 2 Continued

decreased LIG3 protein levels (black arrow) in patient fibroblasts compared with controls. ACTB = beta-actin loading control. Immunoblotting for LIG3 and for ACTB (endogenous control) proteins were performed on the same blot. Cropped images are reported. (**E**) *LIG3* transcript analysis in Patient 2-1 and control cDNAs. *Left*: Agarose gel electrophoresis image of the RT-PCR products. Cropped images of gel electrophoresis are reported, without the marker lane (relevant sizes indicated). *Right*: Sanger sequencing analysis of the products of RT-PCR with primers c–d and primers e–f. Arrows indicate the c.799C>T and c.2996G>A variants in *LIG3* transcript. The electropherogram shows that only the c.2996G>A (p.C999Y) variant is present in the *LIG3* transcript of the patient, and not the c.799C>T (p.R267Ter) variant. (**F**) *LIG3* transcript analysis in Patient 3-2 and control cDNAs. *Left*: Agarose gel electrophoresis image of the RT-PCR products. HPRT = internal control. Cropped images of gel electrophoresis are reported, without the marker lane (relevant sizes indicated). *Right*: Sanger sequencing analysis of the products of RT-PCR with primers 1–2 and primers 3–4. Arrows indicate the c.1826C>T and c.2431C>T variants in *LIG3* transcript. The electropherogram shows that only the c.1826C>T (p.P609L) variant is present in the *LIG3* transcript of the patient, and not the c.2431C>T (p.R811Ter) variant.

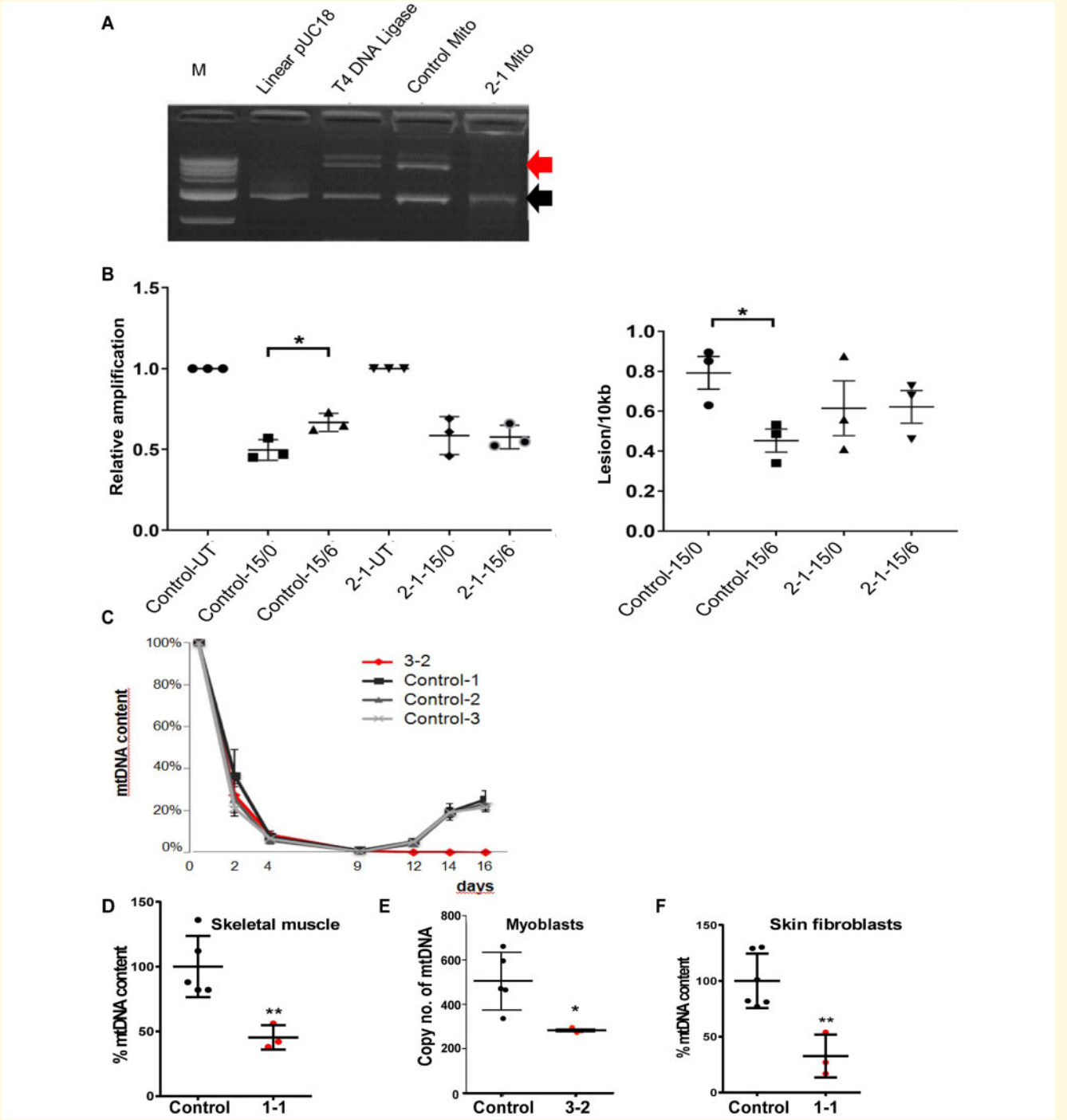

Figure 3 Defects in mtDNA maintenance due to *LIG3* mutations. (**A**) Comparison of ligase activity on linearized pUC18 plasmid DNA (length ~2.6 kb) in mitochondrial extracts between Patient 2-1 and control fibroblasts. T4 DNA ligase = positive control. Black arrow = linearized plasmid; red arrow = expected ligated product. M = molecular weight marker. (**B**) Reduced mtDNA repair kinetics after oxidative damage in control and Patient 2-1-derived fibroblasts. Values were normalized to mtDNA copy number ($n = 3$ experiments). UT = untreated; 15/0 = cells treated for 15 min with H_2O_2 and directly analysed for mtDNA repair kinetics; 15/6 = cells treated 15 min with H_2O_2, recovered for 6 h, then analysed for PCR amplification of a long mtDNA fragment relative to a short PCR fragment (*left*) and the calculated number of lesions per 10 kb of mitochondrial genome (*right*). *$P < 0.05$, ANOVA multiple testing. (**C**) Mitochondrial DNA depletion experiments. Control and Patient 3-2-derived fibroblasts were treated with EtBr for 9 days ($n = 3$ experiments; mean ± standard deviation, SD). (**D**) Quantification of mtDNA in the skeletal muscle of Patient 1-1 (red circles) and controls (black circles). Data shown for $n = 5$ controls and three replicates of the Patient 1-1 muscle biopsy. **$P < 0.01$, Student *t*-test. (**E**) Mitochondrial DNA quantification in myoblasts from Patient 3-2 (in red; three replicates of Patient 3-2 samples) and controls (in black; data shown for five controls). *$P < 0.05$, Student *t*-test. (**F**) Quantification of mtDNA in skin-derived fibroblasts ({atient 1-1); data shown for five samples for control (black circles) and Patient 1-1 (red circles). **$P < 0.01$, Student's *t*-test.

Supplementary Videos 1 and 2 (normal versus abnormal peristalsis) and Supplementary Fig. 7F).

Haematoxylin and eosin staining in the zebrafish gut (8 dpf) showed a reduction of goblet cells in morphants (e11i11) and F0 CRISPR mutants compared with controls (Supplementary Fig. 8A and B, $P < 0.01$ and $P < 0.05$, respectively). We then assayed swim bladder formation at 4 dpf (at which age the swim bladder is fully formed) by quantifying the swim bladder area, in morphants and F0 CRISPR mutants. Swim bladder area was reduced in morphants and F0 CRISPR mutants compared with controls (Supplementary Fig. 9A and B, $P < 0.0001$). Next, we quantified the expression of mitochondrial markers (*mt-nd1*, *mt-co1*) in zebrafish embryos at 4dpf. We observed a significant reduction for *mt-nd1* in morphants (e11i11) ($P < 0.01$; Supplementary Fig. 9C) with a similar trend in F0 CRISPR mutants, and a significant reduction for *mt-co1* in morphants (e11i11) ($P < 0.05$; Supplementary Fig. 9C) and F0 CRISPR mutants ($P < 0.05$; Supplementary Fig. 9C). We also tested whether *lig3* suppression (MO) or ablation (CRISPR) perturbed the morphology of the eye. Haematoxylin and eosin staining in the zebrafish eye (5 dpf), revealed a significant reduction of the outer nuclear layer in morphants (e11i11) and F0 CRISPR mutants, compared with controls (Supplementary Fig. 10A and B; $P < 0.0001$).

Discussion

In this study we described a novel recessive syndrome caused by mutations in the *LIG3* gene. The affected individuals in three independent families showed neurogastrointestinal encephalomyopathy characterized by CIPO, neurogenic bladder, myopathic changes, and neurological impairment with stroke-like episodes, epilepsy and leukoencephalopathy. The underlying cause is a defect in mtDNA ligase activity, leading to decreased mtDNA repair capacity, reduced mtDNA content and impaired mitochondrial function.

It was previously reported that the inactivation of *Lig3* led to loss of cell viability and early embryonic lethality in mice, with profound mitochondrial dysfunction due to reduced mtDNA in the nervous system.[2,5] At the single cell level, viability could be restored by mitochondrial targeting of another DNA ligase, showing that the pathogenic effect was caused by the inability to ligate mtDNA. Neuron-targeted conditional *Lig3* knockout mice showed a reduced brain size and cerebellar abnormalities with increased apoptosis in the granular layer, consistent with our observation of the zebrafish phenotype and brain defects as manifested by affected members of Family 3.[5] Gut peristalsis was not investigated in the *Lig3* mutant mice, so we link for the first time this phenotype to *LIG3* mutations. However, this is not unexpected as *POLG* mutations also cause compromised mtDNA maintenance and gut dysmotility.[39,40]

Given the functional redundancy of different ligases in the nucleus, our study suggests that primary mitochondrial dysfunction is the major, if not the only, contributor to the clinical phenotype, as documented by the downstream disruption of mtDNA maintenance and repair, with the depletion of mitochondrial genomes in skeletal muscle and fibroblasts from patients. This explains the impaired mitochondrial function in tissues with high-energy requirements, such as neurons and muscle cells. Disruption of *lig3* in the zebrafish recapitulated the cerebellar phenotype (a hallmark of $Lig3^{-/-}$ mice) and eye defects, as well as the severe impairment of gut propulsion that was observed in all patients of the three investigated families. Disruption of *lig3* also led to a significant decrease in the expression of mitochondrial markers in the zebrafish.

The features of our patients are reminiscent of known mitochondrial disorders, such as MNGIE, MELAS, and *POLG*-associated phenotypes, which all involve post-mitotic, high-energy dependent tissues, i.e. brain, skeletal muscle, and smooth muscle.[41] Notably, mtDNA depletion occurs in both MNGIE and *POLG*-mutant patients. The latter patients may additionally show migraine and epilepsy with stroke-like episodes, which are features also observed in MELAS as well as in our *LIG3*-mutant patients. Interestingly, multiple deletions in mtDNA, which are frequently observed in both MNGIE and *POLG*-associated phenotypes, were not found in patients with *LIG3* mutations. The overall CNS involvement in patients with *LIG3* mutations was more severe than in MNGIE patients with *TYMP* mutations, who usually have asymptomatic leukoencephalopathy.

The age of onset of major symptoms in patients with *LIG3* mutations was in infancy for Family 3, paediatric age for Family 1 and adult age for Family 2. The rate of progression of disease also seemed faster in Family 3 and slower in Family 2. We hypothesize that the difference in severity is caused by differences in residual protein levels and activity, but this has not been addressed directly. It is possible that the residual level of mitochondrial ligase function is higher in point mutants disrupting the interaction with XRCC1 (Families 1 and 2), which may lead to decreased protein levels but relatively normal function, whereas the mutations in Family 3 may lead to severely reduced protein levels and function. Further identification of patients with additional *LIG3* mutations will increase our understanding of the phenotypes of this new disorder, as well as provide a comparison with other mitochondrial diseases. Moreover, *LIG3* polymorphisms have been associated with a variety of pathological conditions such as tumours, neurodegenerative disorders (i.e. Alzheimer's disease), recurrent depression and neural tube defects,[42-47] suggesting that a better understanding of LIG3 function may have implication also in these diseases.

There is still a limited understanding of the metabolic consequences of mitochondrial defects.[48,49] Glutamine is crucially involved in metabolic fluxes, by replenishing the intermediates of mitochondrial respiration.[50,51] A recent

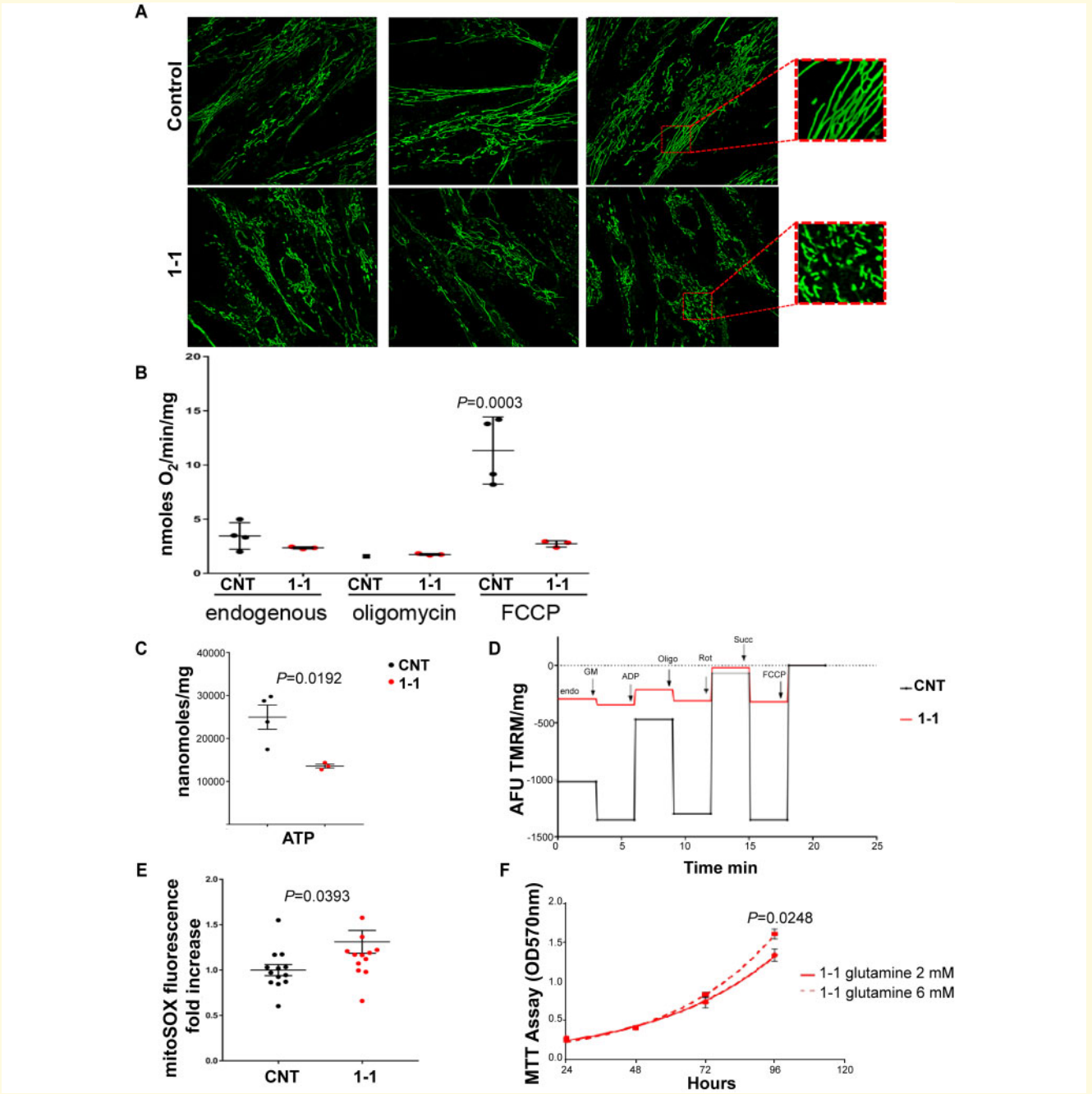

Figure 4 Functional impairment of mitochondria caused by *LIG3* mutations. (**A**) MitoTracker Green staining demonstrated a fragmented mitochondrial network in Patient 1-1 compared to control fibroblasts. Squares on the right are magnified images of the *insets*. (**B**) Mitochondrial oxygen consumption in endogenous and uncoupled conditions. Compared to control (CNT, black circles) cells, fibroblasts from Patient 1-1 (red circles) showed a significantly reduced respiration in the presence of FCCP ($P = 0.0003$; $n = 3$ independent experiments; ANOVA for multiple comparisons). (**C**) ATP content, normalized for protein content, was significantly decreased in patient fibroblasts (red circles) compared with control fibroblasts (black circles; $P = 0.0192$; $n = 3$ independent experiments; Student *t*-test). (**D**) Analysis of mitochondrial membrane potential in digitonin-permeabilized cells. A representative trace (spectrofluorimetric acquisition) of the pattern measured by the sequential addition of specific substrates (ADP = adenosine diphosphate; GM = glutamate-malate; Succ = succinate), inhibitors (Oligo = oligomycin A; Rot = rotenone) and an uncoupler (FCCP) as indicated. Compared to controls (black line), fibroblasts from Patient 1-1 (red line) were less responsive to different respiratory substrates and inhibitors ($P = 0.0012$; $n = 2$ independent experiments; Student *t*-test). AFU = arbitrary fluorescence units. (**E**) Analysis of mitochondrial reactive oxygen species production with MitoSOX shows a significant increase in Patient 1-1 fibroblasts (red circles) compared with control fibroblasts (black circles; $P = 0.0393$; Student *t*-test). (**F**) Growth curve (MTT assay) of Patient 1-1-derived fibroblasts grown in 2 mM (solid line) or 6 mM glutamine (dashed line). Patient cells cultured in 6 mM glutamine show a significantly increased growth after 96 h compared with cells grown in 2 mM glutamine ($P = 0.0248$; ANOVA test; five replicates/each time point).

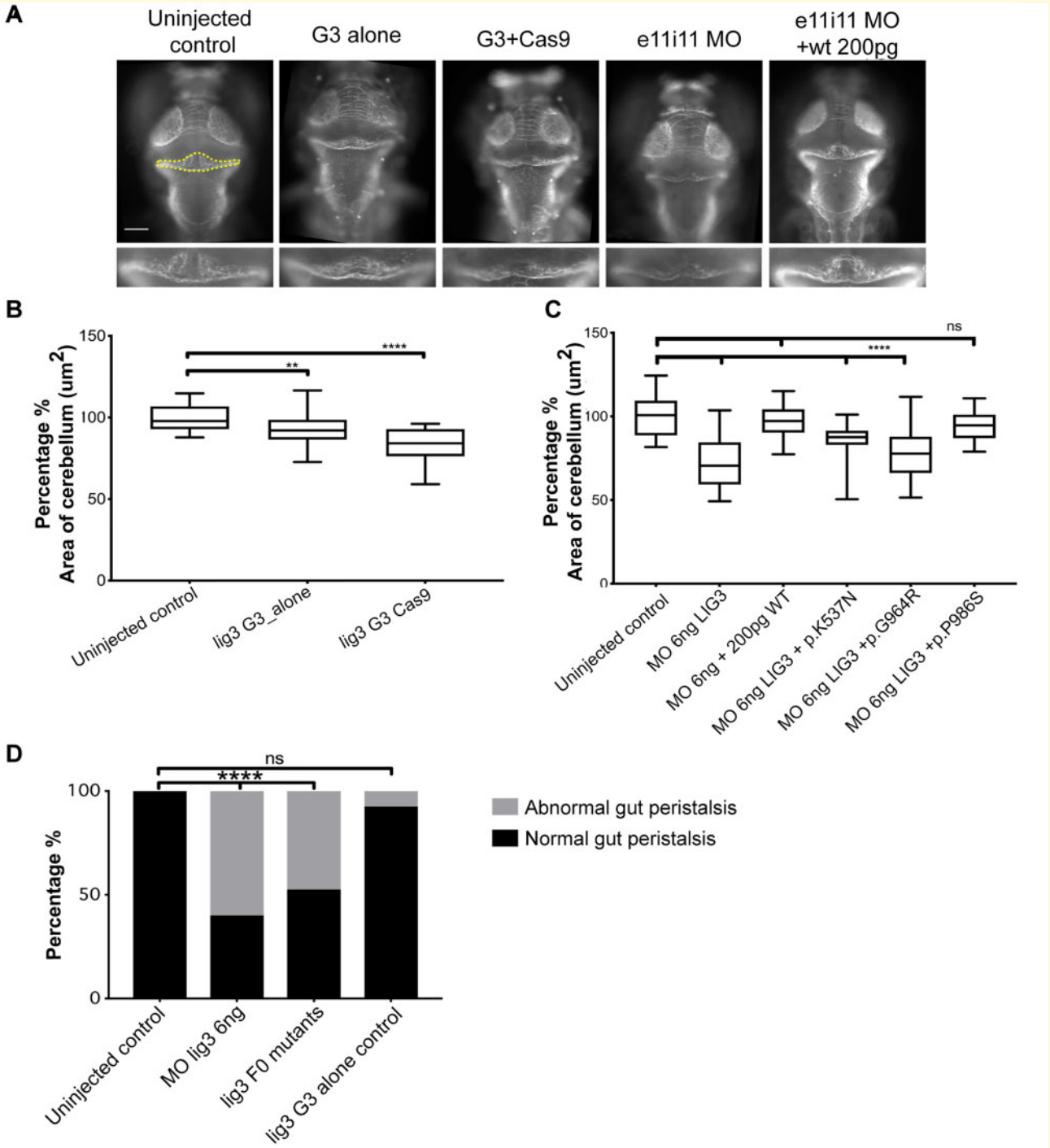

Figure 5 Suppression of *lig3* causes cerebellar hypoplasia and intestinal pseudo-obstruction in the zebrafish. (**A**) Representative dorsal images of larvae (3 dpf) immunostained for acetylated tubulin. To quantify neurons in the cerebellar area, whole-mount acetylated tubulin immunostaining was performed. Cerebellar structures of interest were measured using ImageJ software. Total cerebellar area was measured on acetylated tubulin-stained larvae by outlining structures with a fluorescent signal. Disruption of *lig3* causes cerebellar defects in both F0 CRISPR/Cas9-mutated (G3 + Cas9) zebrafish and morphants (e1i1i1 MO); e1i1i1 MO + 200 pg: complementation of *lig3* MO (e1i1i1 MO) with wild-type (WT) human *LIG3* mRNA (200 pg). Statistical analyses were performed using a nonparametric one-way ANOVA, with the Tukey multiple comparison test. ns = not significant; yellow dashed outline = area of the cerebellum that was measured; G3 = guide alone. (**B**) Quantification of cerebellar area in CRISPR/Cas9 genome edited larvae is shown for a guide targeting exon 8 of *lig3*. Comparison of F0 CRISPR/Cas9 clutches (*lig3* G3 Cas9) with either uninjected embryos or embryos injected with gRNA alone, but no enzyme (*lig3* G3_alone), showed a significant decrease in the overall cerebellar area in F0 mutants ($P < 0.0001$ for each comparison, replicated, scored blind). (**C**) Complementation of *lig3* MO with wild-type (WT) or mutated human mRNA. In contrast to embryos injected with wild-type *LIG3* mRNA or with a benign variant, i.e. not affecting ligase activity (p.P986S, rs498673), which were indistinguishable from the uninjected ones, injection with mRNA encoding p.K537N and p. G964R did not show rescue of the cerebellar phenotype. (**D**) Ablation of *lig3* causes abnormal gut peristalsis in F0 CRISPR/Cas9 mutants and morphants ($P < 0.0001$, $n = 40$ larvae/batch, replicated, χ^2 test). *$P < 0.05$; **$P < 0.01$; ***$P < 0.001$; ****$P < 0.0001$.

study showed that increased glutamine concentration improved the survival of cells carrying mtDNA defects.[34] In our study, glutamine added to *LIG3*-mutant fibroblasts led to an increase in cell growth. These results suggest that the bioenergetic impairment induced by *LIG3* mutations may be ameliorated by boosting the glutamine anaplerotic pathway although the evidence is still limited.[34]

In conclusion, we described a new mitochondrial recessive disorder caused by biallelic variants in *LIG3*, with a clinical phenotype characterized by CIPO and neurologic abnormalities, including brain abnormalities similar to those observed in other mitochondrial diseases, epilepsy and stroke-like episodes, which are clearly associated with mitochondrial dysfunction caused by defective mtDNA maintenance.

Web resources

CHOPCHOP: https://chopchop.rc.fas.harvard.edu/
ClustalOmega: https://www.ebi.ac.uk/Tools/msa/clustalo/
The Single Nucleotide Polymorphism Database (dbSNP): https://www.ncbi.nlm.nih.gov/snp
Genome Aggregation database (gnomAD): http://gnomad.broadinstitute.org/
GraphPad Prism: https://www.graphpad.com/scientific-software/prism/
Genotype-Tissue Expression (GTEx): https://commonfund.nih.gov/gtex
Human Splicing Finder (HSF) v.3.1: http://www.umd.be/HSF3/index.html
The Human Protein Atlas: https://www.proteinatlas.org/
ImageJ (National Institutes of Health, Bethesda, MD): http://rsbweb.nih.gov/ij
Mendelian Clinically Applicable Pathogenicity Score (M-CAP): http://bejerano.stanford.edu/mcap/
Pfam database: https://pfam.xfam.org/
Prediction of functional effects of human nsSNPs (PolyPhen-2): http://genetics.bwh.harvard.edu/pph2/
Primer3: http://bioinfo.ut.ee/primer3/
Protein Data Bank (PDB): http://www.rcsb.org/
Protein Variation Effect Analyzer (Provean): http://provean.jcvi.org/index.php
Zebrafish Information Network (ZFIN): https://zfin.org/

Acknowledgements

We greatly appreciate the cooperation of the patients and their families who participated in the study. We thank A. Astolfi for technical help in NGS, F.M. Santorelli and D. Cassandrini for clinical evaluation of muscle biopsies, G. La Marca for performing the thymidine phosphorylase assay using patient-derived urine. We thank A. Kita, A. Hosoya, M. Kawai, M. Kusunoki, M. Tachikawa and J. Odijk for technical assistance. We also thank H. Inagaki, S. Minamikawa, H. Nagase, M. Nishiyama, H. Awano, Y. Aoki, T. Kawada, M. Matsumoto, N. Matsumoto and N. Taniguchi for their technical support and valuable comments.

Funding

This work was supported by Telethon Grant GGP15171 to E.B. and R.D.G. and by a donation from Kobe city to the Department of General Pediatrics, Kobe University Graduate School of Medicine (K550003302). S.C. was supported by a Dutch Cancer Foundation grant (KWF11011). V.C. and A.M. were supported by the Italian Ministry of Health ("Ricerca Corrente" funding). R.D.G. is the recipient of grants from University of Ferrara (FAR and FIR funds).

Competing interests

The authors report no competing interests.

Supplementary material

Supplementary material is available at *Brain* online.

References

1. Cuneo MJ, Gabel SA, Krahn JM, Ricker MA, London RE. The structural basis for partitioning of the XRCC1/DNA ligase 3-α BRCT-mediated dimer complexes. *Nucleic Acids Res.* 2011;39:7816-7827.
2. Gao Y, Katyal S, Lee Y, et al. DNA ligase 3 is critical for mtDNA integrity but not Xrcc1-mediated nuclear DNA repair. *Nature.* 2011;471:240-244.
3. Odell ID, Barbour JE, Murphy DL, et al. Nucleosome disruption by DNA ligase 3-XRCC1 promotes efficient base excision repair. *Mol Cell Biol.* 2011;31:4623-4632.
4. Shokolenko IN, Fayzulin RZ, Katyal S, McKinnon PJ, Wilson GL, Alexeyev MF. Mitochondrial DNA ligase is dispensable for the viability of cultured cells but essential for mtDNA maintenance. *J Biol Chem.* 2013;288:26594-26605.
5. Simsek D, Furda A, Gao Y, et al. Crucial role for DNA ligase 3 in mitochondria but not in Xrcc1-dependent repair. *Nature.* 2011;471:245-258.
6. DiMauro S, Schon EA, Carelli V, Hirano M. The clinical maze of mitochondrial neurology. [Review]. *Nat Rev Neurol.* 2013;9:429-444.
7. Akbari M, Keijzers G, Maynard S, et al. Overexpression of DNA ligase 3 in mitochondria protects cells against oxidative stress and improves mitochondrial DNA base excision repair. *DNA Repair (Amst).* 2014;16:44-53.
8. Di Nardo G, Di Lorenzo C, Lauro A, et al. Chronic intestinal pseudo-obstruction in children and adults: diagnosis and therapeutic options [Review]. *Neurogastroenterol Motil.* 2017;e12945.
9. Downes TJ, Cheruvu MS, Karunaratne TB, De Giorgio R, Farmer AD. Pathophysiology, diagnosis, and management of chronic intestinal pseudo-obstruction [Review]. *J Clin Gastroenterol.* 2018;52:477-489.
10. Goldstein AM, Thapar N, Karunaratne TB, De Giorgio R. Clinical aspects of neurointestinal disease: pathophysiology, diagnosis, and treatment [Review]. *Dev Biol.* 2016;417:217-228.

11. Nishino I, Spinazzola A, Hirano M. Thymidine phosphorylase gene mutations in MNGIE, a human mitochondrial disorder. *Science*. 1999;283:689-692.
12. Carelli V, La Morgia C. Clinical syndromes associated with mtDNA mutations: where we stand after 30 years [Review]. *Essays Biochem*. 2018;62:235-254.
13. Lakshmipathy U, Campbell C. The human DNA ligase 3 gene encodes nuclear and mitochondrial proteins. *Mol Cell Biol*. 1999;19: 3869-3876.
14. Tomkinson AE, Sallmyr A. Structure and function of the DNA ligases encoded by the mammalian LIG3 gene. *Gene*. 2013;531: 150-157.
15. Giordano C, Iommarini L, Giordano L, et al. Efficient mitochondrial biogenesis drives incomplete penetrance in Leber's hereditary optic neuropathy. *Brain*. 2014;137:335-353.
16. Dimmock D, Tang LY, Schmitt ES, Wong LJ. Quantitative evaluation of the mitochondrial DNA depletion syndrome. *Clin Chem*. 2010;56:1119-1127.
17. Furda A, Santos JH, Meyer JN, Van Houten B. Quantitative PCR-based measurement of nuclear and mitochondrial DNA damage and repair in mammalian cells. *Methods Mol Biol*. 2014;1105: 419-437.
18. Kornblum C, Nicholls TJ, Haack TB, et al. Loss-of-function mutations in MGME1 impair mtDNA replication and cause multisystemic mitochondrial disease. *Nat Genet*. 2013;45:214-219.
19. Lakshmipathy U, Campbell C. Double strand break rejoining by mammalian mitochondrial extracts. *Nucleic Acids Res*. 1999;27: 1198-1204.
20. Diquigiovanni C, Bergamini C, Evangelisti C, et al. Mutant MYO1F alters the mitochondrial network and induces tumor proliferation in thyroid cancer. *Int J Cancer*. 2018;143:1706-1719.
21. Bergamini C, Moruzzi N, Sblendido A, Lenaz G, Fato R. A water soluble CoQ_{10} formulation improves intracellular distribution and promotes mitochondrial respiration in cultured cells. *PLoS One*. 2012;7:e33712.
22. Niederriter AR, Davis EE, Golzio C, Oh EC, Tsai IC, Katsanis N. In vivo modeling of the morbid human genome using Danio rerio. *J Vis Exp*. 2013;24:e50338.
23. Marjoram L, Alvers A, Deerhake ME, et al. Epigenetic control of intestinal barrier function and inflammation in zebrafish. *Proc Natl Acad Sci USA*. 2015;112:2770-2775.
24. Sanna-Cherchi S, Khan K, Westland R, et al. Exome-wide Association Study Identifies GREB1L mutations in congenital kidney malformations. *Am J Hum Genet*. 2017;101:789-802.
25. Loviglio MN, Arbogast T, Jønch AE, et al. The Iimmune signaling adaptor LAT contributes to the neuroanatomical phenotype of 16p11-2 BP2-BP3 CNVs. *Am J Hum Genet*. 2017;101:564-577.
26. Ohkubo H, Iida H, Takahashi H, et al. An epidemiologic survey of chronic intestinal pseudo-obstruction and evaluation of the newly proposed diagnostic criteria. *Digestion*. 2012;86:12-19.
27. Canafoglia L, Franceschetti S, Antozzi C, et al. Epileptic phenotypes associated with mitochondrial disorders. *Neurology*. 2001; 56:1340-1346.
28. El-Gebali S, Mistry J, Bateman A, et al. The Pfam protein families database in 2019. *Nucleic Acids Res*. 2019;47:D427-D432.
29. Madeira F, Park YM, Lee J, et al. The EMBL-EBI search and sequence analysis tools APIs in 2019. *Nucleic Acids Res*. 2019;47: W636-W641.
30. Calabrese R, Capriotti E, Fariselli P, Martelli PL, Casadio R. Functional annotations improve the predictive score of human disease-related mutations in proteins. *Hum Mutat*. 2009;30: 1237-1244.
31. Savojardo C, Fariselli P, Martelli PL, Casadio R. INPS-MD: a web server to predict stability of protein variants from sequence and structure. *Bioinformatics*. 2016;32:2542-2544.
32. Lazzeri E, Ronconi E, Angelotti ML, et al. Human urine-derived renal progenitors for personalized modeling of genetic kidney disorders. *JASN*. 2015;26:1961-1974.
33. Diquigiovanni C, Bergamini C, Diaz R, et al. A novel mutation in SPART gene causes a severe neurodevelopmental delay due to mitochondrial dysfunction with complex I impairments and altered pyruvate metabolism. *FASEB J*. 2019;33:11284-11302.
34. Chen Q, Kirk K, Shurubor YI, et al. Rewiring of glutamine metabolism is a bioenergetic adaptation of human cells with mitochondrial DNA mutations. *Cell Metab*. 2018;27:1007-1025.
35. Pichili VB, Rao KV, Jayakumar AR, Norenberg MD. Inhibition of glutamine transport into mitochondria protects astrocytes from ammonia toxicity. *Glia*. 2007;55:801-809.
36. Rama Rao KV, Jayakumar AR, Norenberg MD. Induction of the mitochondrial permeability transition in cultured astrocytes by glutamine. *Neurochem Int*. 2003;43:517-523.
37. Guissart C, Latypova X, Rollier P, et al. Dual Molecular Effects of dominant RORA mutations cause two variants of syndromic intellectual disability with either autism or cerebellar ataxia. *Am J Hum Genet*. 2018;102:744-759.
38. Bonora E, Bianco F, Cordeddu L, et al. Mutations in RAD21 disrupt regulation of APOB in patients with chronic intestinal pseudo-obstruction. *Gastroenterology*. 2015;148:771-782.
39. Filosto M, Mancuso M, Nishigaki Y, et al. Clinical and genetic heterogeneity in progressive external ophthalmoplegia due to mutations in polymerase gamma. *Arch Neurol*. 2003;60: 1279-1284.
40. Van Goethem G, Schwartz M, Löfgren A, Dermaut B, Van Broeckhoven C, Vissing J. Novel *POLG* mutations in progressive external ophthalmoplegia mimicking mitochondrial neurogastrointestinal encephalomyopathy. *Eur J Hum Genet*. 2003;11: 547-549.
41. Kanungo S, Morton J, Neelakantan M, Ching K, Saeedian J, Goldstein A. Mitochondrial disorders. [Review]. *Ann Transl Med*. 2018;6:475.
42. Corral R, Lewinger JP, Joshi AD, et al. Genetic variation in the base excision repair pathway, environmental risk factors, and colorectal adenoma risk. *PLoS One*. 2013;8:e71211.
43. Czarny P, Kwiatkowski D, Toma M, et al. Impact of single nucleotide polymorphisms of base excision repair genes on DNA damage and efficiency of DNA repair in recurrent depression disorder. *Mol Neurobiol*. 2017;54:4150-4159.
44. Kwiatkowski D, Czarny P, Toma M, et al. Association between single-nucleotide polymorphisms of the *hOGG1, NEIL1, APEX1, FEN1, LIG1*, and *LIG3* genes and Alzheimer's disease risk. *Neuropsychobiology*. 2016;73:98-107.
45. Li D, Suzuki H, Liu B, et al. DNA repair gene polymorphisms and risk of pancreatic cancer. *Clin Cancer Res*. 2009;15:740-746.
46. Li G, Wang X, Wang X, et al. Polymorphism rs1052536 in base excision repair gene is a risk factor in a high-risk area of neural tube defects in China. *Med Sci Monit*. 2018;24:5015-5026.
47. Liao YH, Ren JT, Zhang W, et al. Polymorphisms in homologous recombination repair genes and the risk and survival of breast cancer. *Gene Med*. 2017;19:9-10.
48. Eales KL, Hollinshead KE, Tennant DA. Hypoxia and metabolic adaptation of cancer cells. [Review]. *Oncogenesis*. 2016;5:e190.
49. Smeitink JA, Zeviani M, Turnbull DM, Jacobs HT. Mitochondrial medicine: a metabolic perspective on the pathology of oxidative phosphorylation disorders [Review]. *Cell Metab*. 2006;3:9-13.
50. Daye D, Wellen KE. Metabolic reprogramming in cancer: unraveling the role of glutamine in tumorigenesis [Review]. *Semin Cell Dev Biol*. 2012;23:362-369.
51. Sullivan LB, Gui DY, Hosios AM, Bush LN, Freinkman E, Vander Heiden MG. Supporting aspartate biosynthesis is an essential function of respiration in proliferating cells. *Cell*. 2015;162:552-563.

Human Genetics
https://doi.org/10.1007/s00439-020-02186-8

ORIGINAL INVESTIGATION

The involvement of U-type dicentric chromosomes in the formation of terminal deletions with or without adjacent inverted duplications

Takema Kato[1] · Hidehito Inagaki[1] · Syunsuke Miyai[1] · Fumihiko Suzuki[1] · Yuki Naru[1] · Yasuko Shinkai[1] · Asuka Kato[1] · Kazuo Kanyama[1] · Seiji Mizuno[2] · Yukako Muramatsu[3] · Toshiyuki Yamamoto[4] · Mitsuhisa Shinya[5,6] · Yukiko Tazaki[5,6] · Sayuri Hiwatashi[5,6] · Toshiro Ikeda[5,6] · Mamoru Ozaki[7] · Hiroki Kurahashi[1,2]

Received: 7 April 2020 / Accepted: 22 May 2020

Abstract
An inverted duplication with a terminal deletion (inv-dup-del) is one of the complex constitutional structural rearrangements that can occur in a chromosome. Although breakages of dicentric chromosome have been suggested, the precise mechanism of this is yet to be fully understood. In our present study, we investigated the genomic structure of 10 inv-dup-del cases to elucidate this mechanism. Two recurrent 8p inv-dup-del cases harbored a large copy-number-neutral region between the duplication and deletion in common. Although the other non-recurrent cases did not appear to have this copy-number-neutral region, refined sequencing analysis identified that they contained a small intervening region at the junction between the inverted and non-inverted segment. The size of this small intervening region ranged from 1741 to 3728 bp. Combined with a presence of microhomology at the junction, a resolution of the replication fork stalling through template switching within the same replication fork is suggested. We further observed two cases with mosaicism of the dicentric chromosome and various structural rearrangements related to the dicentric chromosome. Refined analysis allowed us to identify different breakpoints on the same chromosome in the same case, implicating multiple rounds of U-type formation and its breakage. From these results, we propose that a replication-based mechanism generates unstable dicentric chromosomes and that their breakage leads to the formation of inv-dup-dels and other related derivative chromosomes.

Introduction

An inverted duplication with a concomitant terminal deletion (inv-dup-del) is one of the common complex chromosomal rearrangements (CCRs) that arises in humans (Weckselblatt and Rudd 2015). Inv-dup-del rearrangements develop mainly in two successive steps. The first of these is the formation of a symmetric dicentric chromosome, which is unstable during mitosis because two functional centromeres can act bidirectionally. The formation of this unstable intermediate leads to anaphase bridging, followed by asymmetric breakage between the two centromeres in a subsequent mitotic division. Finally, it forms a stable large monocentric chromosome with an inverted duplication contiguous to a distal deletion and a small monocentric chromosome with a deletion (Zuffardi et al. 2009).

Two possible mechanisms are currently proposed for the formation of a dicentric chromosomal structure, the intermediate product of the inv-dup-del rearrangement (Zuffardi et al. 2009). One is a non-allelic homologous recombination (NAHR)-based mechanism. NAHR between segmental duplications with an inverted orientation produces a dicentric chromosome, and it induces breakage between the two centromeres during mitotic division. One of the representative NAHR-mediated inv-dup-dels is chromosome 8p inv-dup-del, which is mediated by homologous recombination between olfactory receptor-gene clusters (Shimokawa et al. 2004; Yu et al. 2010; García-Santiago et al. 2015). Since many 8p inv-dup-dels have been reported in unrelated families, those that are NAHR-mediated are thought to arise recurrently. In addition, NAHR between inverted repeats within the olfactory receptor-gene clusters induces benign polymorphic pericentric inversions. Meiotic recombination within the inverted segment in heterozygotes of polymorphic pericentric inversions produces a dicentric chromosomal structure that serves as an intermediate of the inv-dup-dels (Giglio et al. 2001).

✉ Hiroki Kurahashi
kura@fujita-hu.ac.jp

Extended author information available on the last page of the article

Published online: 02 June 2020

Another proposed mechanism for the generation of dicentric chromosomal structures is a U-type exchange for the formation of a sporadic inv-dup-del (Ballif et al. 2003; Rowe et al. 2009; Yu and Graf 2010). This is based on a replication-based mechanism involving template-switching between sister chromatids. When a DNA replication fork encounters a replication block caused by different types of DNA damage, DNA synthesis may stall and a DNA end will then emerge. Break-induced replication then initiates at the site of microhomology on the opposite strand forming a U-type exchange between sister chromatids. Single stranded DNA nearby can be a potential template for strand switching and is usually present during lagging strand synthesis; it appears in the uncoupling of helicase and polymerase even during leading strand synthesis. Strand switching can facilitate a DNA synthesis restart, which continues to the next fork or as far as the telomere leading to the formation of dicentric chromosomes. This series of events leading to an inv-dup-del rearrangement is consistent with the concepts of replication fork stalling and template switching (FoSTeS) and microhomology-mediated break-induced replication (MMBIR) (Zhang et al. 2009a, b). This pathway can lead to a non-recurrent inv-dup-del rearrangement in a sequence-independent manner.

In our present study, we further elucidated the mechanism of dicentric chromosome formation, and the secondary structural rearrangements that consequently arise, by analyzing the breakpoint junction sequence of 10 cases of inv-dup-del representing 9 different chromosome regions. Breakpoint sequences found in common among the non-recurrent cases suggested the involvement of the replication-based mechanism in the formation of the dicentric chromosome. In addition, we obtained evidence of dynamic structural changes from the dicentric chromosome to the terminal deletion with or without adjacent inverted duplication during cell culture of samples from miscarriage fetuses. Taken together, we hypothesized from our present data that the replication stall model for the formation of a dicentric chromosome followed by a breakage-fusion-bridge (BFB) cycle is required for the generation of an inv-dup-del rearrangement.

Materials and methods

Ethical statement

This study was approved by the Ethical Review Board for Human Genome Studies at Fujita Health University. We obtained informed consent from all of the participating patients. All genetic experiments were carried out in accordance with the relevant guidelines and regulations.

Subjects

We analyzed 10 patients harboring an inv-dup-del that had been identified by initial standard chromosome banding and subsequent cytogenetic microarray. The karyotypes of the inv-dup-dels are summarized in Table 1. The breakpoints of the inv-dup-dels in 2 patients (cases 9 and 10) were almost identical and located at 8p, suggesting that they are recurrent. Two patients had a mosaic ring shaped chromosome (cases 3 and 8). Case 5 harbored an inv-dup-del with an additional triplication. Case 10 showed an inv-dup-del on 8p with an additional duplication of 8q. In addition, to better understand the development of inv-dup-del rearrangement from an intermediate dicentric chromosome, we analyzed 2 miscarriage fetuses (cases 11 and 12), whose karyotype showed mosaic isodicentric chromosomes.

Copy-number-analysis by cytogenetic microarray analyses

Genomic DNA samples were isolated from peripheral blood, cultured cells or chorionic villi using a Gentra Puregene Tissue Kit (Qiagen, Hilden, Germany). To identify the extent of the copy-number-alterations of the inv-dup-del, we employed a CytoScan HD, 750 k Array (Affymetrix, Santa Clara, CA) or Human Genome CGH Microarray (Agilent, Santa Clara, CA) in accordance with the manufacturer's instructions. Regions of copy-number-alteration were visualized using Chromosome Analysis Suite 3.2 (Affymetrix) or Genomics Workbench 7.0 (Agilent).

Copy-number-analysis by next generation sequencing (NGS)

In cases 11 and 12, we performed copy-number-analysis by NGS. The isolation and purification of genomic DNA from cultured cells or chorionic villi was carried out using a Gentra Puregene Tissue Kit (QIAGEN). Genomic DNA samples were diluted and amplified by whole-genome amplification using SurePlex (Illumina, San Diego, CA). One nanogram of each whole-genome amplified DNA sample was prepared for NGS analysis. Shallow whole-genome sequencing was performed for comprehensive copy-number-analysis using the VeriSeq PGS Kit MiSeq (Illumina). The sequencing data were analyzed using BlueFuse Multi Software (Illumina).

Breakpoint characterization by NGS

To identify the breakpoint junctions in our sporadic inv-dup-del study cases, we carried out NGS analysis of each patient's genomic DNA. Mate-pair whole-genome

Table 1 Patients information with inv-dup-dels

Sample no.	Chromosome	Karyotype	Genomic coordinates from microarray analysis	Copy-number-neutral region	Size (bp)	Microhomology (bp)
1	4p	–	arr[GRCh37] 4p16.3(71552_664410)X1,4p16.3p14(703668_36230853)X3	chr4:689,203–690,943	1741	3
2	4q	der(4)(pter→q3?4.3::q?34.3→31.3)(::?2q35.2(177383079_190957473)X1	arr[GRCh37] 4q31.23q34.2(151058587_177382551)X3,4q34	chr4:177,383,829–177,387,559	3728	2
3	9p	r(9)(::?::p24→q34.3::)[27]/45,XY,-9 [3]	arr[GRCh37] 9p24.3p24.1(203861_8216831)X1,9p24.1p21.1(8216910_31620128)X3	chr9:8,215,737–8,218,461	2725	0
4	9p	add(9)(p24)	arr[GRCh37] 9p24.3p23(214367_11573590)X1,9p23p13.1(12048553_39156954)X3	chr9:11,712,793–11,715,125	2333	− 4
5	10q	add(10)(q25.1)	arr[GRCh37] 10q26.12q26.3(122328262_132082817)X3 ~ 4,10q26.3(132942513_135404523)X1	chr10:132,878,450–132,880,484, chr10:122,306,763–122,307,064	2035, 303	2
6	11q	–	arr[GRCh37] 11q23.1q24.1(111612172_121578675)X3,11q24.1q25(121829034_134868407)X1	chr11:121,765,738–121,767,908	2167	3
7	18p	add(18)(p11.2)	arr[GRCh37] 18p11.32p11.31(14,316–3,458,388)X1,18p11.31p11.21(3,572,316–14,733,870)X3	chr18:3,492,546–3,494,355	1810	3
8	21q	r(21) [27]/45,XX,-21[2]/46,XX,?dic r(21) [1]	arr[GRCh37] 21q21.1q22.13(16832706_44518076)X3,21q22.3(44526182_48097372)X1	chr21:44,524,195–44,526,196	2001	0
9	8p	der(8)(::p12→p23.1::p23.1→qter)	arr[GRCh37] 8p23.3p23.1(158048_6981988)X1,8p23.1p11.22(11945855_39451389)X3			
10	8p	der(8)(8qter→8q24.2::8p11.2→8p23.1::8p23.1→8qter)	arr[GRCh37] 8p23.3p23.1(158048_6999114)X1,8p23.1p11.22(12560781_39078328)X3,8q24.21q24.3(129285242_146295771)X3			

sequencing was performed to determine the breakpoints of the inverted duplication in the dicentric chromosome. Since the breakpoint junctions can have palindromic (inverted repeated) characteristic sequences, we generated mate-pair long libraries of 9 kb to minimize the loss of palindromic DNA molecules at the breakpoint junction during library preparation. These 9-kb mate-pair libraries were prepared using a Nextera Mate Pair Library Preparation Kit (Illumina) in accordance with the manufacturer's protocol. The libraries were sequenced with 101 bp-paired-end reads on a HiSeq 1500 platform (Illumina). Sequence reads were trimmed adapter sequences using NxTrim and mapped with BWA 0.7.10 against hg19 (Li and Durbin 2010). Subsequently, discordantly mapped paired-reads were extracted to detect chromosomal structural rearrangements using BreakDancer (Fan et al. 2014). Putative breakpoints produced by inverted duplications, triplications and terminal deletions were confirmed by visual inspection of NGS data using Integrative Genomics Viewer (IGV) (Thorvaldsdottir et al. 2013). The nucleotide sequences of the breakpoint junctions of the inverted duplications and triplications were determined by breakpoint-specific PCR and Sanger sequencing using an ABI3130xl sequencer (Life Technologies, Foster City, CA). The length of the inverted sequence homology at the between copy-number-gain and -loss was searched using a YASS sequence similarity search (Noe and Kucherov 2005). Default parameter setting was used for this analysis.

Product of conception karyotyping

Products of conception (POC) were analyzed for chromosome abnormalities using standard cell culture followed by Giemsa banding.

Results

Copy-number variation features in recurrent and non-recurrent inv-dup-dels

We employed a cytogenetic microarray to characterize the 10 inv-dup-del rearrangements in our study cohort. The copy-number-profile detected by SNP microarray showed a clear difference between the cases involving 8p23.1 (cases 9 and 10) and others (Fig. 1). The two 8p23.1 cases harbored a large copy-number-neutral region between the copy-number-gain and -loss regions (~ 5 Mb). The endpoints of these copy-number-neutral regions were found to be almost identical between the two subjects and located within the olfactory receptor (OR) gene clusters. In contrast, none of the eight sporadic inv-dup-del cases showed

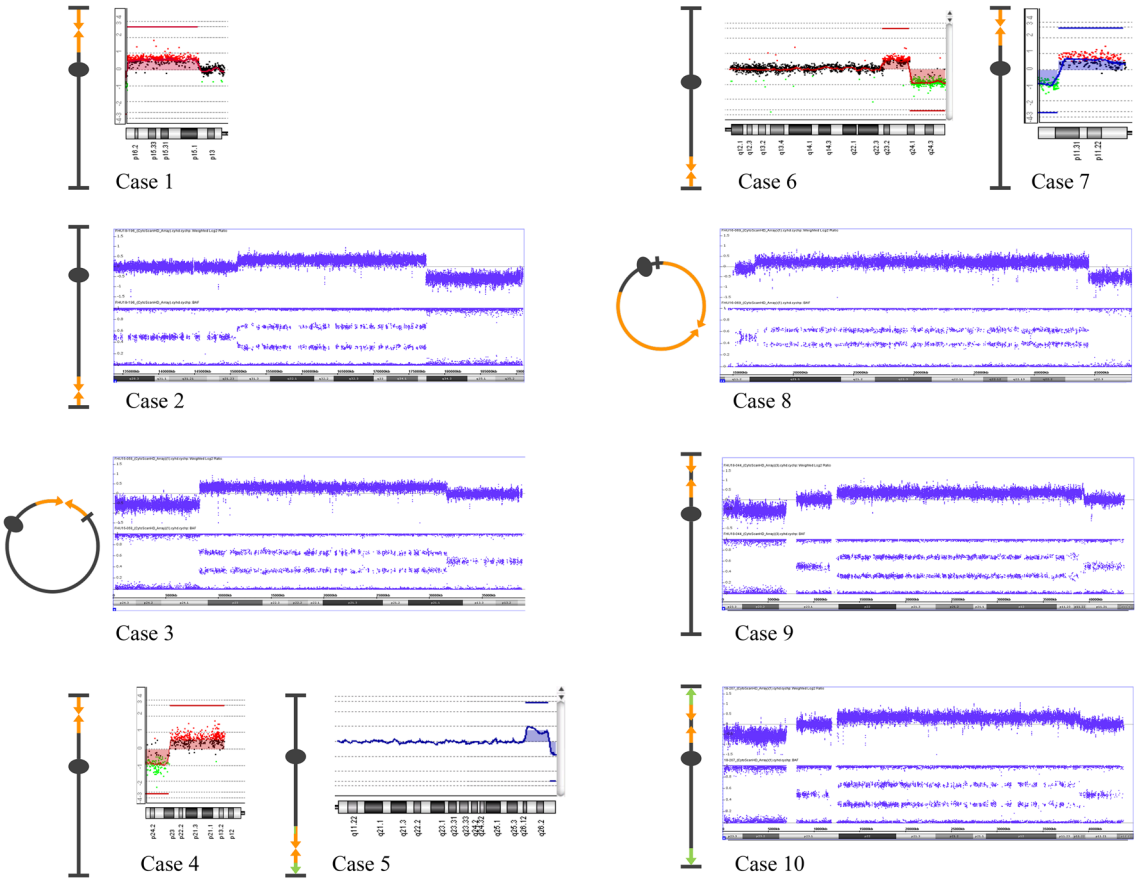

Fig. 1 Copy-number-profile of the inv-dup-dels determined by microarray. Copy-numbers were determined using an Affymetrix CytoScan microarray and visualized with ChAS software (Case 2, 3, 8, 9, 10). The upper blue plots show the signal for the weighted log 2 ratio. The lower plots indicate the B allele frequency. Copy-numbers were also determined using an Agilent CGH microarray and visualized with Genomics Workbench (Case 1, 4, 5, 6, 7). The log 2 ratio of the genomic copy-number is also plotted and indicated by horizontal lines. Illustrative diagrams of chromosomal structure are shown at the left. Inverted duplications are shown by arrows with orange color. Other rearrangements are shown with green color

any detectable copy-number-neutral regions between the copy-number-gain and -loss (cases 1–8; Fig. 1).

Breakpoint analysis of the non-recurrent inv-dup-dels

Whole genome sequencing of the 9-kb mate-pair library was performed to further analyze the breakpoints in our eight study cases with non-recurrent inv-dup-del structures. The inverted duplication structures were confirmed in each case by the presence of a junction for the inverted orientation of the two copy-number-gain regions. The DNA fragment incorporating the junction manifested a characteristic volcano-like pattern in the mapping of the discordant reads (Fig. 2). Some cases had telomeric repeat sequences at the proximal end of the inverted duplication, i.e. mapped at the proximal end of the copy-number-gain regions, reflecting telomere healing of the breakage (data not shown). In the case of ring chromosomes, the proximal end of the inverted duplication possibly contained a 9q subtelomeric repeat sequence (case 3) or 21q repetitive sequence (case 8), suggesting that ring formation was another healing pathway for the breakage (data not shown). Based on the fact that inverted and non-inverted segment was fused in head-to-head orientation and the chromosome end-like sequence appeared at the other end of the inverted segment, the inv-dup-del structures were confirmed in these cases.

Although high-resolution microarray did not detect an intervening copy-number-neutral region between the inverted and non-inverted segment, refined analysis of the breakpoint junction sequences identified a small copy-number-neutral region at the junction in all of the cases with a non-recurrent inv-dup-del (Fig. 2, red arrows). The size of the copy-number-neutral regions ranged from 1741 to 3728 bp (Fig. 3, Table 1). Microhomologies from 1 to 3 bp were found at breakpoint junctions between inverted and

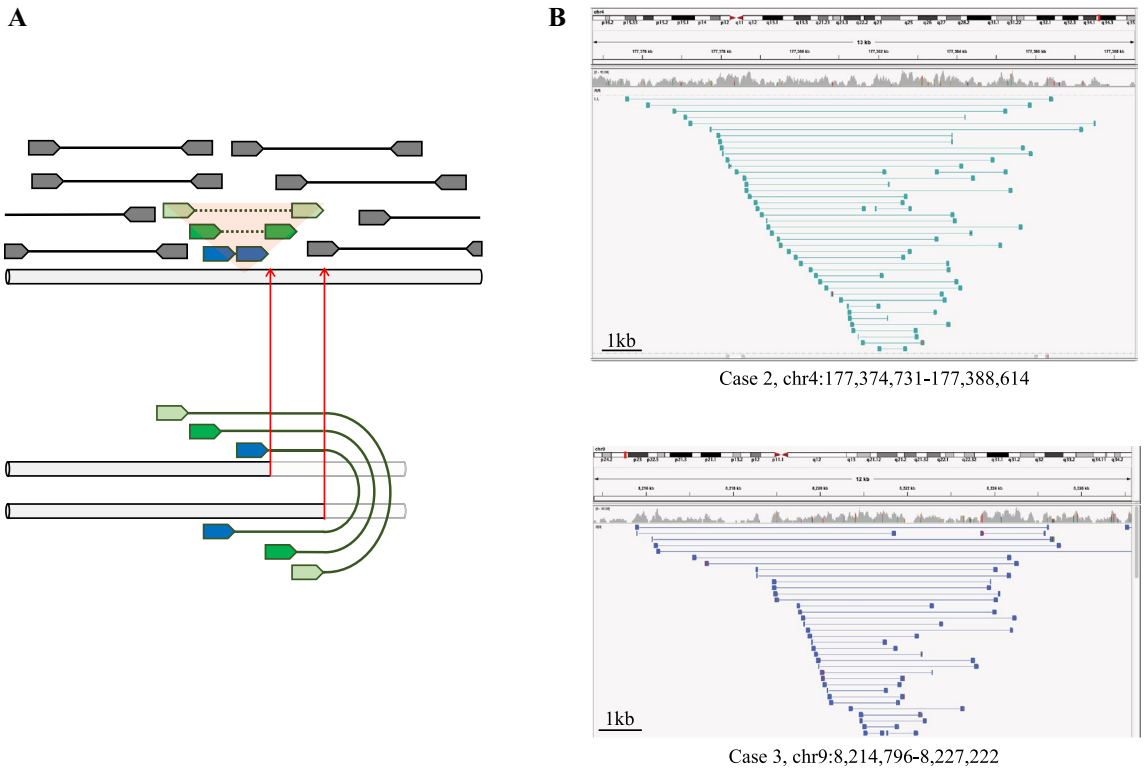

Fig. 2 Discordant reads at the junction of the dicentric chromosome. **a** Strategy for determining mate-pair sequences. The upper panel provides a schematic of the reference human genome structure. The lower panel depicts the assumed structure of the inverted duplication. Gray reads show normal paired-end reads, which were mapped in the forward and reverse direction to the reference genome. Green colored reads indicate discordant reads, which were mapped in the same orientation. Red arrows indicate the putative breakpoints. **b** Mapping of mate-pair sequences on the reference human genome sequence. The region around the breakpoint of dicentric chromosome was shown using IGV browser. A characteristic volcano-like pattern could be observed

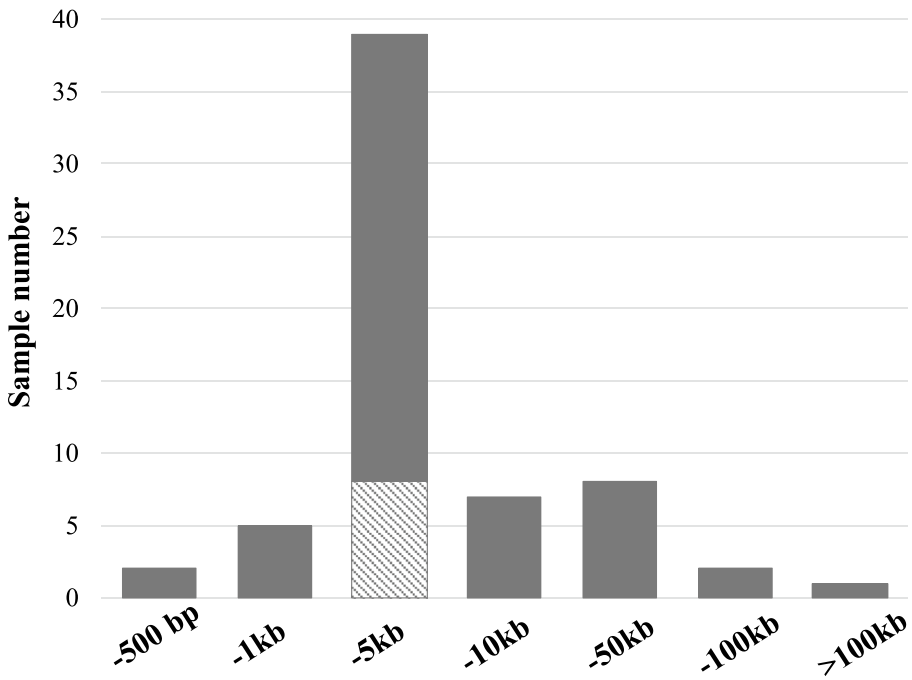

Fig. 3 Distribution of the lengths of the intervening copy-number-neutral regions. Bars indicate the number of analyzed cases in studies published from 2003 to 2014 (black bar) (Ballif et al. 2003; Bonaglia et al. 2008; Hermetz et al. 2014; Rowe et al. 2009) and in this current study (hatched bar)

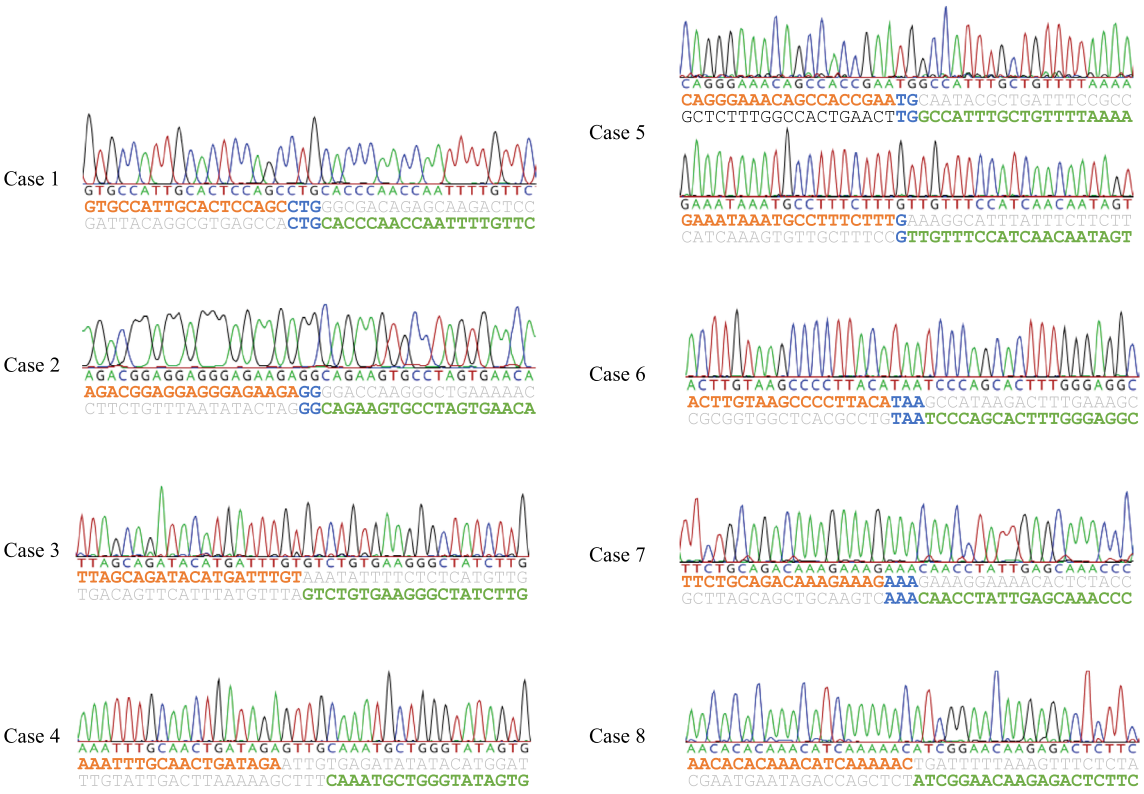

Fig. 4 Junction sequences of fold-back chromosomes. The orange and green characters indicate the plus and minus strands, respectively. Blue characters indicate homologous nucleotides. Gray characters indicate unknown nucleotide insertions

non-inverted segment in 5 cases, but none were evident in 3 cases with the remaining subject carrying a 4 bp microinsertion (Fig. 4, Table 1).

To investigate whether the initial formation of the dicentric chromosome in our study subjects was caused by an inverted repeat sequence at the breakpoint, we conducted sequence similarity analysis around the breakpoint region. Sequences with high similarity were found as expected in the inverted orientation at the proximal and distal end of the copy-neutral-region in the two recurrent 8p inv-dup-del cases (case 9 and 10), suggesting that the breakpoints were located within the olfactory receptor-gene clusters (Fig. 5). In contrast, significant inverted repeat sequences were not observed in any of the other inv-dup-del cases (cases 1–8). It is likely that the inverted duplications were generated in these eight individuals through repeat-independent, microhomology-based mechanisms, such as FoSTeS/MMBIR or microhomology-mediated end joining (MMEJ).

Breakage of the dicentric chromosome to form an inv-dup-del rearrangement

We additionally analyzed two fetal loss cases for which molecular cytogenetic analysis revealed evidence of dicentric chromosomes leading to inv-dup-del formation. Case 11 underwent a miscarriage after 8 gestational weeks. Karyotyping of her POC sample revealed that all clones harbored add(13)(q22). Furthermore, derivative chromosome 13 showed a mirror structure. NGS chromosome analysis further revealed a copy-number-gain adjacent to a deletion on chromosome 13 (Fig. 6a). Based on these results, we concluded that the derivative chromosome was an isodicentric chromosome 13 (idic(13)). When we used uncultured POC cells for NGS copy-number-analysis, we identified an inv-dup-del pattern on the chromosome 13 which was likely to have derived from a breakage of idic(13). Intriguingly, the endpoint of the deletion of the two samples did not show concordance. If the inv-dup-del was a breakage product of idic(13), the deletion endpoint should be concordant, but the position of the deletion endpoint in inv-dup-del was more proximal (see "Discussion").

Case 12 (Fig. 6b) underwent a stillbirth at gestational week 34 due to multiple fetal anomalies. We analyzed three independent cultures of her POC sample. Karyotyping from one of the cultures revealed a 46,XX,del(15)(q26.1)[46]/46,XX,psu idic(15)(q26.3) mosaicism [8]. To analyze for a possible breakage of the idic(15) chromosome, we performed an SNP array of the same sample. We observed

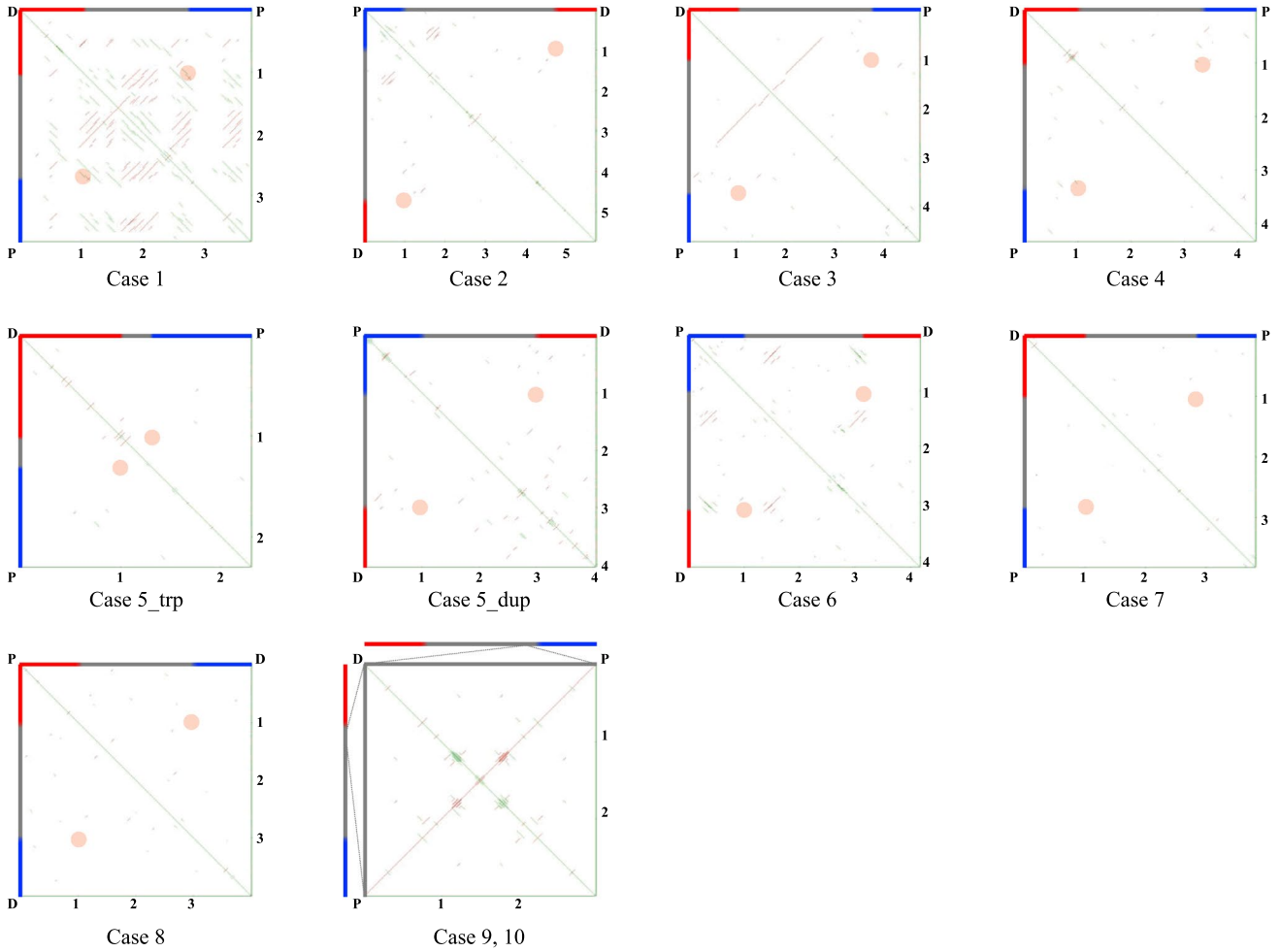

Fig. 5 Sequence similarity analysis of the small intervening regions in our case subjects. Intervening regions which covered ± 1 kb around the copy-number-neutral region are schematically represented on both axes. Black bars indicate copy-number-neutral regions, while blue and red bars indicate copy-number-gain and -loss, respectively. We defined the default parameter values for this analysis. Green line indicates a direct repeat and pink line denotes an inverted repeat. Pink circles indicate sequence similarities between the proximal and distal breakpoints. With regard to cases 9 and 10, parts of the two olfactory receptor-gene cluster regions (REPD[hg19]chr8:7,466,506-7,468,005 and REPP[hg19]chr8:12,466,006-12,467,505) were merged and used for this analysis. P, proximal side; D, distal side. The scale represents size in 1 kb

a stepwise copy-number-loss on chromosome 15q. It was likely that the distal breakpoint corresponded to the idic(15) breakpoint whilst the proximal breakpoint corresponded to a terminal deletion endpoint or inv-dup-del endpoint. We performed karyotype analysis of another culture which revealed 46,XX,add(15)(q26.1)[24]/46,XX,del(15)(q26.1)[19]/46,XX,psu idic(15)(q26.3)[14]. As was the case with the first culture, an SNP array indicated a stepwise copy-number-loss on chromosome 15q. The distal breakpoint was found to be identical to that of the first culture, whilst the position of the proximal breakpoint differed (see "Discussion"). In addition, a copy-number-gain of chromosome 17q was observed, suggesting that the add(15)(q26.1) was der(15)t(15;17)(q26;q21). We also performed SNP array analyses of a frozen uncultured sample for case 12, which indicated a copy-number-gain on chromosome 9q in addition to a stepwise copy-number-loss of chromosome 15q, which might be derived from a line with 46,XX,der(15)t(9;15)(q34;q26). In summary, the unstable idic(15) chromosome may be susceptible to DNA breakage, leading not only to inv-dup-del rearrangement, but also to a terminal deletion such as del(15)(q26.1), or other unbalanced translocations like der(15)t(15;17)(q26;q21) or der(15)t(9;15)(q34;q26).

Discussion

We conducted our current molecular cytogenetic study to clarify how an inv-dup-del rearrangement is generated. We carried out the breakpoint junction analysis of dicentric

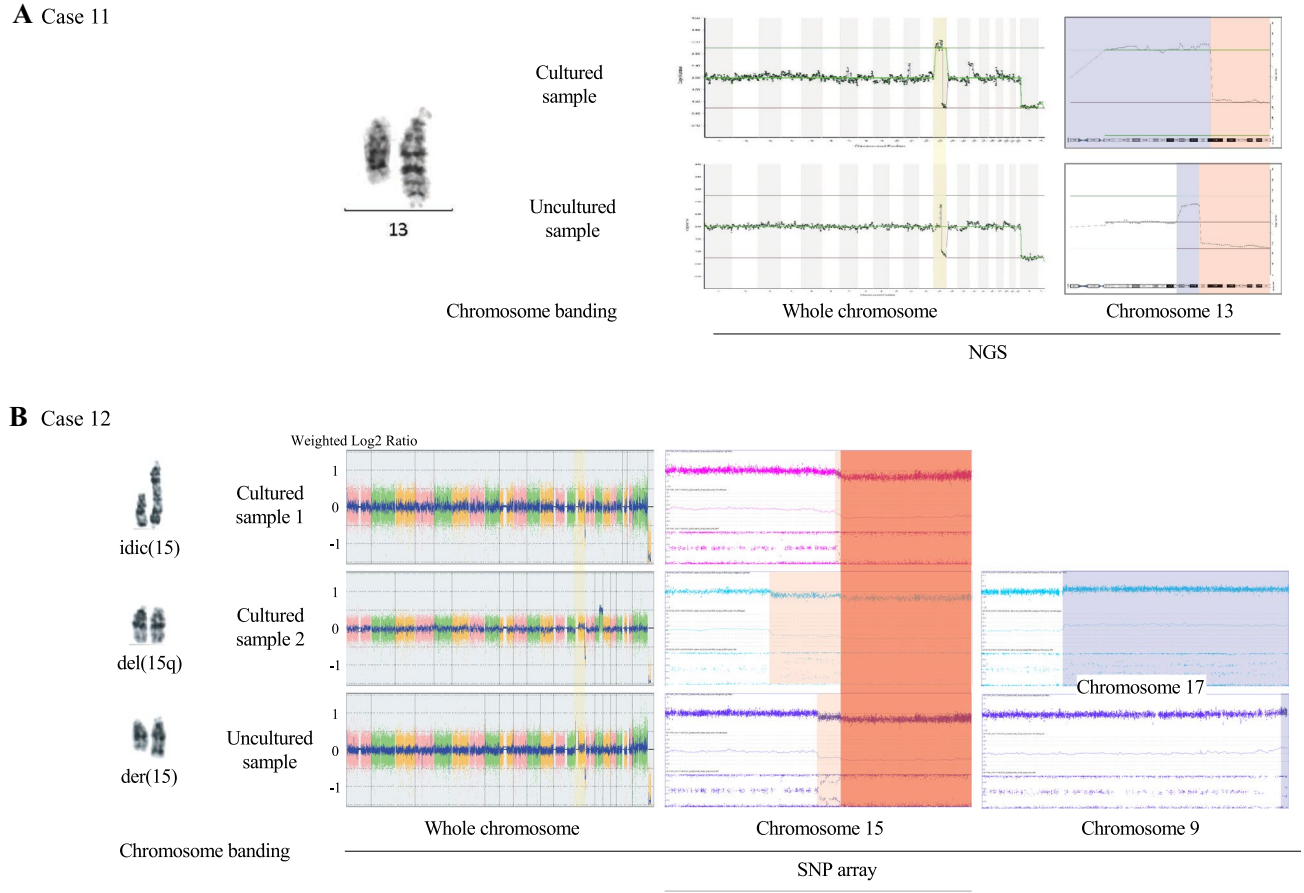

Fig. 6 Chromosome conformation changes during cell culture. Various chromosome analyses of cases 11 and 12 indicating that dicentric chromosomes in both subjects led to secondary structural rearrangements. **a** Case 11 harbors a chromosomal abnormality on chromosome 13. The upper panel shows a cultured sample and the lower panel shows an uncultured sample. Chromosome 13 was painted with a yellow signal. Copy-number-alterations are indicated in blue (copy-number-gain) and red (copy-number-loss). **b** Case 12 harbors chromosomal abnormalities on chromosomes 9, 15 and 17. The upper and middle panels show cultures of sample 1 and 2, respectively. The lower panel shows an uncultured sample. Chromosome 15 was painted with a yellow signal. Copy-number-alterations are indicated in blue (copy-number-gain) or red (copy-number-loss). In cultured sample 2, chromosome banding revealed three different karyotypes

chromosomes and a follow-up survey of secondary rearrangements that arose due to these dicentric chromosomes.

Involvement of a replication-based mechanism in the formation of a U-type dicentric chromosome

SNP microarray data showed a significant difference between recurrent and non-recurrent inv-dup-dels. Recurrent inv-dup-dels harbor large copy-number neutral region between the copy-number-gain and -loss. In contrast, non-recurrent sporadic inv-dup-dels do not have copy-number neutral region. This implicates mechanism leading to the formation of a dicentric chromosome might be different. The endpoints of copy-number-neutral regions were located within the OR gene clusters. This suggested that the repetitive nature of OR gene clusters was involved in the development of the recurrent inv-dup-dels in cases 9 and 10. NAHR between the OR genes may possibly underlie the most common recurrent inv-dup-del (Giglio et al. 2001; García-Santiago et al. 2015). Although we used high-resolution microarray in our current study, any sporadic inv-dup-del cases were not able to detect copy-number-neutral regions between the copy-number-gain and -loss. It was previously proposed that a symmetrical U-type exchange is the underlying mechanism leading to non-recurrent dicentric chromosome formation (Rowe et al. 2009). In our current study however, when we analyzed junction sequences at a nucleotide resolution, asymmetrical dicentric structures with an intervening sequence were observed. The presence of microhomologies or microinsertions at the fusion points of inverted and non-inverted segments (Fig. 4) indicated that the inverted duplications were generated through repeat-independent, microhomology-based mechanisms, such as FoSTeS/MMBIR or microhomology-mediated end joining.

In a previous report, Hermetz et al., proposed a fold-back model for the formation of dicentric chromosomes via a double-strand break (DSB) repair pathway (Hermetz et al. 2014). In this model, a DSB undergoes resection, which generates a long 3′ single-stranded DNA (ssDNA) overhang. This in turn promotes intrastrand pairing to the short inverted repeat via a homology-based mechanism leading to the formation of a dicentric chromosome. Notably however, we did not observe any homology between both ends of the intervening copy-number-neutral region at the boundary of the inverted and non-inverted segments in our current cases (Fig. 5). Further, the size of the intervening sequence showed a unique distribution, ranging from 1 to 5 kb in our analyzed cases. When we increased the number of inv-dup-del cases using data from previous studies in which where the breakpoints of inv-dup cases were analyzed at a nucleotide resolution (Ballif et al. 2003; Bonaglia et al. 2008; Rowe et al. 2009; Hermetz et al. 2014), the size of the intervening sequence peaked at 1–5 kb (Fig. 3).

Uncoupling of the helicase and polymerase leads to a single-stranded DNA in the leading strand, which when stalled can produce an uncoupled nascent lagging strand under certain conditions. Such single-stranded DNA can be up to 3–5 kb in length, depending on the nature of the replication fork block (Lopes et al. 2006). It is likely that the tight distribution of these sizes may reflect a resolution of the replication fork block through template switching within the same replication fork. Interestingly, when we increased our current sample number by including prior data from the literature, another low-pitched distribution curve appeared up to 100 kb (Fig. 3). This possibly reflects a resolution of the stalled replication fork by an adjacent fork which may be distant in a genomic sense but in close proximity within the nucleus. We are thus proposing a replication stall model as a mechanism of formation for U-type dicentric chromosomes.

Dicentric chromosome instability results in secondary rearrangements

In general, dicentric chromosome breakages would produce two reciprocal products: inv-dup-del chromosomes and terminal deletion chromosomes. We observed in our present series that two POC samples had a mosaicism of cells with dicentric chromosomes and inv-dup-del or other rearrangements associated with the dicentric chromosome. This suggested that the formation of the dicentric chromosome and other related rearrangements including the inv-dup-del were sequential events. The breakage of an unstable dicentric chromosome leads to the formation of not only an inv-dup-del chromosome and terminal deletion chromosome after stabilization through telomere healing of the broken ends, but also results in various structural rearrangements via stabilization by telomere capture.

Interestingly, our SNP microarray analysis of case 11 indicates that the endpoint of the deletion of the possible inv-dup-del was more proximal to that of the idic(13) chromosome. This suggested that the inv-dup-del chromosome might have originated from a terminal deletion chromosome reciprocal of the inv-dup-del chromosome derived from a breakage of idic(13). The terminal deletion chromosome might form a U-type dicentric chromosome leading to the second inv-dup-del chromosome having the proximal deletion endpoint. Likewise, SNP microarray data for case 12 indicated a more proximal endpoint of der(15) to that of the idic(15). This also suggested that the der(15) chromosome might have been generated in the second round of breakage of the dicentric chromosome. Dicentric chromosome must be stable and segregate to daughter cells correctly since one of the centromeres is functionally silenced (Stimpson et al. 2010). However, just after the formation of a U-type dicentric chromosome, both of the centromeres might be still active and the dicentric chromosomes are therefore unstable, leading to secondary rearrangements into various derivative chromosomes (Soler et al. 2003; Chabchoub et al. 2007; Schlade-Bartusiak et al. 2013; Pedurupillay et al. 2014). Hence, we can observe multiple clones with different derivative chromosomes.

Finally, in case 12, two types of translocation chromosomes related to the idic(15) chromosome were observed. In general, an unbalanced translocation would originate from segregation of the one of the translocation chromosomes from a balanced translocation carrier. However, our current results suggest that if the unbalanced translocation arises as de novo, it might originate from breakage of dicentric chromosome followed by telomere capture using the other chromosomal end.

In summary, a dicentric chromosome is so unstable that it leads to the generation of an inv-dup-del chromosome, as well as a reciprocal terminal deletion through telomere healing and also an unbalanced translocation via telomere capture.

Acknowledgements We thank the patients and their families for participating in this study.

Author contributions TK—participated in the design of the study, carried out the molecular biology work, and drafted the manuscript. HI—participated in the design of the study, carried out the molecular biology work. SuM—participated in the design of the study, carried out the molecular biology work. FS—participated in the design of the study, carried out the molecular biology work. YN—participated in the design of the study, carried out the molecular biology work. YS—participated in the design of the study, carried out the molecular biology work. AK—participated in the design of the study, carried out the molecular biology work. KK—participated in the design of the study, carried out the molecular biology work. SeM—participated in

the design of the study. YM—participated in the design of the study. TY—participated in the design of the study. MS—participated in the design of the study. YT—participated in the design of the study, carried out the molecular biology work. SH—participated in the design of the study. TI—participated in the design of the study. MO—participated in the design of the study. HK—Coordinated and conceived the study, being involved in the critical revision of the manuscript for important intellectual content.

Funding This study was supported by a Grant-in-Aid for Scientific Research from the Ministry of Education, Culture, Sports, Science, and Technology of Japan (17K11259 to T.K., 15H04710 and 24390085 to H.K.) and from the Ministry of Health, Welfare and Labor (16ek0109067h0003 to H.K.).

Data availability All data analyzed during this study are included in this published article.

Compliance with ethical standards

Conflict of interest The authors declare no competing interests.

Ethical approval This study was approved by the Ethical Review Board for Human Genome Studies at Fujita Health University. The written informed consent was obtained from patients. All experiments were carried out in accordance with the relevant guidelines and regulations.

Informed consent We have obtained consent to participate in the study. We have obtained consent to publication in the study.

References

Ballif BC, Yu W, Shaw CA et al (2003) Monosomy 1p36 breakpoint junctions suggest pre-meiotic breakage-fusion-bridge cycles are involved in generating terminal deletions. Hum Mol Genet 12:2153–2165. https://doi.org/10.1093/hmg/ddg231

Bonaglia MC, Giorda R, Massagli A et al (2008) A familial inverted duplication/deletion of 2p25.1–25.3 provides new clues on the genesis of inverted duplications. Eur J Hum Genet 17:179–186. https://doi.org/10.1038/ejhg.2008.160

Chabchoub E, Rodriguez L, Galan E et al (2007) Molecular characterisation of a mosaicism with a complex chromosome rearrangement: evidence for coincident chromosome healing by telomere capture and neo-telomere formation. J Med Genet 44:250–256. https://doi.org/10.1136/jmg.2006.045476

Fan X, Abbott TE, Larson D, Chen K (2014) BreakDancer: Identification of genomic structural variation from paired-end read mapping. Curr Protoc Bioinformatics 45:15.6.1–11. https://doi.org/10.1002/0471250953.bi1506s45

García-Santiago FA, Martínez-Glez V, Santos F et al (2015) Analysis of invdupdel(8p) rearrangement: clinical, cytogenetic and molecular characterization. Am J Med Genet 167A:1018–1025. https://doi.org/10.1002/ajmg.a.36879

Giglio S, Broman KW, Matsumoto N et al (2001) Olfactory receptor-gene clusters, genomic-inversion polymorphisms, and common chromosome rearrangements. Am J Hum Genet 68:874–883. https://doi.org/10.1086/319506

Hermetz KE, Newman S, Conneely KN et al (2014) Large inverted duplications in the human genome form via a fold-back mechanism. PLoS Genet 10:e1004139–e1004214. https://doi.org/10.1371/journal.pgen.1004139

Li H, Durbin R (2010) Fast and accurate long-read alignment with Burrows-Wheeler transform. Bioinformatics 26:589–595. https://doi.org/10.1093/bioinformatics/btp698

Lopes M, Foiani M, Sogo JM (2006) Multiple mechanisms control chromosome integrity after replication fork uncoupling and restart at irreparable UV lesions. Mol Cell 21:15–27. https://doi.org/10.1016/j.molcel.2005.11.015

Noe L, Kucherov G (2005) YASS: enhancing the sensitivity of DNA similarity search. Nucleic Acids Res 33:W540–W543. https://doi.org/10.1093/nar/gki478

Pedurupillay CRJ, Misceo D, Gamage TH et al (2014) Post-zygotic breakage of a dicentric chromosome results in mosaicism for a telocentric 9p marker chromosome in a boy with developmental delay. Gene 533:403–410. https://doi.org/10.1016/j.gene.2013.09.090

Rowe LR, Lee J-Y, Rector L et al (2009) U-type exchange is the most frequent mechanism for inverted duplication with terminal deletion rearrangements. J Med Genet 46:694–702. https://doi.org/10.1136/jmg.2008.065052

Schlade-Bartusiak K, Tucker T, Safavi H et al (2013) Independent post-zygotic breaks of a dicentric chromosome result in mosaicism for an inverted duplication deletion 9p and terminal deletion 9p. Eur J Med Genet 56:229–235. https://doi.org/10.1016/j.ejmg.2013.01.013

Shimokawa O, Kurosawa K, Ida T et al (2004) Molecular characterization of inv dup del(8p): analysis of five cases. Am J Med Genet 128A:133–137. https://doi.org/10.1002/ajmg.a.30063

Soler A, Sánchez A, Carrió A et al (2003) Fetoplacental discrepancy involving structural abnormalities of chromosome 8 detected by prenatal diagnosis. Prenat Diagn 23:319–322. https://doi.org/10.1002/pd.590

Stimpson KM, Song IY, Jauch A et al (2010) Telomere disruption results in non-random formation of de novo dicentric chromosomes involving acrocentric human chromosomes. PLoS Genet 6:e1001061–e1001119. https://doi.org/10.1371/journal.pgen.1001061

Thorvaldsdottir H, Robinson JT, Mesirov JP (2013) Integrative Genomics Viewer (IGV): high-performance genomics data visualization and exploration. Brief Bioinform 14:178–192. https://doi.org/10.1093/bib/bbs017

Weckselblatt B, Rudd MK (2015) Human structural variation: mechanisms of chromosome rearrangements. Trends Genet. https://doi.org/10.1016/j.tig.2015.05.010

Yu S, Graf WD (2010) Telomere capture as a frequent mechanism for stabilization of the terminal chromosomal deletion associated with inverted duplication. Cytogenet Genome Res 129:265–274. https://doi.org/10.1159/000315887

Yu S, Fiedler S, Stegner A, Graf WD (2010) Genomic profile of copy number variants on the short arm of human chromosome 8. Eur J Hum Genet 18:1114–1120. https://doi.org/10.1038/ejhg.2010.66

Zhang F, Carvalho CMB, Lupski JR (2009a) Complex human chromosomal and genomic rearrangements. Trends Genet 25:298–307. https://doi.org/10.1016/j.tig.2009.05.005

Zhang F, Khajavi M, Connolly AM et al (2009b) The DNA replication FoSTeS/MMBIR mechanism can generate genomic, genic and exonic complex rearrangements in humans. Nat Genet 41:849–853. https://doi.org/10.1038/ng.399

Zuffardi O, Bonaglia M, Ciccone R, Giorda R (2009) Inverted duplications deletions: underdiagnosed rearrangements?? Clin Genet 75:505–513. https://doi.org/10.1111/j.1399-0004.2009.01187.x

Affiliations

Takema Kato[1] · Hidehito Inagaki[1] · Syunsuke Miyai[1] · Fumihiko Suzuki[1] · Yuki Naru[1] · Yasuko Shinkai[1] · Asuka Kato[1] · Kazuo Kanyama[1] · Seiji Mizuno[2] · Yukako Muramatsu[3] · Toshiyuki Yamamoto[4] · Mitsuhisa Shinya[5,6] · Yukiko Tazaki[5,6] · Sayuri Hiwatashi[5,6] · Toshiro Ikeda[5,6] · Mamoru Ozaki[7] · Hiroki Kurahashi[1,2]

Takema Kato
takema@fujita-hu.ac.jp

Hidehito Inagaki
hinagaki@fujita-hu.ac.jp

Syunsuke Miyai
smiyai@fujita-hu.ac.jp

Fumihiko Suzuki
fsuzuki@fujita-hu.ac.jp

Yuki Naru
y.naru@ovus.co.jp

Yasuko Shinkai
y.shinkai@ovus.co.jp

Asuka Kato
asukak@fujita-hu.ac.jp

Kazuo Kanyama
kanyamk@labcorp.com

Seiji Mizuno
seiji_mizuno@aichi-colony.jp

Yukako Muramatsu
murayuka@med.nagoya-u.ac.jp

Toshiyuki Yamamoto
yamamoto.toshiyuki@twmu.ac.jp

Mitsuhisa Shinya
m-shinya@m3.kufm.kagoshima-u.ac.jp

Yukiko Tazaki
tazaki-y@m.kufm.kagoshima-u.ac.jp

Sayuri Hiwatashi
sayuri1030@yahoo.co.jp

Toshiro Ikeda
ikeda@m2.kufm.kagoshima-u.ac.jp

Mamoru Ozaki
m-ozaki@kanazawa-med.ac.jp

[1] Division of Molecular Genetics, Institute for Comprehensive Medical Science, Fujita Health University, 1-98 Dengakugakubo, Kutsukake-cho, Toyoake, Aichi 470-1192, Japan

[2] Department of Clinical Genetics, Central Hospital, Aichi Developmental Disability Center, Kasugai, Kasugai, Japan

[3] Department of Pediatrics, Nagoya University Graduate School of Medicine, Nagoya, Japan

[4] Institute of Medical Genetics, Tokyo Women's Medical University, Shinjuku, Japan

[5] Genetic Counseling Room, Kagoshima University Hospital, Kagoshima, Japan

[6] Department of Obstetrics and Gynecology, Faculty of Medicine, Kagoshima, Japan

[7] Division of Genomic Medicine, Department of Advanced Medicine, Medical Research Institute, Kanazawa Medical University, Uchinada, Japan

Cytogenetic and Genome Research

Short Report

Cytogenet Genome Res
DOI: 10.1159/000507177

Accepted: March 6, 2020
Published online: April 4, 2020

Analysis of the Origin of Double Mosaic Aneuploidy in Two Cases

Takema Kato[a] Miki Kawai[a] Shunsuke Miyai[a] Fumihiko Suzuki[a]
Makiko Tsutsumi[a] Seiji Mizuno[b, c] Toshiro Ikeda[d, e] Hiroki Kurahashi[a]

[a]Division of Molecular Genetics, Institute for Comprehensive Medical Science, Fujita Health University, Toyoake, Japan; [b]Department of Pediatrics, Aichi Human Service Center, Central Hospital, Kasugai, Japan; [c]Department of Clinical Genetics, Aichi Developmental Disability Center, Central Hospital, Kasugai, Japan; [d]Genetic Counseling Room, Kagoshima University Hospital, Kagoshima, Japan; [e]Department of Obstetrics and Gynecology, Faculty of Medicine, Kagoshima University, Kagoshima, Japan

Keywords
Meiotic segregation · Mitotic segregation · Mosaicism · SNP microarray · Trisomy rescue

Abstract
We present 2 cases of double mosaic aneuploidy harboring 2 or more different aneuploid cell lines, but no line with a normal chromosome constitution. One of these cases presented mosaicism of sex chromosome aneuploid cell lines (47,XXX/45,X) along with another line containing an autosomal trisomy (47,XX,+8), while the other case showed mosaicism of 2 different autosomal trisomy cell lines (47,XY,+5 and 47,XY,+8). To elucidate the mechanisms underlying these mosaicisms, we conducted molecular cytogenetic analyses. Genotyping data from the SNP microarray indicated that 2 sequential meiotic or early postzygotic segregation errors likely had occurred followed by natural selection. These cases suggest that frequent segregation errors and selection events in the meiotic and early postzygotic stages lead to this condition.

In the course of blood karyotyping for the etiological analysis of multiple congenital anomalies or intellectual disabilities, or karyotyping of product of conception (POC) samples to investigate pregnancy loss, occasionally aneuploidy of different chromosomes is observed in 2 or more different cell lines as a mosaic. This is known as double mosaic aneuploidy. As this condition generally arises via 2 independent segregation errors in different cells, cells with a normal chromosome constitution are usually also present. However, in rare cases, double mosaic aneuploidy is seen in the absence of normal cell lines [Schofield et al., 1992; Harada et al., 1998; Schubert et al., 2002; Ryu et al., 2010; Kumar et al., 2014]. In these cases, the cytogenetic mechanisms leading to this condition are hard to understand.

In our current study, we describe 2 cases of double (triple) mosaic aneuploidy in which each cell harbored a single trisomic or monosomic chromosome, and no cells with normal chromosome content were observed. We performed molecular analyses and assessed the etiology of these cases.

T.K. and M.K. contributed equally to this work.

karger@karger.com
www.karger.com/cgr

Hiroki Kurahashi, M.D., Ph.D.
Division of Molecular Genetics, Institute for Comprehensive Medical Science
Fujita Health University, 1-98 Dengakugakubo, Kutsukake-cho
Toyoake, Aichi 470-1192 (Japan)
kura@fujita-hu.ac.jp

Material and Methods

For our analyses, we obtained blood samples and buccal mucosa cells from case 1 and POC samples from case 2.

Karyotyping

Chromosomal karyotyping of POC and blood samples was conducted using conventional G-banding methods.

Fluorescence in situ Hybridization

Interphase FISH analysis of peripheral blood and buccal mucosa cells was performed using a mixture of 2 probes: Vysis CEP 8 (D8Z2) Spectrum Green (Abbott Laboratories, IL) and Chromosome X Alpha Satellite (DXZ1) Texas Red (Cytocell Ltd, UK).

SNP Array

For SNP microarray analysis, genomic DNA was extracted from POC and blood specimens using a Gentra Puregene Tissue Kit (Qiagen, Germany). We then used the Affymetrix Cytoscan 750k array (Affymetrix, Santa Clara, CA) and the Illumina HumanCytoSNP-12 array (Illumina, San Diego, CA) for genotyping. Sample preparation was performed following the manufacturer's protocol. Copy number alterations and genotypes on the CytoScan 750k array were analyzed using Affymetrix® Chromosome Analysis Suite Software v4.0 (ChAS). Analysis of the CytoSNP-12 array data was carried out using GenomeStudio software (Illumina).

NGS Copy Number Analysis

Comprehensive copy number analysis was conducted using a next-generation sequencer (NGS), according to the manufacturer's protocol (Illumina). Genomic DNA was diluted and subjected to whole-genome amplification using SurePlex. Then, samples were prepared for NGS analysis. The library was sequenced using the VeriSeq PGS Kit - MiSeq system, and these sequencing data were analyzed using BlueFuse Multi Software (Illumina).

Results

Case 1

The 3-month-old girl was referred to our facility due to growth retardation and relative macrocephaly. She was the first-born child of a 35-year-old healthy mother and a 30-year-old healthy father. No dysmorphic features other than macrocephaly were observed, although agenesis of the corpus callosum was found by cerebral MRI, and a ventricular septal defect was also noted. The karyotype of the peripheral blood of the proband was mos 47,XX,+8[16]/47,XXX[4]. This double mosaic aneuploidy was found to be unique as it consisted of 2 cell lines that were aneuploid for a single different chromosome; no cells with normal chromosome content were observed. Since the proband had no clinical findings of sex chromosome aneuploidy or trisomy 8 mosaicism, we performed additional cytogenetic analyses. Repeated evaluations of the peripheral blood karyotype revealed mos 47,XX,+8[37]/47,XXX[8]/45,X[5]. FISH analysis of her buccal mucosa cells also indicated mosaic aneuploidy but with a different frequency, i.e., mos 47,XX,+8[5]/47,XXX[84]/45,X[11] (Fig. 1A, B). Her mild clinical findings might be explained by the low rate of trisomy 8 mosaicism in non-blood tissues. Unfortunately, we could not obtain the parental samples.

To further investigate the origin of the triple mosaic aneuploidy, we employed SNP microarray analysis of genomic DNA from blood. B allele frequency (BAF) analysis indicated that both chromosomes 8 and X had a 4-allele combination (Fig. 1C). The estimated mosaic rate was 50% for chromosome 8, whilst that for chromosome X was reduced, probably due to an compensation by the 45,X and 47,XXX lines. Since the other chromosomes did not show the 4-allele combination, a chimera of a zygote with trisomy 8 and another zygote with sex chromosome aneuploidy is unlikely. A 6-allele combination was not found in chromosome 8, suggesting an identical haplotype of its 2 copies. These data indicated that the segregation error for chromosome 8 might have been a meiosis II error between 2 sister chromatids without crossover in meiosis I, or a post-zygotic mitosis error. Because trisomy X and monosomy X were observed in case 1, a chromosome X nondisjunction should have occurred at the postzygotic stage.

From the aforementioned findings, we propose 2 possible pathways for this case of triple mosaic aneuploidy. Our first hypothesis is that a nondisjunction of chromosomes 8 and X occurred independently in each cell at the second postzygotic cell division. Monosomy 8 cells were then negatively selected (Fig. 1D-I). The other hypothesis assumes that the zygote is trisomic for chromosome 8 due to a meiosis II error. The extra chromosome 8 might be lost from one cell in the first postzygotic cell division. Then, in the following second cell division, the disomic cell might undergo mitotic nondisjunction of chromosome X (Fig. 1D-II).

Case 2

A 48-year-old woman presented at our clinic due to 3 consecutive miscarriages in which the pregnancy loss occurred at gestational week 7. Chromosome karyotyping of the POC sample dissected from chorionic villi revealed mos 47,XY,+5[48]/47,XY,+8[2] (Fig. 2A). To confirm this rare karyotype, we employed NGS chromosome analysis using genomic DNA from the surface of an uncultured POC sample. Full trisomy of chromosome 8 was observed, but the copy number was neutral for chromo-

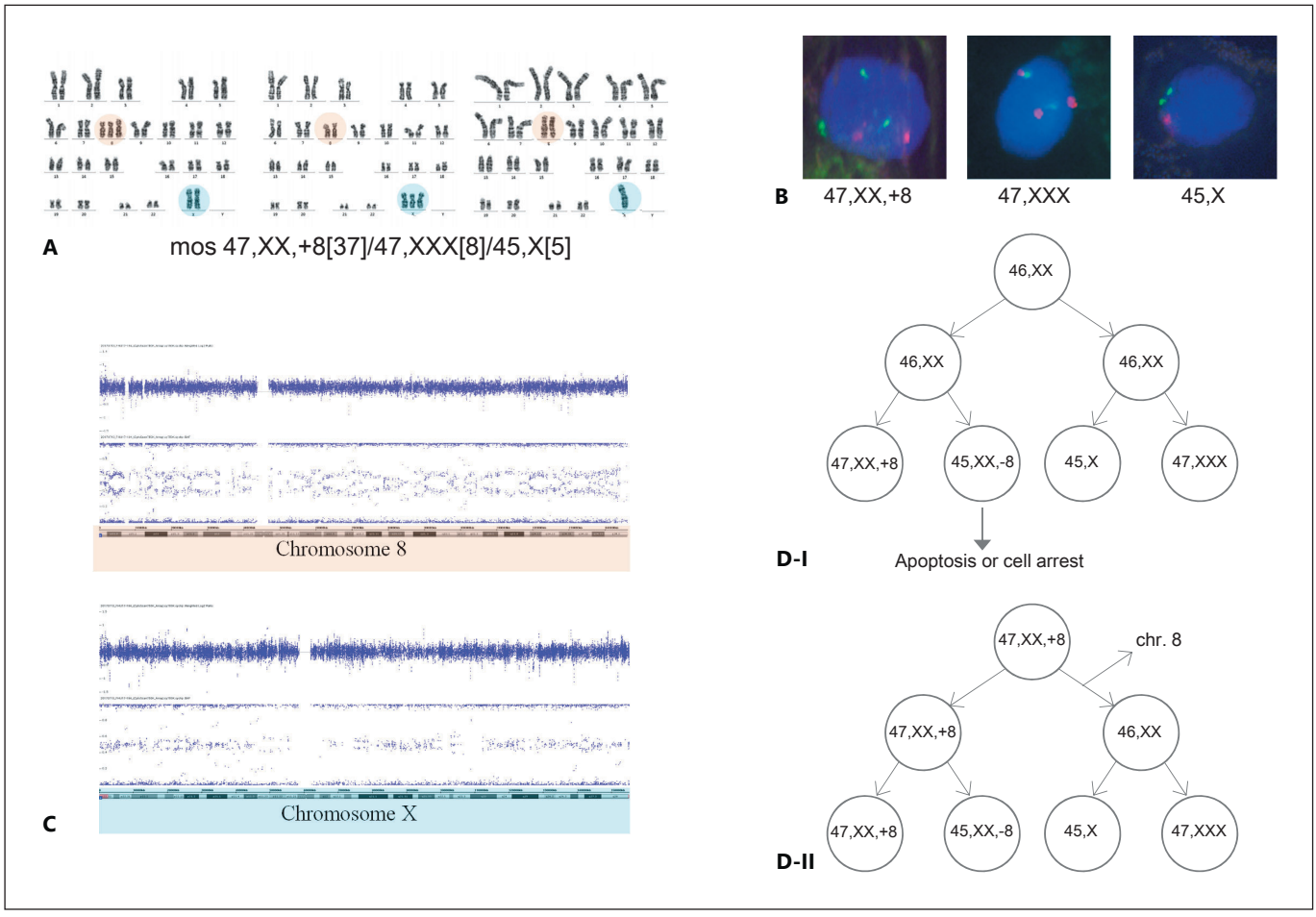

Fig. 1. Mosaic triple aneuploidy was identified in an infant with growth retardation and relative macrocephaly. **A** G-banding of peripheral blood lymphocytes revealed a mos 47,XX,+8/47,XXX/45,X karyotype. **B** Interphase FISH with alpha satellite probes specific for chromosome 8 (green) and chromosome X (red) on buccal mucosa cells. **C** SNP microarray analysis was used to determine a weighted log2 ratio (top) and B allele frequency (bottom) for chromosomes 8 and X. **D** Two possible mechanisms leading to the mosaic triple aneuploidy in this case (see text). The first 2 postzygotic divisions are shown.

some 5 (Fig. 2B). We speculated that this discordance might be attributable to differences in the cell source, i.e., trophoblasts in the uncultured sample and mesenchymal cell lineages in the cultured sample. The double mosaic aneuploidy detected in this POC was unique since it consisted of 2 cell lines that were aneuploid for a single, different chromosome, and no cells with normal chromosome content were observed. Unfortunately, we could not obtain the parental samples.

To determine the origin of the double mosaic aneuploidy in this case, we carried out SNP microarray analysis of genomic DNA isolated from an uncultured POC sample. The BAF results revealed a 4- or 6-allele combination pattern in both chromosomes 5 and 8 but in no other chromosome, indicating that a chimera of different zygotes each with a trisomy 5 or trisomy 8 was unlikely. The mosaic ratio estimated using the BAF was 20–40% for trisomy 5 and 60–70% for trisomy 8. The BAF of chromosome 5 showed a mixture of 4-allele and 6-allele combinations and a 4-allele combination surrounding the centromere, indicating a malsegregation event during meiosis II between sister chromatids with crossover (Fig. 2C). In contrast, chromosome 8 showed only a 4-allele combination throughout. This indicated that the missegregation of chromosome 8 would be due to a postzygotic mitotic error or meiosis II error between sister chromatids without crossover (Fig. 2C).

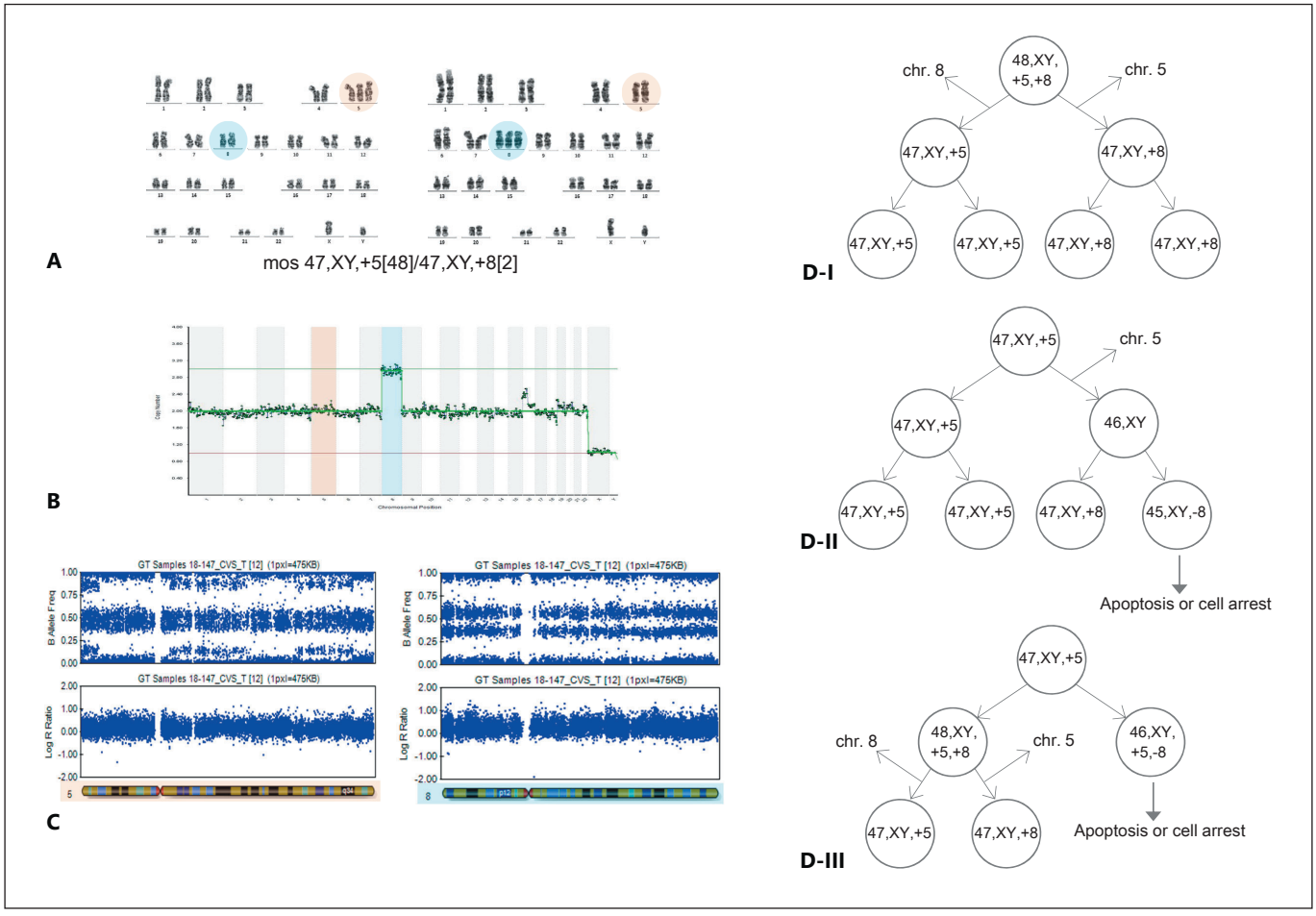

Fig. 2. Mosaic double trisomy was identified in the POC sample of a 48-year-old woman. **A** G-banding revealed a mos 47,XY,+5/47,XY,+8 karyotype in the POC sample. **B** NGS analysis of DNA from an uncultured sample indicated a neutral copy number for chromosome 5 and a full chromosome 8 trisomy. **C** SNP microarray analysis of the B allele frequency (top) and logR ratio (bottom) for chromosomes 5 and 8. **D** Three possible mechanisms for the mosaic double aneuploidy in this case (see text). The first 2 postzygotic divisions are shown.

Based on these observations, we surmised that there were 3 possible pathways that could have led to the double mosaic aneuploidy in case 2. The first was based on an original zygote with 48,XY,+5,+8 possibly derived from meiotic errors. During the first postzygotic mitotic cell division, loss of chromosome 5 or 8 in either of the 2 cells, respectively, resulted in 47,XY,+5 and 47,XY,+8 cells (Fig. 2D-I). A second possibility was that a 47,XY,+5 zygote, derived from a meiotic error, led by loss of chromosome 5 in the first postzygotic cell division to 47,XY,+5 and 46,XY cells, respectively. In the second cell division, the rescued 46,XY cell underwent mitotic nondisjunction of chromosome 8, followed by negative selection of the monosomy 8 cell (Fig. 2D-II). The third possible pathway was that an original zygote with trisomy 5 underwent mitotic nondisjunction of chromosome 8 at the first cell division. This would have generated a 48,XY,+5,+8 and a 46,XY,+5,–8 cell underlying negative selection. In the subsequent second mitotic cell division, the 48,XY,+5,+8 cell would then have lost chromosome 5 or 8 in either of the 2 cells, resulting in 47,XY,+5 and 47,XY,+8 cells (Fig. 2D-III).

Discussion and Conclusion

Double mosaic aneuploidy without a euploid cell line is a very rare condition, and only a small number of cases have been reported to date [Schofield et al., 1992; Harada

et al., 1998; Schubert et al., 2002; Ryu et al., 2010]. This is likely due to a low fetal viability in the absence of euploid cells. When 2 different numerical chromosome abnormalities occur simultaneously or sequentially in the same cell line, a subset of cells should carry these 2 types of aneuploidy parallelly. When 2 different numerical chromosome abnormalities arise independently in different cell lines, each cell line should carry each single aneuploidy separately. In the second situation, original euploid cells should be generally present. However, we have here presented 2 cases of double mosaic aneuploidy in the absence of normal cells, in which the underlying cytogenetic mechanisms are hard to understand.

Our molecular cytogenetic analyses of these 2 cases indicated that the double mosaic aneuploidy arose via 2 successive segregation errors either during maternal meiosis or in early postzygotic stages, which was then followed by natural selection. The errors may have been nondisjunction or predivision during meiosis I or II, or missegregation during mitosis at the early postzygotic stage, such as nondisjunction or anaphase lagging [Conlin et al., 2010]. Such phenomena usually produce monosomy or trisomy, but in some cases can lead to monosomy or trisomy rescue. It has been amply documented that a high level of chromosome instability develops during meiosis in oogenesis and in cleavage-stage embryos [Vanneste et al., 2009; Nagaoka et al., 2012; Fragouli et al., 2013; Potapova and Gorbsky, 2017]. This was further validated by the recent advances in single-cell genomic analysis using NGS [Fiorentino et al., 2014]. Additionally, it has been demonstrated that the large amount of cytoplasm present in oocytes and cleavage stage embryos induces error-prone chromosome segregation via dilution of spindle assembly checkpoint proteins [Kyogoku and Kitajima, 2017]. This instability might contribute to the 2 successive segregation errors at this stage in a single zygote, thereby leading to the development of double mosaic aneuploidy.

Most of the reported double mosaic aneuploidies are combinations of autosomal and gonosomal aneuploidy [Schofield et al., 1992; Harada et al., 1998; Schubert et al., 2002; Ryu et al., 2010; Kumar et al., 2014; present case 1]. Trisomy 13, trisomy 18, trisomy 21, and sex chromosome aneuploidies are often involved due to phenotypic selection. In contrast, the combination of 2 different autosomal aneuploidies is very rare [Huijsdens-van Amsterdam et al., 2012; Jurcă et al., 2018; present case 2]. Notably, many reports of this rare condition, including our present study, have described chromosome 8 mosaic trisomy [Schofield et al., 1992; DeBrasi et al., 1995]. Prior trisomy 8 nondisjunction studies have found that most mosaic trisomy 8 cases are likely due to mitotic duplication, with only a few cases arising from a maternal meiotic nondisjunction. Those results are in contrast to the findings for common autosomal trisomies where the majority of cases are due to errors in maternal meiosis [Karadima et al., 1998]. However, the reasons why chromosome 8 is frequently involved in double mosaic aneuploidy are unclear. Cell lineage-specific mitotic duplication or cell lineage-specific selection may be possible mechanisms. Future detailed case reports will be required to clarify the mechanisms underlying the involvement of specific chromosomes in double mosaic aneuploidy.

Acknowledgements

We thank the patients and their families for agreeing to participate in this study.

Statement of Ethics

This study was approved by the Ethical Review Board for Human Genome Studies at Fujita Health University. Written informed consent was obtained from the patients. All experiments were carried out in accordance with the relevant guidelines and regulations.

Disclosure Statement

The authors have no conflicts of interest to declare.

Funding Sources

This study was supported by a Grant-in-Aid for Scientific Research from the Ministry of Education, Culture, Sports, Science, and Technology of Japan (17K11259 to T.K., 15H04710 and 24390085 to H.K.) and from the Ministry of Health, Welfare and Labor (16ek0109067h0003 to H.K.).

Author Contributions

T.K. and M.K. drafted the manuscript. T.K., M.K., S.M., F.S., M.T., S.M., and T.I. participated in designing the study and carried out the molecular biology work. H.K. coordinated and conceived the study and was involved in the critical revision of the manuscript for important intellectual content.

References

Conlin LK, Thiel BD, Bonnemann CG, Medne L, Ernst LM, et al: Mechanisms of mosaicism, chimerism and uniparental disomy identified by single nucleotide polymorphism array analysis. Hum Mol Genet 19:1263–1275 (2010).

DeBrasi D, Genardi M, D'Agostino A, Calvieri F, Tozzi C, et al: Double autosomal/gonosomal mosaic aneuploidy: study of nondisjunction in two cases with trisomy of chromosome 8. Hum Genet 95:519–525 (1995).

Fiorentino F, Biricik A, Bono S, Spizzichino L, Cotroneo E, et al: Development and validation of a next-generation sequencing-based protocol for 24-chromosome aneuploidy screening of embryos. Fertil Steril 101:1375–1382 (2014).

Fragouli E, Alfarawati S, Spath K, Jaroudi S, Sarasa J, et al: The origin and impact of embryonic aneuploidy. Hum Genet 132:1001–1013 (2013).

Harada N, Abe K, Nishimura T, Sasaki K, Ishikawa M, et al: Origin and mechanism of formation of 45,X/47,XX,+21 mosaicism in a fetus. Am J Med Genet 75:432–437 (1998).

Huijsdens-van Amsterdam K, Barge-Schaapveld DQ, Mathijssen IB, Alders M, Pajkrt E, Knegt AC: Prenatal diagnosis of a trisomy 7/trisomy 13 mosaicism. Mol Cytogenet 5:8 (2012).

Jurcă MC, Bembea M, Iuhas OA, Kozma K, Petcheşi CD, et al: Double autosomal trisomy with mosaicism 47,XY(+8)/47,XY(+21). Morphological and genetic changes of a rare case. Rom J Morphol Embryol 59:985–988 (2018).

Karadima G, Bugge M, Nicolaidis P, Vassilopoulos D, Avramopoulos D, et al: Origin of nondisjunction in trisomy 8 and trisomy 8 mosaicism. Eur J Hum Genet 6:432–438 (1998).

Kumar M, Lal V, Chapadgaonkar S, Bhattacharya SK: A rare case of mosaic 45,X/47,XX,+13 in 28-year-old women with secondary amenorrhoea: a case report and literature review. Meta Gene 3:8–13 (2014).

Kyogoku H, Kitajima TS: Large cytoplasm is linked to the error-prone nature of oocytes. Dev Cell 41:287–298 (2017).

Nagaoka SI, Hassold TJ, Hunt PA: Human aneuploidy: mechanisms and new insights into an age-old problem. Nat Rev Genet 13:493–504 (2012).

Potapova T, Gorbsky G: The consequences of chromosome segregation errors in mitosis and meiosis. Biology (Basel) 6:12 (2017).

Ryu SW, Lee G, Baik CS, Shim SH, Kim JT, et al: Down-Turner syndrome (45,X/47,XY,+21): case report and review (in Korean). Korean J Lab Med 30:195–200 (2010).

Schofield B, Babu A, Punales-Morejon D, Popescu S, Leiter E, et al: Double mosaic aneuploidy: 45,X/47,XY,+8 in a male infant. Am J Med Genet 44:7–10 (1992).

Schubert R, Eggermann T, Hofstaetter C, von Netzer B, Knöpfle G, Schwanitz G: Clinical, cytogenetic, and molecular findings in 45,X/47,XX,+18 mosaicism: clinical report and review of the literature. Am J Med Genet A 110:278–282 (2002).

Vanneste E, Voet T, Le Caignec C, Ampe M, Konings P, et al: Chromosome instability is common in human cleavage-stage embryos. Nat Med 15:577–583 (2009).

Journal of Human Genetics (2020) 65:705–709
https://doi.org/10.1038/s10038-020-0748-4

BRIEF COMMUNICATION

A case of a parthenogenetic 46,XX/46,XY chimera presenting ambiguous genitalia

Rie Kawamura[1] · Takema Kato[1] · Shunsuke Miyai[1] · Fumihiko Suzuki[1] · Yuki Naru[1] · Maki Kato[1] · Keiko Tanaka[2] · Miwako Nagasaka[2,3] · Makiko Tsutsumi[1] · Hidehito Inagaki[1] · Tomoaki Ioroi[4] · Makiko Yoshida[5] · Tomoya Nao[6] · Laura K. Conlin[7] · Kazumoto Iijima[2,3] · Hiroki Kurahashi[1] · Mariko Taniguchi-Ikeda[1,8]

Received: 17 December 2019 / Revised: 12 March 2020 / Accepted: 12 March 2020 / Published online: 10 April 2020

Abstract

Sex-chromosome discordant chimerism (XX/XY chimerism) is a rare chromosomal disorder in humans. We report a boy with ambiguous genitalia and hypospadias, showing 46,XY[26]/46,XX[4] in peripheral blood cells. To clarify the mechanism of how this chimerism took place, we carried out whole-genome genotyping using a SNP array and microsatellite analysis. The B-allele frequency of the SNP array showed a mixture of three and five allele combinations, which excluded mosaicism but not chimerism, and suggested the fusion of two embryos or a shared parental haplotype between the two parental cells. All microsatellite markers showed a single maternal allele. From these results, we concluded that this XX/XY chimera is composed of two different paternal alleles and a single duplicated maternal genome. This XX/XY chimera likely arose from a diploid maternal cell that was formed via endoduplication of the maternal genome just before fertilization, being fertilized with both X and Y sperm.

These authors contributed equally: Rie Kawamura, Takema Kato

Supplementary information The online version of this article (https://doi.org/10.1038/s10038-020-0748-4) contains supplementary material, which is available to authorized users.

✉ Mariko Taniguchi-Ikeda
mtani@fujita-hu.ac.jp

1 Department of Molecular Genetics, Fujita Health University, Toyoake, Japan

2 Division of Genetic Counseling, Kobe University Hospital, Kobe, Japan

3 Department of Pediatrics, Kobe University Graduate School of Medicine, Kobe, Japan

4 Department of Pediatrics, Comprehensive Perinatal Maternal and Child Medical Center, Himeji Red Cross Hospital, Himeji, Japan

5 Department of Pathology, Hyogo Prefectural Kobe Children's Hospital, Kobe, Japan

6 Department of Urology, Hyogo Prefectural Kobe Children's Hospital, Kobe, Japan

7 Division of Genomic Diagnostics, Department of Pathology and Laboratory Medicine, Children's Hospital of Philadelphia, Philadelphia, PA, USA

8 Department of Clinical Genetics, Fujita Health University Hospital, Toyoake, Japan

A chimera is defined as the fusion product of two different zygotes in a single embryo, whereas a mosaic results from a mitotic error in a single zygote. Sex-chromosome discordant chimerism in humans (XX/XY chimerism) is a rare chromosomal abnormality. Although the first case was described in 1962 [1], its incidence is still unknown. The XX/XY chimera manifests variable genital phenotypes, ranging from normal male or female genitalia to different degrees of ambiguous genitalia. Chimeras are thought to result from a defect in the processes near the time of fertilization. The XX/XY chimera is classified into some subtypes; tetragametic chimeras [2–5], parthenogenetic chimeras [5–9], androgenetic chimeras [5, 10, 11] and sesquizygotic twinning chimera [12]. Whereas tetragametic chimeras are known as the most common subtype of XX/XY chimeras, which are derived from the simple fusion of two different zygotes, parthenogenetic chimeras and androgenetic chimeras [8, 11] undergo endoreplication of one of the gametic genomes. Therefore, genotyping of XX/XY chimeras is important not only to clarify its developmental mechanism but also for diagnosis and treatment, as such patients occasionally present with fertility problems. In this report, we present a case of a parthenogenic chimera with a karyotype of XX/XY, together with a literature review.

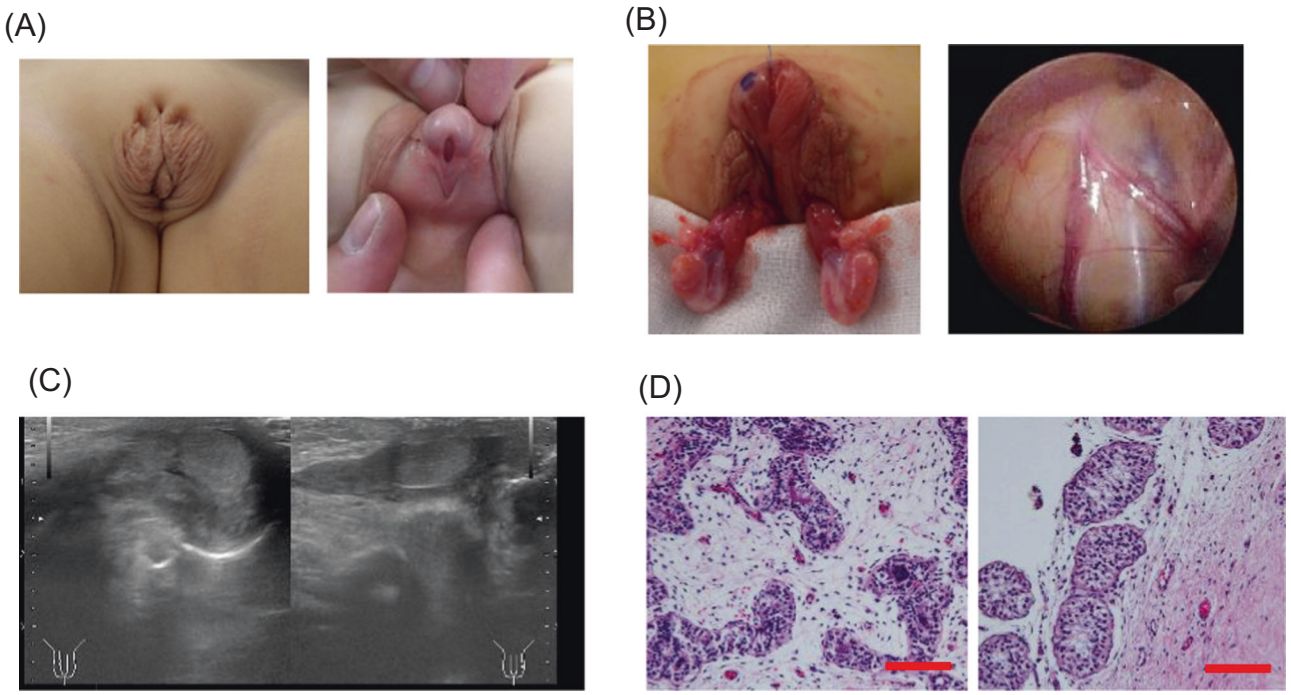

Fig. 1 Clinical findings of the patient. **a** On examination, the patient showed cryptorchidism (left), hypospadias (right), and anterior scrotum (right). **b** On operation, epididymes were identified macroscopically, but the tunica albuginea of the testis was absent bilaterally (left). Laparoscopy demonstrated that the vas deferens and gonadal veins flowed normally into the bilateral inguinal rings, and ovaries and a uterus were not detected (right). The precise position of the external urethral opening was normal. **c** The ultrasound echoic level of both gonads was homogeneous. No other tissue-like structures with margins, suggestive of ovarian tissue, were detected. **d** Testis biopsy of the patient (left). Compared to control tissue (right, age-matched normal testis), interstitial tissue of the patient was edematous and more prominent than the seminiferous tubules, which were tortuous and diverging. The seminiferous tubules appeared dysplastic, but detailed analysis demonstrated that they were not dysplastic. Bar, 100 µm

The patient was born from healthy parents at an affiliated hospital as a boy with ambiguous genitalia, hypospadias cryptorchidism, and an anterior scrotum (Fig. 1a). The pregnancy was not a result of in vitro fertilization treatment. His father was 43 years old and mother was 31 years old. Abdominal magnetic resonance imaging displayed no uterus or ovaries. His growth milestone at 1 year was normal. The patient's toy preference was wheeled vehicles and superheroes. Macro- and microscopically, the patient had ambiguous external genitalia, male-type internal genitalia (epididymis), and bilateral testes (Fig. 1b–d). The family chose a male sex to assign. Hypospadias was repaired. The parents were recommended to undergo genetic counseling regarding detailed genetic analysis as well as recurrence risk. G-banding from peripheral blood cells of the patient showed 46,XY[26]/46,XX[4]. To analyze the XX/XY ratio further, we performed fluorescence in situ hybridization (FISH) analysis on interphase nuclei from the patient's buccal mucosal cells with specific probes for chromosomes X and Y by AneuVysion Assay Kit (Abbott, Tokyo, Japan). FISH showed nuc ish XX[83]/XY[17]. The XY/XX ratio in buccal cells (17%) was lower than that in peripheral blood cells (87%). After receiving approval from the Ethics Review Board for Human Genome Studies at Fujita Health University and written informed consent from the parents to participate in our study, genetic diagnosis was performed.

To confirm chimerism, we carried out SNP microarray analysis using a CytoScan 750 K Array (Affymetrix, Santa Clara, CA). We used genomic DNA, which was isolated from nail as a template for microarray analysis. Scan data were visualized using ChAS 3.2 software (Affymetrix). The copy number state of chromosome X was 1.5, which means that the ratio of XX to XY was about 50% (Fig. 2a). Next, to confirm chimerism, we analyzed the B-allele frequency of autosomes and the X chromosome [13, 14]. We found both a region showing five allele combinations, where possible SNP genotypes were BB–BB, BB–BA, BB–AA, BA–AA, and AA–AA, which means that there were three or four chromosome sets, and a region showing three allele combinations, where the possible SNP genotypes were BB–BB, AB–AB, and AA–AA, which means that there were two identical chromosome sets in the autosomes (Fig. 2b). The region showing four allele combinations, where the possible SNP genotypes were BB–B, BB–A, AA–B, and AA–A, were on chromosome X (Fig. 2b). These allele combinations were detected throughout the whole genome (Supplementary Fig. 1). This indicates the

(A)

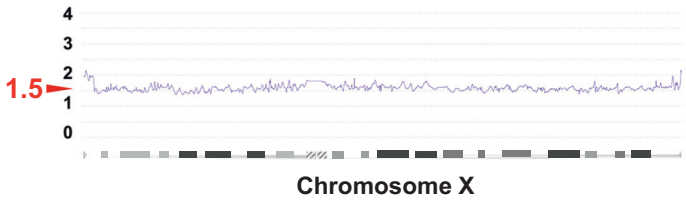

(C)

STR Maker	G-band	Proband	Father	Mother
D1S0859i	1p21.2	319 / 331 / 375	319 / 331	375 / 347
D1S2671	1p21.2	168 / 170 / 178	168 / 170	178 / 182
D2S2110	2p13.2	132 / 136 / 138	132 / 136	138 / 134
D5S1411	5q13.1	246 / 250 / 248	246 / 250	248 / 236
DXS1048	Xp21.3	168 / 170	168	170 / 172
DXS0441i	Xq22.3	264 / 234	264	234 / 262
DXS0633	Xq28	329 / 323	329	323 / 347

(B)

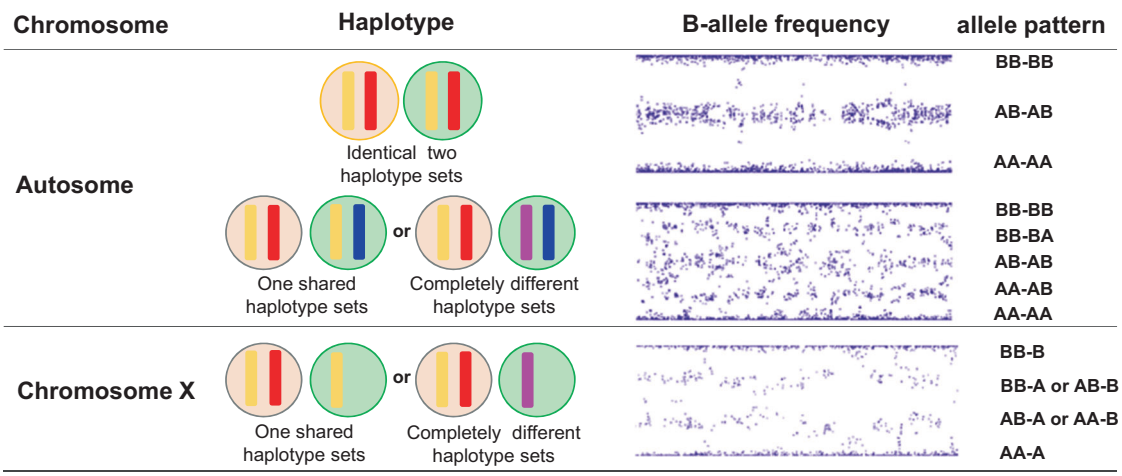

Fig. 2 SNP array and STR analysis. **a** Smooth signal track of the patient's X chromosome. Copy number (*Y* axis) showed 1.5, suggesting that the patient has more than two sets of X chromosomes. **b** A B-allele frequency (BAF) plot and possible allele patterns of the patient's nail DNA, showing a XX to XY ratio of 50% in SNP array analysis. The blue and red colored chromosomes in the circles are both of paternal origin. The yellow and pink colored chromosomes are of maternal origin. **c** STR maker analysis. Red and blue numbers indicate paternal origin, and yellow and pink numbers indicate maternal origin

presence of two different genomes, demonstrating that the patient does not show mosaicism but is an XX/XY chimera. Haplotype sharing region encompasses 1.5 Gbps, which is approximately half of the entire genome (Supplementary Fig. 1), suggesting that the chimera is possibly tetragenic, parthenogenic or androgenic. However, SNP array is not able to classify chimerism.

To investigate the parental origin of the genome in the patient, we performed microsatellite marker analysis, as known as short tandem repeat (STR) analysis. This time, genomic DNA was extracted from the patient's nails and parental peripheral blood cells. We chose STR markers located in the region showing the five allele combinations in autosomes or four allele combinations on chromosome X on SNP array analysis. We first determined the patient's genotype as well as the genotype of the parents. Next, the proband's genotype was determined by using completely different markers in autosomes. All markers showed the contribution of two paternal alleles and one maternal allele in the chimera (Fig. 2c). Therefore, we determined the dispermic origin of the chimera. We concluded that the patient is a parthenogenetic chimera, which is composed of two paternal alleles and one duplicated maternal allele (Fig. 3a).

Although there are various mechanisms that lead to the development of chimeras, our results suggested that this patient was a parthenogenetic chimera [9]. Oocyte possibly started first mitosis before the disappearance of the pronuclear.

From the point of view of genetic counseling, the recurrence risk of this condition in this family is low because of the lack of a family history. On the other hand, careful follow-up of testicular function is important in considering future family planning and gender identity for the patient. However, as the chimeric ratio in this patient is different among various tissues in the body [15], androgen or estrogen exposure to the entire body cannot be assessed and it is difficult to predict the risk of problems, such as gonadoblastoma (Fig. 3b). In addition, genetic counseling should be recommended so that the patient's gender identity can be determined autonomously when the pathological condition is explained to the patient.

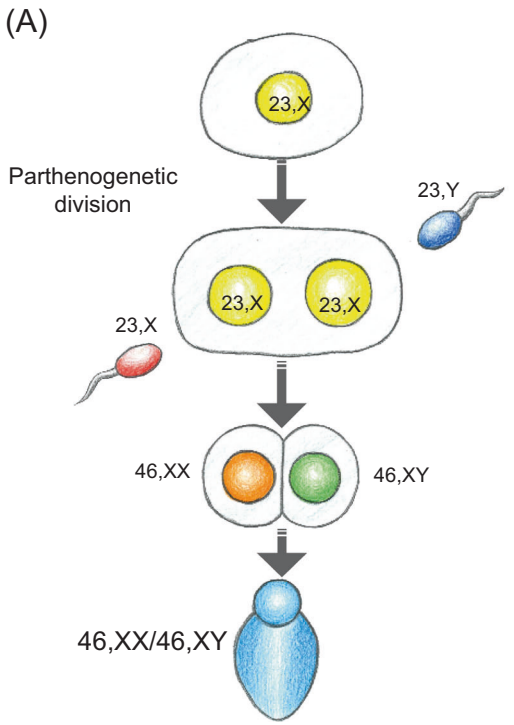

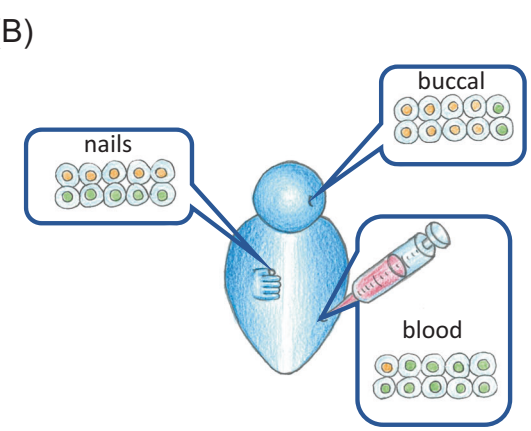

Tissue	XX:XY ratio
Blood	1:9
Nails	5:5
Buccal tissue	8:2

Fig. 3 Schematic drawing of how a parthenogenetic chimera is produced. **a** Schematic drawing of how a parthenogenetic chimera is produced. Endoduplication of the maternal genome occurs just before fertilization with two spermatozoa. The colors of the cells are consistent with Fig. 2b, c. **b** Top, diagram of XX and XY chimeric ratios of three tissues from the patient. Orange cells indicate 46,XX, and green cells indicate 46,XY. Bottom, whereas G-banding from the peripheral blood cells of the patient showed 46,XY[26]/46,XX[4] (XX:XY ratio, 1:9), FISH showed nuc ish XX[83]/XY[17] (XX:XY ratio, 8:2) in buccal cells, and the SNP array suggested that both XX and XY are present at about 50% (XX:XY ratio, 5:5)

In the present case, genotyping determined that the patient had a rare condition (XX/XY chimerism). Furthermore, it was suggested that the patient was not the common tetragametic chimera, but a parthenogenetic chimera. Genotyping of XX/XY chimeras is important not only for clarifying the pathogenesis of chimeras but also for understanding of the disease. Therefore, we expect this method to become the standard for patients who are chimeric for the XX/XY karyotype.

Acknowledgements We would like to thank the patient and the family for participating in this study. We would also like to thank Dr Akiko Helena Popiel for valuable comments, Tatsuro Ikeda for drawing of the Figures. This study was supported by a grant-in-aid for Scientific Research from the Ministry of Education, Culture, Sports, Science, and Technology of Japan (grant number 17K00481 to RK, to 17K11259 to TK).

Compliance with ethical standards

Conflict of interest The authors declare that they have no conflicts of interest.

Publisher's note Springer Nature remains neutral with regard to jurisdictional claims in published maps and institutional affiliations.

References

1. Gartler SM, Waxman SH, Giblett E. An XX/XY human hermaphrodite resulting from double fertilization. Proc Natl Acad Sci USA. 1962;48:332–5.
2. Laursen RJ, Alsbjerg B, Vogel I, Gravholt CH, Elbaek H, Lildballe DL, et al. Case of successful IVF treatment of an oligospermic male with 46,XX/46,XY chimerism. J Assist Reprod Genet. 2018;35:1325–8.
3. Sheets KM, Baird ML, Heinig J, Davis D, Sabatini M, Starr DB. A case of chimerism-induced paternity confusion: what ART practitioners can do to prevent future calamity for families. J Assist Reprod Genet. 2018;35:345–52.
4. Malan V, Gesny R, Morichon-Delvallez N, Aubry MC, Benachi A, Sanlaville D, et al. Prenatal diagnosis and normal outcome of a 46, XX/46,XY chimera: a case report. Hum Reprod. 2007;22:1037–41.
5. Malan V, Vekemans M, Turleau C. Chimera and other fertilization errors. Clin Genet. 2006;70:363–73.
6. Shin SY, Yoo HW, Lee BH, Kim KS, Seo EJ. Identification of the mechanism underlying a human chimera by SNP array analysis. Am J Med Genet A. 2012;158:2119–23.
7. Lee KF, Hsu CS, Kuo PL, Chen JL, Jiang YH, Liu IY. The identification of a spontaneous 47,XX,+21/46,XY chimeric fetus with male genitalia. BMC Med Genet. 2012;13:85.
8. Yamazawa K, Nakabayashi K, Kagami M, Sato T, Saitoh S, Horikawa R, et al. Parthenogenetic chimaerism/mosaicism with a Silver-Russell syndrome-like phenotype. J Med Genet. 2010;47:782–5.
9. Giltay JC, Brunt T, Beemer FA, Wit JM, van Amstel HK, Pearson PL, et al. Polymorphic detection of a parthenogenetic

maternal and double paternal contribution to a 46,XX/46,XY hermaphrodite. Am J Hum Genet. 1998;62:937–40.
10. Kaiser-Rogers KA, McFadden DE, Livasy CA, Dansereau J, Jiang R, Knops JF, et al. Androgenetic/biparental mosaicism causes placental mesenchymal dysplasia. J Med Genet. 2006;43:187–92.
11. Giurgea I, Sanlaville D, Fournet JC, Sempoux C, Bellanné-Chantelot C, Touati G, et al. Congenital hyperinsulinism and mosaic abnormalities of the ploidy. J Med Genet. 2006;43:248–54.
12. Gabbett MT, Laporte J, Sekar R, Nandini A, McGrath P, Sapkota Y, et al. Molecular support for heterogonesis resulting in sesquizygotic twinning. N Engl J Med. 2019;28:842–9.
13. Davidsson J, Johansson B. Methylation and expression analyses of Pallister-Killian syndrome reveal partial dosage compensation of tetrasomy 12p and hypomethylation of gene-poor regions on 12p. Epigenetics. 2016;3:194–204.
14. Conlin LK, Thiel BD, Bonnemann CG, Medne L, Ernst LM, Zackai EH, et al. Mechanisms of mosaicism, chimerism and uniparental disomy identified by single nucleotide polymorphism array analysis. Hum Mol Genet. 2010;19:1263–75.
15. Biesecker LG, Spinner NB. A genomic view of mosaicism and human disease. Nat Rev Genet. 2013;14:307–20.

Tsutsumi et al. BMC Cancer (2020) 20:1162
https://doi.org/10.1186/s12885-020-07653-z

BMC Cancer

RESEARCH ARTICLE Open Access

An aggressive systemic mastocytosis preceded by ovarian dysgerminoma

Makiko Tsutsumi[1†], Hiroki Miura[2†], Hidehito Inagaki[1], Yasuko Shinkai[1], Asuka Kato[1,3], Takema Kato[1], Susumu Hamada-Tsutsumi[4], Makito Tanaka[2], Kazuko Kudo[2], Tetsushi Yoshikawa[2] and Hiroki Kurahashi[1*]

Abstract

Background: Aggressive systemic mastocytosis (ASM) is a rare malignant disease characterized by disordered mast cell accumulation in various organs. We here describe a female ASM patient with a previous history of ovarian dysgerminoma.

Methods: Molecular cytogenomic analyses were performed to elucidate an etiological link between the ASM and dysgerminoma of the patient.

Results: This patient was affected by ovarian dysgerminoma which was treated by chemotherapy and surgical resection. Having subsequently been in complete remission for 2 years, she developed symptoms of ASM. A somatic D816A mutation in the *KIT* gene was detected in her bone marrow, which facilitated the diagnosis of ASM. Unexpectedly, this *KIT* D816A variant was also detected in the prior ovarian dysgerminoma sample. Whole-exome sequencing allowed us to identify a somatic nonsense mutation of the *TP53* gene in the bone marrow, but not in the dysgerminoma. Microarray analysis of the patient's bone marrow revealed a copy-number-neutral loss of heterozygosity at the *TP53* locus, suggestive of the homozygous nonsense mutation in the *TP53* gene. In addition, the loss of heterozygosity at the *TP53* locus was also detected in the dysgerminoma.

Conclusions: These results indicated that either the mast cells causing the ASM in this case had originated from the preceding ovarian dysgerminoma as a clonal evolution of a residual tumor cell, which acquired the *TP53* mutation, or that both tumors developed from a common cancer stem cell carrying the *KIT* D816A variation.

Keywords: Aggressive systemic mastocytosis, *KIT*, Dysgerminoma, Germ cell tumor, *TP53*, Loss of heterozygosity

Background

ASM is one of the advanced forms of systemic mastocytosis (SM) with a poor prognosis. In this disorder, clonal mast cells become abnormally accumulated in the skin, lymph nodes, liver, gastrointestinal tract and bone marrow (BM) where they are activated and release mediators such as histamine, tryptase and cytokines that then cause organ damage [1–3]. The prevalence of ASM is 0.09 per 100,000, and the median age at diagnosis is over 60 years. ASM is quite rare in pediatric population [4–6]. The D816V mutation in *KIT* is frequently found in the tumor cells of SM patients and is an important part of the established diagnostic criteria for ASM. In addition to *KIT* variations, somatic mutations in other genes also occur in ASM that facilitate tumor growth [2, 7].

Ovarian dysgerminoma is one of the common malignant germ cell tumors believed to develop from primordial germ cells (PGCs) due to its morphology. These malignant tumors more frequently occur in adolescents and young adults, and surgical resection accompanied

* Correspondence: kura@fujita-hu.ac.jp
†Makiko Tsutsumi and Hiroki Miura contributed equally to this work.
[1]Division of Molecular Genetics, Institute for Comprehensive Medical Science, Fujita Health University, 1-98 Dengakugakubo, Kutsukake-cho, Toyoake, Aichi 470-1192, Japan
Full list of author information is available at the end of the article

with chemotherapy generally result in a good prognosis [8, 9].

In our present case report, we describe an adolescent case of ASM in a female with a previous history of ovarian dysgerminoma. Genetic analysis indicated a common origin for these malignancies and provided insights into the processes underlying the progression to ASM.

Methods

Samples for genetic analyses

Genomic DNA was isolated from peripheral blood (PB) and BM samples of the study patient using the QuickGene DNA whole blood DNA kit L (Kurabo, Osaka, Japan). Genomic DNA of the buccal mucosa was extracted using the DNeasy Blood and Tissue kit (Qiagen, Tokyo, Japan). A formalin-fixed paraffin-embedded specimen of the surgically dissected ovarian dysgerminoma was deparaffinized in xylene followed by proteinase treatment, phenol/chloroform extraction and ethanol precipitation of DNA. Conventional G-banding of the patient's bone marrow was performed using a standard method.

PCR amplification and sequencing

DNA fragments were amplified by PCR using Ex-Taq or LA-Taq polymerase (Takara, Kusatsu, Japan) followed by direct sequencing with the primers listed in Table S1 of the Additional file 1. Where indicated, PCR products were cloned into the pT7 Blue T-vector (Novagen, Madison, WI, USA) and then sequenced.

Real-time quantitative PCR

Quantitative PCR of the *KIT* gene was performed on the StepOnePlus Real-Time PCR system (Thermo Fisher Scientific, Waltham, MA, USA) using the PowerUp SYBR Green Master Mix (Thermo Fisher Scientific) with the primers listed in Table S1 of the Additional file 1. The *DROSHA* gene was used as an internal control.

Whole-exome sequencing

Whole-exome sequencing of the PB and BM specimens was performed as described previously [10]. The sequencing data were analyzed with Variant Studio 2.3 (Illumina, San Diego, CA, USA), Integrative Genomics Viewer ver.2.4.19 (Broad Institute, Cambridge, MA, USA) and Mutect2 software (Broad Institute). The list of known cancer genes in the Cancer Gene Census [11] was used to identify mutations in the study patient.

Cytogenetic microarray

Whole genomic microarray analysis of the BM sample was performed using the CytoScan 750 K array (Affymetrix, Santa Clara, CA) and analyzed using R package Rawcopy [12].

Results

Case presentation

The study case was affected with ovarian dysgerminoma when she was 13 years old. She received 4 cycles of chemotherapy, consisting of bleomycin, etoposide and cisplatin, followed by complete surgical resection of the tumor. After this resection, the patient's α-fetoprotein (AFP) level fell from 1053 ng/ml (normal range, 0–10.5 ng/ml) to normal levels and she received 2 cycles of postoperative chemotherapy consisting of carboplatin and etoposide.

She had been in complete remission for 2 years but developed recurring episodes of skin rash, bone pain, periodic fever and anaphylactic reactions when she was 16 years old (Fig. 1). A computed tomography scan suggested skeletal involvement with osteosclerosis mainly affecting the spine and osteolysis in a limited area of bones, but no tumor mass was observed suggesting that ovarian dysgerminoma recurrence was unlikely. BM examination of the osteolytic lesions revealed multifocal, dense infiltrates of mast cells that showed positive immunohistochemical staining for mast cell tryptase, CD25, CD33, and c-KIT, but no dysgerminoma cell was observed. A mutation at codon 816 of the KIT gene was further revealed in these cells, as detailed later. In addition, the serum tryptase level was markedly elevated at 276 μg/L (normal range, 1–15 μg/L), but AFP level was normal. The patient was subsequently diagnosed with ASM in accordance with the 2016 WHO classification of mastocytosis. The initial therapeutic intervention, including prednisolone, and histamine H1- and H2- receptor antagonists, improved her general condition, but the frequency of anaphylaxis did not decrease significantly and she became steroid dependence. Furthermore, her serum alkaline phosphatase level, which is indicative of disease activity, temporarily decreased and then rose again from 595 to 2857 U/L (normal range, 115–359 U/L). Mast cell accumulation in the BM was reevaluated before applying a second-line therapy. At that time, the proportion of the mast cells identified by c-KIT staining had decreased to 5% of all nucleated cells. The karyotype of the BM was normal (46,XX). After introducing nilotinib, a potent tyrosine kinase inhibitor for patients harboring a *KIT* codon 816 mutation, her clinical symptoms that had been occurring on an almost daily basis improved moderately and the prednisolone dose could therefore be reduced. Her serum alkaline phosphatase level was also normalized. However, she still suffered with anaphylactic reactions almost once per month, which suggested the existence of uncontrolled residual and reactive mast cells.

Detection of a KIT mutation

To make a definitive diagnosis of ASM in our study patient, the codon 816 region of the *KIT* gene was

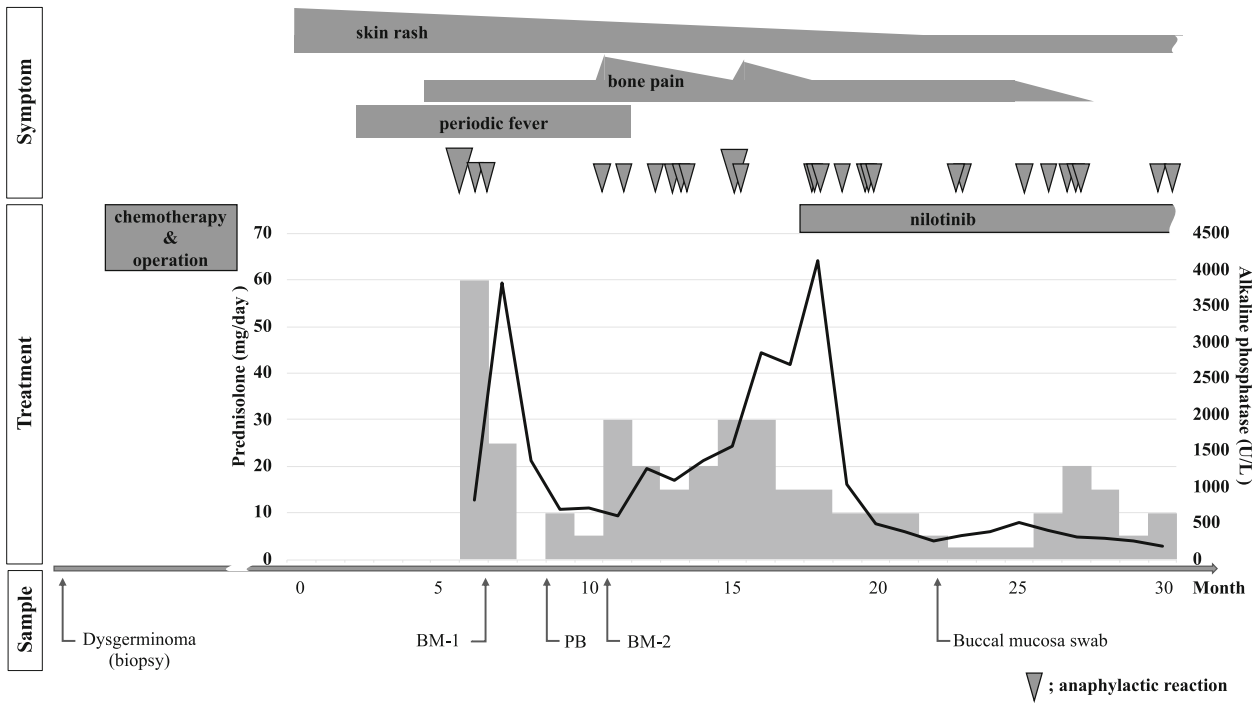

Fig. 1 Clinical course of the study patient, and timeline for the tissue and blood sampling for genetic analysis. The black line and gray bar graphs indicate the kinetics for the alkaline phosphatase disease biomarker and daily prednisolone requirement, respectively. The gray inverse triangles indicate the occurrence of an anaphylactic reaction, with the severity denoted by the size of the symbol

amplified by PCR and directly sequenced (Fig. 2a; Additional file 2: Fig. S1A). A somatic mutation, D816A (NM_000222.2:c.2447A > C, COSM24675) was identified in the patient's BM that had been sampled at the onset of the ASM-associated symptoms (BM-1). This mutation was not detectable in the PB, nor in the BM obtained after the initial treatment (BM-2). The percentage of mast cells in the BM-1 and BM-2 smears determined by microscopic examination was 50 and 5%, respectively. The variant allele frequency (VAF) in the BM-1 sample was 0.34, which may have been due to contamination by normal cells.

D816 mutations in the *KIT* gene are common to germ cell tumors [13] and we thus tested a biopsy specimen that was obtained from the dysgerminoma lesion in our study case prior to chemotherapy. The same D816A *KIT* mutation was detected. Notably also, the mutant allele ratio in the dysgerminoma was considerably higher than that of the normal allele (VAF = 0.75). *KIT* gene amplification was not evident by quantitative PCR (Additional file 2: Fig. S1B), suggesting that the normal allele had been deleted in the dysgerminoma cells. Indeed, the ratio between the two alleles of a heterozygous common single nucleotide polymorphism (SNP), C > T (rs1008658), located 115 bp downstream of the mutation site, was also skewed in samples carrying the D816A variant. PCR products including both the *KIT* D816 and rs1008658 sites were cloned and sequenced individually (Additional file 2: Fig. S1C). The *KIT* D816A mutation was found to be linked to the T allele of the SNP. Since the VAF in the BM-1 sample was 0.64, the normal allele was thought be also lost in the ASM cells.

Genome-wide analysis of genetic alterations

We next explored the additional mutations associated with ASM development in our patient as ASM cells often carry mutations in cancer-related genes in addition to *KIT* [2]. Whole-exome sequencing of the genomic DNA from BM-1 and PB samples was performed and revealed a nonsense mutation in *TP53* and a missense mutation in *TET2* (Additional file 1: Tables S2 and S3). The nonsense mutation in *TP53*, E62X, (NM_000546: c.184G > T) was detected in BM-1, but not in the dysgerminoma nor the other samples (Fig. 2b). Normal cell contamination prevented us from determining the status of the normal allele (VAF = 0.31). When we examined for the presence of a common heterozygous SNP (rs1042522), located 31 bp downstream of the mutation site, an allelic imbalance was found in the BM-1 cells (Fig. 2b). Next-generation sequencing reads demonstrated that the mutant allele was present in the G allele of the SNP (Additional file 3: Fig. S2). From this phasing data, loss of heterozygosity (LOH) at this locus was evident in the BM-1 sample, suggesting a biallelic

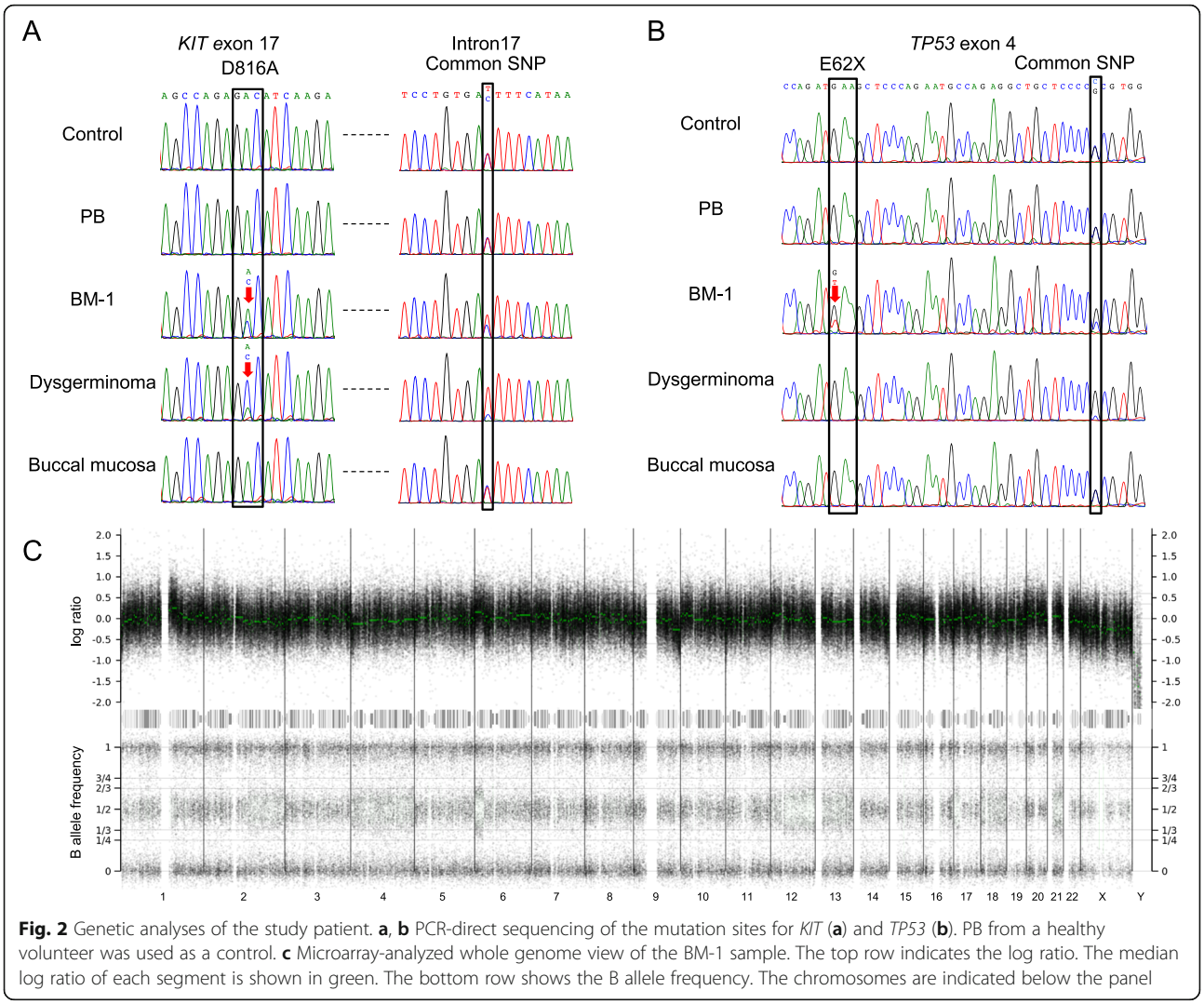

Fig. 2 Genetic analyses of the study patient. **a**, **b** PCR-direct sequencing of the mutation sites for *KIT* (**a**) and *TP53* (**b**). PB from a healthy volunteer was used as a control. **c** Microarray-analyzed whole genome view of the BM-1 sample. The top row indicates the log ratio. The median log ratio of each segment is shown in green. The bottom row shows the B allele frequency. The chromosomes are indicated below the panel

inactivation of the *TP53* gene in the ASM cells. To next determine whether the normal allele of the *TP53* gene had been deleted, its copy number was analyzed by whole-genomic microarray. LOH spanning the 17p13.1 region that incorporates the *TP53* locus was demonstrated in the BM-1 cell genomes, although the copy number of this region was normal (Fig. 2c). This copy-number-neutral LOH (CN-LOH) suggested that second hit was not the deletion, but that both alleles of the *TP53* gene in the ASM cells carried an E62X mutation, possibly due to mitotic recombination. Surprisingly, an LOH of the rs1042522 SNP was also found in the dysgerminoma cells without the E62X mutation (Fig. 2b).

The V1846F missense variant of *TET2* (NM_001127208.3:c.5536G > T) was found from our analysis of a buccal mucosal sample from the current study patient to be a germline variant (Additional file 4: Fig. S3). In silico analysis further predicted this to be a deleterious variation (PolyPhen-2 = 0.852, SIFT = 0.034) that did not appear in the databases (Additional file 1: Table S3). Notably, *TET2* is one of the tumor suppressor genes associated with ASM [14–16]. Both *TET2* and *KIT* are located on the chromosome 4 and we found by microarray analysis that the copy number of chromosome 4 was decreased in BM-1 (Fig. 2c). To then investigate whether the inactivation of the *TET2* gene is involved in development of ASM, we examined the phase of the *TET2* variant and the rs1008658 SNP. According to the determined allele frequencies, the *TET2* mutation was linked to the chromosome harboring the C allele of rs1008658 and was lost in the tumor cells. We thus concluded that the *TET2* variant was not associated with the development of ASM, since this rare mutation had been lost in the ASM cells. Further to this, the presence of this rare *TET2* variant in the healthy father of our patient was consistent with it having a benign nature (Additional file 4: Fig. S3).

In addition to chromosomes 4 and 17, copy-number aberrations or LOHs were detected in chromosomes 1,

2, 6, 9, 12, 13, 14, 16, 18, 20, 21 and X in the BM-1 cells from our patient (Fig. 2c). No other mutations with the potential to be cancer driver candidates were detected by whole-exome sequencing of the affected regions of these chromosomes (Additional file 1: Table S3).

Discussion

We have here presented an adolescent case of ASM which is a rare neoplasm at such a young age. Our female patient developed the ASM after prior treatment for a dysgerminoma. Significantly, the pathogenic *KIT* gene variant, D816A, was identified in both the dysgerminoma and BM samples in this case. *KIT* mutations are frequently found in the tumor cells of SM patients and are an important part of the established diagnostic criteria for ASM, but the most prevalent variant of these is the D816V mutation, which has been observed in > 60% of ASM patients [7]. The D816A mutation has been occasionally identified also in SM with an associated hematologic neoplasm [17–19] but not in ASM. *KIT* D816 mutations are also commonly observed in germ cell tumors, and have been found in one-third of ovarian dysgerminomas [13]. Notably however, the D816A mutation has not been reported previously in these tumors. Thus, the presence of the *KIT* D816A variant in both the ASM and dysgerminoma cells in our present patient is unlikely to be a coincidence. There are considerable number of reports describing the association between mastocytosis and germ cell tumor [20–24]. The etiological linkage between ASM and a preceding germ cell tumor caused by a *KIT* D816 mutation is further supported by a similar prior report of an ASM patient carrying *KIT* D816V who had previously had an ovarian germ cell tumor harboring this same mutation [25]. Another similar case of an ovarian germ cell tumor carrying a *KIT* D816H mutation was also recently reported in which the chemotherapy was complicated by the development of SM with chronic myelomonocytic leukemia harboring this same mutation [26].

One simple hypothesis to explain our current findings is clonal evolution (Fig. 3a). In brief, the *KIT* D816A variation initially induces the development of ovarian dysgerminoma. Although the tumor was removed by surgical resection, minimally residual cells that

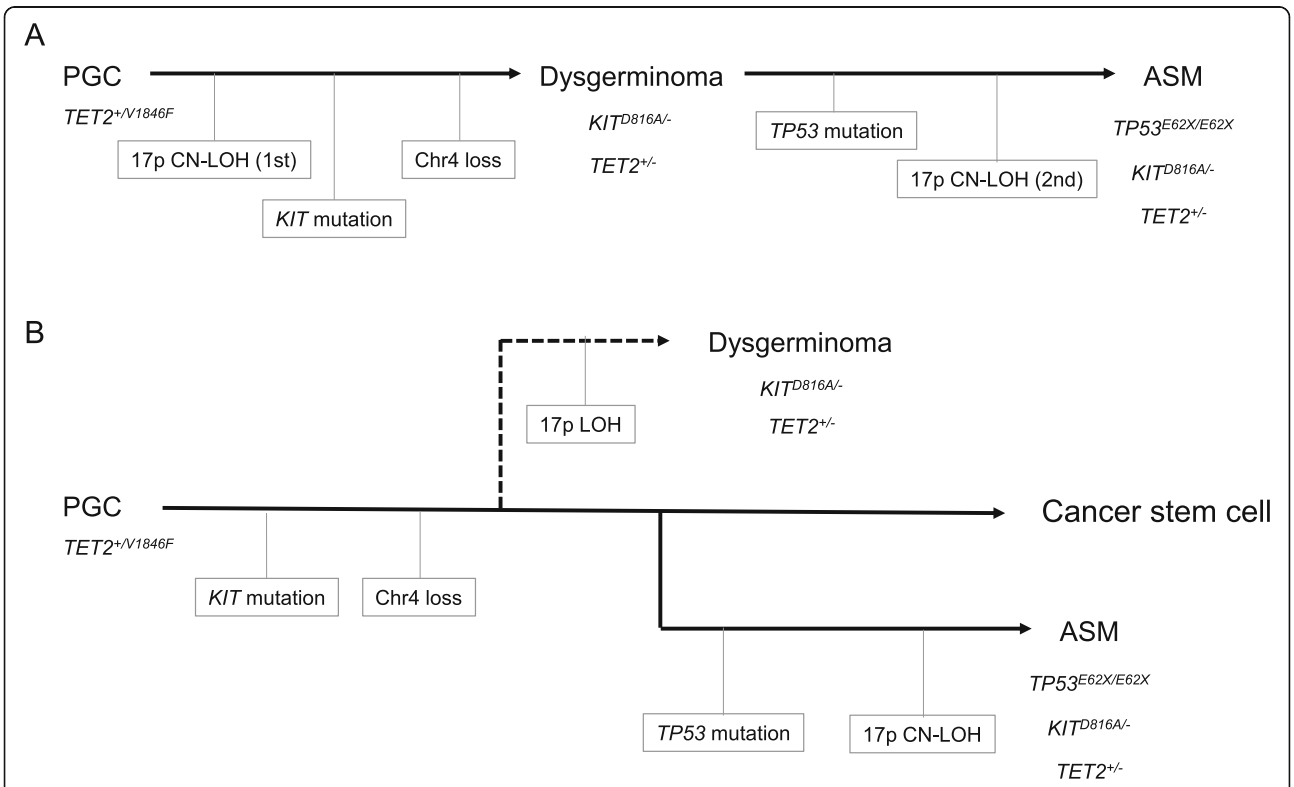

Fig. 3 Schema for two possible mechanisms of ASM development in the study patient. **a** The first CN-LOH of 17p occurred as an incidental event in the PGCs. Subsequently, a cell which acquired the *KIT* mutation and lost one copy of chromosome 4 without that mutation was selected and gave rise to a dysgerminoma. After treatment for that lesion, a residual tumor cell differentiated into a mast cell and acquired the *TP53* mutation in one allele. Finally, a second CN-LOH event involving 17p led to the inactivation of the *TP53* gene in both alleles and caused the ASM. **b** A cancer stem cell carrying the *KIT* mutation arose from the PGCs. One of these cancer stem cells was fated to become the lineage for the dysgerminoma, which underwent a 17p LOH. Another cancer stem cell which acquired the *TP53* mutation was fated to cause the ASM. A cell of this tumor lineage underwent a 17p CN-LOH which inactivated both *TP53* alleles

differentiated into hematologic cells possibly underwent subsequent biallelic mutation of the *TP53* gene, resulting in malignant transformation. Our microarray analysis indicated a complex karyotype and suggested the mast cells underwent repeated genetic rearrangements, although an abnormal karyotype is less common in ASM [5, 27, 28]. *TP53* is a less frequently affected gene in advanced SM [3], but is the most commonly affected gene in therapy-related myeloid neoplasms [29, 30]. The chemotherapy for the previous dysgerminoma in our present patient may have contributed to the mutation induction in a residual tumor cell and then expansion of these mutated mast cells, resulting in the younger onset of ASM in this case.

It is noteworthy that the LOH at the *TP53* locus was present both in the dysgerminoma and ASM, but that the ASM had the CN-LOH. The ASM cells were found to carry a biallelic homozygous E62X mutation of the *TP53* gene, suggesting that the CN-LOH was established by mitotic recombination after acquisition of the *TP53* mutation. However, the dysgerminoma was found to carry a 17p LOH without *TP53* mutation, suggesting that the 17p LOH in the dysgerminoma and ASM were independent events. A possible alternative hypothesis therefore is that the dysgerminoma and ASM originated from a common cancer stem cell harboring the *KIT* D816A mutation and developed independently (Fig. 3b). Briefly, the deletion of 17p possibly occurred in the dysgerminoma lineage. After treatment for this lesion, another cancer stem cell acquired the *TP53* mutation and underwent chromosome rearrangements, which evolved into the origin of another tumor lineage and caused the ASM.

Previously reported experiments using murine cells expressing pathogenic *KIT* mutants have demonstrated that the loss of one copy of *Tet2* accelerates mast cell growth [15, 31]. Although the effect of the *TET2* V1846F variation in tumorigenesis is not clear, cells with only one normal *TET2* allele may have a growth advantage under KIT D816A expression, even after deletion of the *TET2* V1846F allele in our current patient, suggesting that the *TET2* V1846F variant was unlikely to have affected the tumor progression.

Our current genetic analyses were useful in not only reaching a conclusive diagnosis but also for determining the treatment strategies in our study patient. Although the patient's condition had not progressed during the current treatment and the genetic alternations in her bone marrow were not among the negative prognostic indicators reported previously [32], the comprehensive cancer-related genetic alterations that were detected in this case in addition to the *KIT* mutation suggested that a tyrosine kinase inhibitor would not be sufficient to achieve remission. Notably in this regard, the multikinase inhibitor midostaurin is not currently available in Japan. An allogenic bone marrow transplantation from an HLA 1-locus mismatched sibling donor is being planned for our study patient.

Conclusions

Our current cytogenomic analyses demonstrated that mast cells causing the ASM shared a common origin with the dysgerminoma, suggesting that a careful follow-up should be required for the dysgerminoma patients after treatment.

Supplementary Information

The online version contains supplementary material available at https://doi.org/10.1186/s12885-020-07653-z.

Additional file 1: Table S1. PCR primers used in this study. **Table S2.** BM-1-specific candidate variants of cancer-related genes analyzed by Mutect2. **Table S3.** Candidate variants of cancer-related genes identified in the PB of the study patient.

Additional file 2: Figure S1. Genetic analyses of the study patient. (A) PCR-direct sequencing of the *KIT* mutation site in the BM-2 sample. (B) Real-time quantitative PCR of the *KIT* gene. The *SNX25* gene is located on the 4q35.1. Ratio to the healthy control (mean ± SD) obtained from the two independent experiments are shown. (C) Cloning and sequence analysis of the PCR products from the BM-1.

Additional file 3: Figure S2. Integrative Genomics Viewer image of the next-generation sequencing reads of the *TP53* mutation site. The arrow indicates the transcriptional direction of the *TP53* gene. The 'A' at the E62X site and 'C' in the common SNP are the complementary bases of 'T' and 'G' in the context of gene coding, respectively.

Additional file 4: Figure S3. PCR-direct sequencing of the *TET2* mutation site in the PB, BM-1, dysgerminoma, and buccal mucosa samples from the patient, and PB samples from her parents and a healthy control.

Abbreviations

AFP: α-fetoprotein; ASM: Aggressive systemic mastocytosis; BM: Bone marrow; CN-LOH: Copy-number-neutral loss of heterozygosity; LOH: Loss of heterozygosity; PB: Peripheral blood; PGC: Primordial germ cells; SM: Systemic mastocytosis; SNP: Single nucleotide polymorphism; VAF: Variant allele frequency

Acknowledgements

We thank Narumi Kamiya for providing technical assistance.

Authors' contributions

MT_1, HI, YS, AK, TK and SH-T carried out the genetic analysis; HM, MT_2, KK and TY clinically managed the patient; HM carried out sampling; MT_1, HM and HK designed the study and drafted the manuscript. All of the study co-authors have read and approved the final manuscript.

Funding

This study was supported by grants-in-aid for Scientific Research from the Ministry of Education, Culture, Sports, Science, and Technology of Japan, the Ministry of Health, Welfare and Labor, and from the Japan Agency for Medical Research and Development. The funding bodies played no role in the design of the study and collection, analysis, and interpretation of data and in writing the manuscript.

Availability of data and materials

The datasets used and/or analyzed during the current study are available from the corresponding author on reasonable request.

Ethics approval and consent to participate

The genetic testing used in this study was approved by the ethics committee of Fujita Health University in accordance with the principles of the Declaration of Helsinki, and with the Ethical Guidelines for Human Genome/Gene Analysis Research of the Ministry of Education, Culture, Science, and Technology, the Ministry of Health, Labor, and Welfare, and the Ministry of Economy, Trade, and Industry of Japan. Written informed ascent from the participants and consent from their guardians was obtained in accordance with local institutional review board guidelines.

Consent for publication

Written informed consent was obtained from the study patient and her guardians to publish this study.

Competing interests

The authors declare no financial or other competing interests in relation to this study.

Author details

[1]Division of Molecular Genetics, Institute for Comprehensive Medical Science, Fujita Health University, 1-98 Dengakugakubo, Kutsukake-cho, Toyoake, Aichi 470-1192, Japan. [2]Department of Pediatrics, Fujita Health University School of Medicine, Toyoake, Japan. [3]ITOCHU Collaborative Research-Molecular Targeted Cancer Treatment for Next Generation, Graduate School of Medicine, Nagoya University, Nagoya, Japan. [4]Department of Virology and Liver Unit, Nagoya City University Graduate School of Medical Sciences, Nagoya, Japan.

Received: 25 September 2020 Accepted: 17 November 2020
Published online: 27 November 2020

References

1. Theoharides TC, Valent P, Akin C. Mast cells, Mastocytosis, and related disorders. N Engl J Med. 2015;373:163–72.
2. Valent P, Akin C, Hartmann K, Nilsson G, Reiter A, Hermine O, et al. Advances in the classification and treatment of Mastocytosis: current status and outlook toward the future. Cancer Res. 2017;77:1261–70.
3. Leguit R, Hebeda K, Kremer M, van der Walt J, Gianelli U, Tzankov A, et al. The Spectrum of aggressive Mastocytosis: a workshop report and literature review. Pathobiology. 2020;87:2–19.
4. Cohen SS, Skovbo S, Vestergaard H, Kristensen T, Møller M, Bindslev-Jensen C, et al. Epidemiology of systemic mastocytosis in Denmark. Br J Haematol. 2014;166:521–8.
5. Pieri L, Bonadonna P, Elena C, Papayannidis C, Grifoni FI, Rondoni M, et al. Clinical presentation and management practice of systemic mastocytosis. A survey on 460 Italian patients. Am J Hematol. 2016;91:692–9.
6. Méni C, Bruneau J, Georgin-Lavialle S, Le Saché de Peufeilhoux L, Damaj G, Hadj-Rabia S, et al. Paediatric mastocytosis: a systematic review of 1747 cases. Br J Dermatol. 2015;172:642–51.
7. Arock M, Sotlar K, Akin C, Broesby-Olsen S, Hoermann G, Escribano L, et al. KIT mutation analysis in mast cell neoplasms: recommendations of the European competence network on Mastocytosis. Leukemia. 2015;29:1223–32.
8. Kraggerud SM, Hoei-Hansen CE, Alagaratnam S, Skotheim RI, Abeler VM, Rajpert-De Meyts E, et al. Molecular characteristics of malignant ovarian germ cell tumors and comparison with testicular counterparts: implications for pathogenesis. Endocr Rev. 2013;34:339–76.
9. Shaaban AM, Rezvani M, Elsayes KM, Baskin H Jr, Mourad A, Foster BR, et al. Ovarian malignant germ cell tumors: cellular classification and clinical and imaging features. Radiographics. 2014;34:777–801.
10. Boda H, Uchida H, Takaiso N, Ouchi Y, Fujita N, Kuno A, et al. A PDE3A mutation in familial hypertension and brachydactyly syndrome. J Hum Genet. 2016;61:701–3.
11. Cancer Gene Census. https://cancer.sanger.ac.uk/census. Accessed 1 Oct 2019.
12. Mayrhofer M, Viklund B, Isaksson A. Rawcopy: improved copy number analysis with Affymetrix arrays. Sci Rep. 2016;6:36158.
13. Cheng L, Roth LM, Zhang S, Wang M, Morton MJ, Zheng W, et al. KIT gene mutation and amplification in dysgerminoma of the ovary. Cancer. 2011; 117:2096–103.
14. Tefferi A, Levine RL, Lim KH, Abdel-Wahab O, Lasho TL, Patel J, et al. Frequent TET2 mutations in systemic mastocytosis: clinical, KITD816V and FIP1L1-PDGFRA correlates. Leukemia. 2009;23:900–4.
15. Soucie E, Hanssens K, Mercher T, Georgin-Lavialle S, Damaj G, Livideanu C, et al. In aggressive forms of mastocytosis, TET2 loss cooperates with c-KITD816V to transform mast cells. Blood. 2012;120:4846–9.
16. Schwaab J, Schnittger S, Sotlar K, Walz C, Fabarius A, Pfirrmann M, et al. Comprehensive mutational profiling in advanced systemic mastocytosis. Blood. 2013;122:2460–6.
17. Cornet E, Dumézy F, Roumier C, Lepelley P, Jouy N, Philippe N, et al. Involvement of a common progenitor cell in core binding factor acute myeloid leukaemia associated with mastocytosis. Leuk Res. 2012;36:1330–3.
18. Yabe M, Masukawa A, Kato S, Yabe H, Nakamura N, Matsushita H. Systemic mastocytosis associated with t(8;21) acute myeloid leukemia in a child: detection of the D816A mutation of KIT. Pediatr Blood Cancer. 2012;59: 1313–6.
19. Frederiksen JK, Shao L, Bixby DL, Ross CW. Shared clonal cytogenetic abnormalities in aberrant mast cells and leukemic myeloid blasts detected by single nucleotide polymorphism microarray-based whole-genome scanning. Genes Chromosomes Cancer. 2016;55:389–96.
20. Chariot P, Monnet I, LeLong F, Chleq C, Droz JP, de Cremoux H. Systemic mast cell disease associated with primary mediastinal germ cell tumor. Am J Med. 1991;90:381–5.
21. Chariot P, Monnet I, Gaulard P, Abd-Alsamad I, Ruffié P, De Cremoux H. Systemic mastocytosis following mediastinal germ cell tumor: an association confirmed. Hum Pathol. 1993;24:111–2.
22. Delacrétaz F, Stalder M, Meugé-Moraw C, Schmidt PM, Joris F, Kurt AM, et al. Systemic mastocytosis following a malignant ovarian germ cell tumour. Histopathology. 1997;30:582–4.
23. Teitell M, Rowland JM. Systemic mast cell disease associated with primary ovarian mixed malignant germ cell tumor. Hum Pathol. 1998;29:1546–7.
24. Miyagawa S, Hirota S, Park YD, Yamasaki M, Daikoku N, Morikawa H, et al. Cutaneous mastocytosis associated with a mixed germ cell tumour of the ovary: report of a case and review of the literature. Br J Dermatol. 2001;145: 309–12.
25. Lee JW, Yang WS, Chung SY, Kang JH, Cho B, Kim HK, et al. Aggressive systemic mastocytosis after germ cell tumor of the ovary: C-KIT mutation documentation in both disease states. J Pediatr Hematol Oncol. 2007;29: 412–5.
26. Mitchell SG, Bunting ST, Saxe D, Olson T, Keller FG. A variant c-KIT mutation, D816H, fundamental to the sequential development of an ovarian mixed germ cell tumor and systemic mastocytosis with chronic myelomonocytic leukemia. Pediatr Blood Cancer. 2017;64:e26282.
27. Naumann N, Jawhar M, Schwaab J, Kluger S, Lübke J, Metzgeroth G, et al. Incidence and prognostic impact of cytogenetic aberrations in patients with systemic mastocytosis. Genes Chromosomes Cancer. 2018;57:252–9.
28. Shah S, Pardanani A, Elala YC, Lasho TL, Patnaik MM, Reichard KK, et al. Cytogenetic abnormalities in systemic mastocytosis: WHO subcategory-specific incidence and prognostic impact among 348 informative cases. Am J Hematol. 2018;93:1461–6.
29. Ok CY, Patel KP, Garcia-Manero G, Routbort MJ, Peng J, Tang G, et al. TP53 mutation characteristics in therapy-related myelodysplastic syndromes and acute myeloid leukemia is similar to de novo diseases. J Hematol Oncol. 2015;8:45.
30. Chung J, Sallman DA, Padron E. TP53 and therapy-related myeloid neoplasms. Best Pract Res Clin Haematol. 2019;32:98–103.
31. De Vita S, Schneider RK, Garcia M, Wood J, Gavillet M, Ebert BL, et al. Loss of function of TET2 cooperates with constitutively active KIT in murine and human models of mastocytosis. PLoS One. 2014;9:e96209.
32. Rossignol J, Polivka L, Maouche-Chrétien L, Frenzel L, Dubreuil P, Hermine O. Recent advances in the understanding and therapeutic management of mastocytosis. F1000Res. 2019;8. https://doi.org/10.12688/f1000research.19463.1.

Publisher's Note

Received: 6 April 2020 | Revised: 4 September 2020 | Accepted: 14 September 2020

DOI: 10.1002/mgg3.1531

Molecular Genetics & Genomic Medicine Open Access WILEY

ORIGINAL ARTICLE

Molecular analysis of low-level mosaicism of the *IKBKG* mutation using the X Chromosome Inactivation pattern in Incontinentia Pigmenti

Miki Kawai[1,2] | **Takema Kato**[1] | **Makiko Tsutsumi**[1] | **Yasuko Shinkai**[1] | **Hidehito Inagaki**[1] | **Hiroki Kurahashi**[1,2]

[1]Division of Molecular Genetics, Institute for Comprehensive Medical Science, Fujita Health University, Toyoake, Japan

[2]Department of Clinical Genetics, Fujita Health University Hospital, Toyoake, Japan

Correspondence
Hiroki Kurahashi, Division of Molecular Genetics, Institute for Comprehensive Medical Science, Fujita Health University, 1-98 Dengakugakubo, Kutsukake-cho, Toyoake, Aichi 470-1192, Japan.
Email: kura@fujita-hu.ac.jp

Funding information
This work was supported by grants-in-aid for Scientific Research from the Ministry of Education, Culture, Sports, Science and Technology of Japan (15H04710); from the Ministry of Health, Welfare and Labor (H27-Nanchitou-Ippan[nan]-024); and from the Japan Agency for Medical Research and Development

Abstract

Background: Incontinentia pigmenti (IP) is a rare X-linked disorder affecting the skin and other ectodermal tissues that is caused by mutation of the *IKBKG/NEMO* gene. Previous studies have reported that the overall mutation detection rate in IP is ~75%. We hypothesized that a low-level mosaicism existed in the remaining cases.

Methods: Genomic variations in the *IKBKG* gene were examined in 30 IP probands and their family members. Standard mutational analyses were performed to detect common deletions, nucleotide alterations, and copy number variations. To assess skewing of the X chromosome inactivation (XCI) pattern, a HUMARA assay was performed. We compared the results of this analysis with phenotype severity.

Results: Pathogenic variants were identified in 20 probands (66.7%), the rate of detection was suboptimal. The remaining 10 probands tended to manifest a mild phenotype with no skewed X chromosome inactivation that is generally observed in IP patients. Quantitative nested PCR and digital droplet PCR were performed for the 10 patients and mosaicism of the common *IKBKG* deletion were identified in five patients.

Conclusion: Overall, we detected 25 *IKBKG* mutations (83.3%). Determination of the XCI value in advance of mutational analyses for IP could improve the mutation detection rate. Our improved detection rate for these mutations, particularly those with a low-level mosaicism, may present opportunities for appropriate genetic counseling.

KEYWORDS

IKBKG, incontinentia pigmenti, mosaicism, X chromosome inactivation

1 | INTRODUCTION

Incontinentia pigmenti (IP; MIM #308300) is a rare X-linked genodermatosis with an estimated prevalence at birth of 1.2/100,000 (Orphanet, 2018). This disorder affects the skin and other ectodermal tissues including the eyes, teeth, hair, nail, and central nervous system (CNS). Skin lesions are the first diagnostic manifestations of IP

that appear in the neonatal period and comprise a vesicubullous stage (stage I) followed by a verrucous stage (stage II) persisting for months to years, a hyperpigmented stage (stage III), and finally a hypopigmented stage (stage IV) usually continuing throughout life. These skin defects follow Blaschko lines and present in almost all IP patients, thus constituting the principal diagnostic IP criteria for this condition (Landy & Donnai, 1993; Minić et al., 2014). Systemic involvement includes ocular and neurologic impairment. Although IP is X-linked dominant and is usually lethal in males, some affected males have been reported, representing approximately 10% (Fusco et al., 2014) of the patient population. Affected males present with somatic mosaicism and in some reported cases a concomitant diagnosis of Klinefelter syndrome (Conte et al., 2014).

IP is caused by a mutation of the *IKBKG*/*NEMO* gene (Inhibitor of Kappa polypeptide gene enhancer in B-cells, Kinase Gamma/Nuclear Factor κB, Essential Modulator, GenBank NM_003639.3, OMIM#300248). This gene encodes NEMO/IKKγ which is required for the activation of the nuclear factor-kappa B (NF-κB) transcription factor. NEMO/IKKγ acts as a regulatory subunit of the inhibitor of the κB (IκB) kinase (IKK) complex. The absence of NEMO/IKKγ protein renders the cells sensitive to apoptosis, leading to lethality in males (Aradhya, et al., 2001) and selective skewed X-inactivation in females (Fusco et al., 2004). In most patients, IP onset is due to loss-of-function (LoF) mutations, although in some case *IKBKG* hypomorphic mutations have been reported (Fusco et al., 2008) that reduce but do not eliminate NF-κB activation, thus explaining why some affected male patients survive (Döffinger et al., 2001). Female patients carrying these hypomorphic mutations show mild signs of IP (Aradhya, et al., 2001).

IKBKG is a 23-kb gene composed of nine coding exons, four alternative noncoding first exons (from exons 1A to 1D), and two promoters. The *IKBKG* gene also shares a part of a 35.7 kb segmental duplication arranged in the opposite direction, one covering the genuine gene and the other a part of a pseudogene copy. The non-functional *IKBKGP* spans the region between exon 3 to 10. The most frequent IP mutation is a recurrent deletion produced by non-allelic homologous recombination (NAHR) due to a misalignment between approximately two 650 bp short interspersed nuclear element (SINE) of a medium reiterated 67B (MER67B), one of which is located in intron 3 and the other distally to exon 10. This deletion removes exons 4-10, spanning 11.7 kb. In addition, the NAHR mechanism can also generate benign copy number variations (CNVs) through an exon 4-10 deletion in *IKBKGP* or an exon 4-10 duplication in the *IKBKG* gene. However, both benign CNVs are risk alleles for de novo generation of a pathological *IKBKG* exon 4-10 deletion (Fusco et al., 2009). The *IKBKG* region contains many repeat sequences and is considered to be prone to rearrangement.

Previous studies have reported that the overall mutation detection rate in IP is 77.6%. *IKBKG* gene targeted analysis of the exon 4-10 deletion can detect 65% of affected patients, single-nucleotide variant (SNV) analysis can detect 8.6%, and large duplication and deletion analysis can detect 4% of clinically affected individuals (Fusco et al., 2008; Fusco et al., 2007; Fusco et al., 2012). As *IKBKG* is the only gene responsible for IP, these rates are low in comparison with other genetic diseases, even when taking into consideration that the *IKBKG* locus has a complex genomic structure. In the course of the mutational analyses of our own IP patients, we observed that patients with no detectable mutation showed a mild phenotype. We hypothesized that a low-level mosaicism existed in these cases which would have made it difficult to detect the mutations in blood samples.

In this study, we conducted *IKBKG* gene mutational analysis in 30 IP patients. We compared the results of this analysis with phenotype severity and also with the X chromosome inactivation (XCI) pattern that would not appear skewed in patients with mosaicism due to the presence of normal cells presenting with a random XCI pattern. We describe observed relationships between phenotype severity, XCI pattern and somatic mosaicism. We also discuss the clinical implications of our results for future genetic testing and counseling.

2 | MATERIALS AND METHODS

2.1 | DNA samples

All research was performed in accordance with the principles of the Declaration of Helsinki, and the Ethical Guidelines for Human Genome/Gene Analysis Research by the Ministry of Education, Culture, Science, and Technology, the Ministry of Health, Labor, and Welfare, and the Ministry of Economy, Trade, and Industry of Japan.

Peripheral blood samples were obtained from 30 Japanese IP patients (28 females) in accordance with the research protocol approved by the local ethics committee of Fujita Health University. The IP patients enrolled in our study were selected on the basis of the previous Landy and Donnai (Landy & Donnai, 1993) diagnostic criteria, and also because they met the recently updated criteria (Minić et al., 2014). The severity of disease in each patient was evaluated using manifestation score of skin leision, nervous system defect, ocular system defect, dental system defect, hair defect, and nail defect (Table S1). We collected DNA samples from both parents in 10 cases and a single parent in six cases. Written informed consent to participate in the study was obtained from the patients or their parents. Genomic DNA from peripheral

blood was extracted using a conventional salt precipitation technique.

2.2 | Analysis of common Incontinentia Pigmenti deletions

Common IP deletions have previously been characterized (Bardaro et al., 2003). Long-range PCR was performed in our current analysis to detect the specific *IKBKG* exon 4-10 deletion using the primers listed in Table S3. The PCR reactions were performed in 25 µl volumes containing 1 µl of sample, 2.5 U of LA Taq Polymerase (Takara Bio Inc.), LA Taq buffer II, 200 µM dNTPs, 2 mM $MgCl_2$ and 10 pmol of each primer. The amplification protocol comprised 30 cycles of 10 seconds at 98°C and 3 min at 65°C. To detect *IKBKGP*, PCR was performed as described above with the previously reported Rev-2 and JF3R primers (Bardaro et al., 2003).

Nested PCR was performed to detect low-level mosaic deletions. The primers used for these second amplifications are also listed in Table S3. The resulting PCR products were diluted 1:100 with Tris-EDTA Buffer (TE). These nested reactions contained 1 µl of template DNA in an identical reaction mixture for 20 cycles of 10 seconds at 98°C and 1 min at 60°C. PCR products were visualized on a 2% agarose gel, quantified using an image analyzer, and compared with the products amplified from serial dilutions of genomic DNA from patients harboring the common *IKBKG* deletion.

To detect mosaic deletions, we performed droplet digital PCR using the custom probes listed in Table S4. Droplet generation, PCR cycling, and droplet reading were performed in accordance with the manufacturer's protocol (Bio-Rad). The first PCR was performed over 13 cycles with 10 ng of DNA sample as the template. The resulting PCR products were diluted 1:10 with Tris-EDTA Buffer. Probes and primers were mixed with a 2x ddPCR supermix and with 1 µl of template DNA. In total, 22 µl volume reactions were loaded into an 8-channel droplet generator cartridge (Bio-Rad) and droplets were then generated with 70 µl of droplet generation oil (Bio-Rad) using a manual QX200 Droplet Generator. Following droplet generation, samples were transferred to a 96-well PCR plate, heat sealed and then amplified on a thermal cycler using the following cycling conditions: 95℃ for 10 min followed by 40 cycles at 95℃ for 30 seconds and 60℃ for 10 min, one cycle at 98℃ for 10 min, and maintenance at 12℃. Post-PCR products were analyzed on the QX200 droplet reader (Bio-Rad) using QuantaSoft software.

2.3 | Analysis of structural variants

Copy number variations were analyzed at the IP locus, including the *IKBKG* gene and *IKBKGP*, by applying the SALSA MLPA probemix P073-A1 (MRC-Holland). Test fragments have been designed previously to evaluate the *IKBKG* gene and the sizes and locations of most of these test probes as well as reference probes have been defined. MLPA and capillary electrophoresis-based amplification product separation (ABI3130, Life Technologies) was performed in accordance with the manufacturer's instructions. Relative copy numbers were obtained after normalization of the peaks against blood-derived controls. Sequences were analyzed using Gene mapper software.

2.4 | Analysis of nucleotide alterations

To detect SNVs within *IKBKG* coding sequences, the coding exons were amplified using nested PCR without amplification of *IKBKGP*. Electropherograms were then obtained by Sanger sequencing using Big Dye Terminator Cycle Sequencing Reactions on an ABI 3100 device (PE Applied Biosystems) and were compared with those for genomic sequences from control samples. To evaluate the low-level mosaicism of the SNVs, we performed deep sequencing of the *IKBKGP* region using next generation sequencer (NGS). We performed long-range PCR for three regions including the entire *IKBKG* gene and pseudogene. The primers used are listed in Table S5. Three PCR reactions were performed under the following cycling conditions: an initial denaturation of 94℃ for 2 min followed by 5 cycles of 98℃ for 10 s and 74℃ for 5 min, 5 cycles of 98℃ for 10 s and 72℃ for 5 min, 5 cycles of 98℃ for 10 s and 70℃ for 5 min, and 20 cycles of 98℃ for 10 s and 68℃ for 5 min. Successful amplification of the three PCR products was confirmed by agarose gel electrophoresis. Pooled DNA libraries were prepared using a Nextera XT DNA Sample Preparation Kit in accordance with the manufacturer's protocol (Illumina). Paired ends were sequenced for 150 bp using a Miseq Reagent Kit v2 (Illumina). The sequence reads were aligned with the human genome (hg38) reference sequence after manual editing to use between chrX:154541001-154567000 with BWA aligner. Approximately 10,000 reads from a single patient were obtained and analyzed for genotyping. Downstream processing was carried out with the Genome analysis toolkit (GATK), SAMtools (http://samtools.sourceforge.net/) and Picard Tools (http://broadinstitute.github.io/picard/). Substitution and Indel calls were made with a GATK HaplotypeCaller and GenotypeGVCF (Boisson et al., 2019). Approximately 10,000 reads from a single patient were obtained and analyzed for genotyping.

Variants that have not been registered in any database, are submitted as a new variant in Leiden Open variation Database (http://www.lovd.nl/3.0/home).

2.5 | X chromosome inactivation studies

To examine the X chromosome inactivation (XCI) pattern, we performed a HUMARA assay according to a previously described protocol (Beever et al., 2003) to assess skewing of the X chromosome inactivation. We first digested the genomic DNA with the methylation-sensitive restriction enzyme *Hpa*II. PCR primers, one of which was labeled with FAM, were designed across the polymorphic CAG repeat and two *Hpa*II sites in the androgen receptor (*AR*) gene on the X chromosome. In addition to the *AR* locus, the *SLITRK4* and *PCSK1N* loci were used in case the *AR* locus was not informative (Bertelsen & Tümer, 2011). PCR amplification would be achieved only from the inactivated allele harboring methylated *Hpa*II sites. PCR products were analyzed by capillary electrophoresis (ABI3730 Genetic Analyzer) and quantified via the area under the curve using GeneMapper software. A skewed XCI was determined when the inactivated allele was biased at more than 90% (Beever et al., 2003).

2.6 | Statistical analysis

Intergroup comparisons were made using the Student's *t*-test or one way analysis of variance method and *P* values of less than 0.05 were considered statistically significant.

3 | RESULTS

In our current IP cohort, we detected the *IKBKG* exon 4-10 common deletion in 13 patients (03f, 05f, 06f, 08f, 13f, 14f, 16f, 18f, 21f, 22f, 28f, 29f, and 30f; Figure 1a) which was a prevalence (detection rate) of 43.3% among the total series

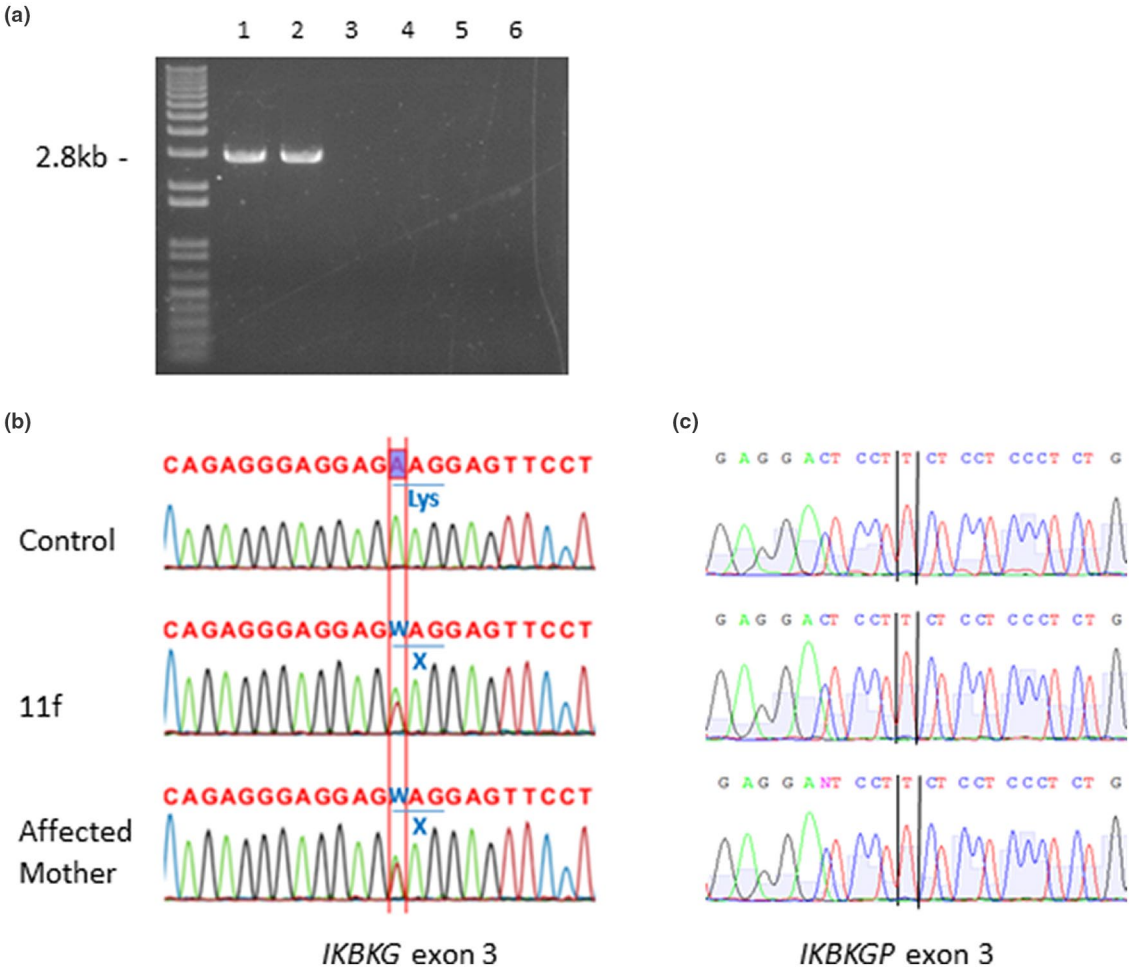

FIGURE 1 Mutational analysis of the *IKBKG* gene in the IP study patients. (a) PCR analysis of the IP patient blood samples. Lane 1, *IKBKG* deletion exon 4-10 control. Lane 2, patient 18f. The *IKBKG* deletion was detected. Lanes 3 and 4 are the father and mother of 18f. Lanes 5 and 6 are a healthy control and distilled water (DW). (b) Sanger sequencing of patient 11f and her affected mother. Coding exons for the *IKBKG* gene were amplified by PCR, being not amplified together with IKBKGP.NM_001099857.2:c.268A>T, NP_001093327.1: p.Lys90X is confirmed. (c) Pseudogene-specific sequencing. Sequencing of 11f and her mother did not show the pathogenic variant at chrX:154648193 on *IKBKGP*.

TABLE 1 Summary of the mutation.

Patient	Age at genetic testing	Female/male	Mutation[a]	Exon/ intron	Inheritance	Phenotype[b] Score	XCI pattern
01f	0	F	ND	—	Sporadic	2	91.8%
02f	3	F	ND	—	Sporadic	2	79.0%
03f	0	F	ex 4-10 deletion	ex 4-10	Familial	4	91.3%
04m	0	M	ND	—	Sporadic	2	(male)
05f	0	F	ex 4-10 deletion	ex 4-10	Sporadic	3	NI
06f	0	F	ex 4-10 deletion	ex 4-10	Sporadic	3	99.0%
07f	0	F	c.343A>T (K115X)	ex 3-10	Familial	3	82.4%
08f	3	F	ex 4-10 deletion	ex 4-10	Sporadic	3	100.0%
09f	0	F	c.896delC (P299RfsX3)	ex 7-10	Familial	4	99.1%
10f	0	F	94 kb deletion	ex 3-10	Familial	4	97.3%
11f	0	F	c.268A>T (K90X)	ex 3-10	Familial	3	98.4%
12f	2	F	Mosaic ex 4-10 deletion	ex 4-10	Sporadic	2	67.1%
13f	0	F	ex 4-10 deletion	ex 4-10	Sporadic	3	100.0%
14f	48	F	ex 4-10 deletion	ex 4-10	Familial	5	100.0%
15f	0	F	ND	—	Sporadic	2	72.2%
16f	0	F	ex 4-10 deletion	ex 4-10	Familial	3	100.0%
17f	0	F	c.184C>T (R62X)	ex 2	ND	3	97.4%
18f	0	F	ex 4-10 deletion	ex 4-10	Sporadic	5	NI
19f	0	F	Mosaic ex 4-10 deletion	ex 4-10	Sporadic	1	50.0%
20f	0	F	Mosaic ex 4-10 deletion	ex 4-10	Sporadic	1	58.4%
21f	2	F	ex 4-10 deletion	ex 4-10	Sporadic	3	100.0%
22f	34	F	ex 4-10 deletion	ex 4-10	ND	3	100.0%
23f	44	F	c.913-2A>G (p.spl)	int 7	Familial	5	100.0%
24m	0	M	Mosaic ex 4-10 deletion	ex 4-10	Sporadic	2	(male)
25f	0	F	Mosaic ex 4-10 deletion	ex 4-10	Sporadic	2	65.3%
26f	2	F	c.976_978delAAG (K326del)	ex 8	ND	3	75.7%
27f	33	F	ND	—	Sporadic	2	92.8%
28f	30's	F	ex 4-10 deletion	ex 4-10	ND	5	98.5%
29f	1	F	ex 4-10 deletion	ex 4-10	Sporadic	3	51.3%
30f	1	F	ex 4-10 deletion	ex 4-10	Sporadic	3	98.3%

Note: Homozygote for the polymorphic CAG repeat in the *AR* gene.

Abbreviations: ND, not determined. NI, not informative.

[a]The mutation numbering is based on the IKBKG cDNA sequence according to the GenBank Accession number NM_003639.3. Codon numbering starts from the translation initiation codon 1 according to the GenBank Accession number NP_003630.1.

[b]Phenotype score was allocated from Table S2.

of 30 patients (Table 1). Among these 13 patients with the common deletion, three were familial cases (03f, 14f, 16f) and we confirmed in one case that the same deletion was present in the mother (03f). We next performed Sanger sequencing in the 17 IP patients who did not carry the recurrent deletion. Pathogenic SNVs were detected in 6 cases [07f, c.343A>T (p.K115X); 09f, c.896delC (p.P299RfsX3); 11f, c.268A>T (p.K90X; Figure 1b,c); 17f, c.184C>T (p.R62X); 23f, c.913-2A>G; 26f, c.976_978delAAG (p.K326del)]. These identified mutations included three nonsense mutations (07f, 11f, 17f), one frameshift mutation (09f), one in-frame amino acid deletion (26f), and one splicing mutation (23f). To identify structural rearrangements caused by large deletions or duplications at the IP locus, including *IKBKG* and neighboring genes, we performed MLPA analysis to investigate copy number variation in the region. We thereby identified a large deletion including the *IKBKGP* pseudogene (10f). Although we identified pathogenic variants in 20 of the 30 study patients (66.7%), this rate of detection was suboptimal.

In the remaining 10 patients with no detectable mutations via standard analyses, we observed that their skin symptoms were less severe than the patient with detectable *IKBKG* mutations. In the evaluations of phenotype severity using our scoring system, the detected mutation cases had a score of 3.55 (n = 20), and those without a detectable mutation had a score of 1.8 (n = 10), which was significantly low ($p < 0.01$; Table 1, Table S1). To exclude the possibility that these patients had another autosomal disease that mimics IP, their XCI status was analyzed using a HUMARA assay since female X-linked IP patients generally manifest a selective skewed X-inactivation. We performed the HUMARA assay on all of the female patients in our current IP cohort (n = 28) as well as some of their female family members (n = 16; Figure 2a, Table S2). We could not however determine the allelic status in some of the cases since the polymorphic CAG repeat in the *AR* gene was homozygous in five of the women, including the mother of 03f, whose values of XCI pattern was determined by the other method (described later). We obtained the values of XCI pattern of 40 females (31 patients and 9 unaffected family members).

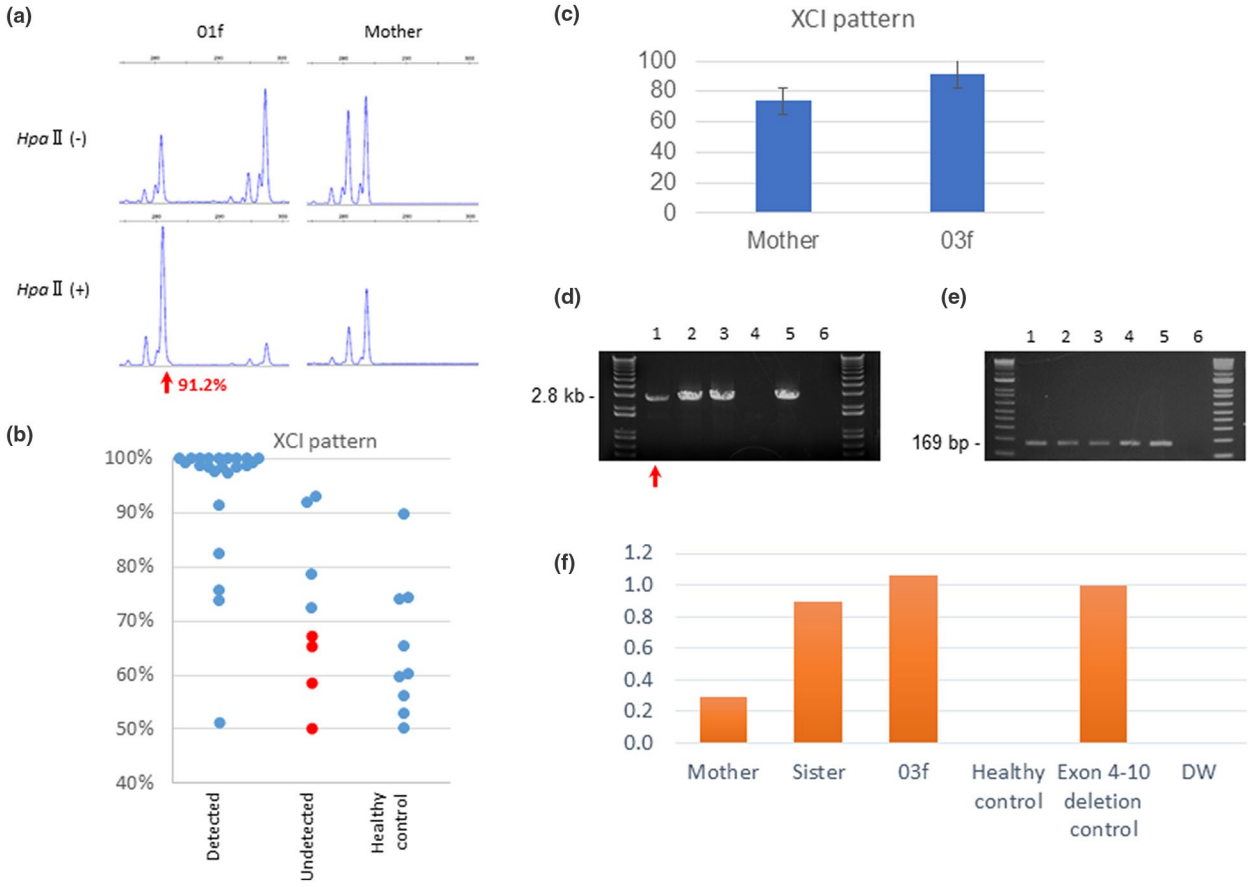

FIGURE 2 XCI patterns among IP patients in the study cohort. (a) Electropherogram of the HUMARA assay data showing the fragment analysis of PCR products amplified from undigested and digested DNA of patient 01f and her mother. The two major peaks represent two alleles with different numbers of short tandem repeats at the HUMARA locus (red arrows). After digestion, the DNA of the mother displayed a matching pattern of preferential loss of the short alleles. (b) Scatter plot of the informative XCI pattern of female IP probands and their mothers. "Detected" represents 18 probands, 4 carrier mothers, and 1 carrier sisters in whom an *IKBKG* mutation was detected. The median XCI value was 98.5% in these 23 cases. "Undetected" represents 8 probands with a median XCI value of 69.7%. The median XCI value of the healthy controls was 60.2%. Mosaic mutations are denoted by red dots. 11 probands, 1 carrier mother and 1 carrier sister carried the exon 4-10 deletion; one patient harbored a 94 kb deleted rearrangement; six probands and their three carrier mothers harbored SNVs; eight female probands had unknown mutations. The median age of the patients was 0 years and of the healthy controls was 40 years. (c) Median XCI values at the *AR*, *ZDHHC15*, *SLITRK4*, and *PCSK1N* loci. A lower XCI level in the mother may indicate somatic and germline mosaicism. (d) Common deletion-specific PCR analysis. 2.8 kb PCR products indicate the common exon 4-10 deletion of the *IKBKG* gene. Lanes 1-3 represent the mother of 03f, the sister of 03f and 03f, respectively. Lane 4 is a healthy control. Lane 5 is an *IKBKG* exon 4-10 deletion control and lane 6 is DW. (e) Internal standard for semi-quantitative PCR. The same DNA samples were used as templates for control PCR to amplify intron 45 of the *DMD* gene. (f) Semi-quantitative PCR. Using image analyzer, measurements of deletion specific PCR products were divided by that of internal control PCR products (lane 5). Mother of 03f is likely to have a mosaic deletion since the amount of the PCR products was less than that of 03f and her sister with heterozygous deletion.

Among the informative 31 patients, the skewed XCI values ranged from 50% to 100%, indicating that some patients showed a selectively skewed XCI pattern while others showed a random XCI pattern. We divided the patients into two categories: patients with an already detected or undetected *IKBKG* mutation. The mean value for the XCI patterns of the patients with a detected mutation was 98.5% (n = 23). In contrast, the XCI pattern values of the patients without a detected mutation (n = 8) ranged from 50% to 92.8% (mean 69.7%), which was significantly low ($p < 0.01$; Figure 2b, Table S2). The mean value for the unaffected family members was 60.2% (n = 9; Figure 2b). It is possible that our remaining 10 patients without a detected mutation and with a mild IP phenotype might have had a disorder other than X-linked IP. However, one of our patients with an in-frame deletion of a single amino acid (p.K326del) in the *IKBKG* gene (26f) had an XCI value of 75.7%, indicating that a hypomorphic variant does not lead to a selectively skewed XCI. Although the K326 residue in the *IKBKG* gene product is located at a linear polyubiquitinated site (Ikeda et al., 2011) and is an evolutionarily conserved position, protein products with an in-frame deletion may possibly have some residual activity that prevents cellular lethality. Hence, it is likely that the patients with a mild phenotype and with an almost random XCI pattern harbor weak variants such as somatic mosaicism.

Further evidence of the relationship between phenotype severity and the XCI pattern was observed in patient 03f and her mildly affected mother, both of whom carried the common *IKBKG* deletion (Table 2). Since the polymorphic CAG repeat in the *AR* gene was homozygous in the mother, we instead assessed three alternative methylation–sensitive restriction enzyme sites in the *ZDHHC15*, *SLITRK4* and *PCSKIN* genes, respectively. The XCI patterns for patient 03f were 89.2% in *SLITRK4*; 93.1% in *PCSKIN*, a median of 91.3%, whereas those for the mother were 67.7% in the *ZDHHC15* locus; 73.3% in *SLITRK4*; 82.5% in *PCSKIN*, a median of 73.7% (Figure 2c, Table 3). These data indicated that patient 03f manifests a selective skewed pattern, but that her mildly affected mother does not. Retrospectively, the amount of deletion-specific PCR products in the mother was less than that of the proband (Figure 2d). This finding indicated that the mother, who had a mild phenotype, may have somatic mosaicism of the common *IKBKG* deletion.

This means that the patients who are positive in PCR for common *IKBKG* deletion might possibly include those with somatic mosaicism. We reanalyzed the PCR-positive patients (03f, 05f, 06f, 08f, 15f, 17f, 28f, 29f, 30f, mother of 03f) by less sensitive MLPA. MLPA detected the common *IKBKG* deletion in all patients except for 29 f. Although the possibility of the effect of duplication polymorphism has not been ruled out, this results suggest that 29f might also harbor somatic mosaicism since the XCI pattern of 29f (51.3%) support this speculation.

A nested PCR assay in the remaining 10 patients revealed low-level mosaicisms of the common deletion in five cases (12f, 19f, 20f, 24m, 25f; Figure 3a-d). Using an image analyzer, the mosaic ratios in 12f, 19f, 20f, 24m and 25f were found to be 1/70, 1/20, 1/43, 1/20, and 1/62, respectively. With the ddPCR assay, the mosaic ratios in those patients were 1/75, 1/57, 1/39, 1/76, and 1/56, respectively (Figure 3e). Except for one male patient, we reviewed the XCI pattern in four of the female IP patients with a mosaic deletion and found XCI patterns of 67.1%, 50%, 58.4%, and 65.3%, respectively, with a mean value of 61.9%. The mean XCI value of the remaining four cases with undetected mutations was 79.0%, compared to 60.2% in the healthy controls. These XCI values thus showed distinct differences. Hence, as the XCI pattern of the mother, who had clinical symptoms, of 03f was 73.3%, this lower XCI may indicate a somatic and germline

TABLE 2 Phenotype score of the 03f family.

Patient	Age at genetic testing	Female/male	Skin leision[a]	Nervous system defect[b]	Ocular system defect[c]	Dental system defect[d]	Hair defect[e]	Nails defect[f]	Phenotype score[g]
03f (proband)	0	F	3	1	ND	ND	ND	ND	4
Sister of 03f	3	F	3	0	0	0	1	0	4
Mother of 03f	38	F	2	0	0	0	0	0	2

Note: IP phenotype score analysis. A phenotype score of clinical severity was derived when possible in IP patients whose clinical data were available.

Abbreviation: ND, not determined.

Phenotype score represents the addition of the single score values for each system/organ.

[a]We assigned a score 1 for little skin abnormality in limbs; a score 2 for skin abnormality in some parts of limbs or trunk; a score of 3 for skin abnormality in all limbs and trunk. All IP reported patients suffered skin abnormality.

[b]A score of 1 was added for each nervous system (NS) defect (seizures, or spastic paresis, or motor retardation, or mental retardation or microcephaly).

[c]A score of 1 was added for each ocular system defect (strabismus, or cataracts, or optic atrophy, or retinal vascular pigmentary abnormalities, ormicrophthalmos, or pseudogliomas).

[d]A score of 1 was added for each Dental System defect (partial anodontia, or delayed dentition, or cone/peg shaped teeth, or impactions).

[e]A score of 1 was added for each Hair defect (vertex alopecia, or wooly hair nevus, or eyelash and eyebrow hypogenesis).

[f]A score of 1 was added for each Nails defect (onychogryposis, or pitting, or ridging).

[g]Phenotype score represents the addition of the single score values for each system/organ.

	AR	*ZDHHC15*	*SLITRK4*	*PCSKIN*	Median (%)
03f	91.3	NI	89.2	93.1	91.3
Sister of 03f	98.3	—	—	—	98.3
Mother of 03f	NI	67.7	73.7	82.5	73.7

Abbreviation: NI, not informative.

TABLE 3 XCI value of AR and three alternative methylation-sensitive restriction enzyme site.

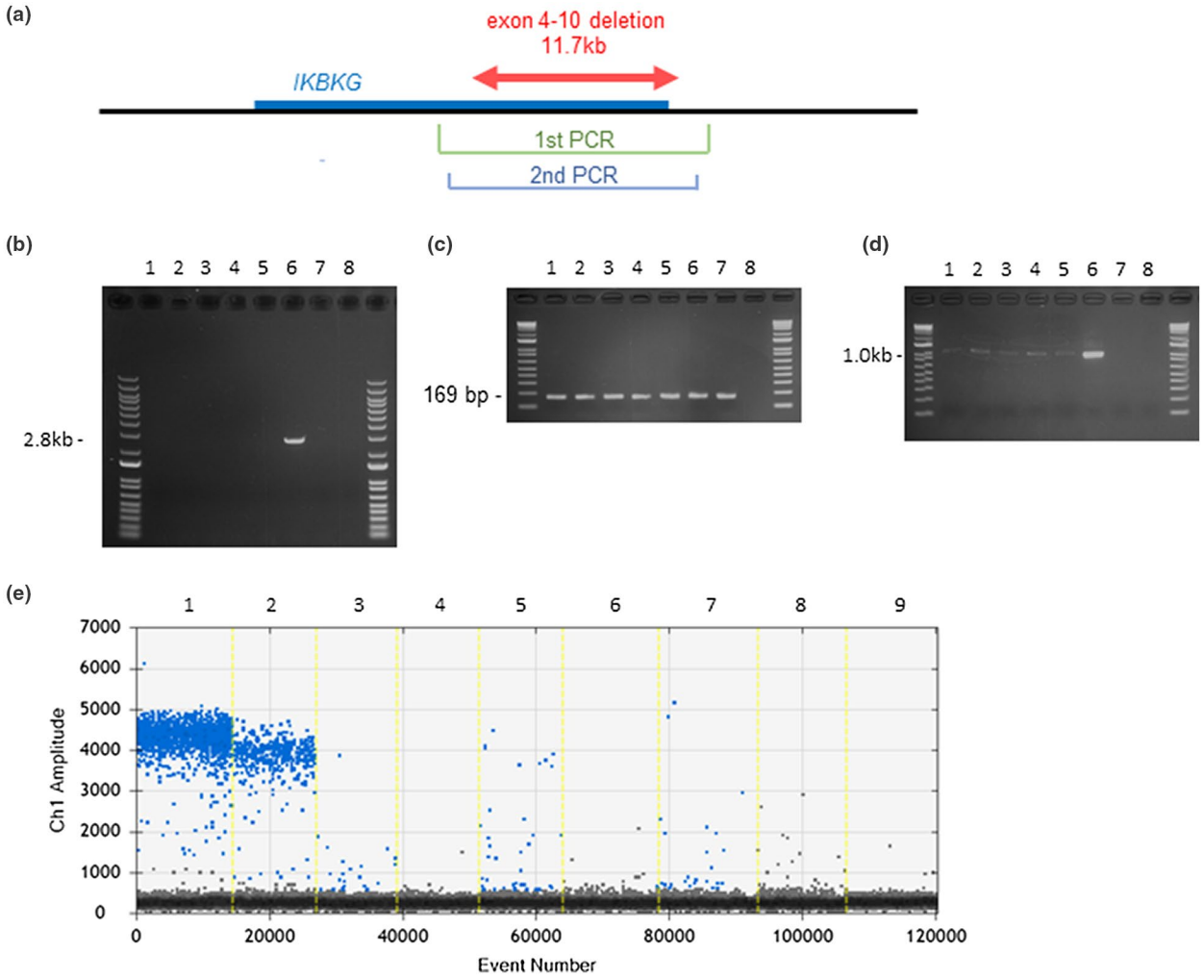

FIGURE 3 Mosaic analysis of the *IKBKG* gene. (a) Schematic showing the relative location of the *IKBKG* gene and its exons 4-10. The position of the common exon 4-10 deletion in IP is indicated by red arrows. The green line denotes the region of the first PCR and the blue line the second PCR. (b) First PCR. A 2.8 kb amplified product indicates an *IKBKG* exon 4-10 deletion. Lanes 1-5 represent 12f, 19f, 20f, 20m, and 25f, respectively. Lane 6, *IKBKG* exon 4-10 deletion control; lane 7, healthy control; lane 8; DW. (c) Internal standard for semi-quantitative PCR. The same DNA samples were used as templates for control PCR to amplify intron 45 of the *DMD* gene. (d) Second PCR. A 1.0 kb amplified product indicates a mosaic deletion, which was evident in lanes 1-5. Lanes 6-8 are as described in (b). (e) ddPCR. Plots show a quantification of fluorescence signal of droplet. Green dots indicate fluorescence-positive droplets, while black dots indicate negative droplets. Lane 1 represent *IKBKG* exon 4-10 deletion control. Lane 2, 3, 4, 5, 6, 7 represent the mother of 03f, 12f, 19f, 20f, 24m, 25f, respectively. Lane 8,9 represent healthy control and DW, respectively.

mosaicism. Our result of PCR assay and ddPCR assay revealed a mosaic ratio of 1/4 and 1/5 for the mother of 03f, respectively (Figure 3e). To confirm the somatic mosaicism, we attempted to obtain somatic tissues other than blood in these patients. Cheek swab sample was obtained only from 24 m, which did not show the common deletion by the nested PCR (data not shown).

We finally performed NGS analysis to detect mosaic SNVs in the remaining subjects (01f, 02f, 04m, and 15f).

Approximately, 90% of the cumulative target region was covered with a sequence depth of more than 200X. We evaluate SNVs and indels at a greater than 1% frequency in the coding exons of the *IKBKG* gene and *IKBKGP* pseudogene. No SNVs that indicated low-level mosaicism were identified in these patients. These data are summarized in Table 1. When including the low-level mosaic mutations, we detected a total of 25 *IKBKG* mutations in 30 samples (83.3%).

4 | DISCUSSION

In our current study of 30 unrelated IP families from Japan, we identified *IKBKG* mutations in 25 families, including 5 low-level mosaic mutations. In a previous large-scale study of IP, 65% of the cases had the common exon 4-10 deletion in the *IKBKG* gene (Fusco et al., 2008), 8.6% harbored SNVs (Fusco et al., 2007), and 4% had a larger deletion at the *IKBKG* locus (Conte et al., 2014). In our current standard protocol, we initially identified the common *IKBKG* deletion at a much reduced frequency of 43.3% (13/30), which made our initial mutation detection efficiency low (20/30, 66.7%) in comparison to previous studies. This outcome might have partly been due to ethnic differences. Another possible reason may be that there was a bias in the patients referred to our institute, that is, they were mainly non-deleted cases that came via deletion screening in a prior facility. We finally identified a total of 25 mutations in 30 IP patients after introducing a detection system for low-level mosaicism (83.3%).

We identified low-level mosaicism of the common *IKBKG* deletion in 16.7% of our current IP cases (5/30). Thus, as much as 27.8% of the common deletions in our current study series were mosaic (5/18). This suggested that our diagnosis system, semi-quantitative nested PCR and ddPCR, could efficiently detect low-level mosaicism. We conclude from this that clinical geneticists should become aware of the high incidence of low-level mosaicism in this disorder. Our present data have indicated that IP patients with mild symptoms only affecting the skin and those with low XCI values tended to include cases of low-level mosaic mutations in the *IKBKG* gene. It is well documented that XCI values are elevated with age (Hatakeyama et al., 2004). Our current patients median age was 0 years old in both groups (no significant difference), although that of the unaffected family members was 38.5 years. Thus, these are likely predictors of a low-level mosaicism when a mutation survey fails to detect mutations in the *IKBKG* gene. Hence, a HUMARA assay may be a powerful method of differentiating the mutational status of the *IKBKG* gene in IP patients. We recommend the use of this assay when the standard mutational analyses fail to detect mutations in the *IKBKG* gene in IP patients.

It is well acknowledged that random XCI in humans occurs in early embryogenesis after the blastocyst stage (Lee & Bartolomei, 2013). If a zygote with a germinal mutation in the *IKBKG* gene undergoes random XCI, about half of the cells carry the mutation on the activated X chromosome and the other half carry the mutation on the inactive X. During early embryogenesis, the cells with the mutation on the activated X chromosome would undergo apoptosis and be negatively selected. Thus, a skewed XCI pattern would be established. A small number of surviving cells harboring the *IKBKG* mutation on the activated X chromosome would then induce local mild symptoms. In contrast, if the mutation in the *IKBKG* gene arises in the very early embryonic stages prior to XCI determination, most of the cells would be normal and lack the mutation. Even if the cells with the mutation on the activated X chromosome would be negatively selected, XCI data would show a random XCI pattern reflecting a majority of normal cells. Finally, if the mutation in the *IKBKG* gene arises after XCI determination, XCI data would show a random XCI pattern reflecting the majority of normal cells regardless of whether the mutation occurred on the activated or inactivated X chromosome. According to their mosaic ratio, our current study probands were found to have undergone the somatic mutation event at the embryonic stage from the end of the morula stage, which consists of 16-36 cells, to the blastocyst stage. However, whether these mutations occurred before or after the XCI patterns are determined, patients with low-level mosaicism would not manifest skewed XCI patterns.

We did not detect any mutations in the *IKBKG* gene in four patients (01f, 02f, 04m, 15f and 27f). One of these cases (27f) showed a skewed XCI pattern (92.8%), suggesting that she had a germline mutation that we could not detect with our methods. Two of our current study patients (02f and 15f) did not show a skewed XCI pattern (79.0% and 72.2%, respectively). The other case (04m) was a male patient with a normal karyotype. These three IP patients may therefore have low-level mosaic mutations not of the common deletion, but at the nucleotide level. The detection sensitivity of the deep sequencing we used prevented us from identifying mosaic nucleotide mutations. With a read depth of 200-400, up to a 1% mutation frequency in the coding exons of the *IKBKG* gene could be theoretically detected in spite of the presence of random artifacts such as misincorporations during DNA synthesis. However, a level of mosaicism below 1% could not be detected even when this deep sequencing was performed. Further investigations using ultra deep sequencing might elucidate the mutations of these remaining patients.

IP females have a risk of having an affected baby, with the risk of inheritance generally thought to be 50%, that is, male embryonic lethality and the birth of affected females. However, our current analyses indicate that the apparently affected IP females include those harboring germline mutations and those with a low level of mosaicism. Given that IP females can have low-level mosaic somatic mutations, the risk of inheritance becomes very small. In sporadic IP

cases, a mother with an apparently normal phenotype may have a hidden low level of mosaicism. Among the IP patients who carry the *IKBKG* exon 4-10 deletion, 65% are sporadic cases (Fusco et al., 2009). In addition, 3.8% of IP offspring with a de novo mutation have parents who shows 1% mosaicism in their blood cells (Rahbari et al., 2015). Clinical symptoms of IP appearing in patients with low-level mosaic mutations might be too mild to be diagnosed properly. Our current findings suggest that most mothers of sporadic cases may have no germline mutation, but some might show a low level of mosaicism when a highly sensitive mutation search is performed. Furthermore, even when the mother of a child with IP is correctly diagnosed with a low level of mosaicism, they would not necessarily have a small risk of having affected children. The mother of our current study patient 03f showed a 1/4 mosaic mutation, but was a parent of three girls of which two were affected with IP. A noteworthy limitation of our current analysis is that we only have the mosaicism information from blood samples and not from the germinal cells. In any event, a correct diagnosis of germline or somatic mosaicism in relation to IP will facilitate more informed genetic counseling for family planning purposes.

In conclusion, we have here identified five patients with low level of mosaicism of the common *IKBKG* exon 4-10 deletion that causes IP. These patients manifest a mild IP phenotype only and no skewed XCI pattern, suggesting that XCI pattern values can predict the possibility of mosaicism for this disorder. Determination of the XCI value in advance of mutational analyses for IP could improve the mutation detection rate. Detecting mosaic mutations will also be beneficial for genetic counseling of affected individuals.

ACKNOWLEDGMENTS

The authors thank the patients, their families, and their attending physicians for participating in this study. The authors also thank in particular Dr. M. Miyata, Dr. H. Nishizawa, Dr. R. Suda, Dr. Y. Fukui, H. Dr. Wakita, F. Dr. Tanaka, Dr. T. Inozume, Dr. A. Noguchi, Dr. T. Hukuda, Dr. A. Sugimoto, Dr. K. Yamane, Dr. T. Nishimura, Dr. T. Kusaka, Dr. Y. Kosugi, Dr. M. Matsuo, Dr. H. Arai, Dr. R. Matsunaga, Dr. S. Akashi, Dr. Y. Murai. Dr. T. Nishimura, Dr. T. Kaji, Dr. S. Kato, Dr. A. Yara, and Dr. S. Kanai, Dr. H. Sueoka, T. Fujii, and Dr. Y. Fukuhara. Additionally, the authors also thank Asami Kuno and Narumi Kamiya for technical assistance.

CONFLICT OF INTEREST

The authors declare no competing interests in relation to this study.

AUTHOR CONTRIBUTIONS

MK carried out the genomic analysis and drafting of the manuscript. TK, MT, and HI was responsible for genomic analysis. YS carried out NGS analysis. HK conceived the study and participated in its design and drafted the manuscript. All authors read and approved the final version of the manuscript and agree with the order of presentation of the authors.

DATA AVAILABILITY STATEMENT

The datasets used and/or analyzed during the current study are available from the corresponding author on reasonable request.

ORCID

Hiroki Kurahashi https://orcid.org/0000-0002-5690-5218

REFERENCES

Aradhya, S., Bardaro, T., Galgóczy, P., Yamagata, T., Esposito, T., Patlan, H., Ciccodicola, A., Munnich, A., Kenwrick, S., Platzer, M., & D'Urso, M. (2001). Multiple pathogenic and benign genomic rearrangements occur at a 35 kb duplication involving the NEMO and LAGE2 genes. *Human Molecular Genetics*, *10*(22), 2557-2567. https://doi.org/10.1093/hmg/10.22.2557

Aradhya, S., Courtois, G., Rajkovic, A., Lewis, R. A., Levy, M., Israël, A., & Nelson, D. L. (2001). Atypical forms of incontinentia pigmenti in male individuals result from mutations of a cytosine tract in Exon 10 of NEMO (IKK- g). *American Journal of Human Genetics*, *68*(3), 765-771.

Bardaro, T., Falco, G., Sparago, A., Mercadante, V., Gean Molins, E., Tarantino, E., Valeria Ursini, M., & D'Urso, M. (2003). Two cases of misinterpretation of molecular results in incontinentia pigmenti, and a PCR-based method to discriminate NEMO/IKKγ gene deletion. *Human Mutation*, *21*(1), 8-11. https://doi.org/10.1002/humu.10150

Beever, C. L., Stephenson, M. D., Peñaherrera, M. S., Jiang, R. H., Kalousek, D. K., Hayden, M., Field, L., Brown, C. J., & Robinson, W. P. (2003). Skewed X-chromosome inactivation is associated with trisomy in women ascertained on the basis of recurrent spontaneous abortion or chromosomally abnormal pregnancies. *The American Journal of Human Genetics*, *72*(2), 399-407. https://doi.org/10.1086/346119

Bertelsen, B., Tümer, Z., & Ravn, K. (2011). Three new loci for determining X chromosome inactivation patterns. *The Journal of Molecular Diagnostics*, *13*(5), 537–540. https://doi.org/10.1016/j.jmoldx.2011.05.003

Boisson, B., Honda, Y., Ajiro, M., Bustamante, J., Bendavid, M., Gennery, A. R., Kawasaki, Y., Ichishima, J., Osawa, M., Nihira, H., Shiba, T., Tanaka, T., Chrabieh, M., Bigio, B., Hur, H., Itan, Y., Liang, Y., Okada, S., Izawa, K., … Yasumi, T. (2019). Rescue of recurrent deep intronic mutation underlying cell type – dependent quantitative NEMO deficiency Find the latest version : Rescue of recurrent deep intronic mutation underlying cell type – dependent quantitative NEMO deficiency. *The Journal of Clinical Investigation*, *129*(2), 583-597. https://doi.org/10.1172/JCI124011

Conte, M. I., Pescatore, A., Paciolla, M., Esposito, E., Miano, M. G., Lioi, M. B., McAleer, M. A., Giardino, G., Pignata, C., Irvine, A. D., & Scheuerle, A. E. (2014). Insight into IKBKG/NEMO locus: Report of new mutations and complex genomic rearrangements

leading to incontinentia pigmenti disease. *Human Mutation*, *35*(2), 165-177. https://doi.org/10.1002/humu.22483

Döffinger, R., Smahi, A., Bessia, C., Geissmann, F., Feinberg, J., Durandy, A., Bodemer, C., Kenwrick, S., Dupuis-Girod, S., Blanche, S., Wood, P., Rabia, S. H., Headon, D. J., Overbeek, P. A., Le Deist, F., Holland, S. M., Belani, K., Kumararatne, D. S., Fischer, A., … Casanova, J.-L. (2001). X-linked anhidrotic ectodermal dysplasia with immunodeficiency is caused by impaired NF- κ B signaling. *Nature Genetics*, *27*, 277-285.

Fusco, F.,Bardaro, T., Fimiani, G., Mercadante, V., Miano, M. G., Falco, G., Israël, A., Courtois, G., D'Urso, M., & Ursini, M. V. (2004). Molecular analysis of the genetic defect in a large cohort of IP patients and identification of novel NEMO mutations interfering with NF-κB activation. *Human Molecular Genetics*, *13*(16), 1763-1773. https://doi.org/10.1093/hmg/ddh192

Fusco, F., Fimiani, G., Tadini, G., Michele, D'. U., & Ursini, M. V. (2007). Clinical diagnosis of incontinentia pigmenti in a cohort of male patients. *Journal of the American Academy of Dermatology*, *56*(2), 264-267. https://doi.org/10.1016/j.jaad.2006.09.019

Fusco, F., Mariateresa, P., Alessandra, P., Brigida, L. M., Carmen, A., Francesca, F., Mattia, G., Marcella, Z., Michele, D. U., Giuseppina, M. M., & Valeria, U. M. (2009). Microdeletion/duplication at the Xq28 IP Locus causes a de novo IKBKG/NEMO/IKKgamma exon4-10 deletion in families with incontinentia pigmenti. *Human Mutation*, *30*(9), 1284-1291. https://doi.org/10.1002/humu.21069

Fusco, F., Paciolla, M., Conte, M., Pescatore, A., Esposito, E., Mirabelli, P., Lioi, M., & Ursini, M. (2014). Incontinentia pigmenti: Report on data from 2000 to 2013. *Orphanet Journal of Rare Diseases*, *9*(1), 1-5. https://doi.org/10.1186/1750-1172-9-93

Fusco, F., Paciolla, M., Napolitano, F., Pescatore, A., D'Addario, I., Bal, E., Lioi, M. B., Smahi, A., Miano, M. G., & Ursini, M. V. (2012). Genomic architecture at the incontinentia pigmenti locus favours de novo pathological alleles through different mechanisms. *Human Molecular Genetics*, *21*(6), 1260-1271. https://doi.org/10.1093/hmg/ddr556

Fusco, F., Pescatore, A., Bal, E., Ghoul, A., Paciolla, M., Lioi, M. B., D'Urso, M., Rabia, S. H., Bodemer, C., Bonnefont, J. P., Munnich, A., Miano, M. G., Smahi, A., & Ursini, M. V. (2008). Alterations of the IKBKG locus and diseases: An update and a report of 13 novel mutations. *Human Mutation*, *29*(5), 595-604. https://doi.org/10.1002/humu.20739

Hatakeyama, C., Anderson, C. L., Beever, C. L., Peñaherrera, M. S., Brown, C. J., & Robinson, W. P. (2004). The dynamics of X-inactivation skewing as women age. *Clinical Genetics*, *66*(4), 327-332. https://doi.org/10.1111/j.1399-0004.2004.00310.x

Ikeda F., Deribe Y. L., Skånland S. S., Stieglitz B., Grabbe C., Franz-Wachtel M., van Wijk S. J. L., Goswami P., Nagy V., Terzic J., Tokunaga F., Androulidaki A., Nakagawa T., Pasparakis M., Iwai K., Sundberg J. P., Schaefer L., Rittinger K., Macek B., Dikic I. (2011). SHARPIN forms a linear ubiquitin ligase complex regulating NF-κB activity and apoptosis. *Nature*, *471*, (7340), 637–641. http://dx.doi.org/10.1038/nature09814.

Landy, S. J., & Donnai, D. (1993). Incontinentia pigmenti (Bloch-Sulzberger syndrome). *Journal of Medical Genetics*, *30*(1), 53-59.

Lee, J. T., & Bartolomei, M. S. (2013). Review X-inactivation, imprinting, and long noncoding RNAs in health and disease. *Cell*, *152*(6), 1308-1323. https://doi.org/10.1016/j.cell.2013.02.016

Minić, S., Trpinac, D., & Obradović, M. (2014). Incontinentia pigmenti diagnostic criteria update. *Clinical Genetics*, *85*(6), 536-542. https://doi.org/10.1111/cge.12223

Orphanet. (2018). Prevalence and incidence of rare diseases: Bibliographic data. *Number*, 1(1). www.orpha.net%0Awww.orpha.net

Rahbari, R., Wuster, A., Lindsay, S. J., Hardwick, R. J., Alexandrov, L. B., Al Turki, S., Dominiczak, A., Morris, A., Porteous, D., Smith, B., Stratton, M. R., & Hurles, M. E. (2015). Articles Timing, rates and spectra of human germline mutation. *Nature Genetics*, *48*(2), 126-133. https://doi.org/10.1038/ng.3469

SUPPORTING INFORMATION

Additional supporting information may be found online in the Supporting Information section.

Supplementary Material

How to cite this article: Kawai M, Kato T, Tsutsumi M, Shinkai Y, Inagaki H, Kurahashi H. Molecular analysis of low-level mosaicism of the *IKBKG* mutation using the X Chromosome Inactivation pattern in Incontinentia Pigmenti. *Mol Genet Genomic Med*. 2020;00:e1531. https://doi.org/10.1002/mgg3.1531

Received: 19 May 2020 | Revised: 19 June 2020 | Accepted: 24 June 2020

DOI: 10.1111/cas.14553

ORIGINAL ARTICLE

Cancer Science WILEY

Impact of *DPYD*, *DPYS*, and *UPB1* gene variations on severe drug-related toxicity in patients with cancer

Katsuyuki Yokoi[1,2] | Yoko Nakajima[1] | Hiroshi Matsuoka[3] | Yasuko Shinkai[2] | Takuma Ishihara[4] | Yasuhiro Maeda[5] | Takema Kato[2] | Hidetoshi Katsuno[3] | Koji Masumori[3] | Kenji Kawada[6] | Tetsushi Yoshikawa[1] | Tetsuya Ito[1] | Hiroki Kurahashi[2]

[1]Department of Pediatrics, Fujita Health University School of Medicine, Toyoake, Japan

[2]Division of Molecular Genetics, Institute for Comprehensive Medical Science, Fujita Health University, Toyoake, Japan

[3]Department of Gastrointestinal Surgery, Fujita Health University School of Medicine, Toyoake, Japan

[4]Innovative and Clinical Research Promotion Center, Gifu University Hospital Gifu University, Gifu, Japan

[5]Center for Joint Research Facilities Support, Fujita Health University, Toyoake, Japan

[6]Department of Medical Oncology, Fujita Health University School of Medicine, Toyoake, Japan

Correspondence
Yoko Nakajima, Department of Pediatrics, Fujita Health University School of Medicine, 1-98 Dengakugakubo, Kutsukake-cho, Toyoake, Aichi 470-1192, Japan.
Email: yonaka@fujita-hu.ac.jp

Abstract

Cancer treatment with a fluoropyrimidine (FP) is often accompanied by severe toxicity that may be dependent on the activity of catalytic enzymes encoded by the *DPYD*, *DPYS*, and *UPB1* genes. Genotype-guided dose individualization of FP therapy has been proposed in western countries, but our knowledge of the relevant genetic variants in East Asian populations is presently limited. To investigate the association between these genetic variations and FP-related high toxicity in a Japanese population, we obtained blood samples from 301 patients who received this chemotherapy and sequenced the coding exons and flanking intron regions of their *DPYD*, *DPYS*, and *UPB1* genes. In total, 24 single nucleotide variants (15 in *DPYD*, 7 in *DPYS* and 2 in *UPB1*) were identified including 3 novel variants in *DPYD* and 1 novel variant in *DPYS*. We did not find a significant association between FP-related high toxicity and each of these individual variants, although a certain trend toward significance was observed for p.Arg181Trp and p.Gln334Arg in *DPYS* ($P = .0813$ and .087). When we focused on 7 *DPYD* rare variants (p.Ser199Asn, p.Ile245Phe, p.Thr305Lys, p.Glu386Ter, p.Ser556Arg, p.Ala571Asp, p.Trp621Cys) which have an allele frequency of less than 0.01% in the Japanese population and are predicted to be loss-of-function mutations by in silico analysis, the group of patients who were heterozygous carriers of at least one these rare variants showed a strong association with FP-related high toxicity ($P = .003$). Although the availability of screening of these rare loss-of-function variants is still unknown, our data provide useful information that may help to alleviate FP-related toxicity in Japanese patients with cancer.

KEYWORDS

5-fluorouracil, *DPYD*, *DPYS*, fluoropyrimidine, *UPB1*

Abbreviations: 5FU, 5-fluorouracil; CDDP, cisplatin; CPT-11, irinotecan hydrochloride hydrate; CTCAE, Common Terminology Criteria for Adverse Events; DHP, dihydropyrimidinase; DPD, dihydropyrimidine dehydrogenase; DTX, docetaxel hydrate; FP, fluoropyrimidine; GEM, gemcitabine hydrochloride; Jmorp, Japanese Multi Omics Reference Panel; L-OHP, oxaliplatin; PTX, paclitaxel; SIFT, Sorting Intolerant From Tolerant; βUP, β-ureidopropionase.

1 | INTRODUCTION

Fluoropyrimidines including 5 5FU and its prodrugs are widely used in the treatment of various malignancies including head and neck, gastrointestinal, or breast cancers.[1-3] FPs have a narrow therapeutic index and up to 30% of treated patients develop early-onset severe toxicity such as diarrhea, nausea, mucositis, stomatitis, myelosuppression, neurotoxicity, and hand-foot syndrome.[4-6] FP toxicity is largely dependent on its catabolism. Most FP molecules are inactivated by DPD and FP-related toxicity is often caused by an inherited reduced activity of this enzyme.[7-9] Patients with a DPD deficiency have an increased risk of developing severe treatment-related toxicity from a standard dose of FP.[10] A partial DPD deficiency is present in 3%-5% of the North American and European general population.

The DPD gene, *DPYD*, is located on chromosome 1p21 and is comprised of 23 exons.[11] The 4 *DPYD* variants considered most clinically relevant with statistically significant associations with severe toxicity are c.1905 + 1G>A (*DPYD**2A, rs3918290, IVS14 + 1G>A), c.2846A>T (rs67376798, D949V), c.1679T>G (rs55886062, *DPYD*13, I560S) and c.1236G>A (rs56038477, E412E, in haplotype B3).[12,13] Hence, *DPYD* genotype-guided dose individualization of FP therapy has now been conducted in some western countries.[10] However, to our knowledge it has not been performed yet in Japan, possibly because none of these *DPYD* variants have been identified in the Asian population.[14] Recently, 21 *DPYD* allelic variants were identified in 1070 healthy Japanese individuals.[15] The functional alterations caused by these variants were analyzed in vitro and their enzyme activities were characterized.[14] However, there has been no report to date on the clinical relevance of *DPYD* variants as predictors of FP-associated toxicity in Japanese people.

It is thought that decreased activity of the enzymes DHP and βUP, which are located downstream of DPD in FP catabolism, may also play a role in FP-associated toxicity.[16] The DHP-encoding gene, *DPYS*, is located on chromosome 8q22,[17] and the βUP-encoding gene, *UPB1*, is located on chromosome 22q11.[18] A relationship between *DPYS* and *UPB1* gene variations and severe FP-related toxicity has been reported,[16] but no other data currently support this association, which thus remains to be fully elucidated. It is known that the Japanese prevalence of βUP deficiency is relatively high (1 per 6000 newborns).[19] We have also reported that some *DPYS* variants may be more common than expected in East Asian groups.[20] These findings have prompted us to screen for variants of the genes associated with FP-related toxicity in Japanese subjects.

We have here evaluated the association between *DPYD*, *DPYS*, and *UPB1* gene variations and severe FP-related toxicity in Japanese patients with cancer. This is the first report to assess the clinical relevance of *DPYD*, *DPYS*, and *UPB1* variants as predictors of severe FP-associated toxicity in East Asians.

2 | MATERIALS AND METHODS

2.1 | Patients and sample collection

Blood samples of 301 consenting patients who received or were receiving FP-based chemotherapy were collected between 2018 and 2020. All patients were of East Asian origin. These 301 patients were recruited at Fujita Health University. All treatments, patient characteristics, concurrent therapy and adverse effects (gastrointestinal [nausea, vomiting, diarrhea, oral mucositis], neutropenia, hand-foot syndrome, acute kidney injury) developed within the first 2 cycles of treatment in this cohort and were classified according to the CTCAE v4.0. We divided these subjects into 2 groups in accordance with the grade of toxicity for statistical purposes. The high-toxicity group included patients who experienced severe toxicity presenting with CTCAE grade 3-5 adverse events in any category. The low-toxicity group included patients who experienced low toxicity involving CTCAE grade 0-2 adverse events.

2.2 | DPYD, DPYS, UPB1 sequencing analysis

Genomic DNA was extracted from aliquots of the study patient blood specimens using a standard procedure. We designed a custom AmpliSeq panel for the sequencing of coding exons and flanking intron regions (± 10 bp) of *DPYD*, *DPYS*, and *UPB1*. Library preparation for amplicon sequencing was performed using AmpliSeq Library PLUS for Illumina. Libraries were sequenced on the MiSeq platform with 150 bp paired-end reads (Illumina, San Diego, CA). Sequencing data were analyzed with Illumina Basespace DNA Amplicon App. We used the UCSC genome browser (http://genome-asia.ucsc.edu/human GRCh37/hg19) as the human genome assembly. Illumina Variant Studio was used for annotation and filtration of genomic variants with a Pass Filter read depth > 50×. Allele frequency was investigated with gnomAD browser beta (http://gnomad.broadinstitute.org/) and Jmorp https://jmorp.megabank.tohoku.ac.jp).

The in silico analysis of each variant was performed using Polymorphism Phenotyping ver. 2 (PolyPhen-2; http://genetics.bwh.harvard.edu/pph2) and SIFT (http://sift-dna.org) to predict the functional impact on the protein product. In the PolyPhen-2 program, the investigated variant is categorized as probably damaging (probability score > 0.85), possibly damaging (probability score between 0.16 and 0.85), or benign (probability score less than or equal to 0.15). SIFT is a tool for sorting intolerant from tolerant amino acids. The evaluated amino acid substitution is predicted as damaging if the score is <.05 and is predicted to be tolerated if the score is greater than or equal to .05.

2.3 | Statistical analyses

The study patient characteristics were presented using median and range for continuous variables, and frequencies and proportions for categorical variables. The Fisher exact test was used to identify the association of

DPYD, *DPYS*, and *UPB1* variations with FP-related high toxicity because some categories would have an expected count of 5 or less. The frequencies of high-toxicity and low-toxicity groups were compared between each genotype. Due to the exploratory nature of this study, a *P*-value less than .05 was considered statistically significant, and $.05 < P < .1$ was recognized as indicating a certain trend toward significance. Statistical analyses were conducted using R software version 3.6.2 (www.r-project.org).

3 | RESULTS

3.1 | Patient characteristics

The age, treatments, and cancer types of the 301 patients are listed in Table 1. The most commonly used regimen in this cohort was 5FU + L-OHP/CPT-11 + α(molecular target) (54.5%, n = 164), followed by 5FU monotherapy (28.9%, n = 87). A majority of patients (68.1%) had a colorectal tumor (n = 205). During the first 2 cycles of chemotherapy, 18.3% (n = 55) of the patients developed high-toxicity responses (CTCAE grade 3-4), and 81.7% (n = 246) showed low toxicity (CTCAE grade 0-2). No patient in our current series developed a grade 5 adverse event. The most frequent adverse event category observed in the high-toxicity group was neutropenia, followed by gastrointestinal-related issues (Table 2).

Toxicity rates varied and significantly depended on the FP regimen (Table 1). 80% (n = 4/5) and 53.8% (n = 7/13) of patients who received DTX + CDDP+5FU and FOLFOXIRI + α, respectively, developed high toxicity, while, only 1 patient (1.8%) showed high toxicity in 5FU monotherapy.

3.2 | Variant analysis of the *DPYD*, *DPYS*, and *UPB1* genes

In total, 24 non-synonymous single nucleotide variants (15 *DPYD*, 7 *DPYS* and 2 *UPB1*) were identified in our present study population including 3 novel variants in *DPYD* and 1 novel variant in *DPYS*. (Table 3) Seven *DPYD* variants and 2 *DPYS* variants were rare variants with a minor allele frequency in the Japanese population of less than 0.01% (Jmorp). (Table 3) Out of the 24 variants identified, we excluded 1 *DPYD* nonsense variant and one *DPYS* noncoding variant and analyzed the remaining 22 by PolyPhen-2 and SIFT. The results indicated that 18 variants, including all of the rare variants, were predicted to be probably damaging by PolyPhen-2 and/or damaging by SIFT (Table 3). The number of heterozygous and homozygous individuals in the high-toxicity and low-toxicity groups for each of the 24 variants is shown in Table S1.

3.3 | Association of *DPYD*, *DPYS*, and *UPB1* variations with FP-related high toxicity

The *P*-values for each of the variants in relation to an association with FP-related high toxicity are shown in Table 4. In the single

TABLE 1 Baseline characteristics of the study population: n = 301

	Total sample	Low toxicity (grade 0-2) n (%)	High toxicity (grade 3-4) n (%)
Total	301	246	55
Age			
Median	67	66	68
Range	22-85	25-85	22-81
Sex			
Male	179	155 (86.6%)	24 (13.4%)
Female	122	91 (74.6%)	31 (25.4%)
Tumor			
Stomach	70	59 (84.3%)	11 (15.7%)
Colorectal	205	167 (81.5%)	38 (18.5%)
Other tumors	26	20 (76.9%)	6 (23.1%)
5FU + CDDP	17	15 (88.2%)	2 (11.8%)
5FU + L-OHP/CPT-11 + α(molecular target)	164	127 (77.4%)	37 (22.6%)
5FU mono	87	86 (98.9%)	1 (1.1%)
DTX + CDDP+5FU	5	1 (20%)	4 (80%)
FOLFOXIRI + α	13	6 (46.2%)	7 (53.8%)
5FU + PTX	1	1 (100%)	0 (0%)
5FU + GEM/DTX	14	10 (71.4%)	4 (28.6%)

Abbreviations: 5FU, 5 fluorouracil; CDDP, cisplatin; L-OHP, oxaliplatin; CPT-11, irinotecan hydrochloride hydrate; DTX, docetaxel hydrate; PTX, paclitaxel; GEM, gemcitabine hydrochloride.

TABLE 2 Numbers and proportions (%) of patients experiencing different categories of toxicity during the first 2 therapy cycles

Toxicity category	Total sample (n = 301) n (%)	Low toxicity (grade 1-2) (n = 246) n (%)	High toxicity (grade 3-4) (n = 55) n (%)
Gastrointestinal			
Nausea	61 (20.3%)	58 (23.6%)	3 (5.5%)
Vomiting	21 (7%)	18 (7.3%)	3 (5.5%)
Diarrhea	43 (14.3%)	36 (14.6%)	7 (12.7%)
Oral Mucositis	29 (9.6%)	28 (11.4%)	1 (1.8%)
Neutropenia	125 (41.5%)	82 (33.3%)	43 (78.2%)
Hand-foot syndrome	30 (10%)	30 (12.2%)	0 (0%)
Acute kidney injury	10 (3.3%)	10 (4.1%)	0 (0%)

variant analysis, in which we analyzed each variant individually, we did not find any significant association with high toxicity, although a certain trend toward significance was observed for p.Arg181Trp and p.Gln334Arg of *DPYS* ($P = .081$ and .087). *DPYS* p.Arg181Trp was a common variant and was heterozygous in 14 patients who were all classified as low-toxicity group cases. In contrast, heterozygosity for *DPYS* p.Gln334Arg was observed in only 3 patients, 2 of whom developed high toxicity (Table 4). Clinical and genetic information for these 2 heterozygous *DPYS* p.Gln334Arg patients with high toxicity are provided in Table 5. Both patients received 5FU + L-OHP and developed grade 3 neutropenia. In addition, 1 patient presented with grade 1 vomiting and the other presented with grade 2 nausea. Although both patients were simultaneous carriers of other variants including *DPYD* p.Arg29Cys, *DPYD* p.Ile543Val and *DPYS* c.-1T>C, these additional variants are common benign variants found in the total cohort with an allele frequency of 96%, 27% and 68%, respectively. Hence, our results suggested that p.Gln334Arg may contribute to the susceptibility to severe FP-related toxicity.

We next focused on 7 rare *DPYD* variants that have an allele frequency in the Japanese population of less than 0.01%. Six show loss-of-function by in silico analysis ie probably damaging by PolyPhen-2 and/or deleterious by SIFT (p.Ser199Asn, p.Ile245Phe, p.Thr305Lys, p.Ser556Arg, p.Ala571Asp, p.Trp621Cys), and one is a nonsense mutation (p.Glu386Ter). We divided our patients into a rare pathogenic *DPYD* variant group consisting of individuals heterozygous for these 7 rare variants (n = 7), and a group of all other individuals without these rare variants (n = 294). Using the Fisher exact test, we found that the rare pathogenic *DPYD* variant group showed a significant association with FP-related high toxicity ($P = .003$; Table 4). Detail information on the 7 patients in the rare *DPYD* variant group is presented in Table 6. Although these 7 patients also carried other variants (*DPYD* p.Arg29Cys, *DPYD* p.Met166Val, *DPYD* p.Ile543Val, *DPYD* p.Thr768Lys and *DPYS* c.-1T>C), these additional variants showed a frequency of more than 1% and appeared benign. In the rare *DPYD* variant group also, 1 patient carrying a heterozygous *DPYD* p.Ala571Asp variant received 5FU monotherapy which is known as a more tolerable chemotherapy protocol, but developed severe toxicity including grade 3 nausea, grade 3 diarrhea, and grade 1 neutropenia.

4 | DISCUSSION

More than 450 *DPYD* variants have been identified to date as a cause of 5FU-related toxicity in patients with cancer.[14] In the context of 5FU, 4 *DPYD* variants identified in the White population are known to have an impact on enzyme function and FP-related toxicity risk.[21] However, none of these *DPYD* variants has been identified to date in an Asian population.[22] Prospective *DPYD* genotyping has thus proved feasible and effective in White but not in Japanese cases. In our present study, we revealed that *DPYD* nonsynonymous variants with allele frequencies of less than 0.01% in the Japanese population, and with an in silico analysis prediction of loss of function, may be associated with severe FP-related toxicity. Our data lend support to the concept that *DPYD* variants exist also in East Asian populations that affect the enzymatic activity of the protein product and thereby the severity of FP-related toxicity. In this study, we found 7 rare *DPYD* variants that were not found in Japanese genome variation databases. For Japanese allele frequency, we used the Jmorp database, which is based on the data of approximately 4000 Japanese individuals mainly living in the northeastern area of Japan. Since our 301 patients were recruited at our hospital at the central area of Japan, the discordance might be due to regional difference in the allele frequency.

The aim of our present study was the establishment of *DPYD* genotype-guided dose individualization of FP therapy in Japanese patients with cancer that have been performed in some western countries. However, we could not find a specific common variant in our present Japanese cohort that was highly associated with FP-related high toxicity. Sequencing of all coding DNA in the *DPYD* gene has some advantages in relation to screening high-risk individuals for severe FP-related toxicity, although it would not seem reasonable to reduce an FP treatment dose based on insufficient in silico findings. It may therefore be difficult to introduce *DPYD* genotyping as useful prospective screening in Japan. Previously, analysis of DPD enzyme activity has been proposed to be the most reliable method for identifying at-risk patients.[23] For the interpretation of a novel or very rare *DPYD* variant, it is useful to measure the DPD activity in the individuals who carry the variants.

TABLE 3 Information and *P*-values for the variants examined in this study

Genotype	dbSNP	In silico function (PolyPhen-2)	In silico function (SIFT)	Allele frequency (%) (Japanese/east Asian/Total)	*P*-value
DPYD					
NM_000110.3:c.85C>T NP_000101.2:p.Arg29Cys	rs1801265	Benign (0)	Tolerated (0.18)	96.85/92.8/76.6	.507
NM_000110.3:c.496A>G NP_000101.2:p.Met166Val	rs2297595	Probably damaging (1)	Tolerated (0.07)	2.18/1.524/8.585	.146
NM_000110.3:c.596G>A NP_000101.2:p.Ser199Asn	rs776973423	Probably damaging (1)	Damaging (0.02)	No data/0/0.006371	.183
NM_000110.3:c.733A>T NP_000101.2:p.Ile245Phe	rs767836989	Possibly damaging (0.853)	Damaging (0)	No data/0/0.004376	.183
NM_000110.3:c.914C>A NP_000101.2:p.Thr305Lys	No number	Probably damaging (0.999)	Damaging (0.01)	No data/no data/no data	1
NM_000110.3:c.1003G>A NP_000101.2:p.Val335Met	rs72549306	Probably damaging (1)	Damaging (0)	0.12/0.01632/0.001989	1
NM_000110.3:c.1156G>T NP_000101.2:p.Glu386Ter	rs78060119			No data/0/0.0007974	.183
NM_000110.3:c.1627A>G NP_000101.2:p.Ile543Val	rs1801159	Benign (0)	Tolerated (0.44)	27.62/25.34/19.52	.974
NM_000110.3:c.1666A>C NP_000101.2:p.Ser556Arg	rs755407188	Probably damaging (1)	Damaging (0)	No data/0.02176/0.001596	1
NM_000110.3:c.1712C>A NP_000101.2:p.Ala571Asp	No number	Probably damaging (1)	Damaging (0)	No data/no data/no data	.183
NM_000110.3:c.1863G>T NP_000101.2:p.Trp621Cys	No number	Probably damaging (1)	Damaging (0)	No data/no data/no data	.183
NM_000110.3:c.2194G>A NP_000101.2:p.Val732Ile	rs1801160	Probably damaging (0.999)	Damaging (0)	19.7/1.887/4.531	.266
NM_000110.3:c.2303C>A NP_000101.2:p.Thr768Lys	rs56005131	Possibly damaging (0.579)	Damaging (0)	24.1/0.236/0.01948	.429
NM_000110.3:c.2476G>A NP_000101.2:p.Val826Met	No number	Probably damaging (0.975)	Damaging (0)	0.14/no data/no data	1
NM_000110.3:c.2678A>G NP_000101.2:p.Asn893Ser	rs188052243	Benign (0)	Tolerated (0.41)	0.22/0.04903/0.003989	1
DPYS					
NM_001385.2:c.-1T>C	rs2959023			69.14/70.45/59.17	.45
NM_001385.2:c.17G>A NP_001376.1:p.Arg6Gln	rs199618701	Benign (0.028)	Damaging (0.02)	0.13/0.3628/0.05538	1
NM_001385.2:c.541C>T NP_001376.1:p.Arg181Trp	rs36027551	Benign (0.024)	Tolerated (0.18)	3.02/5.928/0.9123	.0813
NM_001385.2:c.884A>G NP_001376.1:p.His295Arg	rs996605020	Probably damaging (0.985)	Tolerated (0.27)	No data/no data/no data	1
NM_001385.2:c.1001A>G NP_001376.1:p.Gln334Arg	rs121964923	Probably damaging (1)	Damaging (0)	0.41/0.06516/0.004597	.087
NM_001385.2:c.1253C>T NP_001376.1:p.Thr418Ile	No number	Probably damaging (1)	Damaging (0)	0.01/no data/no data	1
NM_001385.2:c.1469G>A NP_001376.1:p.Arg490His	rs189448963	Probably damaging (1)	Damaging (0)	0.06/0.01504/0.02369	1
UPB1					
NM_016327.2:c.91G>A NP_057411.1:p.Gly31Ser	rs200145797	Probably damaging (1)	Damaging (0)	0.12/0.4612/0.03339	1
NM_016327.2:c.977G>A NP_057411.1:p.Arg326Gln	rs118163237	Probably damaging (1)	Tolerated (0.29)	0.85/2.611/0.192	.671

A recent study has reported the functional characterization of 21 allelic variants of *DPYD* identified in 1070 Japanese individuals.[14] Five of the variants (p.Val335Met, p.Ile543Val, p.Val732Ile, p.Thr768Lys, p.Asn893Ser) identified in our present analysis were among those described in that earlier study. Among these 5 variants, the activity of the p.Val335Met and p.Thr768Lys mutant DPDs exhibited significantly lower intrinsic clearance (*CLint* = *Vmax*/*Km*) values compared to the wild-type enzyme (47.4% and 47.9% respectively). However, our present analysis did not find an association between any of these previously reported *DPYD* single variants and severe FP-related toxicity. This may be due to the small number of subjects we analyzed and a further investigation with an increased number of patients is thus warranted to further clarify this issue.

DHP is the second enzyme in the catabolic pathway of uracil and thymine. There are some reports of variants in *DPYS* that may explain the occurrence of severe toxicity from FP-based chemotherapy. For example, c.−1T>C is a common noncoding variant in this gene reported to have an impact on toxicity in patients receiving FP.[24] Our current results have also revealed a high allele frequency of 68% for c.−1T>C, but did not demonstrate a clear relationship between FP-related high toxicity and this variant. With regard to *DPYS* gene coding regions, a prior study has described a patient with severe adverse events from FP therapy harboring the *DPYS* compound heterozygous missense and nonsense variants p.Gly334Arg and p.Arg465Ter.[7] The p.Gln334Arg variant had been previously identified in Japanese patients with DHP deficiency and functional analysis revealed that the corresponding mutant enzyme had only 2.5% residual activity.[17] Until now, it was unknown whether a heterozygous p.Gly334Arg patient would be at a high risk for severe FP-related toxicity, but our current findings have suggested that this might be a possibility. Because the frequency of the p.Gly334Arg is higher in Japanese people than in other ethnic groups (0.41% vs 0.004597% Jmorp, genomeAD), genetic analysis of the *DPYS* gene is important, at least in Japanese patients. Conversely, our present data have indicated that no patients who are heterozygous for *DPYS* p.Arg181Trp developed a severe adverse event following FP treatment. The kinetic parameters of the corresponding mutant enzyme were assessed in a previous report and no markedly reduced activity relative to wild-type DHP was evident.[25] This variant may have protective effects against the development of FP-related toxicity in vivo, but the mechanism is unknown.

The contribution of the some *UPB1* gene alterations to the development of FP-related toxicity was also analyzed previously in White patients with cancer.[1] There have been few reports to date however on coding region variants in this gene. In our previous study, we revealed that the *UPB1* pathogenic variant c.977G>A p.Arg326Gln was prevalent in the Japanese population at a rate of 1.8% but was not found in more than 8000 European and more than 4000 African American alleles.[26] However, the association of this variant with FP-related toxicity is unknown. Our current results found no clear association between this *UPB1* variant and FP-related toxicity, suggesting that a standard regimen with this chemotherapeutic would be tolerated by heterozygous carriers of this pathogenic variant.

Rare *DPYD* variants that cause loss of function in silico and a *DPYS* pathogenic variant p.Gly334Arg may be associated with severe FP-related toxicity in Japanese patients with cancer. However, the common *UPB1* pathogenic variant p.Arg326Gln in the Japanese population does not show a clear association with toxicity in heterozygous individuals.

TABLE 4 Frequency of *DPYS* p.Arg181Trp, *DPYS* p.Gln334Arg and rare pathogenic *DPYD* variants found in the high-toxicity and low-toxicity groups

Genotype	Low toxicity (grade 0-2)	High toxicity (grade 3-4)	Total
DPYS c.541C>T (p.Arg181Trp)			
TT	0	0	0
CT	14	0	14
CC	232	55	287
Total	246	55	301
P-value = .0813			
DPYS c.1001A>G (p.Gln334Arg)			
GG	0	0	0
AG	1	2	3
AA	245	53	298
Total	246	55	301
P-value = .087			
Frequency of patients who had a rare and pathogenic variant of DPYD			
Hetero	2	5	7
Reference	244	50	294
Total	246	55	301
P-value = .0271			

TABLE 5 Clinical and genetic information for 2 heterozygous *DPYS* p.Gln334Arg patients with high toxicity

Patient no.	Age	Sex	Cancer	Regimen	Side effects	Other DPYD variants	Other DPYS variants	Other UPB1 variants
Patient 1	68	Female	Colorectal	5FU + L-OHP	Vomiting Grade 1 Neutropenia Grade 3	p.Ile543Val het p.Arg29Cys hom	c.-1T>C hom	No variant
Patient 2	81	Female	Colorectal	5FU + L-OHP	Nausea Grade 2 Neutropenia Grade 3	p.Arg29Cys het	c.-1T>C hom	No variant

TABLE 6 Detailed information on the 7 patients in the rare pathogenic *DPYD* variant group

Rare pathogenic variant	Age	Sex	Cancer	Regimen	Side effects	Other DPYD variants	Other DPYS variants	Other UPB1 variants
c.596G>A (p.Ser199Asn)	67	Female	Colorectal	5FU + L-OHP	Vomiting Grade 3 Diarrhea Grade 3 Neutropenia Grade 3	p.Ile543Val hom p.Arg29Cys hom	c.-1T>C het	No variant
c.733A>T (p.Ile245Phe)	63	Female	Stomach	5FU + L-OHP	Nausea Grade 2 Vomiting Grade 2 Diarrhea Grade 3	p.Ile543Val het p.Met166Val het p.Arg29Cys hom	c.-1T>C hom	No variant
c.914C>A (p.Thr305Lys)	66	Female	Colorectal	5FU + L-OHP	Diarrhea Grade 1 Oral Mucositis Grade 1 Hand-foot syndrome Grade 1 Neutropenia Grade 2	p.Arg29Cys hom	c.-1T>C het	No variant
c.1156G>T (p.Glu386Ter)	48	Male	Colorectal	FOLFOXIRI + α	Nausea Grade 1 Neutropenia Grade 3	p.Arg29Cys hom	c.-1T>C hom	No variant
c.1666A>C (p.Ser556Arg)	25	Male	Colorectal	5FU + L-OHP	Nausea Grade 1 Vomiting Grade 1 Oral Mucositis Grade 1 Neutropenia Grade 1	p.Arg29Cys hom	c.-1T>C hom	No variant
c.1712C>A (p.Ala571Asp)	70	Female	Colorectal	5FU mono	Nausea Grade 3 Diarrhea Grade 3 Neutropenia Grade 1	p.Arg29Cys het	c.-1T>C hom	No variant
c.1863G>T (p.Trp621Cys)	72	Female	Colorectal	5FU + L-OHP	Nausea Grade 1 Neutropenia Grade 3	p.Ile543Val het p.Arg29Cys hom p.Thr768Lys het	c.-1T>C hom	No variant

ACKNOWLEDGMENTS

The authors thank all of the participating patients, and the investigators, co-investigators, and study teams at Fujita Health University.

CONFLICT OF INTEREST

The authors have no conflict of interest.

ETHICAL APPROVAL

We obtained approval for this study from the Ethical Review Board for Human Genome Studies at Fujita Health University. Written informed consent was obtained from all patients. All experiments were carried out in accordance with the relevant guidelines and regulations.

ORCID

Katsuyuki Yokoi https://orcid.org/0000-0002-4760-0420

REFERENCES

1. Fidlerova J, Kleiblova P, Kormunda S, Novotny J, Kleibl Z. Contribution of the β-ureidopropionase (UPB1) gene alterations to the development of fluoropyrimidine-related toxicity. *Pharmacol Rep*. 2012;64(5):1234-1242.
2. Jennings BA, Loke YK, Skinner J, et al. Evaluating predictive pharmacogenetic signatures of adverse events in colorectal cancer patients treated with fluoropyrimidines. *PLoS One*. 2013;8(10):e78053.
3. Longley DB, Harkin DP, Johnston PG. 5-fluorouracil: mechanisms of action and clinical strategies. *Nat Rev Cancer*. 2003;3(5):330-338.
4. Kuilenburg ABPV, Meijer J, Tanck MWT, et al. Phenotypic and clinical implications of variants in the dihydropyrimidine dehydrogenase gene. *Biochim Biophys Acta*. 2016;1862(4):754-762.
5. Lunenburg CATC, Henricks LM, Guchelaar HJ, et al. Prospective DPYD genotyping to reduce the risk of fluoropyrimidine-induced severe toxicity: Ready for prime time. *Eur J Cancer*. 2016;54:40-48.
6. Wigle TJ, Tsvetkova EV, Welch SA, Kim RB. DPYD and fluorouracil-based chemotherapy: mini review and case report. *Pharmaceutics*. 2019;11(5):199.
7. Hiratsuka M, Yamashita H, Akai F, et al. Genetic polymorphisms of dihydropyrimidinase in a Japanese patient with capecitabine-induced toxicity. *PLoS One*. 2015;10(4):e0124818.
8. Loganayagam A, Arenas Hernandez M, Corrigan A, et al. Pharmacogenetic variants in the DPYD, TYMS, CDA and MTHFR genes are clinically significant predictors of fluoropyrimidine toxicity. *Br J Cancer*. 2013;108(12):2505-2515.
9. van Kuilenburg AB, Meinsma R, Zonnenberg BA, et al. Dihydropyrimidinase deficiency and severe 5-fluorouracil toxicity. *Clin Cancer Res*. 2003;9(12):4363-4367.
10. Henricks LM, Lunenburg CATC, de Man FM, et al. DPYD genotype-guided dose individualisation of fluoropyrimidine therapy in patients with cancer: a prospective safety analysis. *Lancet Oncol*. 2018;19(11):1459-1467.
11. Lu ZH, Zhang R, Diasio RB. Purification and characterization of dihydropyrimidine dehydrogenase from human liver. *J Biol Chem*. 1992;267(24):17102-17109.
12. Meulendijks D, Henricks LM, Sonke GS, et al. Clinical relevance of DPYD variants c.1679T>G, c.1236G>A/HapB3, and c.1601G>A as predictors of severe fluoropyrimidine-associated toxicity: a systematic review and meta-analysis of individual patient data. *Lancet Oncol*. 2015;16(16):1639-1650.
13. van Kuilenburg AB, Meijer J, Maurer D, et al. Severe fluoropyrimidine toxicity due to novel and rare DPYD missense

mutations, deletion and genomic amplification affecting DPD activity and mRNA splicing. *Biochim Biophys Acta Mol Basis Dis*. 2017;1863(3):721-730.
14. Hishinuma E, Narita Y, Saito S, et al. Functional Characterization of 21 Allelic Variants of Dihydropyrimidine Dehydrogenase Identified in 1070 Japanese Individuals. *Drug Metab Dispos*. 2018;46(8):1083-1090.
15. Nagasaki M, Yasuda J, Katsuoka F, et al. Rare variant discovery by deep whole-genome sequencing of 1,070 Japanese individuals. *Nat Commun*. 2015;21(6):8018.
16. Kummer D, Froehlich TK, Joerger M, et al. Dihydropyrimidinase and β-ureidopropionase gene variation and severe fluoropyrimidine-related toxicity. *Pharmacogenomics*. 2015;16(12):1367-1377.
17. Hamajima N, Kouwaki M, Vreken P, et al. Dihydropyrimidinase deficiency: structural organization, chromosomal localization, and mutation analysis of the human dihydropyrimidinase gene. *Am J Hum Genet*. 1998;63(3):717-726.
18. Vreken P, van Kuilenburg AB, Hamajima N, et al. cDNA cloning, genomic structure and chromosomal localization of the human BUP-1 gene encoding beta-ureidopropionase. *Biochim Biophys Acta*. 1999;1447(2-3):251-257.
19. Kuhara T, Ohse M, Inoue Y, Shinka T. Five cases of beta-ureidopropionase deficiency detected by GC/MS analysis of urine metabolome. *J Mass Spectrom*. 2009;44(2):214-221.
20. Nakajima Y, Meijer J, Dobritzsch D, et al. Dihydropyrimidinase deficiency in four East Asian patients due to novel and rare DPYS mutations affecting protein structural integrity and catalytic activity. *Mol Genet Metab*. 2017;122(4):216-222.
21. Froehlich TK, Amstutz U, Aebi S, Joerger M, Largiadèr CR. Clinical importance of risk variants in the dihydropyrimidine dehydrogenase gene for the prediction of early-onset fluoropyrimidine toxicity. *Int J Cancer*. 2015;136(3):730-739.
22. Maekawa K, Saeki M, Saito Y, et al. Genetic variations and haplotype structures of the DPYD gene encoding dihydropyrimidine dehydrogenase in Japanese and their ethnic differences. *J Hum Genet*. 2007;52(10):804-819.
23. Thomas F, Hennebelle I, Delmas C, et al. Genotyping of a family with a novel deleterious DPYD mutation supports the pretherapeutic screening of DPD deficiency with dihydrouracil/uracil ratio. *Clin Pharmacol Ther*. 2016;99(2):235-242.
24. Fidlerova J, Kleiblova P, Bilek M, et al. Contribution of dihydropyrimidinase gene alterations to the development of serious toxicity in fluoropyrimidine-treated cancer patients. *Cancer Chemother Pharmacol*. 2010;65(4):661-669.
25. Hishinuma E, Akai F, Narita Y, et al. Functional characterization of 21 allelic variants of dihydropyrimidinase. *Biochem Pharmacol*. 2017;1(143):118-128.
26. Nakajima Y, Meijer J, Dobritzsch D, et al. biochemical and molecular analysis of 13 Japanese patients with β-ureidopropionase deficiency demonstrates high prevalence of the c.977G>A (p. R326Q) mutation. *J Inherit Metab Dis*. 2014;37(5):801-812.

SUPPORTING INFORMATION

Additional supporting information may be found online in the Supporting Information section.

How to cite this article: Yokoi K, Nakajima Y, Matsuoka H, et al. Impact of *DPYD*, *DPYS*, and *UPB1* gene variations on severe drug-related toxicity in patients with cancer. *Cancer Sci*. 2020;111:3359–3366. https://doi.org/10.1111/cas.14553

The Journal of Infectious Diseases

MAJOR ARTICLE

Inherited Chromosomally Integrated Human Herpesvirus 6 Is a Risk Factor for Spontaneous Abortion

Hiroki Miura,[1] Yoshiki Kawamura,[1] Tamae Ohye,[2] Fumihiko Hattori,[1] Kei Kozawa,[1] Masaru Ihira,[3] Hiroshi Yatsuya,[4] Haruki Nishizawa,[5] Hiroki Kurahashi,[6] and Tetsushi Yoshikawa[1]

[1]Department of Pediatrics, Fujita Health University School of Medicine, Toyoake, Japan, [2]Department of Clinical Laboratory Medicine, Graduate School of Health Sciences, Fujita Health University, Toyoake, Japan, [3]Faculty of Clinical Engineering, Fujita Health University School of Health Sciences, Toyoake, Japan, [4]Department of Public Health, Fujita Health University School of Medicine, Toyoake, Japan, [5]Department of Obstetrics and Gynecology, Fujita Health University School of Medicine, Toyoake, Japan, and [6]Division of Molecular Genetics, Institute for Comprehensive Medical Science, Fujita Health University, Toyoake, Japan

Background. Human herpesvirus 6 (HHV-6) can be genetically transmitted from parent to child as inherited chromosomally integrated HHV-6 (iciHHV-6). HHV-6 reactivation occurs in pregnant women with iciHHV-6. We found no sex differences in the frequency of index cases with iciHHV-6 but inheritance from the father was more common. We evaluated the association between iciHHV-6 status and spontaneous abortion.

Methods. iciHHV-6 was confirmed by high viral DNA copy numbers in whole blood and somatic cells. The origin of integrated viral genome, paternal or maternal, was examined using the same method. The pregnancy history of 23 mothers in families with iciHHV-6 and 285 mothers in families without iciHHV-6 was abstracted.

Results. Of 23 iciHHV-6 index cases, 8 mothers and 15 fathers had iciHHV-6. Spontaneous abortion rates in mothers with and mothers without/fathers with iciHHV-6 and mothers in families without iciHHV-6 were 27.6%, 10.3%, and 14.8%, respectively ($P = .012$). Mothers with iciHHV-6 (odds ratio [OR], 6.41; 95% confidence interval [CI], 1.10–37.4) and maternal age at the most recent pregnancy ≥40 years (OR, 3.91; 95% CI, 1.30–11.8) were associated with 2 or more spontaneous abortions.

Conclusions. Mothers with iciHHV-6 is a risk factor for spontaneous abortion.

Keywords. iciHHV-6; spontaneous abortion; pregnancy.

Human herpesvirus 6 (HHV-6) was the sixth human herpesvirus discovered. It belongs to the β-Herpesvirinae subfamily. This virus is categorized into 2 distinct species (HHV-6A and HHV-6B) with 90% overall nucleotide sequence identity [1, 2]. Primary HHV-6B infection generally occurs in infancy and causes exanthema subitum, a common febrile exanthematous disease [3, 4]. In contrast to HHV-6B, the clinical features of primary HHV-6A infection remain unclear. Although HHV-6B is a ubiquitous virus throughout the world, HHV-6A infection is considered to be endemic only in a limited geographical area [5].

Although horizontal transmission is considered to be the main route of HHV-6 infection, it can be genetically transmitted from parent to child as inherited chromosomally integrated HHV-6 (iciHHV-6) [6, 7]. The complete HHV-6 genome is integrated into every nucleated cell of an individual with iciHHV-6. Extremely high copy numbers of HHV-6 DNA can be detected in clinical specimens containing nucleated cells, which can lead to a misdiagnosis of active viral infection [8]. The frequency of iciHHV-6 in the general population is approximately 0.8%–1.5% in the United Kingdom [9, 10] compared with 0.2%–0.6% in Japan [6, 7]. This low frequency has hampered the elucidation of the link between iciHHV-6 and disease.

Previous studies have suggested that iciHHV-6 is associated with clinical manifestations such as encephalitis [11, 12], cognitive dysfunction, fatigue [13, 14], and angina pectoris [15]. However, the precise relationship between iciHHV-6 and these conditions remains under investigation. In addition, viral reactivation from the integrated viral genome has been demonstrated in an immunocompromised patient with iciHHV-6 [16] and pregnant women with iciHHV-6 [17, 18]. Moreover, viral reactivation can be induced in iciHHV-6 cells by some chemical compound treatments [19]. These findings suggest that iciHHV-6 may cause physiological changes in the host through viral reactivation from the integrated viral genome. For example, hematopoietic stem cell transplant recipients with iciHHV-6 have been shown to have an increased frequency of acute graft-versus-host disease [20].

Theoretically, a parent with iciHHV-6 has a 50% chance of transmitting the integrated HHV-6 genome to the next generation. Our previous study demonstrated no sex difference among index cases with iciHHV-6. However, when we examined the

Received 6 August 2020; editorial decision 17 September 2020; accepted 25 September 2020; published online September 28, 2020.

Correspondence: Hiroki Miura, MD, PhD, Department of Pediatrics, Fujita Health University School of Medicine, 1–98 Dengakugakubo, Kutsukake-cho, Toyoake, Aichi, Japan (hiroki-m@fujita-hu.ac.jp).

The Journal of Infectious Diseases® 2020;XX:1–7

DOI: 10.1093/infdis/jiaa606

origin of the viral genome, we noticed that there are many cases of paternal origin [21]. Therefore, to determine if paternal origin is more common than maternal origin and to evaluate the association between iciHHV-6 and spontaneous abortion, we sought to examine the origin of the HHV-6 genome and pregnancy history of mothers in families with iciHHV-6.

METHODS

Subjects and Samples

Individuals with iciHHV-6 with a confirmed origin of the viral genome were enrolled in this study. Index cases were diagnosed with iciHHV-6 based on the following procedures. Screening for HHV-6 was performed using peripheral whole blood or serum obtained from patients with febrile illness enrolled in another clinical study at Fujita Health University (ethics committee accession number 14-096). In addition, harvested cord blood from healthy neonates born at Fujita Health University Hospital underwent HHV-6 screening. Furthermore, whole blood or serum samples obtained from patients with suspected iciHHV-6 at other hospitals were also analyzed.

Screening and Criteria for iciHHV-6

To screen for HHV-6 infection, DNA was extracted from 200 µL of whole blood or serum samples using the QIAamp DNA Blood Mini kit (QIAGEN). DNA samples were stored at −30°C until polymerase chain reaction (PCR) analysis. HHV-6 DNA loads were measured in these samples using real-time PCR [22]. If a high copy number of HHV-6 DNA (whole blood, $>5.5 \times 10^5$ copies/mL; serum, $>1.0 \times 10^5$ copies/mL) was detected, the subject was suspected of having iciHHV-6. HHV-6 species were determined by restriction fragment length polymorphism (RFLP) analysis of loop-mediated isothermal amplification products as previously described [23].

If a subject was suspected of having iciHHV-6, additional whole blood, hair follicle, or buccal mucosa swab samples were collected for further investigation. Whole blood, hair follicle, or buccal mucosa swab samples were used to measure HHV-6 DNA load with real-time PCR analysis. Whole blood samples were used for fluorescent in situ hybridization (FISH) assays to identify the integration site. A subject was defined as having iciHHV-6 if either of the following 2 criteria was fulfilled: (1) detection of more than 5.5×10^5 copies/mL of HHV-6 DNA in whole blood and HHV-6 DNA in somatic cells (hair follicle or buccal mucosa swab samples) or (2) confirmation of HHV-6 DNA integration in a chromosome by FISH.

To determine the origin of the endogenous HHV-6 genome, whole blood, hair follicle, or buccal mucosa swab samples were collected from the parents of the index cases. The samples were used to measure HHV-6 DNA load and for FISH analysis. The origin of iciHHV-6 was confirmed using the criteria described above.

FISH Analysis for Integration Site Determination

To identify the site of chromosomal integration, 5 mL of heparinized peripheral blood was collected from subjects with iciHHV-6 to perform FISH analysis as previously described [24]. Briefly, phytohemagglutinin-stimulated lymphocytes or Epstein-Barr virus-transformed lymphoblasts were arrested by treatment with colcemid. Metaphase preparations were obtained via hypotonic treatment with 0.075 M KCl followed by methanol and acetate fixation. PCR products from HHV-6 sequences were used as probes for FISH, which were labelled by nick translation with biotin-16-dUTP or digoxigenin-11-dUTP. After hybridization, the probes were detected using either Alexa Fluor 488-conjugated streptavidin or rhodamine-conjugated antidigoxigenin and visualized through counter-staining with 4′,6-diamino-2-phenylindole. Chromosome-specific probes were used as reference standards.

Pregnancy History of Mothers in Families with iciHHV-6

Pregnancy history was obtained from mothers in families with icHHV-6 and 285 women in families without iciHHV-6 as a control group for comparison of the incidence of spontaneous abortion. Control subjects had given birth at Fujita Health University Hospital between December 2017 and March 2019. Pregnancy histories of cases and controls who could be reviewed from medical records were abstracted and those of the others were elicited by telephone interview. These reviews and interviews were performed by a person blinded to the subjects' iciHHV-6 status. All cord blood samples obtained from control subjects did not contain HHV-6 DNA.

Statistical Analysis

The sex of iciHHV-6 index cases and the maternal/paternal origin were compared using the binomial test for differences in proportion. The number of spontaneous abortions per mother and maternal age at the most recent pregnancy in the iciHHV-6 versus non–iciHHV-6 groups were evaluated using the Kruskal-Wallis test. The proportion of mothers having 2 or more spontaneous abortions in the 2 groups was evaluated using Fisher exact test. Univariable associations between potential factors described below and history of spontaneous abortion were evaluated using Fisher exact test. We analyzed the association between 2 or more spontaneous abortion and the following factors: iciHHV-6 family, iciHHV-6 species, iciHHV-6 integration site, mother with iciHHV-6, and maternal age at the most recent pregnancy. Variables that were statistically significantly associated with spontaneous abortion in univariable analyses were included in multivariable logistic regression analyses. Statistical significance was defined as a 2-sided $P < .05$. JMP version 13.1 (SAS Institute) was used for analyses.

Ethics Approval

This study was approved by the Ethics Review Board for Human Genome Studies at Fujita Health University (accession number HG19-006), 12 June 2019. If the subjects had suspected iciHHV-6 based on HHV-6 DNA loads in blood samples, written informed consent was obtained from subjects or their guardians to carry out examinations for definitive diagnosis of iciHHV-6 and collection of clinical information.

RESULTS

Characteristics of Index Cases With iciHHV-6

Twenty-three iciHHV-6 index cases were enrolled in this study. Sex, iciHHV-6 origin, iciHHV-6 integration site, iciHHV-6 species, and maternal pregnancy history are summarized in Table 1. No sex difference was observed among index cases ($P = .84$) but paternal origin accounted for 68% of iciHHV-6 cases ($P = .088$). The site of integration was determined in 21 of 23 subjects with iciHHV-6 using FISH analysis. One copy of the HHV-6 genome was integrated in 20 of 21 cases (22q, 11 cases; Xp, 2 cases; Yp, 2 cases; 1q, 2 cases; 16q, 1 case; 17p, 1 case; and 20p, 1 case). Two copies of the HHV-6 genome were integrated in patient 8; 1 copy was derived from each parent. The copy integrated on chromosome 20p was of paternal origin whereas the copy integrated on chromosome 22q was of maternal origin. RFLP analysis indicated that 11 (48%) of the 23 iciHHV-6 cases were HHV-6A and 12 (52%) were HHV-6B.

Regarding the birth history of the 8 index cases whose mothers had iciHHV-6, 1 was preterm, 1 had low birth weight, and 1 was preterm and had low birth weight. The remaining 5 index cases had no abnormalities at the time of birth. In the 15 index cases whose mothers did not have iciHHV-6, 1 was preterm and had low birth weight and another was born through emergency cesarean delivery because of reduced baseline variability. The remaining 13 index cases had no abnormalities.

Maternal Pregnancy History by iciHHV-6 Status

In 23 families with iciHHV-6, 8 mothers with iciHHV-6 (patients 1 to 8) had 8 spontaneous abortions in 29 pregnancies whereas 15 mothers without/fathers with iciHHV-6 (patients 9 to 23) had 3 spontaneous abortions in 29 pregnancies (Table 1). In the control group, 285 mothers in families without iciHHV-6 had 87 spontaneous abortions in 589 pregnancies. The spontaneous abortion rate and numbers of mothers having 2 or more spontaneous abortions were compared among 3 groups (mothers with iciHHV-6, mothers without/fathers with iciHHV-6, and control mothers in families without iciHHV-6) (Table 2). Spontaneous abortion rates among mothers with iciHHV-6, mothers without/fathers with iciHHV-6 and control

Table 1. Characteristics of Index Cases With iciHHV-6 and Maternal Pregnancy History

					Maternal Pregnancy History		
Patient	Sex	Origin[a]	Integration Site	iciHHV6 Species	No. of Pregnancies	No. of Spontaneous Abortions	Maternal Age at Most Recent Pregnancy, y
1	M	Maternal	22q	HHV-6A	5	2	NA
2	F	Maternal	22q	HHV-6A	3	1	35
3	F	Maternal	22q	HHV-6A	4	1	25
4	F	Maternal	22q	HHV-6A	2	0	34
5	M	Maternal	22q	HHV-6A	2	0	33
6	M	Maternal	16p	HHV-6B	2	0	32
7	M	Maternal	20p	HHV-6B	6	2	40
8	F	Paternal and maternal	20p and 22q	HHV-6B	5	2	32
9	F	Paternal	22q	HHV-6A	3	0	34
10	F	Paternal	22q	HHV-6A	1	0	25
11	F	Paternal	22q	HHV-6A	2	0	25
12	M	Paternal	22q	HHV-6A	2	0	NA
13	M	Paternal	22q	HHV-6B	2	1	30
14	F	Paternal	22q	HHV-6B	1	0	NA
15	F	Paternal	Xp	HHV-6B	2	0	27
16	M	Paternal	Xp	HHV-6B	2	0	NA
17	M	Paternal	Yp	HHV-6B	4	1	34
18	M	Paternal	Yp	HHV-6B	2	0	39
19	F	Paternal	1q	HHV-6B	2	1	26
20	M	Paternal	1q	HHV-6B	2	0	NA
21	M	Paternal	17p	HHV-6A	1	0	30
22	M	Paternal	ND	HHV-6A	1	0	36
23	M	Paternal	ND	HHV-6B	2	0	32

Abbreviations: [a]Paternal or maternal origin of chromosomally integrated HHV-6.

Table 2. Prevalence of Spontaneous Abortion by iciHHV-6 Status

Status	Spontaneous Abortion Rate, %	No. of Mothers With 2 or More Spontaneous Abortions, n (%)	Maternal Age at Most Recent Pregnancy, y, Median (IQR)
Mother with iciHHV-6 (n = 8)	27.6	3 (37.5)	33.0 (28.0–36.0)
Mother without/father with iciHHV-6 (n = 15)	10.3	0 (.0)	30.0 (26.5–34.0)
Mother in family without iciHHV-6 (n = 285)	14.8	18 (6.3)	33.0 (32.0–34.5)
P value	**.012**	**.002**	.46

Bold values are statistically significant.

Abbreviations: iciHHV-6, inherited chromosomally integrated human herpesvirus 6; IQR, interquartile range.

mothers in families without iciHHV-6 were 27.6% (8/29), 10.3% (3/29), and 14.8% (87/589), respectively ($P = .012$). Because recurrent pregnancy loss is defined as 2 or more spontaneous abortions, the number of mothers with a history of 2 or more abortions was compared among the 3 groups. Of 8 mothers with iciHHV-6, 3 (37.5%) had repeated spontaneous abortions. None (0%) of the mothers without/fathers with iciHHV-6 had repeated spontaneous abortions and 18 of 285 (6.3%) mothers in the control group had repeated spontaneous abortions. There was a statistically significant difference among the 3 groups ($P = .002$). Maternal age at the most recent pregnancy was not significantly different among the 3 groups ($P = .46$).

Risk Factors for Spontaneous Abortion

To elucidate potential risk factors for 2 or more spontaneous abortions, we examined characteristics associated with iciHHV-6 status and maternal age at the most recent pregnancy (Table 3). Univariable analyses indicated that iciHHV-6 family status did not affect the risk of spontaneous abortion ($P = .20$), but mother with iciHHV-6 and maternal age at the most recent pregnancy of 40 years or older were associated with 2 or more spontaneous abortions ($P = .012$ and $P = .021$, respectively). Among 23 families with iciHHV-6, there was no correlation between spontaneous abortion and HHV-6 species ($P = 1.00$) and HHV-6 integration site ($P = 1.00$). Multivariable analyses revealed that mother with iciHHV-6 (odds ratio [OR], 6.41; 95% confidence interval [CI], 1.10–37.4; $P = .001$) and maternal age at the most recent pregnancy of 40 years or older (OR, 3.91; 95% CI, 1.30–11.8; $P = .016$) were significantly associated with 2 or more spontaneous abortions (Table 3).

DISCUSSION

Similar to our previous study [7], there was no sex difference in index cases with iciHHV-6, but iciHHV-6 of maternal origin was lower than expected (32% instead of 50%) in this study. In contrast to our studies, Hall et al [25] (who first demonstrated that HHV-6 can be genetically transmitted from parent to child) reported that 60% (18/30) of children with iciHHV-6 inherited it from their mother. An insufficient number of cases may be the main reason for this

Table 3. Risk Factors for 2 or More Spontaneous Abortions

	Univariable		Multivariable	
Risk Factor	Odds Ratio (95% CI)	*P* Value	Odds Ratio (95% CI)	*P* Value
iciHHV-6 family				
No (n = 285)	Ref			
Yes (n = 23)	2.23 (.60–8.20)	.20		
iciHHV-6 species				
iciHHV-6A (n = 11)	Ref			
iciHHV-6B (n = 12)	2.00 (.16–25.8)	1.00		
iciHHV-6 integration site				
Other (n = 9)	Ref			
22q (n = 12)	2.00 (.16–25.8)	1.00		
Mother with iciHHV-6				
No (n = 300)	Ref		Ref	
Yes (n = 8)	9.40 (2.08–42.5)	**.012**	6.41 (1.10–37.4)	**.040**
Maternal age at most recent pregnancy, y				
<35 (n = 194)	Ref		Ref	
35–39 (n = 74)	1.05 (.32–3.46)	1.00	1.11 (.33–3.68)	.87
≥40 (n = 35)	3.81 (1.29–11.3)	**.021**	3.91 (1.30–11.8)	**.016**

Bold values are statistically significant.

Abbreviations: CI, confidence interval; iciHHV-6, inherited chromosomally integrated human herpesvirus 6; Ref, reference.

discrepancy, but the exact reason is unknown. Common viral genome integration sites are different between Japan and Western countries; 22q is the most common site in Japan and 17p is the most common site in Western countries [7, 26]. Nine of 10 index case of iciHHV-6A had the 22q integration site in this study. This pattern has been found in the majority of Japanese cases and our previous study suggested that iciHH-6A in 22q likely derived from a common ancestor [27]. Furthermore, genetic diversity of the viral genome in each region has been demonstrated by phylogenetic tree analysis of integrated viral genomes from different regions [28]. Thus, it is possible that differences in chromosome of integration and genetic diversity of the integrated viral genome may be associated with different patterns of inheritance between Japanese and the Western populations.

Spontaneous abortion rates in mothers without/fathers with iciHHV-6 and mothers in families without iciHHV-6 were 10.3% and 14.8%, respectively, which is consistent with findings from previous studies [29, 30]. The spontaneous abortion rate and number of mothers with repeated spontaneous abortions were significantly higher in mothers with iciHHV-6 than in the other 2 groups ($P = .012$ and $P = .002$). In addition, univariable analyses showed that iciHHV-6 family status, integration in chromosome 22q, and HHV-6 species did not increase the risk of spontaneous abortion, but maternal age at the most recent pregnancy of 40 years or older and mother with iciHHV-6 were the only risk factors for 2 or more spontaneous abortions identified by multivariable analyses. Because older maternal age is an expected risk factor for spontaneous abortion [31], the reliability of this study is considered to be high. Furthermore, it is well known that older maternal age, genetic abnormalities, selected maternal autoantibodies, endocrine dysfunction, and uterine abnormalities are risk factors for spontaneous abortion [32]. However, the cause of approximately 50% of recurrent spontaneous abortions is unknown. Therefore, the present findings may help explain the cause of some unexplained recurrent pregnancy loss.

It is necessary to elucidate mechanisms by which iciHHV-6 increases the risk of spontaneous abortion. This study suggests that mother with iciHHV-6 can be a risk factor for spontaneous abortion but fetal iciHHV-6 is not, because in families with iciHHV-6, father with iciHHV-6 was not a risk factor. Thus, maternal factors may play an important role in iciHHV-6–related spontaneous abortion. Results of previous studies on the association between maternal HHV-6 infection and spontaneous abortion may be helpful for future research. It has been suggested that active HHV-6 infection during pregnancy may cause spontaneous abortion [33, 34] as well as premature delivery with neonatal hypotonia [35]. Furthermore, a series of Italian studies has demonstrated that some infertile women have HHV-6A infection in endometrial epithelial cells accompanied by alterations in the maternal immune system [36–38]. Their in vitro study demonstrated that endometrial cells infected with HHV-6A are less permissive to the attachment of trophoblast cells and microRNA expression patterns of endometrial cells were altered by HHV-6A infection [39].

As described above, HHV-6 reactivation from integrated viral genomes has been demonstrated in both in vivo and in vitro studies [16–19]. Recently, HHV-6 transcripts have been detected in placentas of pregnant women with iciHHV-6 and preeclampsia, and the risk of preeclampsia was significantly higher in mothers with iciHHV-6 than control mothers [40]. Detection of HHV-6 mRNA in placentas with iciHHV-6 suggests viral reactivation in placental tissue. Taken together with the results of this study, HHV-6 reactivation in pregnant women with iciHHV-6 may cause spontaneous abortion or preeclampsia. There are 2 possible mechanisms by which reactivation of HHV-6 from an integrated viral genome can affect the host cells: direct cellular damage induced by viral infection and bystander effects induced by viral reactivation. Recent studies have suggested that iciHHV-6 can exacerbate acute graft-versus-host disease via upregulation of inflammatory cytokines [41]. Furthermore, Kumata et al reported that host transcripts in the certain tissues are modified by iciHHV-6 [42]. Although a prospective study might be difficult because of the limited number of cases, a study following pregnant women with iciHHV-6 is necessary to explore the mechanisms underlying iciHHV-6–related spontaneous abortion. In addition, although no notable clinical manifestations were observed in neonates with iciHHV-6 delivered from mothers with iciHHV-6 in this study, more neonates with iciHHV-6 should be examined and followed for longer periods to understand the effects of iciHHV-6 during the embryonic period.

In conclusion, although there was no sex difference among iciHHV-6 index cases, the frequency of iciHHV-6 inherited from the mother was lower than expected in this study. In addition to maternal age at the most recent pregnancy of 40 years or older, mother with iciHHV-6 was a risk factor for 2 or more spontaneous abortions. Therefore, careful management may be required for pregnant women with iciHHV-6, who may be predisposed to spontaneous abortion.

Notes

Acknowledgments. The authors gratefully acknowledge the technical support of Akiko Yoshikawa, Chieko Mori, and Yoko Osakabe, and helpful suggestions from Dr Benedikt B. Kaufer and Dr Nicholas F. Parrish.

Financial support. This work was supported by the Japanese Society for the Promotion of Science KAKENHI (grant number JP 19K17346).

Potential conflicts of interest. All authors: No reported conflicts. All authors have submitted the ICMJE Form for Disclosure of Potential Conflicts of Interest. Conflicts that the

editors consider relevant to the content of the manuscript have been disclosed.

References

1. Dominguez G, Dambaugh TR, Stamey FR, Dewhurst S, Inoue N, Pellett PE. Human herpesvirus 6B genome sequence: coding content and comparison with human herpesvirus 6A. J Virol **1999**; 73:8040–52.
2. Isegawa Y, Mukai T, Nakano K, et al. Comparison of the complete DNA sequences of human herpesvirus 6 variants A and B. J Virol **1999**; 73:8053–63.
3. Yamanishi K, Okuno T, Shiraki K, et al. Identification of human herpesvirus-6 as a causal agent for exanthem subitum. Lancet **1988**; 1(8594):1065–7.
4. Asano Y, Suga S, Yoshikawa T, Urisu A, Yazaki T. Human herpesvirus type 6 infection (exanthem subitum) without fever. J Pediatr **1989**; 115:264–5.
5. Bates M, Monze M, Bima H, et al. Predominant human herpesvirus 6 variant A infant infections in an HIV-1 endemic region of Sub-Saharan Africa. J Med Virol **2009**; 81:779–89.
6. Tanaka-Taya K, Sashihara J, Kurahashi H, et al. Human herpesvirus 6 (HHV-6) is transmitted from parent to child in an integrated form and characterization of cases with chromosomally integrated HHV-6 DNA. J Med Virol **2004**; 73:465–73.
7. Miura H, Kawamura Y, Hattori F, et al. Chromosomally integrated human herpesvirus 6 in the Japanese population. J Med Virol **2018**; 90:1636–42.
8. Lee SO, Brown RA, Razonable RR. Chromosomally integrated human herpesvirus-6 in transplant recipients. Transpl Infect Dis **2012**; 14:346–54.
9. Leong HN, Tuke PW, Tedder RS, et al. The prevalence of chromosomally integrated human herpesvirus 6 genomes in the blood of UK blood donors. J Med Virol **2007**; 79:45–51.
10. Ward KN, Thiruchelvam AD, Couto-Parada X. Unexpected occasional persistence of high levels of HHV-6 DNA in sera: detection of variants A and B. J Med Virol **2005**; 76:563–70.
11. Troy SB, Blackburn BG, Yeom K, Caulfield AK, Bhangoo MS, Montoya JG. Severe encephalomyelitis in an immunocompetent adult with chromosomally integrated human herpesvirus 6 and clinical response to treatment with foscarnet plus ganciclovir. Clin Infect Dis **2008**; 47:e93–6.
12. Wittekindt B, Berger A, Porto L, et al. Human herpes virus-6 DNA in cerebrospinal fluid of children undergoing therapy for acute leukaemia. Br J Haematol **2009**; 145:542–5.
13. Montoya JG, Neely MN, Gupta S, et al. Antiviral therapy of two patients with chromosomally-integrated human herpesvirus-6A presenting with cognitive dysfunction. J Clin Virol **2012**; 55:40–5.
14. Pantry SN, Medveczky MM, Arbuckle JH, et al. Persistent human herpesvirus-6 infection in patients with an inherited form of the virus. J Med Virol **2013**; 85:1940–6.
15. Gravel A, Dubuc I, Morissette G, Sedlak RH, Jerome KR, Flamand L. Inherited chromosomally integrated human herpesvirus 6 as a predisposing risk factor for the development of angina pectoris. Proc Natl Acad Sci U S A **2015**; 112:8058–63.
16. Endo A, Watanabe K, Ohye T, et al. Molecular and virological evidence of viral activation from chromosomally integrated human herpesvirus 6A in a patient with X-linked severe combined immunodeficiency. Clin Infect Dis **2014**; 59:545–8.
17. Hall CB, Caserta MT, Schnabel KC, et al. Transplacental congenital human herpesvirus 6 infection caused by maternal chromosomally integrated virus. J Infect Dis **2010**; 201:505–7.
18. Gravel A, Hall CB, Flamand L. Sequence analysis of transplacentally acquired human herpesvirus 6 DNA is consistent with transmission of a chromosomally integrated reactivated virus. J Infect Dis **2013**; 207:1585–9.
19. Arbuckle JH, Medveczky MM, Luka J, et al. The latent human herpesvirus-6A genome specifically integrates in telomeres of human chromosomes in vivo and in vitro. Proc Natl Acad Sci U S A **2010**; 107:5563–8.
20. Hill JA, Magaret AS, Hall-Sedlak R, et al. Outcomes of hematopoietic cell transplantation using donors or recipients with inherited chromosomally integrated HHV-6. Blood **2017**; 130:1062–9.
21. Miura H, Kawamura Y, Kudo K, et al. Virological analysis of inherited chromosomally integrated human herpesvirus-6 in three hematopoietic stem cell transplant patients. Transpl Infect Dis **2015**; 17:728–31.
22. Tanaka N, Kimura H, Hoshino Y, et al. Monitoring four herpesviruses in unrelated cord blood transplantation. Bone Marrow Transplant **2000**; 26:1193–7.
23. Ihira M, Ohta A, Sugata K, Suga S, Asano Y, Yoshikawa T. Loop-mediated isothermal amplification for discriminating between human herpesvirus 6 A and B. J Virol Methods **2008**; 154:223–5.
24. Ohye T, Kawamura Y, Inagaki H, et al. A simple cytogenetic method to detect chromosomally integrated human herpesvirus-6. J Virol Methods **2016**; 228:74–8.
25. Hall CB, Caserta MT, Schnabel K, et al. Chromosomal integration of human herpesvirus 6 is the major mode of congenital human herpesvirus 6 infection. Pediatrics **2008**; 122:513–20.
26. Tweedy J, Spyrou MA, Pearson M, Lassner D, Kuhl U, Gompels UA. Complete genome sequence of germline chromosomally integrated human herpesvirus 6A and analyses integration sites define a new human endogenous virus with potential to reactivate as an emerging infection. Viruses **2016**; 8:19.

27. Kawamura Y, Ohye T, Miura H, et al. Analysis of the origin of inherited chromosomally integrated human herpesvirus 6 in the Japanese population. J Gen Virol **2017**; 98:1823–30.
28. Greninger AL, Knudsen GM, Roychoudhury P, et al. Comparative genomic, transcriptomic, and proteomic reannotation of human herpesvirus 6. BMC Genomics **2018**; 19:204.
29. Ammon Avalos L, Galindo C, Li DK. A systematic review to calculate background miscarriage rates using life table analysis. Birth Defects Res A Clin Mol Teratol **2012**; 94:417–23.
30. Wilcox AJ, Weinberg CR, O'Connor JF, et al. Incidence of early loss of pregnancy. N Engl J Med **1988**; 319:189–94.
31. Magnus MC, Wilcox AJ, Morken NH, Weinberg CR, Håberg SE. Role of maternal age and pregnancy history in risk of miscarriage: prospective register based study. BMJ **2019**; 364:l869.
32. El Hachem H, Crepaux V, May-Panloup P, Descamps P, Legendre G, Bouet PE. Recurrent pregnancy loss: current perspectives. Int J Womens Health **2017**; 9:331–45.
33. Ando Y, Kakimoto K, Ekuni Y, Ichijo M. HHV-6 infection during pregnancy and spontaneous abortion. Lancet **1992**; 340:1289.
34. Revest M, Minjolle S, Veyer D, Lagathu G, Michelet C, Colimon R. Detection of HHV-6 in over a thousand samples: new types of infection revealed by an analysis of positive results. J Clin Virol **2011**; 51:20–4.
35. Drago F, Broccolo F, Zaccaria E, et al. Pregnancy outcome in patients with pityriasis rosea. J Am Acad Dermatol **2008**; 58:S78–83.
36. Marci R, Gentili V, Bortolotti D, et al. Presence of HHV-6A in endometrial epithelial cells from women with primary unexplained infertility. PLoS One **2016**; 11:e0158304.
37. Bortolotti D, Gentili V, Rotola A, et al. HHV-6A infection of endometrial epithelial cells affects immune profile and trophoblast invasion. Am J Reprod Immunol **2019**; 82:e13174.
38. Caselli E, Bortolotti D, Marci R, et al. HHV-6A infection of endometrial epithelial cells induces increased endometrial NK cell-mediated cytotoxicity. Front Microbiol **2017**; 8:2525.
39. Bortolotti D, Soffritti I, D'Accolti M, et al. HHV-6A infection of endometrial epithelial cells affects miRNA expression and trophoblast cell attachment. Reprod Sci **2020**; 27:779–86.
40. Gaccioli F, Lager S, de Goffau MC, et al. Fetal inheritance of chromosomally integrated human herpesvirus 6 predisposes the mother to pre-eclampsia. Nat Microbiol **2020**; 5:901–8.
41. Weschke DP, Leisenring WM, Lawler RL, et al. Inflammatory cytokine profile in individuals with inherited chromosomally integrated human herpesvirus 6. Biol Blood Marrow Transplant **2020**; 26:254–61.
42. Kumata R, Ito J, Sato K. Inherited chromosomally integrated HHV-6 possibly modulates human gene expression. Virus Genes **2020**; 56:386–9.

Molecular Therapy
Methods & Clinical Development
Original Article

Unexpected Mutations by CRISPR-Cas9 CTG Repeat Excision in Myotonic Dystrophy and Use of CRISPR Interference as an Alternative Approach

Miki Ikeda,[1] Mariko Taniguchi-Ikeda,[2,3] Takema Kato,[3] Yasuko Shinkai,[3] Sonoko Tanaka,[1] Hiroki Hagiwara,[4] Naomichi Sasaki,[5] Toshihiro Masaki,[5] Kiichiro Matsumura,[1] Masahiro Sonoo,[1] Hiroki Kurahashi,[3] and Fumiaki Saito[1]

[1]Department of Neurology, School of Medicine, Teikyo University, Tokyo 1738606, Japan; [2]Department of Clinical Genetics, Fujita Health University Hospital, Aichi 4701192, Japan; [3]Division of Molecular Genetics, Institute for Comprehensive Medical Science, Fujita Health University, Aichi 4701192, Japan; [4]Department of Medical Science, Teikyo University of Science, Uenohara Campus, Yamanashi 4090193, Japan; [5]Department of Medical Science, Teikyo University of Science, Senju Campus, Tokyo 1200045, Japan

Myotonic dystrophy type 1 is the most common type of adult-onset muscular dystrophy. This is an autosomal dominant disorder and caused by the expansion of the CTG repeat in the 3′ untranslated region of the dystrophia myotonica protein kinase (*DMPK*) gene. Messenger RNAs containing these expanded repeats form aggregates as nuclear RNA foci. Then, RNA binding proteins, including muscleblind-like 1, are sequestered to the RNA foci, leading to systemic abnormal RNA splicing. In this study, we used CRISPR-Cas9 genome editing to excise this CTG repeat. Dual cleavage at the 5′ and 3′ regions of the repeat using a conventional Cas9 nuclease and a double nicking with Cas9 nickase successfully excised the CTG repeat. Subsequently, the formation of the RNA foci was markedly reduced in patient-derived fibroblasts. However, contrary to expectations, a considerable amount of off-target digestions and on-target genomic rearrangements were observed using high-throughput genome-wide translocation sequencing. Finally, the suppression of *DMPK* transcripts using CRISPR interference significantly decreased the intensity of RNA foci. Our results indicate that close attention should be paid to the unintended mutations when double-strand breaks are generated by CRISPR-Cas9 for therapeutic purposes. Alternative approaches independent of double-strand breaks, including CRISPR interference, may be considered.

INTRODUCTION

Myotonic dystrophy type 1 (DM1) is the most common type of adult-onset muscular dystrophy, affecting 1 in 8,000 individuals.[1] DM1 is an autosomal dominant disorder that is characterized by systemic symptoms, including progressive muscular atrophy, muscular weakness, myotonia, cardiac arrhythmia, insulin resistance, gastrointestinal dysfunctions, cataract, and cognitive impairment.[1] It is caused by the expansion of the CTG repeat in the 3′ untranslated region (UTR) of the dystrophia myotonica protein kinase (*DMPK*) gene.[2,3] Healthy subjects have 5–37 CTG repeats, whereas DM1 symptoms are identified in individuals with more than 50 CTG repeats.[2–4] The larger repeat sizes tend to be associated with worse clinical manifestations, and several thousand repeats are typically observed in severe congenital DM1 patients.[5,6] The expanded CTG repeats exhibit somatic and intergenerational instability with a bias toward expansion.[7,8]

The expanded CTG repeats in the 3′ UTR of *DMPK* are transcribed to mRNA as CUG repeats. It was previously demonstrated that the expanded CUG repeat forms stable hairpin structures that aggregate as RNA foci.[9–11] The intranuclear RNA foci sequester RNA binding proteins, including muscleblind-like 1 (MBNL1), a known splicing regulator.[12–14] This in turn leads to the depletion of soluble MBNL1 with normal regulatory function.[15] In addition, the RNA foci upregulate the activity of another splicing regulator, CUGBP Elav-like family member 1 (CELF1), by activating the protein kinase C pathway and suppressing the expression of specific microRNAs for CELF1.[16,17] The altered function of these splicing regulators results in the abnormal splicing of many genes, including *CLCN1*, *BIN1*, or *IRα*, which account for some aspects of the systemic features of DM1.[18–21]

The CRISPR-Cas9 system was first discovered as a microbial adaptive immune system.[22] It has since been successfully applied in the genome editing of eukaryotic cells and in a variety of research fields.[23–25] The most basic CRISPR-Cas9 system uses Cas9 nuclease derived from *Streptococcus pyogenes* and a single-guide RNA (sgRNA) with a complementary sequence to the target region of interest. These two components form a complex that is able to induce double-strand breaks (DSBs) at the target site. After cleavage, the DSBs are repaired by one of the two major repair pathways, that is,

Received 12 May 2020; accepted 20 May 2020;
https://doi.org/10.1016/j.omtm.2020.05.024.

Correspondence: Fumiaki Saito, Department of Neurology, School of Medicine, Teikyo University, 2-11-1 Kaga, Itabashi-ku, Tokyo 1738606.
E-mail: f-saito@med.teikyo-u.ac.jp

non-homologous end joining (NHEJ) or homology-directed repair (HDR).[26] This powerful tool has been adapted for medical therapeutics, including DM1. Thus far, several groups have successfully excised the CTG repeat of the *DMPK* gene using the conventional Cas9 nuclease system in cultured cells and model mice.[27–30]

Although CRISPR-Cas9 is an innovative technology, care must be taken to avoid causing undesirable mutations when used for therapeutic purposes.[31] One way to avoid this lies in the use of the double nicking strategy.[32] In this system, Cas9 nickase, a D10A mutant of Cas9, is utilized with a pair of offset sgRNAs complementary to opposite strands of the target site. The nicks of both of the DNA strands lead to a DSB with a 5′ overhang. A large reduction in off-target cutting is expected due to the need for two sgRNAs, since it is unlikely that two off-target nicks will be generated by chance in close proximity.[32,33] Importantly, by dual DSBs, the region encompassed by up to several Mb can be removed and the 5′ and 3′ cut ends can be rejoined using the NHEJ or HDR repair systems.[34] Another candidate is CRISPR interference (CRISPRi), a strategy in which the transcription of any gene is downregulated without inducing DSBs.[35,36] This strategy utilizes catalytically inactive Cas9 (dCas9) fused with a transcription suppressor, KRAB, and sgRNA designed at the vicinity of transcription start sites (TSSs). This DSB-free method is expected to be much safer than DSB-dependent genome editing.

In the present study, we demonstrated that both a conventional Cas9 nuclease and a double nicking strategy using Cas9 nickase successfully excised the CTG repeat tract by designing sgRNAs at the 5′ and 3′ flanking regions. Using these procedures, the formation of RNA foci was markedly inhibited. However, the unbiased detection of genomic alterations using linear amplification-mediated high-throughput genome-wide translocation sequencing (LAM-HTGTS)[37,38] revealed unexpected on- and off-target mutations as a result of using these procedures. Lastly, we showed that the downregulation of *DMPK* transcription by CRISPRi significantly suppressed the formation of RNA foci. Based on these observations, we propose that approaches that are independent of a DSB formation, such as CRISPRi, should be considered when applying the CRISPR-Cas9 technologies for therapeutic purposes in the future.

RESULTS

Excision of *DMPK* CTG Repeat by Cas9 Nuclease

First, we tested whether the conventional CRISPR-Cas9 system using Cas9 nuclease and a pair of sgRNAs designed at the 5′ and 3′ region of the CTG repeat could be used to remove the repeat sequence in HEK293 cells. We confirmed by Sanger sequencing that the strain of HEK293 cells we used contained five CTG repeats (data not shown). As shown in Figure 1A, three sgRNAs were designed on both the 5′ and the 3′ regions of the CTG repeats. Each sgRNA was expressed with Cas9 nuclease in HEK293 cells and showed similar indel frequencies, according to the result of a T7 endonuclease 1 assay (Figure S1). Then, Cas9 nuclease and two sgRNAs, one targeting the 5′ region and another targeting the 3′ region of the repeat, were co-transfected. Three days after transfection, genomic PCR was performed using primers designed at the outer sites of the sgRNA targeting loci (Figure 1A). Upon these co-expressions, lower molecular weight bands were observed (Figure 1B), suggesting the excision of the CTG repeats.

We investigated whether similar events could be observed in the fibroblasts of DM1, denoted as GM03991, which contains 50–80 CTG repeats. Using PCR amplification, the control fibroblasts (mock electroporation) exhibited two distinct bands at 400 and 700 bp, corresponding to the wild-type and mutant allele, respectively. Based on the CRISPR design tool score, we chose two combinations of sgRNA pairs: (1) 5′ guide 2/3′ guide 2 and (2) 5′ guide 3/3′ guide 2. These showed the lowest likelihood of off-target digestion. By electroporation with these sgRNAs, the lower molecular weight bands appeared above 200 bp (Figure 1C). Sanger sequencing confirmed that these bands consisted of amplicons lacking the CTG repeat (Figures 1D, S2A, and S2B). Although several junctional sequences were obtained, they were mostly homogeneous (57.1% for type deletion [del] 2 in HEK293 cells and 83.3% for type del 1 in fibroblasts; Figure S2C). In the following experiments, we used the sgRNA pair 5′ guide 3/3′ guide 2 for Cas9 nuclease cleavage. The T7 endonuclease 1 assay did not reveal any obvious off-target mutations at the top five sites predicted by the CRISPR design tool in fibroblasts (Figure S3).

When designing *in vivo* gene therapy for DM1 using CRISPR-Cas9 technology, it is of particular importance to remove the CTG repeats from as many cells as possible. To this purpose, we investigated whether repeated genome editing may facilitate the excision. The repeated genome editing of HEK293 cells and fibroblasts using Cas9 nuclease increased the intensity of the lower bands gradually, indicating it facilitated repeat excision (Figure 1E).

Excision of *DMPK* CTG Repeat by Cas9 Nickase

In order to adapt the CRISPR-Cas9 technology for clinical usage, it is critical to reduce the potential for off-target effects. For this purpose, we tested whether the CTG repeat was excised using the CRISPR-Cas9 double nicking strategy. We designed seven (Nick 1, 2, 5, 6, 7, 8, and 9) and two (Nick 3 and 4) nicking pairs of sgRNAs on the 5′ and 3′ regions of the CTG repeat, respectively (Figure 2A). Upon transfection of these nicking pairs into HEK293 cells, a T7 endonuclease 1 assay demonstrated indel frequencies ranging from 30% to 40% or more (Figure S4). We then co-transfected HEK293 cells with Cas9 nickase and two pairs of sgRNAs, one targeting the 5′ region and another the 3′ region of the repeat. Genomic PCR showed lower molecular weight bands in all of the combinations of sgRNA pairs (Figure 2B). Among them, we chose the nicking pairs of Nick 1 and Nick 3 for the subsequent experiments, since the lower band was robust and the decrease in molecular weight was small, and the latter may only minimally affect the 3′ UTR structure of the *DMPK* gene. Sanger

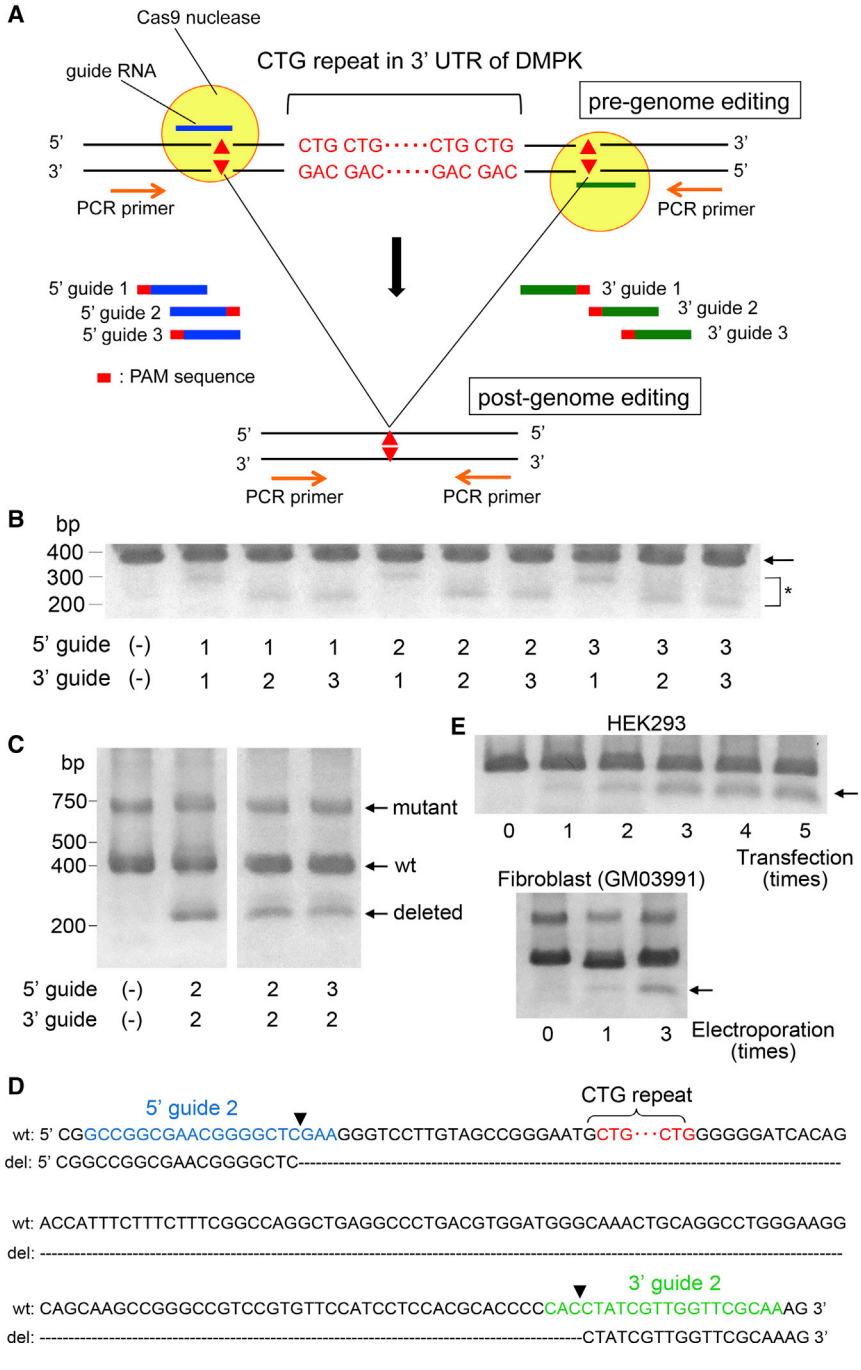

Figure 1. Excision of *DMPK* CTG Repeat Using Cas9 Nuclease

(A) Schematic representation of 3′ UTR of the *DMPK* gene is shown. The CTG repeat sequence is indicated in red characters. Three guide RNAs were designed at the 5′ and 3′ region of the CTG repeat (guide 1, 2, and 3). This region was amplified by PCR using the primers flanking the target sequence. (B) HEK293 cells were co-transfected with guide RNAs designed at the 5′ and 3′ regions with Cas9 nuclease, and genomic PCR was performed. By mock transfection, i.e., 5′ guide (–), 3′ guide (–), a PCR product of 400 bp was observed (arrow). Upon transfection with each combination of guide RNA, lower molecular weight bands were observed (asterisk). (C) Genomic PCR of DM1 patient-derived fibroblasts GM03991, harboring 50–80 CTG repeats, showed two distinct bands with an apparent molecular mass of 400 and 700 bp, corresponding to the wild-type and the mutant allele with an expanded CTG repeat, respectively. By genome editing using 5′ guide 2/3′ guide 2 and 5′ guide 3/3′ guide 2, the bands with a lower molecular mass above 200 bp were observed. (D) Sanger sequencing revealed that the lower molecular weight bands consisted of amplicons in which the CTG repeat region was excised. A typical junctional sequence is shown here. The blue, green, and red characters represent the position of the 5′ guide 2, 3′ guide 2, and CTG repeat, respectively. Arrowheads indicate the position of the expected DSBs. (E) Genome editing was repeated five times with an interval of 3 days to HEK293 cells (upper panel) and three times with an interval of 7 days to DM1-derived fibroblasts (lower panel). The CTG repeat excision was facilitated by repeating the genome editing (arrow).

sequencing demonstrated that the lower band consisted of amplicons lacking the CTG repeat (Figures 2C, S5A, and S5B). By aligning the sequence data, it was evident that the junctional sequences were heterogeneous, compared to those observed using the conventional Cas9 nuclease (Figures S2B and S5B). No identical junctional sequence was observed among the clones we tested (Figure S5C). Repeated genome editing of HEK293 cells using the double nicking strategy gradually increased the intensity of the lower bands, indicating that it facilitated the excision of the repeat (Figures 2D and 2E).

Suppression of RNA Foci Formation by CRISPR-Cas9 Genome Editing

As described above, the fibroblast GM03991, harboring 50–80 CTG repeats, was found to contain a wild-type allele at 400 bp and a mutant allele at 700 bp, according to the PCR results. In contrast, the fibroblast GM05163, harboring 400 repeats, showed only a wild-type allele, suggesting that the PCR failed to amplify the large mutant allele (Figure 3A, mock). Upon the genome editing of these fibroblasts using conventional Cas9 nuclease or double nicking with Cas9 nickase, the lower molecular weight bands appeared above 200 bp, indicating the successful excision of the CTG repeat (Figure 3A).

RNA foci were not detected in GM03991 using the RNA-fluorescence *in situ* hybridization (FISH) assay. As such, we studied GM05163 to evaluate the formation of RNA foci, one of the major pathological hallmarks of DM1 (Figure S6). To determine whether

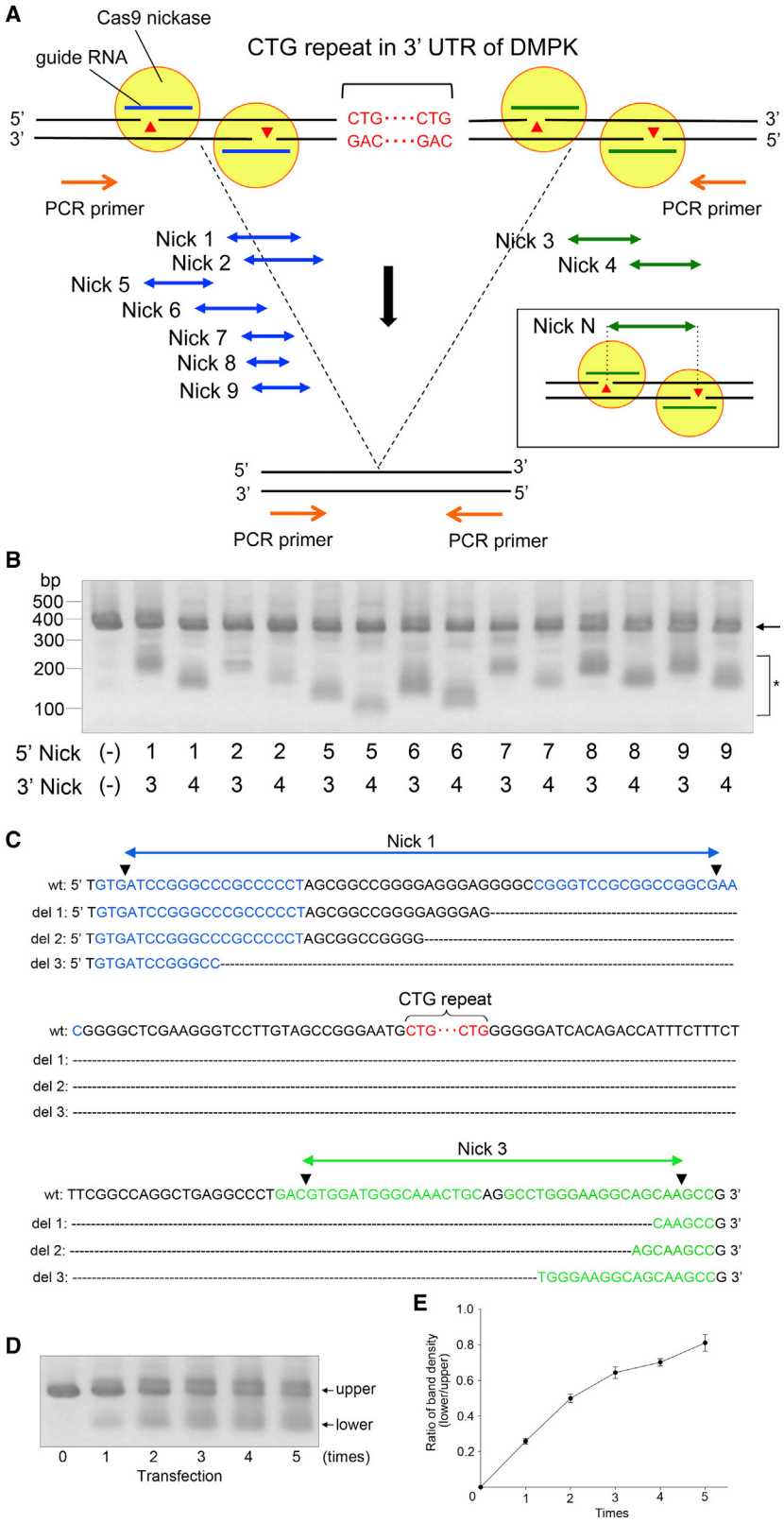

Figure 2. Excision of *DMPK* CTG Repeat Using Cas9 Nickase

(A) Schematic representation of the 3′ UTR of the *DMPK* gene. The CTG repeat sequence is indicated in red characters. Seven (Nick 1, 2, 5, 6, 7, 8, and 9) and two (Nick 1 and 2) nicking pairs of guide RNAs were designed at the 5′ and 3′ regions of the CTG repeat, respectively. This region was amplified by PCR using the primers flanking the target sequence. (B) HEK293 cells were co-transfected with two pairs of guide RNAs, one against the 5′ region and another against the 3′ region of the repeat together with Cas9 nickase. Genomic PCR showed a PCR product of 400 bp by mock transfection i.e., 5′ Nick (–), 3′ Nick (–) (arrow). Upon transfection with each combination of nicking pairs of guide RNAs, lower molecular weight bands were observed (asterisk). (C) Sanger sequencing of the lower molecular weight band observed in Figure 3B by 5′ Nick 1 and 3′ Nick 3 revealed that it consisted of amplicons lacking the CTG repeat. A few junctional sequences are shown here. The blue, green, and red characters represent the position of Nick 1, Nick 3, and the CTG repeat, respectively. Arrowheads indicate the position of expected nicks. (D) Genome editing with Cas9 nickase was repeated five times with an interval of 3 days to HEK293 cells. The CTG repeat excision was facilitated by repeating the genome editing. (E) Quantitative densitometric analyses of the lower bands in (B) confirmed that the repeated genome editing increases the efficiency of repeat excision. The results are expressed as the mean ± SEM (n = 3).

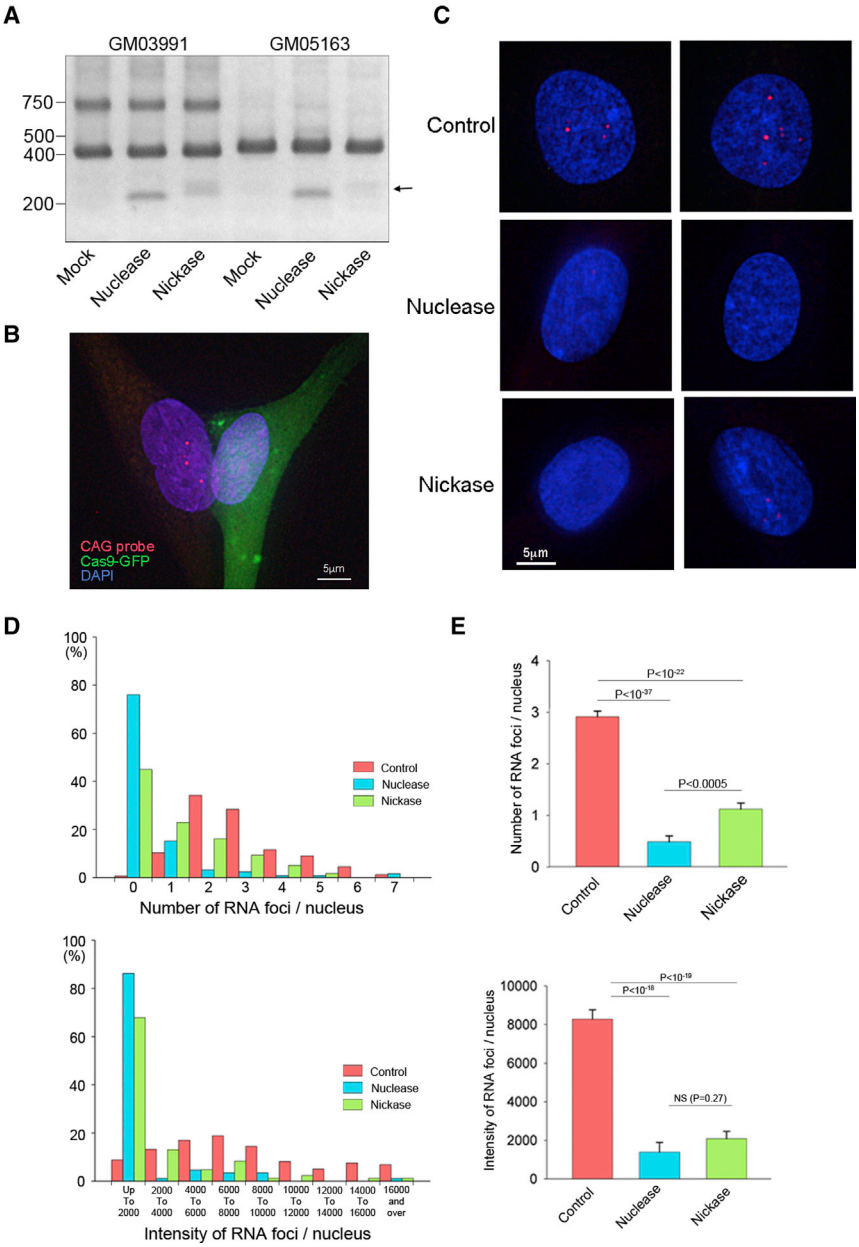

Figure 3. Suppression of RNA Foci Formation by the Repeat Excision

(A) Fibroblast GM03991, harboring 50–80 CTG repeats, was found to consist of a wild-type allele at 400 bp and a mutant allele at 700 bp by PCR. However, fibroblast GM05163, with 400 CTG repeats, exhibited only the wild-type allele, presumably because the PCR failed to amplify the highly repetitive sequence of the mutant allele. Genome editing was performed to these cells using conventional Cas9 nuclease and two sgRNAs (5′ guide 3 and 3′ guide 2) or the double nicking strategy with Cas9 nickase and four sgRNAs (Nick 1 and Nick 3 pairs). Using both of the procedures, lower molecular weight bands were observed above 200 bp (arrow), indicating the successful excision of the CTG repeat. (B) Fibroblast GM05163 was co-transfected with GFP-tagged Cas9 nuclease or Cas9 nickase together with sgRNAs. The RNA-FISH image shows intense RNA foci in the GFP-negative fibroblast (left) but not in the GFP-positive Cas9 nuclease-expressing cell (right). (C) In the nuclei of the control fibroblasts (no plasmids), several RNA foci were consistently observed. However, the RNA foci were mostly undetectable in fibroblasts expressing Cas9 nuclease or nickase. (D) Quantitative analyses of the number and the total intensity of intranuclear RNA foci were performed. Histograms of both the number (upper panel) and the intensity (lower panel) with a left-side skew were obtained for Cas9 nuclease and nickase. (E) The average number of RNA foci was significantly reduced by both Cas9 nuclease and nickase. When compared between Cas9 nuclease and nickase, the nuclease-treated cells exhibited significantly fewer foci (upper panel). The average intensity of RNA foci was significantly decreased by both Cas9 nuclease and nickase. There was no significant difference between the nuclease and nickase by this parameter (lower panel). The results are expressed as the mean ± SEM.

the removal of the CTG repeat affected the formation of foci, fibroblasts were co-transfected with GFP-tagged Cas9 nuclease or Cas9 nickase together with sgRNAs targeting the 5′ and 3′ regions flanking the CTG repeat. A typical RNA-FISH image 3 days after genome editing is provided in Figure 3B. In the nucleus of the GFP-negative fibroblasts (Figure 3B, left), several intense dot-shaped RNA foci were detected, which were not observed in GFP-positive Cas9-expressing fibroblasts (Figure 3B, right). In the nuclei of the control fibroblasts (mock electroporation), several RNA foci were consistently observed. However, the RNA foci were mostly undetectable in the nuclei of fibroblasts expressing Cas9 nuclease and nickase (Figure 3C). Furthermore, to ascertain the sequestration of MBNL1 to the RNA foci, an RNA-FISH assay was performed, followed by immunofluorescent analysis using anti-MBNL1 antibody. As a result, we found that MBNL1 colocalized with RNA foci in the DM1 patient-derived fibroblasts. Upon genome editing using Cas9 nuclease, both of the signals of the RNA foci and MBNL1 were abolished, indicating that the trapped MBNL1 was released from the foci (Figure S7).

Subsequently, we obtained more than 100 images of the nuclei from each group to quantitatively analyze the formation of the RNA foci. The number of RNA foci and the total intensity of RNA foci in each nucleus were measured. Histograms of both the number (Figure 3D, upper panel) and the total intensity (Figure 3D, lower panel) showed a left-sided skew resulting from Cas9 nuclease and nickase compared to the control. These data demonstrated that both genome editing strategies suppressed the formation of RNA foci.

Furthermore, the average number of RNA foci was significantly reduced by both Cas9 nuclease and nickase. When comparing Cas9 nuclease and nickase, the nuclease-treated cells exhibited significantly fewer foci (Figure 3E, upper panel). The average intensity of the RNA foci was also significantly decreased by these procedures. There was no significant difference between the nuclease and nickase with regard to this parameter (Figure 3E, lower panel).

Unbiased Genome-wide Detection of On- and Off-Target Mutations

To evaluate the unexpected mutations caused by CRISPR-Cas9, we performed LAM-HTGTS. Generally, DSBs generated by genome editing are rejoined via the classic NHEJ pathway, with occasional indels at the break site, and rarely by HDR. However, some DSBs, which are not rejoined immediately at the original loci, are fused with the separate cut ends when the other DSBs occur due to off-target cleavage. This leads to translocations to other chromosomes or intra-chromosomal deletions. By designing the sequence-specific primers at the fixed "bait" (DMPK locus in this case), LAM-HTGTS analyzes the genome-wide off-target "prey" DSBs captured by the on-target bait DSBs using next-generation sequencing (Figure 4A).

First, as a positive control, we induced a DSB using Cas9 nuclease and one sgRNA at the *RAG1* locus in HEK293 cells. Using this single DSB, the translocation hotspots were identified in chromosomes 7, 12, 15, and 19, as shown in a Circos plot (Figure 4B). This pattern of hotspots was consistent with that reported in a previous study.[37] Next, we performed genome editing to the *DMPK* 3′ UTR using Cas9 nuclease and two sgRNAs to excise the CTG repeat, and detected translocations using *DMPK* as a bait. Although no hotspots were found in the negative control (no editing) (Figure 4C), six translocation hotspots were observed in chromosomes 1, 14, 15, 17, 19, and X by the dual DSBs (Figure 4D). Furthermore, we attempted the double nicking strategy using Cas9 nickase and four sgRNAs to generate dual DSBs in the *DMPK* locus. We anticipated that off-target effects would be strikingly reduced by this procedure. However, contrary to our expectation, as many as 25 translocation hotspots were identified using double nicking genome editing (Figures 4E and 4F). The frequency of translocation to each hotspot is shown in Table S1. The total frequency of these translocations in total mapped reads by a DSB at the *RAG1* locus with Cas9 nuclease was 0.002625%. Comparably, the total frequencies by DSBs at the *DMPK* locus using Cas9 nuclease and Cas9 nickase were 0.001592% and 0.002169%, respectively.

Furthermore, to evaluate the on-target mutations neighboring the cutting sites, we mapped the paired reads obtained by LAM-HTGTS using integrative genomics viewer software.[39] Upon generation of a single DSB at the *RAG1* locus, the left-sided reads of some of the paired reads were mapped several kb apart from the breakpoint (Figure S8A). The non-edited samples using *DMPK* as a bait, which were used as negative controls for Cas9 nuclease and Cas9 nickase, exhibited only minimal gaps between the paired reads (Figures S8B and S8C). However, dual DSBs, generated by both Cas9 nuclease and Cas9 nickase, resulted in much larger gaps between the paired reads. These large gaps indicate that genomic rearrangements occurred including large deletions. Among them, paired reads with opposite orientations facing each other and with inferred insert sizes larger than expected, such as several hundred bp or larger, represent possible deletions. We extracted the paired reads with these possible deletions and ranked the top 20 according to their size (Figure 4G; Table S2). Using *RAG1* cleavage with a single sgRNA, potential on-target deletions ranging from several hundred bp to several kb were observed. However, the dual digestion at *DMPK* by Cas9 nuclease and nickase led to the generation of much larger deletions spanning beyond 20 and 60 kb, respectively.

Suppression of RNA Foci by CRISPRi

The generation of unexpected mutagenesis is of great concern when DSBs are generated using CRISPR-Cas9, as described above. Therefore, we examined whether the RNA foci were suppressed by the downregulation of *DMPK* transcription using CRISPRi, a DSB-free method. We searched the TSS of the human *DMPK* gene using the FANTOM5 database and identified the most enriched peak at chromosome 19 (ch19), 46,285,748 (hg19). Then, three sgRNAs neighboring the peak were designed (Figure 5A). Three days after the transfection of HEK293 cells with dCas9-KRAB and each sgRNA, the RNA was extracted from the whole cell population without selection. Quantitative RT-PCR revealed a significant reduction in the level of *DMPK* mRNA by guide 2 (Figure 5B). Next, to evaluate the formation of RNA foci, an RNA-FISH assay was performed using the fibroblast GM05163. Several RNA foci were clearly observed in the control fibroblasts, whereas RNA foci were mostly inconspicuous in the transfected cells with the guide 2, according to the red fluorescent protein (RFP) fluorescence of EF1-RFP-U6-gRNA plasmid (Figure 5C). Finally, the number and total intensity of the RNA foci were quantitatively analyzed. Histograms of both the number (Figure 5D, upper panel) and the total intensity (Figure 5D, lower panel) of RNA foci with a left-sided skew were obtained using CRISPRi. Although the average foci number was not significantly different (Figure 5E, upper panel), the average intensity of foci was significantly decreased by CRISPRi (Figure 5E, lower panel).

DISCUSSION

Thus far, no therapeutic strategy has been successfully applied in clinical use for the treatment of DM1, although many experimental approaches have been attempted in the past two decades. These include small molecular therapeutic strategies and posttranscriptional silencing using nucleotide sequences. For example, small molecules, such as erythromycin, and several designer small molecular compounds have been reported to block the interaction between CUG repeat and MBNL1.[40,41] It was also demonstrated that RNase-H active gapmer antisense oligonucleotides (ASOs) modified by 2′-*O*-methoxyethyl and 2′-4′-constrained ethyl effectively corrected the phenotype of DM1 in model mice.[42,43] Note that a gapmer ASO developed by Ionis Pharmaceuticals (IONIS-DMPKRX) entered a phase I/IIa trial, but enough concentration of the drug was not achieved in skeletal muscle to provide a therapeutic benefit (ClinicalTrials.gov: NCT02312011). Recently, genome editing technologies

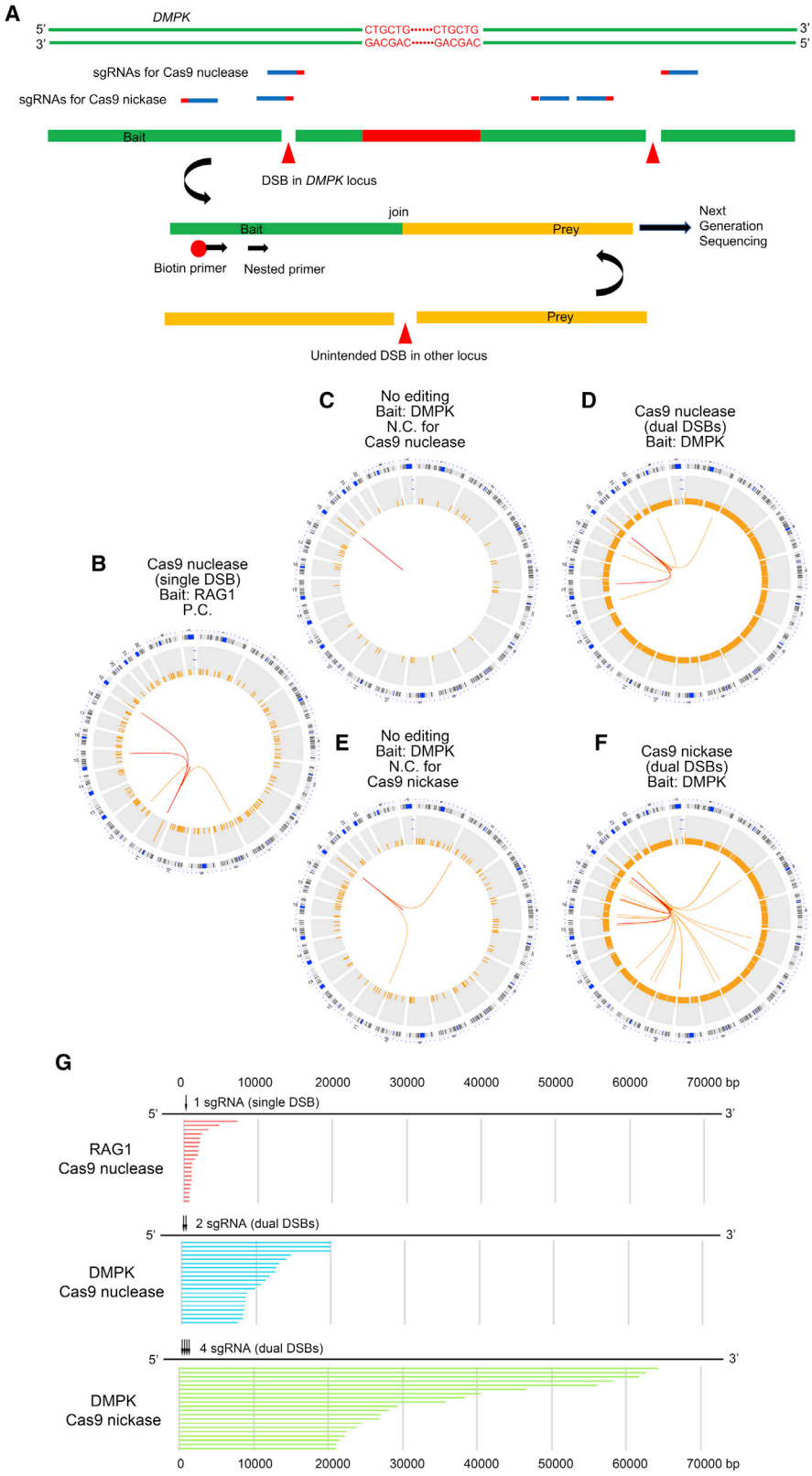

(legend on next page)

based on CRISPR-Cas9 have been found to have a robust applicability in a variety of research fields, including medical therapeutics. Several groups have reported successful excision of the CTG repeat in DM1 with conventional Cas9 nuclease by designing sgRNAs at the 5′ and 3′ region flanking the repeats.[27–30] In alternative approaches, polyadenylation signals were inserted in the 3′ UTR upstream of the CTG repeat using CRISPR-Cas9 or transcription activator-like effector nuclease (TALEN).[44,45] This insertion led to the premature termination of transcription and the reversal of aberrant splicing. In terms of the delivery method for *in vivo* gene targeting, one of the most attractive vectors is the adeno-associated virus (AAV).[46] AAV does not integrate into the genome and produces high levels of long-term gene expression. A variety of serotypes are available that provide increased delivery efficiencies for the specific cell/tissue types. However, AAV has some disadvantages, including (1) a prolonged and uncontrollable expression that potentially increases the off-target mutagenesis, (2) a production of antibodies against AAV that may reduce the therapeutic effectiveness, and (3) a limited packing capacity that sometimes requires separate vector systems. Alternatively, CRISPR-Cas9 components can be delivered as a ribonucleoprotein (RNP) complex, which is generally considered to be safe since it is rapidly degraded. Although a local injection of RNP itself was shown to successfully induce genome editing,[47] many non-viral delivery systems are currently under development for more efficient RNP delivery. These include lipid nanoparticles,[48] gold nanoparticles,[49] cell-penetrating peptides,[50] and extracellular nanovesicles.[51]

In this study, we tried to validate the excision of expanded CTG repeats using a conventional CRISPR-Cas9 system. By designing sgRNAs at the 5′ and 3′ region of the repeats, Cas9 nuclease successfully removed the targeted region. Upon this procedure, RNA foci were suppressed, and trapped MBNL1 was released from the foci. Although we have not examined the correction of the mis-splicing of mRNAs, including *CLCN1*, *BIN1*, or *IRα*, it is presumed to be difficult to validate this using fibroblasts.[21] CRISPR-Cas9 is an innovative tool that has potential applications in clinical use in the future; however, it can lead to unintended mutagenesis. To reduce this possibility, we excised the CTG repeats using the double nicking strategy, by which the off-target cuttings are considered to be strictly inhibited. We found that the repeat sequence was successfully deleted in HEK293 cells and DM1 fibroblasts using this procedure. Note that on-target junctional sequences were found to be heterogeneous using Sanger sequencing after double nicking. The breakpoints spanned widely, from the upstream of 5′ nicking sgRNAs to the downstream of 3′ sgRNAs. This is in contrast to Cas9 nuclease, which mostly generated the expected junctions. It is difficult to predict the exact on-target cutting sites when the double nicking strategy is employed, which is a potential disadvantage of this procedure. In addition to the accuracy, a degree of effectiveness is required to apply the genome editing to clinical use, especially for disorders in which the pathogenic mechanism is based on the gain of toxic functions, including DM1. We found that the excision of CTG repeats was facilitated by genome editing. Thus, several rounds of repeating genome editing therapies could be used in severe cases to obtain an additive efficacy, such as in chemotherapy for cancer or immunosuppressive therapies for autoimmune-related disorders.[52]

Although both the conventional Cas9 nuclease and the double nicking strategy with Cas9 nickase significantly reduced the RNA foci, Cas9 nuclease seems to have a subtle advantage over Cas9 nickase in terms of its efficiency. One possible reason for this difference may be that four sgRNAs are necessary to exert an effect simultaneously at each targeting loci in the double nicking strategy, in contrast to Cas9 nuclease, which requires two sgRNAs. Alternatively, the efficiency of the DSB formation by paired nickase may be lower than that by Cas9 nuclease. The former is more likely since D10A Cas9 nickase used in this study was recently reported to have a higher cutting efficiency than Cas9 nuclease.[53]

So far, many methodologies for the detection of unintended mutations by genome editing have been reported, and they are grouped into two categories: "biased" methods and "unbiased" methods.[54] In the biased methods, potential off-target sites are predicted using *in silico* homology searches, and the resulting sites are analyzed by

Figure 4. Unbiased Genome-wide Detection of On- and Off-Target Mutations

(A) A diagram of LAM-HTGTS for the detection of unbiased genome-wide off-target effects is shown. The broken end of the *DMPK* locus generated by on-target DSB works as a "bait" and captures genome-wide "prey" induced by unintended DSBs in other loci. Following PCR using a biotinylated primer, enrichment with avidin beads, and nested PCR, the bait-prey hybrid sequences are read using next-generation sequencing. (B) Using Cas9 nuclease and one sgRNA targeting the *RAG1*A site, a single DSB was generated in the HEK293 cells as a positive control. With *RAG1* as a bait, LAM-HTGTS was used to reveal several translocation hotspots. The chromosomal location is indicated in the outermost part of the Circos plot. Split reads binned into 50-Mb regions (orange bars) have been plotted on a log scale. Colored lines (orange and red) connect the *RAG1* bait site on chromosome 11 to the genome-wide prey hotspots binned into 100-bp regions. The orange and red line colors indicate a split-reads frequency of 3–9 and of more than 10, respectively. (C) LAM-HTGTS was performed without genome editing using *DMPK* as a bait, a negative control for Cas9 nuclease. No translocation hotspot was detected. (D) Using Cas9 nuclease and two sgRNAs targeting the *DMPK* locus, dual DSBs were generated. Using *DMPK* as a bait, six translocation hotspots were identified. (E) LAM-HTGTS was performed without genome editing using *DMPK* as a bait, a negative control for the double nicking strategy with Cas9 nickase. (E) differs from (C) in the filtering process of split reads since the deduced on-target breakpoint is different between them (details are found in Materials and Methods). (F) Using Cas9 nickase and four sgRNAs, dual DSBs were generated. Using *DMPK* as a bait, as many as 24 translocation hotspots were identified. (G) Split reads obtained by LAM-HTGTS were mapped in integrative genomics viewer. Possible deletions, jugged from the orientation of the paired reads and their intervals, were extracted and the top 20 were sorted according to their size. By generating a single DSB on the *RAG1* locus using Cas9 nuclease, possible on-target deletions ranging from several hundred bp to several kb were observed (upper panel). By generating dual DSBs on the *DMPK* locus using Cas9 nuclease and two sgRNAs, larger deletions with an estimated size ranging from several to 20 kb were observed (middle panel). By generating dual DSBs on the *DMPK* locus using Cas9 nickase and four sgRNA, larger deletions with an estimated size ranging from 20 to 60 kb were observed (lower panel). Arrows indicate the position of sgRNA.

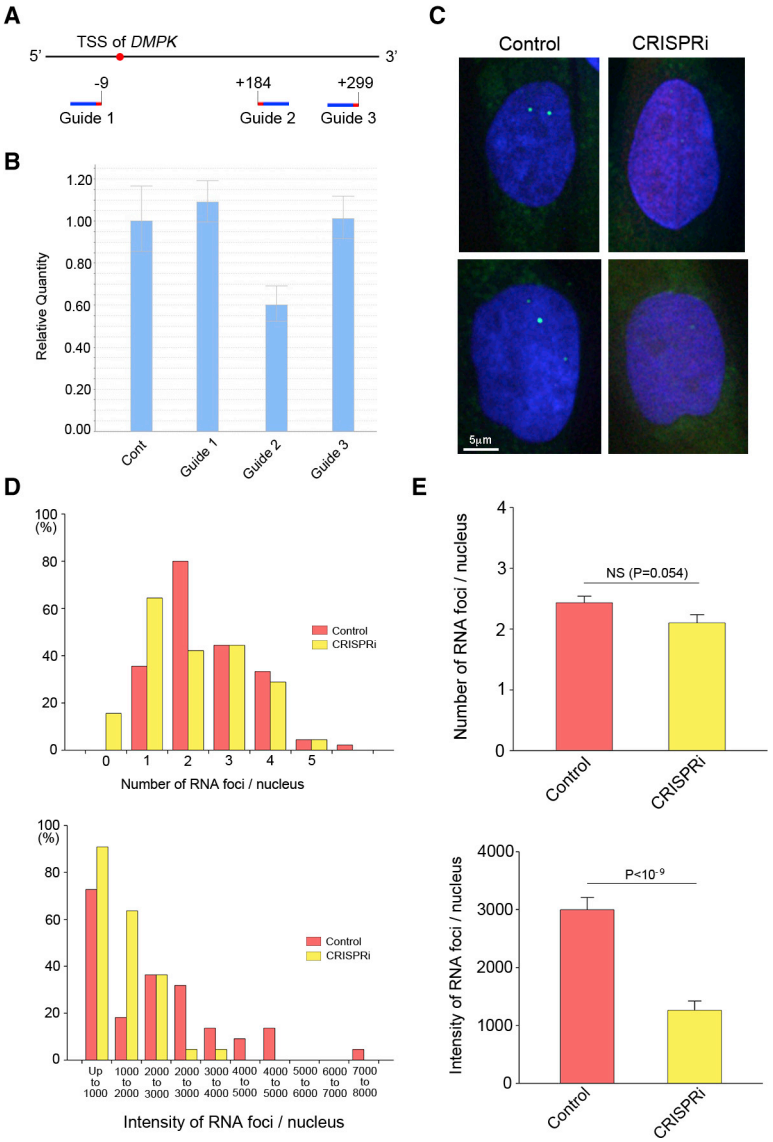

Figure 5. Suppression of RNA Foci by CRISPRi

(A) To suppress the transcription of the *DMPK* gene by CRISPRi, three sgRNAs, one upstream and two downstream of the TSS, were designed. (B) After the transfection of the HEK293 cells, total RNA was extracted from the whole cell population without selection. Quantitative RT-PCR revealed a significant reduction in the level of *DMPK* mRNA by guide 2. The results are expressed as the mean ± SEM (N = 3). (C) An RNA-FISH assay was performed using fibroblast GM05163 after CRISPRi using guide 2. Several RNA foci were clearly observed in the control fibroblasts, but they were mostly inconspicuous in the transfected cells. (D) Quantitative analysis of the number and total intensity of the intranuclear RNA foci was performed. Histograms of both the number (upper panel) and the total intensity (lower panel) shifted toward the left side by CRISPRi compared to control. (E) Although the fibroblasts transfected for CRISPRi tended to show fewer foci, the difference in the average foci number was not statistically significant (upper panel). The average intensity of the RNA foci was significantly decreased by CRISPRi (lower panel). The results are expressed as the mean ± SEM.

a T7 endonuclease 1 assay or deep sequencing.[26] However, these methods have only a limited capability to detect off-target mutations and cannot reveal unpredicted genomic alterations. In contrast, the unbiased methods directly detect mutations at the genome-wide level independent of *in silico* prediction tools.[54] Therefore, to develop medical therapeutics for human diseases using genome editing, on- and off-target mutations need to be thoroughly assessed using the unbiased method, although most studies in the context of disease treatment do not use them. Using LAM-HTGTS, we clearly demonstrated a significant translocation hotspot, even in the case of the double nicking strategy, against our expectations.[37] One possible explanation for the off-target cleavages is that the Cas9 nickase may exert residual nuclease activity. Indeed, D10A Cas9 nickase with a single sgRNA (not a double nicking) exhibited low levels of on-target indels.[24,55] The sgRNAs we used for the double nicking strategy may have relatively frequent homologous sequences along the genome, thereby generating DSBs individually without pairing. Another possibility is that the single-strand breaks (SSBs; nicks) generated by Cas9 nickase led to the formation of DSBs during the replication of the chromosome. SSBs are mainly repaired via the base excision repair pathway with a high degree of fidelity.[56] However, if they are left unrepaired, replicative polymerases encounter these SSBs, which can result in the collapse of the replication fork, and subsequently in the formation of DSBs.[57–59] In the presence of Cas9 nickase, the cycles of nick formation and their repair will be continuously repeated until the enzyme is inactivated. This may result in the formation of frequent DSBs, especially in the actively dividing cells, such as HEK293 cells.

Apart from the off-target effects, LAM-HTGTS revealed on-target genomic rearrangements, including possible large deletions. The largest deletion size estimated was several kb, resulting from a single DSB at the *RAG1* locus. However, this was exceeded by 20 and 60 kb by dual DSBs at the *DMPK* locus as a result of Cas9 nuclease and Cas9 nickase, respectively. Recently, on-target large deletions caused by CRISPR-Cas9 have been reported by several research groups. They have found deletions ranging from several hundred bp up to several kb in mouse embryonic stem cells (ESCs) or cultured cell lines using long PCR and Sanger sequencing.[60–63] However, larger deletions, such as those identified in our study, are difficult to detect using these strategies, since PCR primer binding sites are lost. In another report, an unbiased mutation detection methodology, UDiTaS (uni-directional targeted sequencing), was used to detect on-target mutations.[64] They generated dual DSBs using Cas9 nuclease at the *DMD* locus and found large deletions of up to several kb in mice.[65] The difference in the deletion size between these studies and our own study (several kb versus

several 10s of kb) may be attributed to the differences in the targeting species, locus, or the procedures used. In our study, the dual DSBs rather than the single DSB, and the double nicking rather than the conventional Cas9 nuclease, induced larger deletions. However, no general conclusions can be currently drawn due to the limited number of experiments. As such, further investigations will be required to confirm our findings.

As discussed above, DSBs can exert potential deleterious effects on genomic structure, even when the double nicking strategy is used. In addition, recent reports found that DSBs induced by CRISPR-Cas9 trigger a p53-mediated DNA damage response and cell cycle arrest.[66,67] Prompted by these observations, we sought to clarify the effects of CRISPRi, a methodology independent of a DSB formation, using dCas9. Since it was demonstrated that the FANTOM5 promoter atlas represented the most reliable source of TSS annotations, we used this online database for the prediction of TSSs.[68] Although the position of sgRNA spanning −50 to +150 relative to the TSS is generally recommended, its functionality also depends on the chromatin accessibility of the target site.[68] In our case, using the sgRNA designed at +184 relative to the *DMPK* TSS, the transcription and the formation of RNA foci were successfully suppressed. Although this procedure inhibits the transcription of both the normal and mutant allele of *DMPK*, serious undesired effects were not presumed since a targeted deletion of *DMPK* exhibited no significant phenotypic alteration in mice.[69] So far, two studies have reported on the use of dCas9 to inhibit the pathogenic pathway of DM1. The strategies reported in these studies differ from our own in that the CTG or CUG repeat sequence on the genome or mRNA was directly targeted by sgRNAs.[70,71] These approaches allow for the selective reduction of mutant *DMPK* mRNA, while non-selectively affecting the CTG repeat tracts found in the form of microsatellite sequences on the human genome.

In conclusion, we demonstrated that both a conventional Cas9 nuclease method and a double nicking strategy using Cas9 nickase can be used to successfully excise CTG repeats in the DM1 locus and suppress the formation of RNA foci. However, contrary to our expectations, off-target cleavage and on-target genomic rearrangements were observed as a result of using the double nicking strategy, to a comparable degree as that observed when using Cas9 nuclease excision. By reducing the transcription of *DMPK* using CRISPRi, a DSB-free procedure, the formation of RNA foci was significantly inhibited. We propose that this alternative approach should be used for the development of a safer therapeutic strategy for the treatment of DM1 in the future.

MATERIALS AND METHODS

Plasmid Construction

The expression plasmids for Cas9 nuclease (pSpCas9(BB)-2A-GFP) and Cas9 nickase, a D10A mutant version of Cas9 nuclease (pSpCas9n(BB)-2A-GFP), were gifts from Dr. Feng Zhang (Addgene, plasmid nos. 48138 [http://addgene.org/48138] and 48140 [http://addgene.org/48140]). The target sites of sgRNA were selected using the online CRISPR design tool (http://zlab.bio/guide-design-resources). Based on the input of the sequences flanking the 5′ and 3′ regions of the CTG repeat of the *DMPK* gene, several targeting sites were chosen to generate the fewest number of off-target sites as close to the CTG repeat as possible. The sgRNAs were cloned into the plasmids as described previously.[26] Briefly, the top and bottom strands of oligonucleotides with BbsI restriction sites on their 5′ termini were chemically synthesized at FASMAC (Atsugi, Japan). The oligonucleotides were phosphorylated and annealed in a thermal cycler using the following program: 37°C for 30 min; 95°C for 5 min; ramp down to 25°C at 5°C/min. Then, pSpCas9(BB)-2A-GFP and pSpCas9n(BB)-2A-GFP were digested by BbsI (NEB, Ipswich, MA, USA) and ligated with each sgRNA. The insertions of the sgRNAs were confirmed by Sanger sequencing. For the CRISPRi experiments, AAV CMV-dSaCas9-KRAB-bGHpA, gifted by Dr. Charles Gersbach (Addgene, plasmid no. 106219 [http://addgene.org/106219]) and EF1-RFP-U6-gRNA (System Biosciences, Palo Alto, CA, USA) were used to express dCas9 and sgRNA, respectively.[72] The TSS of the human *DMPK* gene was identified using the online database FANTOM5 (https://fantom.gsc.riken.jp/5/).[73] sgRNAs with a PAM sequence of NNGRRT or NNGRR were designed in the vicinity using Benchling software (https://www.benchling.com). The corresponding oligonucleotides were synthesized, annealed, and ligated to the EF1-RFP-U6-gRNA plasmid according to the manufacturer's instructions. The sgRNA sequences used are listed in Table S3.

Cell Culture, Transfection, and Electroporation

HEK293 cells and DM1 patient-derived fibroblasts were obtained from RIKEN BioResource Research Center (BRC) (Tsukuba, Japan) and the Coriell Institute (Camden, NJ, USA), respectively. The fibroblast GM03991, harboring 50–80 CTG repeats, was obtained from a mildly affected patient, while the fibroblast GM05163, with 400 CTG repeats, was obtained from a moderately affected individual. HEK293 cells were plated on plastic culture dishes or six-well plates (Corning Life Sciences, Oneonta, NY, USA) and grown in the Dulbecco's modified Eagle's medium (Thermo Fisher Scientific, Waltham, MA, USA) supplemented with 10% fetal bovine serum and antibiotic-antimycotic (Thermo Fisher Scientific, Waltham, MA, USA). Fibroblasts were plated on six-well plates and grown in minimal essential medium (Thermo Fisher Scientific, Waltham, MA, USA) with 10% fetal bovine serum and antibiotic-antimycotic. All cells were grown in a humidified 37°C incubator with 5% CO_2 and 95% air. The HEK293 cells were transfected with the expression plasmids using Effectene (QIAGEN, Hilden, Germany). The fibroblasts were transfected using electroporation with an Amaxa 4D-Nucleofector (Lonza, Basel, Switzerland) by condition CA-137 according to the manufacturer's instructions. The cells were harvested 3 days after the transfection.

PCR Amplification and T7 Endonuclease 1 Assay

Genomic DNA was extracted from the cultured cells using a DNeasy Blood & Tissue kit (QIAGEN, Hilden, Germany) and quantified using a Qubit 2.0 fluorometer (Thermo Fisher Scientific, Waltham, MA, USA). The PCR amplification of the on-target *DMPK* locus was

performed using the extracted genomic DAN as a template with KOD FX (Toyobo, Osaka, Japan). The PCR primers used are indicated in Table S3. The following program was used: an initial denaturation at 94°C for 2 min; 35 cycles at 98°C for 10 s, 68°C for 3 min. After the separation of the PCR products in 2% agarose gel, the DNA was extracted using a QIAquick gel extraction kit (QIAGEN, Hilden, Germany) and analyzed by Sanger sequencing. A T7 endonuclease 1 assay was performed using a Surveyor mutation detection kit (Integrated DNA Technologies, Coralville, IA, USA), according to the manufacturer's protocol. Briefly, after genome editing with Cas9 nuclease or Cas9 nickase, the genomic DNA was extracted from HEK293 cells or fibroblasts. On- and off-target loci were amplified by PCR using LA Taq DNA polymerase (Takara Bio, Shiga, Japan) and the primers listed in Table S3. The PCR products were heat-denaturated and then re-annealed according to the following program in a thermal cycler: 95°C for 10 min; ramp down to 25°C at 1°C/15 s; hold at 4°C. Heteroduplex PCR products comprised of wild-type and mutant alleles were digested by incubating with Surveyor nuclease at 42°C for 60 min. The PCR products were separated by 4%–20% gradient polyacrylamide gel electrophoresis, and the band intensities were measured using ImageJ software. Indel occurrence (indel %) was estimated as previously described.[26]

Quantitative RT-PCR

The RNA was extracted from cultured cells using an RNeasy mini kit (QIAGEN, Hilden, Germany) and quantified using a Qubit 2.0 fluorometer (Thermo Fisher Scientific, Waltham, MA, USA). Then, the cDNA was reverse transcribed using ReverTra Ace (Toyobo, Osaka, Japan) according to the manufacturer's instructions. Quantitative RT-PCR was conducted with a 7500 Fast real-time PCR system (Thermo Fisher Scientific, Waltham, MA, USA) using the cDNAs as templates. The gene expression was quantitatively analyzed by TaqMan assay using TaqMan probes Hs01094329_m1 and Hs02786624_g1 for *DMPK* and *GAPDH*, where the latter was used as an internal control.

RNA-FISH and Quantitative Analysis of RNA Foci

For the RNA-FISH assay, a DNA/locked nucleic acid (LNA) chimeric oligonucleotide labeled with Cy3 or Alexa Fluor 488 was synthesized as follows (GeneDesign, Osaka, Japan): 5′-Cy3/Alexa 488-CAGCAG CAGCAGCAGCAGCA-3′, where underlining denotes LNAs. The fibroblasts were grown on non-coated coverslips. The cells were fixed with cold 4% paraformaldehyde for 30 min at 4°C and permeabilized for 5 min at 4°C with 2% acetone in PBS pre-chilled at −20°C. Hybridization was performed with 2 ng/μL of DNA/LNA probe in hybridization buffer (30% formamide, 2× SSC, 200 ng/mL single-stranded DNA [ssDNA], 0.02% BSA, 10% dextran sulfate, and 2 mM vanadyl ribonucleoside) overnight at 37°C. Then, the cells were washed with 30% formamide in 2× SSC for 30 min at 45°C and 30% formamide in 1× SSC for 30 min at 37°C. For the immunofluorescence detection of the transfected cells, fibroblasts were blocked with 3% BSA in PBS for 1 h and incubated with anti-GFP (Thermo Fisher Scientific, Waltham, MA, USA) or anti-RFP (MBL International, Nagoya, Japan) antibody. After washing, the coverslips were mounted with ProLong Diamond antifade mountant with DAPI (Thermo Fisher Scientific, Waltham, MA, USA), and fluorescent images were taken using an FSX100 fluorescence microscope (Olympus, Tokyo, Japan). For the quantitative analysis of the RNA foci, images of more than 100 nuclei were captured from each group. The numbers of RNA foci in the nuclei were counted by visual observation, and the intensities of the RNA foci in the nuclei were measured using ImageJ software. Statistical differences were evaluated using Student's t test. p values <0.05 were considered statistically significant. For the detection of MBNL1, the RNA-FISH assay was followed by immunofluorescent staining with anti-MBNL1 MB1a (Developmental Studies Hybridoma Bank, Iowa City, IA, USA), according to the standard protocol.

Unbiased Genome-wide Detection of Off-target DSBs

LAM-HTGTS was performed as previously reported with some modifications.[37,38] Briefly, HEK293 cells (6×10^6 cells for each group) were transfected with Cas9 nuclease or Cas9 nickase with the respective sgRNAs (5′ guide 3 and 3′ guide 2 for Cas9 nuclease, Nick 1 and Nick 3 for Cas9 nickase). As a positive control of the off-target effects, the cells were transfected with Cas9 nuclease and sgRNA targeting *RAG1* gene site A (RAG1A) (Table S3).[37] Three days after the transfection, genomic DNA was extracted from the cells with a DNeasy Blood & Tissue kit (QIAGEN, Hilden, Germany) and incubated overnight at 56°C. Then, the genomic DNA was sheared using a Covaris Focused-ultrasonicator (Covaris, Woburn, MA, USA). After purification using Agencourt AMPure XP beads (Beckman Coulter, Brea, CA, USA), the sheared DNA was amplified by LAM-PCR using KOD FX (Toyobo, Osaka, Japan) and sequence-specific biotinylated primers for *DMPK* and *RAG1* (Table S4) under the following conditions: an initial denaturation at 98°C for 2 min; 80 cycles at 95°C for 30 s, 58°C for 30 s, 72°C for 90 s; a final extension at 72°C for 2 min. The PCR products were incubated with Dynabeads MyONE streptavidin C1 beads (Thermo Fisher Scientific, Waltham, MA, USA) for 4 h. The DNA-beads complex was then captured by the magnetic stand. After annealing the upper and lower strands of the oligonucleotides for the bridge adaptor (Table S4), this was ligated to the DNA-beads complex using T4 DNA ligase (Promega, Madison, WI, USA) by incubating at 25°C for 1 h, 92°C for 2 h, and 16°C for 1 h. The on-beads ligation products were again captured by the magnetic stand and washed twice. Nested PCR was performed using the on-beads ligation products as templates with the primers indicated in Table S4. The PCR conditions were as follows: an initial denaturation at 95°C for 5 min; 15 cycles at 95°C for 60 s, 60°C for 30 s, 72°C for 60 s; a final extension at 72°C for 6 min. The PCR products were centrifuged at 15,000 × *g* for 5 min and the supernatants were concentrated using a QIAquick gel extraction kit (QIAGEN, Hilden, Germany). The DNA samples were barcoded for multiplexing using dual index primer sets (Illumina, San Diego, CA, USA) (Table S4) using the following conditions: an initial denaturation at 95°C for 3 min; 16 cycles at 95°C for 30 s, 62°C for 30 s, 72°C for 60 s; a final extension at 72°C for 6 min. The PCR products were run on a 1% agarose gel and the DNA was extracted from an area ranging from 500 to 1,000 bp using a QIAquick gel extraction kit. After barcoding, the samples were pooled in equal mass ratios. A denatured and diluted

library pool of 600 μL of PhiX control was sequenced with the 300-bp paired-end sequencing reactions on the MiSeq sequencer using the a V3 600 cycle kit (Illumina, San Diego, CA, USA). After trimming the adaptor sequences, the sequence reads were mapped to the hg19 reference genome, and any PCR duplicates were removed. The reads, which contain 20 bp of an adjacent to on-target breakpoint locus and at least 10 bp of uncertain nucleotides beyond the breakpoint, were specifically extracted for subsequent analysis. Off-target digestion and genomic rearrangements were detected as split reads, which mapped more than two different genomic loci in the same reads. Split reads were counted in a series of 100-bp equal-sized bins of entire genome. Off-target sites and the number of split reads were drawn using a Circos plot.[74]

SUPPLEMENTAL INFORMATION

Supplemental Information can be found online at https://doi.org/10.1016/j.omtm.2020.05.024.

AUTHOR CONTRIBUTIONS

F.S. conducted the study and wrote the manuscript. M.I. performed most of the experiments. M.T.-I. and T.K. performed deep sequencing. Y.S. performed bioinformatics analysis. S.T., H.H., N.S., and T.M. analyzed the experiments. K.M., M.S., and H.K. supervised the project.

CONFLICTS OF INTEREST

The authors declare no competing interests.

ACKNOWLEDGMENTS

F.S. was supported by an Intramural Research Grant (29-4) for Neurological and Psychiatric Disorders of NCNP from the Ministry of Health, Labour and Welfare of Japan and a Grant-in-Aid for Scientific Research C (19K07981) from the Ministry of Education, Culture, Sports, Science and Technology of Japan. F.S. received research support from Eisai, Takeda Pharmaceutical, Daiichi Sankyo, and Novartis. K.M. was supported by a Grant-in-Aid for Scientific Research C (19K07406) from the Ministry of Education, Culture, Sports, Science and Technology of Japan. H.H. was supported by a Grant-in-Aid for Scientific Research C (19K11359) from the Ministry of Education, Culture, Sports, Science and Technology of Japan. T.M was supported by a Grant-in-Aid for Scientific Research C (18K10693) from the Ministry of Education, Culture, Sports, Science and Technology of Japan. M.T.I. was supported by the Naito Foundation and the Hoansya Foundation.

REFERENCES

1. Turner, C., and Hilton-Jones, D. (2010). The myotonic dystrophies: diagnosis and management. J. Neurol. Neurosurg. Psychiatry *81*, 358–367.
2. Mahadevan, M., Tsilfidis, C., Sabourin, L., Shutler, G., Amemiya, C., Jansen, G., Neville, C., Narang, M., Barceló, J., O'Hoy, K., et al. (1992). Myotonic dystrophy mutation: an unstable CTG repeat in the 3′ untranslated region of the gene. Science *255*, 1253–1255.
3. Fu, Y.H., Pizzuti, A., Fenwick, R.G., Jr., King, J., Rajnarayan, S., Dunne, P.W., Dubel, J., Nasser, G.A., Ashizawa, T., de Jong, P., et al. (1992). An unstable triplet repeat in a gene related to myotonic muscular dystrophy. Science *255*, 1256–1258.
4. Zerylnick, C., Torroni, A., Sherman, S.L., and Warren, S.T. (1995). Normal variation at the myotonic dystrophy locus in global human populations. Am. J. Hum. Genet. *56*, 123–130.
5. Harley, H.G., Rundle, S.A., MacMillan, J.C., Myring, J., Brook, J.D., Crow, S., Reardon, W., Fenton, I., Shaw, D.J., and Harper, P.S. (1993). Size of the unstable CTG repeat sequence in relation to phenotype and parental transmission in myotonic dystrophy. Am. J. Hum. Genet. *52*, 1164–1174.
6. Tsilfidis, C., MacKenzie, A.E., Mettler, G., Barceló, J., and Korneluk, R.G. (1992). Correlation between CTG trinucleotide repeat length and frequency of severe congenital myotonic dystrophy. Nat. Genet. *1*, 192–195.
7. Lavedan, C., Hofmann-Radvanyi, H., Shelbourne, P., Rabes, J.P., Duros, C., Savoy, D., Dehaupas, I., Luce, S., Johnson, K., and Junien, C. (1993). Myotonic dystrophy: size- and sex-dependent dynamics of CTG meiotic instability, and somatic mosaicism. Am. J. Hum. Genet. *52*, 875–883.
8. Ashizawa, T., Anvret, M., Baiget, M., Barceló, J.M., Brunner, H., Cobo, A.M., Dallapiccola, B., Fenwick, R.G., Jr., Grandell, U., Harley, H., et al. (1994). Characteristics of intergenerational contractions of the CTG repeat in myotonic dystrophy. Am. J. Hum. Genet. *54*, 414–423.
9. Davis, B.M., McCurrach, M.E., Taneja, K.L., Singer, R.H., and Housman, D.E. (1997). Expansion of a CUG trinucleotide repeat in the 3′ untranslated region of myotonic dystrophy protein kinase transcripts results in nuclear retention of transcripts. Proc. Natl. Acad. Sci. USA *94*, 7388–7393.
10. Michalowski, S., Miller, J.W., Urbinati, C.R., Paliouras, M., Swanson, M.S., and Griffith, J. (1999). Visualization of double-stranded RNAs from the myotonic dystrophy protein kinase gene and interactions with CUG-binding protein. Nucleic Acids Res. *27*, 3534–3542.
11. Mooers, B.H., Logue, J.S., and Berglund, J.A. (2005). The structural basis of myotonic dystrophy from the crystal structure of CUG repeats. Proc. Natl. Acad. Sci. USA *102*, 16626–16631.
12. Miller, J.W., Urbinati, C.R., Teng-Umnuay, P., Stenberg, M.G., Byrne, B.J., Thornton, C.A., and Swanson, M.S. (2000). Recruitment of human muscleblind proteins to $(CUG)_n$ expansions associated with myotonic dystrophy. EMBO J. *19*, 4439–4448.
13. Mankodi, A., Urbinati, C.R., Yuan, Q.P., Moxley, R.T., Sansone, V., Krym, M., Henderson, D., Schalling, M., Swanson, M.S., and Thornton, C.A. (2001). Muscleblind localizes to nuclear foci of aberrant RNA in myotonic dystrophy types 1 and 2. Hum. Mol. Genet. *10*, 2165–2170.
14. Fardaei, M., Rogers, M.T., Thorpe, H.M., Larkin, K., Hamshere, M.G., Harper, P.S., and Brook, J.D. (2002). Three proteins, MBNL, MBLL and MBXL, co-localize in vivo with nuclear foci of expanded-repeat transcripts in DM1 and DM2 cells. Hum. Mol. Genet. *11*, 805–814.
15. Kanadia, R.N., Johnstone, K.A., Mankodi, A., Lungu, C., Thornton, C.A., Esson, D., Timmers, A.M., Hauswirth, W.W., and Swanson, M.S. (2003). A muscleblind knockout model for myotonic dystrophy. Science *302*, 1978–1980.
16. Kuyumcu-Martinez, N.M., Wang, G.S., and Cooper, T.A. (2007). Increased steady-state levels of CUGBP1 in myotonic dystrophy 1 are due to PKC-mediated hyperphosphorylation. Mol. Cell *28*, 68–78.
17. Kalsotra, A., Singh, R.K., Gurha, P., Ward, A.J., Creighton, C.J., and Cooper, T.A. (2014). The Mef2 transcription network is disrupted in myotonic dystrophy heart tissue, dramatically altering miRNA and mRNA expression. Cell Rep. *6*, 336–345.
18. Mankodi, A., Takahashi, M.P., Jiang, H., Beck, C.L., Bowers, W.J., Moxley, R.T., Cannon, S.C., and Thornton, C.A. (2002). Expanded CUG repeats trigger aberrant splicing of ClC-1 chloride channel pre-mRNA and hyperexcitability of skeletal muscle in myotonic dystrophy. Mol. Cell *10*, 35–44.
19. Charlet-B, N., Savkur, R.S., Singh, G., Philips, A.V., Grice, E.A., and Cooper, T.A. (2002). Loss of the muscle-specific chloride channel in type 1 myotonic dystrophy due to misregulated alternative splicing. Mol. Cell *10*, 45–53.
20. Fugier, C., Klein, A.F., Hammer, C., Vassilopoulos, S., Ivarsson, Y., Toussaint, A., Tosch, V., Vignaud, A., Ferry, A., Messaddeq, N., et al. (2011). Misregulated alternative splicing of BIN1 is associated with T tubule alterations and muscle weakness in myotonic dystrophy. Nat. Med. *17*, 720–725.
21. Savkur, R.S., Philips, A.V., and Cooper, T.A. (2001). Aberrant regulation of insulin receptor alternative splicing is associated with insulin resistance in myotonic dystrophy. Nat. Genet. *29*, 40–47.

22. Garneau, J.E., Dupuis, M.È., Villion, M., Romero, D.A., Barrangou, R., Boyaval, P., Fremaux, C., Horvath, P., Magadán, A.H., and Moineau, S. (2010). The CRISPR/Cas bacterial immune system cleaves bacteriophage and plasmid DNA. Nature *468*, 67–71.

23. Cong, L., Ran, F.A., Cox, D., Lin, S., Barretto, R., Habib, N., Hsu, P.D., Wu, X., Jiang, W., Marraffini, L.A., and Zhang, F. (2013). Multiplex genome engineering using CRISPR/Cas systems. Science *339*, 819–823.

24. Mali, P., Yang, L., Esvelt, K.M., Aach, J., Guell, M., DiCarlo, J.E., Norville, J.E., and Church, G.M. (2013). RNA-guided human genome engineering via Cas9. Science *339*, 823–826.

25. Komor, A.C., Badran, A.H., and Liu, D.R. (2017). CRISPR-based technologies for the manipulation of eukaryotic genomes. Cell *168*, 20–36.

26. Ran, F.A., Hsu, P.D., Wright, J., Agarwala, V., Scott, D.A., and Zhang, F. (2013). Genome engineering using the CRISPR-Cas9 system. Nat. Protoc. *8*, 2281–2308.

27. van Agtmaal, E.L., André, L.M., Willemse, M., Cumming, S.A., van Kessel, I.D.G., van den Broek, W.J.A.A., Gourdon, G., Furling, D., Mouly, V., Monckton, D.G., et al. (2017). CRISPR/Cas9-induced $(CTG{\cdot}CAG)_n$ repeat instability in the myotonic dystrophy type 1 locus: implications for therapeutic genome editing. Mol. Ther. *25*, 24–43.

28. Provenzano, C., Cappella, M., Valaperta, R., Cardani, R., Meola, G., Martelli, F., Cardinali, B., and Falcone, G. (2017). CRISPR/Cas9-mediated deletion of CTG expansions recovers normal phenotype in myogenic cells derived from myotonic dystrophy 1 patients. Mol. Ther. Nucleic Acids *9*, 337–348.

29. Dastidar, S., Ardui, S., Singh, K., Majumdar, D., Nair, N., Fu, Y., Reyon, D., Samara, E., Gerli, M.F.M., Klein, A.F., et al. (2018). Efficient CRISPR/Cas9-mediated editing of trinucleotide repeat expansion in myotonic dystrophy patient-derived iPS and myogenic cells. Nucleic Acids Res. *46*, 8275–8298.

30. Lo Scrudato, M., Poulard, K., Sourd, C., Tomé, S., Klein, A.F., Corre, G., Huguet, A., Furling, D., Gourdon, G., and Buj-Bello, A. (2019). Genome editing of expanded CTG repeats within the human *DMPK* gene reduces nuclear RNA foci in the muscle of DM1 mice. Mol. Ther. *27*, 1372–1388.

31. Zhang, X.H., Tee, L.Y., Wang, X.G., Huang, Q.S., and Yang, S.H. (2015). Off-target effects in CRISPR/Cas9-mediated genome engineering. Mol. Ther. Nucleic Acids *4*, e264.

32. Ran, F.A., Hsu, P.D., Lin, C.Y., Gootenberg, J.S., Konermann, S., Trevino, A.E., Scott, D.A., Inoue, A., Matoba, S., Zhang, Y., and Zhang, F. (2013). Double nicking by RNA-guided CRISPR Cas9 for enhanced genome editing specificity. Cell *154*, 1380–1389.

33. Shen, B., Zhang, W., Zhang, J., Zhou, J., Wang, J., Chen, L., Wang, L., Hodgkins, A., Iyer, V., Huang, X., and Skarnes, W.C. (2014). Efficient genome modification by CRISPR-Cas9 nickase with minimal off-target effects. Nat. Methods *11*, 399–402.

34. Canver, M.C., Bauer, D.E., Dass, A., Yien, Y.Y., Chung, J., Masuda, T., Maeda, T., Paw, B.H., and Orkin, S.H. (2014). Characterization of genomic deletion efficiency mediated by clustered regularly interspaced short palindromic repeats (CRISPR)/Cas9 nuclease system in mammalian cells. J. Biol. Chem. *289*, 21312–21324.

35. Qi, L.S., Larson, M.H., Gilbert, L.A., Doudna, J.A., Weissman, J.S., Arkin, A.P., and Lim, W.A. (2013). Repurposing CRISPR as an RNA-guided platform for sequence-specific control of gene expression. Cell *152*, 1173–1183.

36. Gilbert, L.A., Larson, M.H., Morsut, L., Liu, Z., Brar, G.A., Torres, S.E., Stern-Ginossar, N., Brandman, O., Whitehead, E.H., Doudna, J.A., et al. (2013). CRISPR-mediated modular RNA-guided regulation of transcription in eukaryotes. Cell *154*, 442–451.

37. Frock, R.L., Hu, J., Meyers, R.M., Ho, Y.J., Kii, E., and Alt, F.W. (2015). Genome-wide detection of DNA double-stranded breaks induced by engineered nucleases. Nat. Biotechnol. *33*, 179–186.

38. Hu, J., Meyers, R.M., Dong, J., Panchakshari, R.A., Alt, F.W., and Frock, R.L. (2016). Detecting DNA double-stranded breaks in mammalian genomes by linear amplification-mediated high-throughput genome-wide translocation sequencing. Nat. Protoc. *11*, 853–871.

39. Robinson, J.T., Thorvaldsdóttir, H., Winckler, W., Guttman, M., Lander, E.S., Getz, G., and Mesirov, J.P. (2011). Integrative genomics viewer. Nat. Biotechnol. *29*, 24–26.

40. Nakamori, M., Taylor, K., Mochizuki, H., Sobczak, K., and Takahashi, M.P. (2015). Oral administration of erythromycin decreases RNA toxicity in myotonic dystrophy. Ann. Clin. Transl. Neurol. *3*, 42–54.

41. Rzuczek, S.G., Colgan, L.A., Nakai, Y., Cameron, M.D., Furling, D., Yasuda, R., and Disney, M.D. (2017). Precise small-molecule recognition of a toxic CUG RNA repeat expansion. Nat. Chem. Biol. *13*, 188–193.

42. Wheeler, T.M., Leger, A.J., Pandey, S.K., MacLeod, A.R., Nakamori, M., Cheng, S.H., Wentworth, B.M., Bennett, C.F., and Thornton, C.A. (2012). Targeting nuclear RNA for in vivo correction of myotonic dystrophy. Nature *488*, 111–115.

43. Jauvin, D., Chrétien, J., Pandey, S.K., Martineau, L., Revillod, L., Bassez, G., Lachon, A., MacLeod, A.R., Gourdon, G., Wheeler, T.M., et al. (2017). Targeting DMPK with antisense oligonucleotide improves muscle strength in myotonic dystrophy type 1 mice. Mol. Ther. Nucleic Acids *7*, 465–474.

44. Gao, Y., Guo, X., Santostefano, K., Wang, Y., Reid, T., Zeng, D., Terada, N., Ashizawa, T., and Xia, G. (2016). Genome therapy of myotonic dystrophy type 1 iPS cells for development of autologous stem cell therapy. Mol. Ther. *24*, 1378–1387.

45. Wang, Y., Hao, L., Wang, H., Santostefano, K., Thapa, A., Cleary, J., Li, H., Guo, X., Terada, N., Ashizawa, T., and Xia, G. (2018). Therapeutic genome editing for myotonic dystrophy type 1 using CRISPR/Cas9. Mol. Ther. *26*, 2617–2630.

46. Wang, D., Zhang, F., and Gao, G. (2020). CRISPR-based therapeutic genome editing: strategies and in vivo delivery by AAV vectors. Cell *181*, 136–150.

47. Staahl, B.T., Benekareddy, M., Coulon-Bainier, C., Banfal, A.A., Floor, S.N., Sabo, J.K., Urnes, C., Munares, G.A., Ghosh, A., and Doudna, J.A. (2017). Efficient genome editing in the mouse brain by local delivery of engineered Cas9 ribonucleoprotein complexes. Nat. Biotechnol. *35*, 431–434.

48. Finn, J.D., Smith, A.R., Patel, M.C., Shaw, L., Youniss, M.R., van Heteren, J., Dirstine, T., Ciullo, C., Lescarbeau, R., Seitzer, J., et al. (2018). A single administration of CRISPR/Cas9 lipid nanoparticles achieves robust and persistent in vivo genome editing. Cell Rep. *22*, 2227–2235.

49. Lee, K., Conboy, M., Park, H.M., Jiang, F., Kim, H.J., Dewitt, M.A., Mackley, V.A., Chang, K., Rao, A., Skinner, C., et al. (2017). Nanoparticle delivery of Cas9 ribonucleoprotein and donor DNA *in vivo* induces homology-directed DNA repair. Nat. Biomed. Eng. *1*, 889–901.

50. Ramakrishna, S., Kwaku Dad, A.B., Beloor, J., Gopalappa, R., Lee, S.K., and Kim, H. (2014). Gene disruption by cell-penetrating peptide-mediated delivery of Cas9 protein and guide RNA. Genome Res. *24*, 1020–1027.

51. Gee, P., Lung, M.S.Y., Okuzaki, Y., Sasakawa, N., Iguchi, T., Makita, Y., Hozumi, H., Miura, Y., Yang, L.F., Iwasaki, M., et al. (2020). Extracellular nanovesicles for packaging of CRISPR-Cas9 protein and sgRNA to induce therapeutic exon skipping. Nat. Commun. *11*, 1334.

52. Schwab, I., and Nimmerjahn, F. (2013). Intravenous immunoglobulin therapy: how does IgG modulate the immune system? Nat. Rev. Immunol. *13*, 176–189.

53. Gopalappa, R., Suresh, B., Ramakrishna, S., and Kim, H.H. (2018). Paired D10A Cas9 nickases are sometimes more efficient than individual nucleases for gene disruption. Nucleic Acids Res. *46*, e71.

54. Yee, J.K. (2016). Off-target effects of engineered nucleases. FEBS J. *283*, 3239–3248.

55. Alateeq, S., Ovchinnikov, D., Tracey, T., Whitworth, D., Al-Rubaish, A., Al-Ali, A., and Wolvetang, E. (2018). Identification of on-target mutagenesis during correction of a β-thalassemia splice mutation in iPS cells with optimised CRISPR/Cas9-double nickase reveals potential safety concerns. APL Bioeng. *2*, 046103.

56. Caldecott, K.W. (2008). Single-strand break repair and genetic disease. Nat. Rev. Genet. *9*, 619–631.

57. Kuzminov, A. (2001). Single-strand interruptions in replicating chromosomes cause double-strand breaks. Proc. Natl. Acad. Sci. USA *98*, 8241–8246.

58. Ensminger, M., Iloff, L., Ebel, C., Nikolova, T., Kaina, B., and Löbrich, M. (2014). DNA breaks and chromosomal aberrations arise when replication meets base excision repair. J. Cell Biol. *206*, 29–43.

59. Cannan, W.J., and Pederson, D.S. (2016). Mechanisms and consequences of double-strand DNA break formation in chromatin. J. Cell. Physiol. *231*, 3–14.

60. Adikusuma, F., Piltz, S., Corbett, M.A., Turvey, M., McColl, S.R., Helbig, K.J., Beard, M.R., Hughes, J., Pomerantz, R.T., and Thomas, P.Q. (2018). Large deletions induced by Cas9 cleavage. Nature *560*, E8–E9.

61. Shin, H.Y., Wang, C., Lee, H.K., Yoo, K.H., Zeng, X., Kuhns, T., Yang, C.M., Mohr, T., Liu, C., and Hennighausen, L. (2017). CRISPR/Cas9 targeting events cause complex deletions and insertions at 17 sites in the mouse genome. Nat. Commun. *8*, 15464.

62. Kosicki, M., Tomberg, K., and Bradley, A. (2018). Repair of double-strand breaks induced by CRISPR-Cas9 leads to large deletions and complex rearrangements. Nat. Biotechnol. *36*, 765–771.

63. Owens, D.D.G., Caulder, A., Frontera, V., Harman, J.R., Allan, A.J., Bucakci, A., Greder, L., Codner, G.F., Hublitz, P., McHugh, P.J., et al. (2019). Microhomologies are prevalent at Cas9-induced larger deletions. Nucleic Acids Res. *47*, 7402–7417.

64. Giannoukos, G., Ciulla, D.M., Marco, E., Abdulkerim, H.S., Barrera, L.A., Bothmer, A., Dhanapal, V., Gloskowski, S.W., Jayaram, H., Maeder, M.L., et al. (2018). UDiTaS™, a genome editing detection method for indels and genome rearrangements. BMC Genomics *19*, 212.

65. Nelson, C.E., Wu, Y., Gemberling, M.P., Oliver, M.L., Waller, M.A., Bohning, J.D., Robinson-Hamm, J.N., Bulaklak, K., Castellanos Rivera, R.M., Collier, J.H., et al. (2019). Long-term evaluation of AAV-CRISPR genome editing for Duchenne muscular dystrophy. Nat. Med. *25*, 427–432.

66. Haapaniemi, E., Botla, S., Persson, J., Schmierer, B., and Taipale, J. (2018). CRISPR-Cas9 genome editing induces a p53-mediated DNA damage response. Nat. Med. *24*, 927–930.

67. Ihry, R.J., Worringer, K.A., Salick, M.R., Frias, E., Ho, D., Theriault, K., Kommineni, S., Chen, J., Sondey, M., Ye, C., et al. (2018). p53 inhibits CRISPR-Cas9 engineering in human pluripotent stem cells. Nat. Med. *24*, 939–946.

68. Radzisheuskaya, A., Shlyueva, D., Müller, I., and Helin, K. (2016). Optimizing sgRNA position markedly improves the efficiency of CRISPR/dCas9-mediated transcriptional repression. Nucleic Acids Res. *44*, e141.

69. Carrell, S.T., Carrell, E.M., Auerbach, D., Pandey, S.K., Bennett, C.F., Dirksen, R.T., and Thornton, C.A. (2016). *Dmpk* gene deletion or antisense knockdown does not compromise cardiac or skeletal muscle function in mice. Hum. Mol. Genet. *25*, 4328–4338.

70. Pinto, B.S., Saxena, T., Oliveira, R., Méndez-Gómez, H.R., Cleary, J.D., Denes, L.T., McConnell, O., Arboleda, J., Xia, G., Swanson, M.S., and Wang, E.T. (2017). Impeding transcription of expanded microsatellite repeats by deactivated Cas9. Mol. Cell *68*, 479–490.e5.

71. Batra, R., Nelles, D.A., Pirie, E., Blue, S.M., Marina, R.J., Wang, H., Chaim, I.A., Thomas, J.D., Zhang, N., Nguyen, V., et al. (2017). Elimination of toxic microsatellite repeat expansion RNA by RNA-targeting Cas9. Cell *170*, 899–912.e10.

72. Thakore, P.I., Kwon, J.B., Nelson, C.E., Rouse, D.C., Gemberling, M.P., Oliver, M.L., and Gersbach, C.A. (2018). RNA-guided transcriptional silencing in vivo with S. aureus CRISPR-Cas9 repressors. Nat. Commun. *9*, 1674.

73. Noguchi, S., Arakawa, T., Fukuda, S., Furuno, M., Hasegawa, A., Hori, F., Ishikawa-Kato, S., Kaida, K., Kaiho, A., Kanamori-Katayama, M., et al. (2017). FANTOM5 CAGE profiles of human and mouse samples. Sci. Data *4*, 170112.

74. Hu, Y., Yan, C., Hsu, C.H., Chen, Q.R., Niu, K., Komatsoulis, G.A., and Meerzaman, D. (2014). OmicCircos: a simple-to-use R package for the circular visualization of multidimensional omics data. Cancer Inform. *13*, 13–20.

令和 3 年 5 月 13 日

国立保健医療科学院長　殿

機関名　藤田医科大学

所属研究機関長　職　名　学長

氏　名　才藤　栄一

次の職員の令和２年度厚生労働科学研究費の調査研究における、倫理審査状況及び利益相反等の管理については以下のとおりです。

１．研究事業名　難治性疾患政策研究事業

２．研究課題名　染色体微細欠失重複症候群の包括的診療体制の構築

３．研究者名　（所属部局・職名）　総合医科学研究所・分子遺伝学・教授

（氏名・フリガナ）　倉橋浩樹・クラハシヒロキ

４．倫理審査の状況

	該当性の有無		左記で該当がある場合のみ記入（※1）		
	有	無	審査済み	審査した機関	未審査（※2）
ヒトゲノム・遺伝子解析研究に関する倫理指針	■	□	■	藤田医科大学	□
遺伝子治療等臨床研究に関する指針	□	■	□		□
人を対象とする医学系研究に関する倫理指針（※3）	□	■	□		□
厚生労働省の所管する実施機関における動物実験等の実施に関する基本指針	□	■	□		□
その他、該当する倫理指針があれば記入すること（指針の名称：　　）	□	■	□		□

（※1）当該研究者が当該研究を実施するに当たり遵守すべき倫理指針に関する倫理委員会の審査が済んでいる場合は、「審査済み」にチェックし一部若しくは全部の審査が完了していない場合は、「未審査」にチェックすること。

その他（特記事項）

（※2）未審査の場合は、その理由を記載すること。

（※3）廃止前の「疫学研究に関する倫理指針」や「臨床研究に関する倫理指針」に準拠する場合は、当該項目に記入すること。

５．厚生労働分野の研究活動における不正行為への対応について

研究倫理教育の受講状況	受講 ■　未受講 □

６．利益相反の管理

当研究機関におけるＣＯＩの管理に関する規定の策定	有 ■　無 □（無の場合はその理由：　　）
当研究機関におけるＣＯＩ委員会設置の有無	有 ■　無 □（無の場合は委託先機関：　　）
当研究に係るＣＯＩについての報告・審査の有無	有 ■　無 □（無の場合はその理由：　　）
当研究に係るＣＯＩについての指導・管理の有無	有 □　無 ■（有の場合はその内容：　　）

（留意事項）　・該当する□にチェックを入れること。
・分担研究者の所属する機関の長も作成すること。

令和 3 年 5 月 1 日

国立保健医療科学院長　殿

機関名埼玉県立小児医療センター

所属研究機関長　職　名　病院長

氏　名　岡　明

次の職員の令和２年度厚生労働科学研究費の調査研究における、倫理審査状況及び利益相反等の管理については以下のとおりです。

１．研究事業名　難治性疾患政策研究事業

２．研究課題名　染色体微細欠失重複症候群の包括的診療体制の構築

３．研究者名　（所属部局・職名）　遺伝科・科長兼部長

（氏名・フリガナ）　大橋博文・オオハシヒロフミ

４．倫理審査の状況

	該当性の有無	左記で該当がある場合のみ記入（※1）		
	有　無	審査済み	審査した機関	未審査（※2）
ヒトゲノム・遺伝子解析研究に関する倫理指針	□　■	□		□
遺伝子治療等臨床研究に関する指針	□　■	□		□
人を対象とする医学系研究に関する倫理指針（※3）	■　□	■	埼玉県立小児医療センター	□
厚生労働省の所管する実施機関における動物実験等の実施に関する基本指針	□　■	□		□
その他、該当する倫理指針があれば記入すること（指針の名称：　）	□　■	□		□

（※1）当該研究者が当該研究を実施するに当たり遵守すべき倫理指針に関する倫理委員会の審査が済んでいる場合は、「審査済み」にチェックし一部若しくは全部の審査が完了していない場合は、「未審査」にチェックすること。

その他（特記事項）

（※2）未審査の場合は、その理由を記載すること。
（※3）廃止前の「疫学研究に関する倫理指針」や「臨床研究に関する倫理指針」に準拠する場合は、当該項目に記入すること。

５．厚生労働分野の研究活動における不正行為への対応について

研究倫理教育の受講状況	受講 ■　未受講 □

６．利益相反の管理

当研究機関におけるＣＯＩの管理に関する規定の策定	有 ■　無 □（無の場合はその理由：　）
当研究機関におけるＣＯＩ委員会設置の有無	有 ■　無 □（無の場合は委託先機関：　）
当研究に係るＣＯＩについての報告・審査の有無	有 ■　無 □（無の場合はその理由：　）
当研究に係るＣＯＩについての指導・管理の有無	有 □　無 ■（有の場合はその内容：　）

（留意事項）　・該当する□にチェックを入れること。
・分担研究者の所属する機関の長も作成すること。

国立保健医療科学院長　殿

令和３年３月２５日

機関名　地方独立行政法人神奈川県立病院機構
神奈川県立こども医療センター

所属研究機関長　職　名　総　長

氏　名　町田　治郎

次の職員の令和２年度厚生労働科学研究費の調査研究における、倫理審査状況及び利益相反等の管理については以下のとおりです。

１．研究事業名　難治性疾患政策研究事業

２．研究課題名　染色体微細欠失重複症候群の包括的診療体制の構築

３．研究者名　（所属部局・職名）　遺伝科　部長

（氏名・フリガナ）　黒澤　健司・クロサワ　ケンジ

４．倫理審査の状況

	該当性の有無		左記で該当がある場合のみ記入（※1）		
	有	無	審査済み	審査した機関	未審査（※2）
ヒトゲノム・遺伝子解析研究に関する倫理指針	■	□	■	神奈川県立こども医療センター	□
遺伝子治療等臨床研究に関する指針	□	■	□		□
人を対象とする医学系研究に関する倫理指針（※3）	□	■	□		□
厚生労働省の所管する実施機関における動物実験等の実施に関する基本指針	□	■	□		□
その他、該当する倫理指針があれば記入すること（指針の名称：　）	□	■	□		□

（※1）当該研究者が当該研究を実施するに当たり遵守すべき倫理指針に関する倫理委員会の審査が済んでいる場合は、「審査済み」にチェックし一部若しくは全部の審査が完了していない場合は、「未審査」にチェックすること。

その他（特記事項）

（※2）未審査に場合は、その理由を記載すること。

（※3）廃止前の「疫学研究に関する倫理指針」や「臨床研究に関する倫理指針」に準拠する場合は、当該項目に記入すること。

５．厚生労働分野の研究活動における不正行為への対応について

研究倫理教育の受講状況	受講 ■　未受講 □

６．利益相反の管理

当研究機関におけるＣＯＩの管理に関する規定の策定	有 ■　無 □（無の場合はその理由：　）
当研究機関におけるＣＯＩ委員会設置の有無	有 ■　無 □（無の場合は委託先機関：　）
当研究に係るＣＯＩについての報告・審査の有無	有 ■　無 □（無の場合はその理由：　）
当研究に係るＣＯＩについての指導・管理の有無	有 □　無 ■（有の場合はその内容：　）

（留意事項）　・該当する□にチェックを入れること。
・分担研究者の所属する機関の長も作成すること。

令和 3 年 3 月 4 日

国立保健医療科学院長　　殿

機関名　東京女子医科大学

所属研究機関長　職　名　学長

氏　名　丸　義朗

次の職員の令和２年度厚生労働科学研究費の調査研究における、倫理審査状況及び利益相反等の管理については以下のとおりです。

１．研究事業名　難治性疾患政策研究事業

２．研究課題名　染色体微細欠失重複症候群の包括的診療体制の構築

３．研究者名　（所属部局・職名）　医学部 ・ 教授

（氏名・フリガナ）　山本　俊至 ・ ヤマモト　トシユキ

４．倫理審査の状況

	該当性の有無		左記で該当がある場合のみ記入　(※1)		
	有	無	審査済み	審査した機関	未審査(※2)
ヒトゲノム・遺伝子解析研究に関する倫理指針	■	□	■	東京女子医科大学	□
遺伝子治療等臨床研究に関する指針	□	■	□		□
人を対象とする医学系研究に関する倫理指針（※3）	□	■	□		□
厚生労働省の所管する実施機関における動物実験等の実施に関する基本指針	□	■	□		□
その他、該当する倫理指針があれば記入すること（指針の名称：　　）	□	■	□		□

（※1）当該研究者が当該研究を実施するに当たり遵守すべき倫理指針に関する倫理委員会の審査が済んでいる場合は、「審査済み」にチェックし一部若しくは全部の審査が完了していない場合は、「未審査」にチェックすること。

その他（特記事項）

（※2）未審査に場合は、その理由を記載すること。

（※3）廃止前の「疫学研究に関する倫理指針」や「臨床研究に関する倫理指針」に準拠する場合は、当該項目に記入すること。

５．厚生労働分野の研究活動における不正行為への対応について

研究倫理教育の受講状況	受講 ■　未受講 □

６．利益相反の管理

当研究機関におけるＣＯＩの管理に関する規定の策定	有 ■　無 □（無の場合はその理由　：　）
当研究機関におけるＣＯＩ委員会設置の有無	有 ■　無 □（無の場合は委託先機関：　）
当研究に係るＣＯＩについての報告・審査の有無	有 ■　無 □（無の場合はその理由　：　）
当研究に係るＣＯＩについての指導・管理の有無	有 □　無 ■（有の場合はその内容　：　）

（留意事項）・該当する□にチェックを入れること。

・分担研究者の所属する機関の長も作成すること。

令和　3年　3月29日

国立保健医療科学院長　殿

機関名　国立大学法人信州大学

所属研究機関長　職　名　学　長

氏　名　濱　田　州　博

次の職員の令和２年度厚生労働科学研究費の調査研究における、倫理審査状況及び利益相反等の管理については以下のとおりです。

１．研究事業名　難治性疾患政策研究事業

２．研究課題名　染色体微細欠失重複症候群の包括的診療体制の構築

３．研究者名　（所属部局・職名）　医学部　遺伝医学教室・講師

（氏名・フリガナ）　涌井　敬子（ワクイ　ケイコ）

４．倫理審査の状況

	該当性の有無		左記で該当がある場合のみ記入（※1）		
	有	無	審査済み	審査した機関	未審査（※2）
ヒトゲノム・遺伝子解析研究に関する倫理指針	□	■	□		□
遺伝子治療等臨床研究に関する指針	□	■	□		□
人を対象とする医学系研究に関する倫理指針（※3）	□	■	□		□
厚生労働省の所管する実施機関における動物実験等の実施に関する基本指針	□	■	□		□
その他、該当する倫理指針があれば記入すること（指針の名称：　）	□	■	□		□

（※1）当該研究者が当該研究を実施するに当たり遵守すべき倫理指針に関する倫理委員会の審査が済んでいる場合は、「審査済み」にチェックし一部若しくは全部の審査が完了していない場合は、「未審査」にチェックすること。

その他（特記事項）

（※2）未審査に場合は、その理由を記載すること。
（※3）廃止前の「疫学研究に関する倫理指針」や「臨床研究に関する倫理指針」に準拠する場合は、当該項目に記入すること。

５．厚生労働分野の研究活動における不正行為への対応について

研究倫理教育の受講状況	受講 ■　未受講 □

６．利益相反の管理

当研究機関におけるＣＯＩの管理に関する規定の策定	有 ■　無 □（無の場合はその理由：　）
当研究機関におけるＣＯＩ委員会設置の有無	有 ■　無 □（無の場合は委託先機関：　）
当研究に係るＣＯＩについての報告・審査の有無	有 ■　無 □（無の場合はその理由：　）
当研究に係るＣＯＩについての指導・管理の有無	有 □　無 ■（有の場合はその内容：　）

（留意事項）　・該当する□にチェックを入れること。
・分担研究者の所属する機関の長も作成すること。